

SEISMIC STRATIGRAPHY AND ARCHITECTURE OF THE JURASSIC ABENAKI
MARGIN, AT COHASSET-MIGRANT, AND POTENTIAL FOR DISTAL ORGANIC-
RICH FACIES

by

Taylor Jane Campbell

Submitted in partial fulfilment of the requirements
for the degree of Master of Science

at

Dalhousie University
Halifax, Nova Scotia
April 2018

© Copyright by Taylor Jane Campbell, 2018

Table of Contents

List of Tables	vi
List of Figures	vii
Abstract	xi
List of Abbreviations Used	xii
Acknowledgements	xiii
Chapter 1: Introduction	1
1.1 Project Overview	1
1.2 Motivation	3
1.3 Hypothesis and objectives	4
1.4 Thesis organization	4
Chapter 2: Geological Background	6
2.1 Introduction	6
2.2 Stratigraphic charts and maps	7
2.3 Scotian Basin	12
2.3.1 Geological Background of the Scotian Basin	13
2.4 Comparison of the Scotian and Moroccan Margins and the Lusitanian Basin	15
2.5 Study area	17
2.5.1 Abenaki Formation	18
2.6 Source Rocks	20
Chapter 3: Methods	23
3.1 Introduction	23
3.2 Project workflow	23
3.3 Datasets	25
3.4 Geology	29

3.4.1 Carbonate geology (models)	29
3.4.2 Siliciclastic geology	32
3.4.3 Core analysis	33
3.4.4 Microfacies analysis.....	34
3.5 Petrophysics	35
3.5.1 Well ties	36
3.5.2 Wireline logs	37
3.6 Geophysics	39
3.6.1 Seismic facies analysis.....	39
3.6.2 Seismic stratigraphy	39
3.6.3 Seismic interpretation	41
3.6.4 Seismic attributes	42
3.6.5 Genetic seismic inversion	42
3.6.6 Geocellular framework (initial model with no properties)	43
3.6.7 Geocellular modeling (with properties)	44
Chapter 4: Results	45
4.1 Introduction.....	45
4.2 Geology.....	45
4.2.1 Core Analysis.....	45
4.2.2 Cored wells cross section.....	46
4.2.3 Lithofacies.....	49
4.3 Petrophysics	56
4.3.1 Well log Analysis.....	56
4.4 Geophysics	58
4.4.1 Seismic interpretation: seismic facies	58

4.4.2 Seismic interpretation: Horizons and faults	66
4.4.3 Genetic seismic inversion	67
4.4.4 Depth model.....	68
4.4.5 Geocellular framework results.....	69
4.4.6 Geocellular model results	71
Chapter 5: Discussion	75
5.1 Introduction.....	75
5.2 Geology.....	76
5.2.1 Summary of lithofacies from core analysis	76
5.2.2 Modern Analog: Great Barrier Reef and Fly River Delta.....	76
5.2.3 Ancient analogs: Lusitanian Basin and Moroccan Margin.....	79
5.3 Well log correlation and source rock sampling	81
5.3.1 Key well log cross section	81
5.4 Geophysics.....	84
5.4.1 Seismic facies.....	84
5.4.2 Stratigraphic architecture of third-order depositional sequences of the Abenaki carbonate bank.....	86
5.4.3 Discussion of the Late Jurassic-Early Cretaceous siliciclastics on published stratigraphic charts	95
5.5 Source rock potential of distal third-order depositional sequences of the Abenaki carbonate bank	97
5.6 Controlling factors on the growth of the Abenaki carbonate bank.....	105
5.6.1 Influx of siliciclastics from the Sable Delta.....	105
5.6.2 Northern termination.....	107
5.6.3 Steep slope to shallow ramp transition	109
5.7 Uncertainties	112
5.7.1 Seismic uncertainties	112

5.7.2 Source rock potential uncertainties	112
Chapter 6: Conclusions and recommendations for future work	114
6.1 Conclusions.....	114
6.2 Recommendations for future work	117
References.....	118
Appendix A: Ancient analogs: Moroccan Margin and Lusitanian Basin.....	130
Appendix B: Wireline logs used within the study area.....	139
Appendix C: Seismic acquisition and processing applied to the Sable Sub-basin	141
Appendix D: Core descriptions.....	151
Appendix E: Seismic traverses	164

List of Tables

Table 3.1: Information on the 13 key wells used for this study. Information from BASIN database, Natural Resources Canada, 2018.....	27-28
Table 3.2: Well names of the cored intervals of the Abenaki Formation along with depth of the cored intervals and the member it belongs to.....	34
Table 5.1: Summary of lithofacies examined from core and petrographic examination.....	76
Table 5.2: Summary of the ten seismic facies used for interpreted the seismic structural and stratigraphic framework.....	85

List of Figures

Figure 1.1: Map of the Scotian Basin and associated sub-basins..	1
Figure 2.1: Paleo-reconstruction map of the Early Triassic (237 Ma).	6
Figure 2.2: Updated magnetic anomalies map along the Scotian margin.....	7
Figure 2.3: Simplified lithostratigraphic charts of the conjugate margins of offshore Nova Scotia and Atlantic Morocco (Central Nova Scotia chart modified from Wade and MacLean 1990 by Tari et al. 2012).....	8
Figure 2.4: Simplified lithostratigraphic charts of the Scotian shelf (modified from Wade and MacLean 1990) and the Lusitanian Basin (modified from Wach et al. 2014, from Azerêdo 2003, Rey 2006).	9
Figure 2.5: Paleogeographic map of the Early Jurassic (Sinemurian – Toarcian) end Sinemurian 190 Ma. Modified from Sibuet et al. 2011 with annotated formation names.	10
Figure 2.6: Paleogeographic map of the Middle Jurassic at Middle Bajocian, 170 Ma. Map modified from Sibuet et al. 2011 with annotated formation names for the Scotian and Moroccan margins and the Lusitanian Basin.	10
Figure 2.7: Paleogeographic map at Late Jurassic, Tithonian, 150 Ma. Map modified from Sibuet et al. 2011 with annotated formation names for the Scotian and Moroccan margins and the Lusitanian Basin.	11
Figure 2.8: Paleogeographic map of the Early Cretaceous (Berriasian-Barremian) at Valanginian, 136 Ma. Map modified from Sibuet et al. 2011 with annotated formation names for the Scotian and Moroccan margins and the Lusitanian Basin.	12
Figure 2.9: Seismic inline 3970 from the 3-D Sable MegaMerge dataset.....	17
Figure 2.10: Zonation depositional environments for a continental margin setting (modified from Veeken et al. 2013).	21
Figure 3.1: Project workflow outlining the integration of well logs and seismic to perform a depositional system analysis of the Middle Jurassic to Early Cretaceous interval.	24
Figure 3.2: Location of the seven 3D seismic surveys included in the Sable MegaMerge survey (modified from Morrison 2017).	25
Figure 3.3: Location of the regional 2D NovaSpan seismic lines..	26
Figure 3.4: Location of 2D seismic (grey lines) in relation to the 3D Sable MegaMerge (purple polygon) and the 2D regional NovaSpan line 1600 (longer black line).	27

Figure 3.5: Location of 10 key wells (yellow points) across the study area. Pink polygon is the outline of the 3D Sable MegaMerge, black lines are 64, 2D seismic lines across the Scotian Shelf. Blue dashed line is the Abenaki bank margin.	28
Figure 3.6: Schematic sequence stratigraphic chart of the Iroquois through Abenaki formations..	31
Figure 3.7: Simplified facies model of the Abenaki Formation, offshore Nova Scotia (modified from Weissenberger et al. 2000)..	31
Figure 3.8: Schematic of J.L. Wilson carbonate sequence stratigraphic model from Kidston et al. (2005) modified from Waite (1998), also identifying where potential organic-rich materials can be deposited within a carbonate ramp depositional system.	32
Figure 3.9: Basinward progradation of a delta, which builds a coarsening upwards facies succession that transition from marine into non-marine top set deposits (modified from Scruton 1960)..	33
Figure 3.10: Dunham classification of the subdivision of limestones based on their matrix content (modified by Kendall 2005 after Dunham 1962)..	35
Figure 3.11: Well cross section from the Encana Deep Panuke Offshore Gas Development Plan (2006)..	36
Figure 3.12: Reflection configurations (A) divergent, (B) concordant, (C) sub-parallel, (D) sigmoid, oblique and shingled, (E) chaotic (F) hummocky, (G) hyperbolic, (H) climbing waves, (I) accretionary channel, (J) cut-and-fill channel (modified from Mitchum et al. 1977)..	40
Figure 3.13: Relationship of strata to the upper and lower boundaries of a depositional sequence (Mitchum et al. 1977)..	41
Figure 4.1: Location of the four wells (L-97, M-79, H-08 and PI-1A- J-99) with cored intervals of the Abenaki Formation (four black dots) from the Middle-Late Jurassic that were analyzed and described for this study.	46
Figure 4.2: Cross section of wells used for core description of the Abenaki Formation for this study. Red arrows point to cored intervals of wells..	48
Figure 4.3: A, B and C: A: Cohasset L-97 Core 1, at approximately 3407m depth.....	50
Figure 4.4: A, B and C: A: Cohasset L-97 core 1, at approximately 3417.5m depth.....	51
Figure 4.5: A, B and C: A: Cohasset L-97 core 1, at approximately 3424m depth.....	52
Figure 4.6: A, B and C: A: Panuke H-08 core 1, at approximately 3450.7m depth.....	53
Figure 4.7: A, B and C: A: Panuke H-08 Core 1, at approximately 3457.5m depth..	54
Figure 4.8: A, B and C: A: Panuke M-79 core 1, at approximately 4532m depth.	55
Figure 4.9: A, B and C: A: Panuke PI-1A core 1, at approximately 4031.9 m depth.	56

Figure 4.10: Key well log cross section.....	57
Figure 4.11: Location of wells for the cross section in Figure 4.10 (A-A').	58
Figure 4.12 Location of the six seismic traverses seen in Figures 4.13 to 4.18..	59
Figure 4.13: Seismic traverse showing the transition from the continental shelf margin where the carbonate platform grew, to the slope on the eastern edge of the study area.....	60
Figure 4.14: Seismic traverse showing the transition from continental shelf margin where the carbonate platform grew, to slope, to distal foreslope/deep basin within the east-central region of the study area..	61
Figure 4.15: Seismic traverse close to the Cohasset L-97 well..	62
Figure 4.16: Seismic traverse showing the transition from continental shelf margin where the carbonate platform grew, through to the slope, to distal foreslope/deep basin within the central region of the study area.....	63
Figure 4.17: Seismic traverse showing the transition from continental shelf margin where the carbonate platform grew, to slope, to distal foreslope/deep basin within the western region of the study area..	64
Figure 4.18: Seismic traverse showing the third-order depositional sequences of the Abenaki carbonate bank distally.....	65
Figure 4.19: Fourteen faults interpreted in the west region of the Sable MegaMerge within the Jurassic.....	66
Figure 4.20: Location of A-A', which is the inline 3960, used for cross sections in Figures 4.21 and 4.22 and 4.25 and 4.26..	67
Figure 4.21: Vertical section (inline 3960, Fig.4.20, 5X vertical exaggeration) showing the results of the genetic inversion..	67
Figure 4.22: Vertical section (inline 3960, Fig. 4.20) showing the depth converted seismic from the genetic inversion.	69
Figure 4.23: 3D display of fault interpretation model..	70
Figure 4.24: 3D display of pillar gridding..	70
Figure 4.25: Vertical section (inline 3970, Fig. 4.20, 5X vertical exaggeration) demonstrating the use of the zone index.....	71
Figure 4.26: Vertical section (inline 3970, Fig. 4.20, 5X vertical exaggeration) demonstrating the sequence thicknesses based from cell heights.....	72
Figure 4.27: Geocellular model of the genetically inverted seismic data for the carbonate depositional system.....	73
Figure 4.28: Geocellular model of the genetically inverted seismic data for the mixed siliciclastic and carbonate depositional system..	74

Figure 5.1 A and B: Both show the locations of the northern extent of the Great Barrier Reef, offshore Queensland, Australia in relation to the Fly River Delta located on the southeastern region of Papua New Guinea.	79
Figure 5.2: Simplified geological map of the Lusitanian Basin, highlighting the locations of interest (Silva et al. 2014).....	81
Figure 5.3: Regional 2D NovaSpan seismic line.	88
Figure 5.4: Inline 3920 from the Sable MegaMerge.....	89
Figure 5.5: Zoom in of seismic traverse 4.13 near the Dominion J-14 well.....	90
Figure 5.6: Refined schematic of the third-order depositional sequences of the Abenaki Formation modified from Weissenberger et al. 2000 and Encana 2006.....	95
Figure 5.7 A and B are stratigraphic charts of the Late Jurassic to Early Cretaceous of the Scotian Basin. A is from Weston et al. 2012..	96
Figure 5.8: Vertical section (inline 3960, Fig. 4.20, 5X vertical exaggeration) showing both geocellular models (mud-rich and sand-rich depositional systems).....	99
Figure 5.9 A-E: Figure A shows the carbonate depositional model in which the environment of deposition maps were created from for Abenaki 2, 3 and 4..	101
Figure 5.10 A-D: Figure A shows the carbonate depositional model from which the environment of deposition maps were created from for Abenaki 5, 6 and 7..	104
Figure 5.11 Schematic illustrating faulting of the Abenaki Formation in the Sable sub-basin interpreted from 2D seismic modified from Wade and MacLean (1990)..	106
Figure 5.12: Cohasset L-97 lithological and gamma ray logs with lithostratigraphic picks from the Play Fairway Analysis from the Nova Scotia Department of Energy in 2011..	106
Figure 5.13 A and B: Generalized facies distribution of the Abenaki Formation (blue) the Verrill Canyon Formation (grey), Lower Missisauga Formation (orange) and the MicMac- Mohawk Formation (yellow)..	108
Figure 5.14: Dip angle map for Abenaki 4..	110
Figure 5.15: Updated magnetic anomalies map along the Scotian margin.....	110
Figure 5.16 A: Inline 3440 from the Sable MegaMerge.....	111

Abstract

This study uses well data, extensive 3D seismic data and geologic analogs to test and extend stratigraphic concepts and models in a mixed clastic-carbonate depositional setting: the Middle Jurassic to Early Cretaceous of the Sable Sub-basin, offshore Nova Scotia. The study incorporates stratigraphic concepts and models developed by government, industry and academic workers during the hydrocarbon exploration, development and production phases of the Sable Sub-basin. The study focuses on basinward mapping of third-order depositional sequences identified in the Abenaki carbonate bank at Deep Panuke Field. Source rock potential in coeval basinal calcareous mudstones; changes in bank margin morphology related to underlying basement; the transition from a dominantly carbonate system at the shelf margin to a fluvio-deltaic system of the Sable Delta adjacent to basinal mudstones outboard of the carbonate bank are discussed.

These depositional systems are imaged by 3D seismic data in the area around the Cohasset L-97 and Migrant N-20 well penetrations. Core studies of wells which penetrated the Abenaki carbonate bank and field studies in the Lusitanian Basin, onshore Portugal, provide calibration and analogs to shallow water carbonates in the Cohasset area. Further ancient and modern analogues are discussed from Morocco and at the termination of the Great Barrier Reef in the Gulf of Papua.

Using multiple geological, petrophysical and geophysical interpretation methods, the depositional cycles of limestones and calcareous shales that were deposited in increasingly deeper water outboard of the Abenaki margin were mapped within a stratigraphic framework. This framework formed the basis for a 3D geocellular model that was then populated with lithologies from well data via a seismic inversion. This model was then interpreted in terms of environments of deposition and source rock potential.

The third-order sequence stratigraphic framework employed here was extrapolated from a framework established at Deep Panuke gas field, where commercial production began in August 2013. This third-order chrono-stratigraphic framework (“Abenaki 1-7 surfaces”) incorporates multiple litho-stratigraphically defined formations: the Mohican, Mohawk, Mic Mac, Abenaki, Missisauga and Verrill Canyon formations. Thick fluvio-deltaic successions adjacent to basinal mudstones in the Migrant N-20 well are interpreted to be structurally controlled, deposited in local depocentres that formed in response to sediment loading, normal faulting and mobile salt substrate.

It is proposed from the 3D geocellular model, from examining analogous basins (Lusitanian Basin in Portugal and the Moroccan Margin), and from a published carbonate source rock model, that condensed sections of the distal carbonate depositional system within Abenaki 1-4 sequences have potential to host organic-rich material. The basinal shales of these sequences are estimated to have been deposited in up to 200 m water depths and have type 2 source rock potential. A change in seismic signatures and facies occurs between Abenaki sequences 1-4 and Abenaki sequences 5-7, reflecting encroachment of the Sable Delta, and it is interpreted that the Abenaki 5-7 sequences have predominantly type 3 source potential, with some potential for a type 2 source in intervening calcareous mudstones.

List of Abbreviations Used

TOC	Total Organic Carbon
OM	Organic Matter
CNSOPB	Canada-Nova Scotia Offshore Petroleum Board
km	Kilometre
m	Metre
TD	Total depth
MD	Measured depth
Wt %	Weight percent
Ma	Million years
ms	Millisecond
TWT	Two-way-time
Fm	Formation
Gp	Group

Acknowledgements

There are many people I would like to thank for their guidance and support throughout the completion of my thesis.

I am very grateful to my supervisor, Dr. Grant Wach, for his guidance, expertise and kind support throughout the completion of this study. I also cannot thank you enough for all the travel, work and learning opportunities you have given me over the past five years.

I would also like to acknowledge my supervisory committee member, Mr. Bill Richards for all the hours spent teaching me the ins and outs of Petrel and for all his constructive feedback throughout the writing process (I will never use the word “represent” again). Thank you for all the thought-provoking conversations and for always bringing me back to reality whenever I became overwhelmed. Thank you to Mr. Dave Brown, Dr. Mladen Nedimovic and Dr. Owen Sherwood, the other members of my supervisory committee.

I acknowledge Schlumberger Canada Ltd. for their donation of the Petrel software and to ExxonMobil Canada and the Operators of the Sable Project (SOEP) for providing excellent 3D seismic data to work with. Thank you to Canstrat Ltd. for providing lithological data from well logs. I also thank the Natural Resources Canada and the Canada-Nova Scotia Offshore Petroleum Board for maintaining databases of information important to the success of this study. I also acknowledge the late Mary Jean Verall, Debra Wheeler and the entire staff from the CNSOPB’s Geoscience Research Centre.

I also thank past and present members of the Basin and Reservoir Laboratory, especially Dr. Ricardo Silva for giving me the opportunity to expand upon my interest in carbonate microfacies and for all your guidance throughout the past three years; and Carlos Wong for your endless support and willingness to help. I am also extremely grateful to everyone I have met during my time at Dalhousie University; Rachel, Laura, Natasha, Erin, Bryan, Anne, Trudy, Ken and Trevor. You all have gotten me through the most stressful of days.

I acknowledge my family and friends outside of geology who were so patient, and understanding throughout my master’s studies and gave me constant love and encouragement. Lastly, I acknowledge RJ, for always being there when I needed someone most and for always pushing me to reach the finish line.

Chapter 1: Introduction

1.1 Project Overview

This study focuses on the early post-rift Middle to Late Jurassic section in the Sable sub-basin at Cohasset-Migrant. The Middle Jurassic to Early Cretaceous Abenaki Formation in the Scotian Basin, offshore Nova Scotia (Fig 1.1) was deposited early in the post-rift phase of the opening of the north Atlantic. It comprises a carbonate platform and associated basinal sediments. The Abenaki carbonate bank lies at the northern end of a continental-scale giga-platform that extends south to modern-day carbonates in the Caribbean (Jansa 1981). The Abenaki carbonate bank has been studied extensively by the petroleum industry, academia, and the Geological Survey of Canada (e.g. Eliuk 1978; 2016, Wade & Maclean 1990, Weissenberger et al. 2000, 2006 and Kidston et al. 2005) using data from 127 exploration wells; extensive 3D and 2D seismic surveys (29,512 km² and 400,954 km respectively) and a commercial gas field at Deep Panuke. The platform margin has been studied extensively for commercial reasons, but the connection between the platform margin and associated basinal sediments has received far less attention, due to lack of well penetrations and less direct commercial interest.

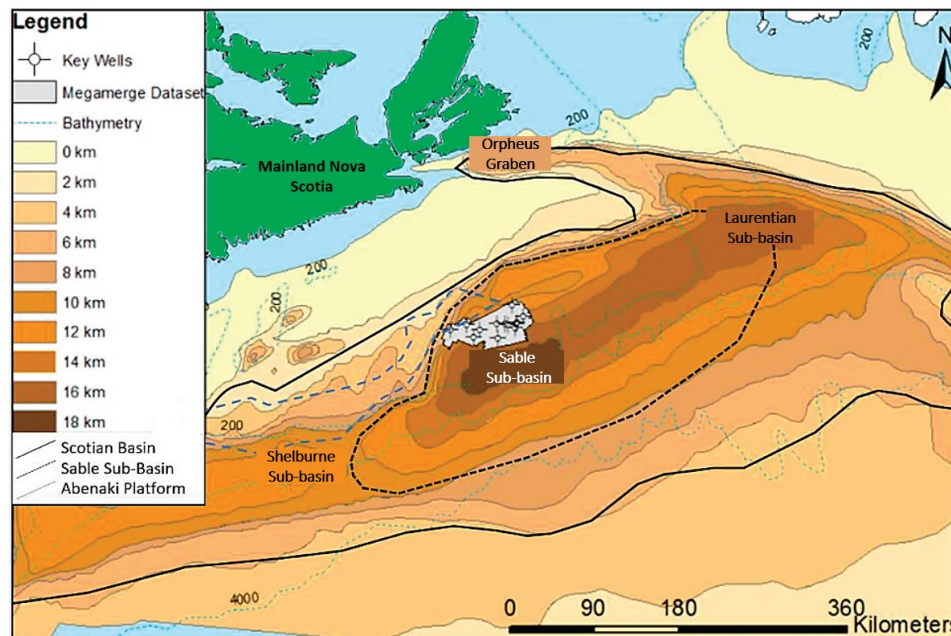


Figure 1.1: Map of the Scotian Basin and associated sub-basins. It also shows the combined thickness of the Mesozoic and Cenozoic sediments; the Sable Sub-basin and MegaMerge dataset area (modified by Wong 2015 from Wade 2000); outlines of the Scotian Basin and Sable Sub-basin are based on Williams et al. 1990 and modified from Morrison 2017.

The Cohasset-Migrant area within the 3D Sable MegaMerge seismic survey can be tied to the Cohasset L-97, Dominion J-14 and Migrant N-20 wells which provides the opportunity to study: i) the stratigraphic architecture of the carbonate platform-basin transition in detail seismically; ii) the possible source-prone intervals; iii) the stratigraphic and structural relationship between the carbonate depositional system and the deltaic depositional system that subsequently overwhelms it.

Eliuk (2016) focused on examining core and cuttings of the Abenaki carbonate bank to establish a depositional setting and stratigraphic framework, inboard of the study area of this thesis. Weissenberger et al. (2000) and Encana (2006) examined and schematically illustrated the platform-basin transition using Panuke M-79, although did not extend the transition basinward at a more regional scale. This study tests the stratigraphic concepts presented by Weissenberger et al. (2000), Encana (2006) and Eliuk (2016) in a basinal setting, using seismic data, calibration of well and cored intervals up dip of the study area, and provides a refined stratigraphic framework for a mixed depositional system. It focuses on depositional architecture and source rock potential (an inferred depositional environment that has potential for deposition and preservation of organic-rich facies) in the transition between two major depositional systems: The Middle-Late Jurassic Abenaki carbonate bank-to-basin system and the Late Jurassic-Early Cretaceous Sable Island Delta. These systems are uniquely imaged by 3D seismic data in the area around the Cohasset L-97 and Migrant N-20 well penetrations. Three well penetrations into the Middle Jurassic in the study area provide calibration of the transition from a carbonate depositional system to a deltaic depositional system: Cohasset L-97 (Mobil et al. 1979) penetrated over 1400 m of tight shallow water carbonates at the seaward margin of the Abenaki bank; Dominion J-14 (Encana-Marauder 2005) penetrated approximately 500 m of tight limestones and basinal mudstones; Migrant N-20 (Mobil 1978) penetrated approximately 1000 m of Jurassic siliciclastics. Stratigraphic relationships between these systems were discussed regionally by Wade and MacLean (1990) by Eliuk and Wach (2008) and Eliuk (2016), but without the benefit of 3D seismic data.

The source rock potential of the Abenaki margin has been inferred by Mukhopadhyay (1990, 1991, 1994) and Kidston et al. (2005), although there is very little well control

outboard of the platform margin, but with sufficient seismic imaging and resolution, it is possible to infer potential source rocks from stratigraphic and structural architecture.

1.2 Motivation

Despite considerable commercial production from the Sable Sub-basin, source rocks of the petroleum system are poorly understood (Silva et al. 2015) and have been the subject of considerable publicly funded research (e.g. Play Fairway Analysis 2011; Central Scotian Slope Play Fairway Analysis 2016). The Abenaki margin has been the location of several hydrocarbon discoveries along the hinge line margin separating the LaHave Platform from the western part of the Sable Sub-basin (Fig. 1.1). The source rock interval is not certain, and an analysis of the condensate from Panuke M-79A (Sassen and Post 2007) revealed that there is a mature liquid confirmed by the low values of aromatic fraction and the high level of diamondoids. The proposed source interval was a shaly and marly limestone. Hydrocarbons are found all along this margin, understanding the relationships between the units and related depositional facies might help in better understanding and predicting the elements and processes of the area's petroleum system.

The study presented here is the second of four recent Sable Sub-basin projects conducted at the Basin and Reservoir Lab at Dalhousie University, that are part of the source rock and geochemistry of the Central Atlantic Margins consortium (e.g. Morrison 2017, Hargreaves *in prep*, Wong *in prep*). A small pilot study by Campbell et al. 2015 established the potential for sequence stratigraphic analysis, seismic facies analysis (amplitude, frequency, geometry and continuity) and 3D acoustic inversion to discriminate carbonate, mixed carbonate and siliciclastics and siliciclastic systems and depositional environments. Following on from this, published depositional models (e.g. Waite, 1997, in Kidston et al. 2005) enable source rock potential to be inferred within the distal mudstones of a carbonate bank, subject to favorable basin morphology, climatic and oceanic conditions. A third-order sequence stratigraphic framework published by Encana (2006) (Weissenberger et al. 2000) at Deep Panuke Field established seven third-order depositional sequences of the Abenaki carbonate bank (Abenaki 1-7). These third-order depositional sequences were extended northward and basinward in this study.

1.3 Hypothesis and objectives

The combination of high quality 3D and 2D seismic data, Jurassic well control and geologic setting, allows the opportunity to address two hypotheses:

1. The 3rd order carbonate sequence stratigraphic framework of the Abenaki carbonate bank established at Deep Panuke (Weissenberger et al. 2000 and Encana 2006) can be extended southeastward into the 3D Sable MegaMerge area.

2D seismic data and well penetrations on the continental shelf margin that provide up dip calibration for this stratigraphic interval.

2. Low impedance calcareous shales (potential source rocks) can be interpreted down dip of the Abenaki carbonate bank and provides evidence for outer neritic to bathyal depositional conditions.

Inferred depositional environments in this area from published depositional models indicate that these shales may have been deposited at a time of high organic productivity and subsequent preservation by being compared to analog studies.

Objectives of this study are:

1. Investigate structural, stratigraphic and depositional relationships between the two different depositional systems;
2. Interpret the interplay of the growth and cessation of the carbonates of the Abenaki Formation as a result of the influx of siliciclastics from the Sable Delta in the north;
3. Investigate the source rock potential of Middle Jurassic basinal mudstones (Verrill Canyon Formation) that preceded the deltaic influx;
4. Determine why the Abenaki carbonate bank transitions from a steeply dipping ramp ($\sim 30^\circ$) to a gently dipping slope ($\sim 10^\circ$) in the 10 km north of the Cohasset L-97 well.

1.4 Thesis organization

Chapter 1 reviews the motivation for the study, background, the hypotheses and the objectives of the study. The geological background and the evolution of the Scotian Basin in comparison to the Lusitanian Basin and the Moroccan Margin, an introduction to the

study area and our definition of what classifies a source rock is presented in Chapter 2. The datasets and the workflow for this study, including the seismic interpretation software which lead to a geocellular model are in Chapter 3. The geocellular model was populated with properties (primarily lithologies) to interpret paleo-water depths, environments of deposition, and inferred source rock potential. This section also introduces the methods and presents information on seismic interpretation (2D and 3D), seismic stratigraphy, and the seismic attributes that were used to interpret depositional environments and source rock potential of the third-order depositional sequences of the Abenaki carbonate bank. Chapter 3 also describes the well logs and petrophysics that were used for this study. Chapter 4 is the results of this study, including analyses of core, seismic interpretation; geocellular and depositional modeling. Chapter 5 discusses the implications of the results in terms of depositional systems, depositional environments and source rock potential. Chapter 6 provides the conclusions and recommendations for future work. The appendices contain background information on seismic acquisition and processing, wireline logs, geological background of the Lusitanian Basin and the Moroccan Margin. The appendices also contain full core descriptions and seismic traverses that are discussed in Chapter 5.

Chapter 2: Geological Background

2.1 Introduction

This chapter describes the tectonic history and stratigraphy of the Scotian Basin in comparison to the Moroccan Margin (conjugate to the Scotian Margin) and the Lusitanian Basin, onshore Portugal (where field work was conducted for this study). This is done by a comparison of stratigraphic charts of all margins and using paleogeographic maps constructed by Sibuet et al. (2011) (Figs. 2.5-2.8). Both the Moroccan Margin and the Lusitanian Basin have stratigraphic similarities to the Scotian Basin from Middle Triassic to Late Jurassic due to the opening of the Atlantic at that time. They are examined here to understand if the depositional environments that lead to prospective source rock intervals within the Jurassic in Morocco and the Lusitanian Basin, are also present within the similar time interval in the Scotian Basin, which is discussed in Chapter 5. Chapter 2 discusses the geology of the study area that can be seen on the 2D and 3D seismic. This chapter also introduces background information on the formation of interest for this study (Abenaki Formation) and on what classifies a source rock.

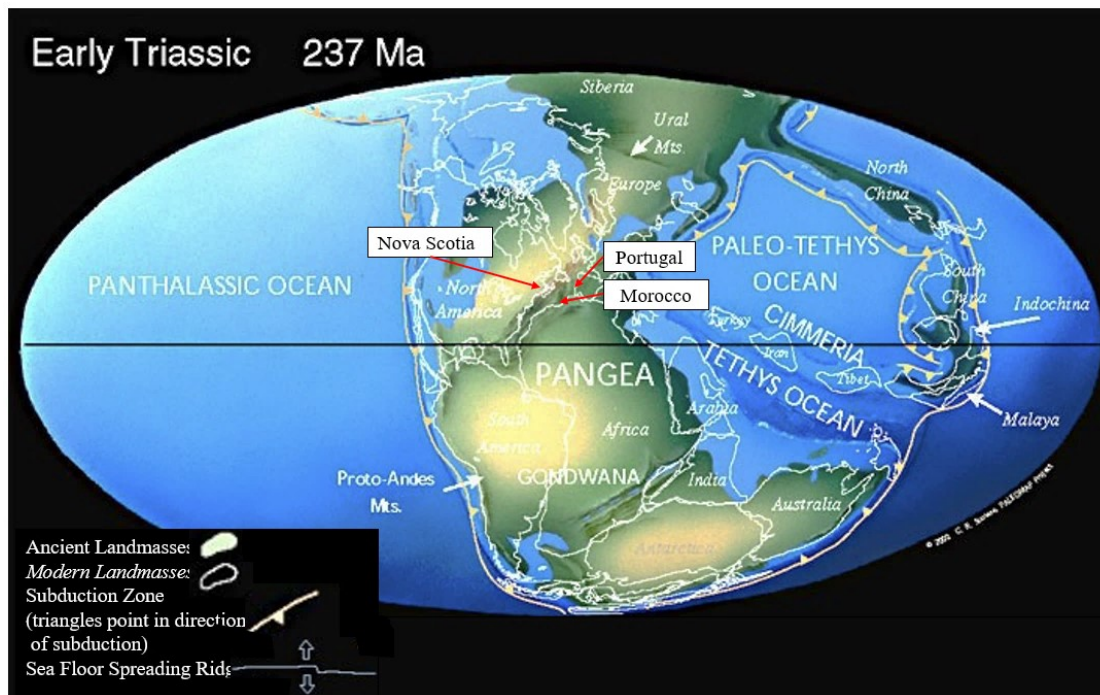


Figure 2.1: *Paleo-reconstruction map of the Early Triassic (237 Ma). Figure shows the location of the ancient landmasses (green) and the modern outline of the landmasses (white). The Scotian Margin and the Moroccan Margin are conjugate margins, whereas*

the Lusitanian Basin in Portugal to the north is conjugate to the Grand Banks of Newfoundland (although it experienced similar depositional environments to that of Nova Scotia and Morocco from the Early Triassic to Middle Jurassic) (modified from Scotese 2001).

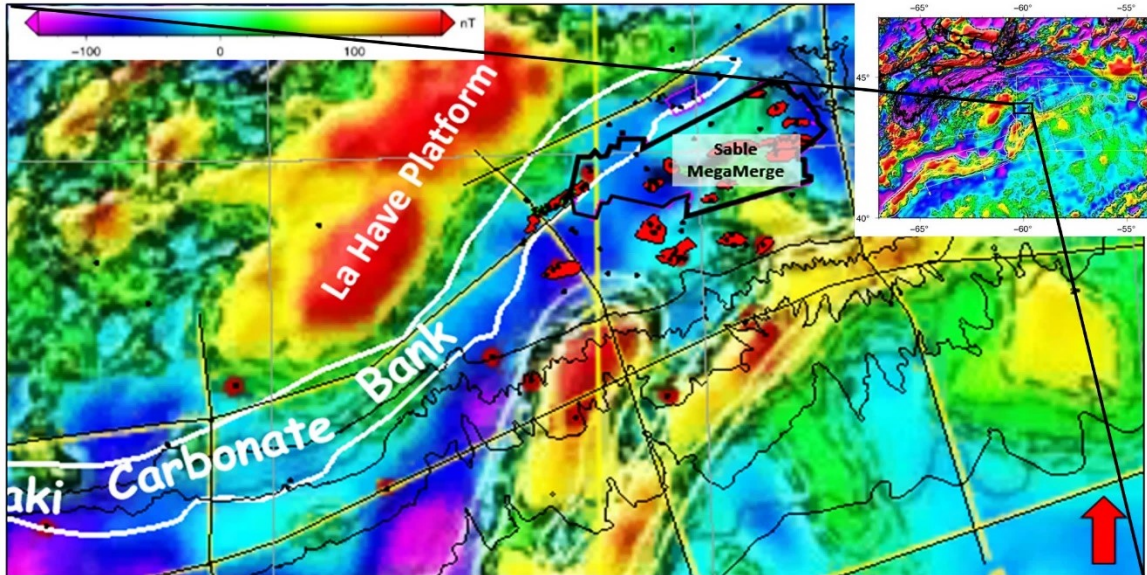


Figure 2.2: Updated magnetic anomalies map along the Scotian margin, overlain with an outline of the approximate boundaries of the Abenaki carbonate bank (white) and the outline of the Sable MegaMerge (black) showing how the Abenaki carbonate bank (white) developed on the basement hinge zone (modified from Verhoef et al. 1996 and Dehler, 2010). Inset map in top right corner of approximate location.

2.2 Stratigraphic charts and maps

Figures 2.3 and 2.4 are simplified lithostratigraphic charts of the Scotian Basin, Central Atlantic Morocco, and the Lusitanian Basin. The stratigraphic chart of Central Atlantic Morocco (Tari et al. 2012) is compared to the stratigraphic chart of the Scotian Basin (Wade and MacLean 1990; modified by Tari et al. 2012) in Figure 2.3. In Figure 2.4, the stratigraphic chart of the Lusitanian Basin (Pereira 2013, modified by Wach et al. 2002) is compared to that of the Scotia Basin. The potential source rock intervals and main tectonic events have been added to both Figure 2.3 and 2.4. These figures will be used within this chapter to compare the stratigraphy and petroleum systems of the margins.

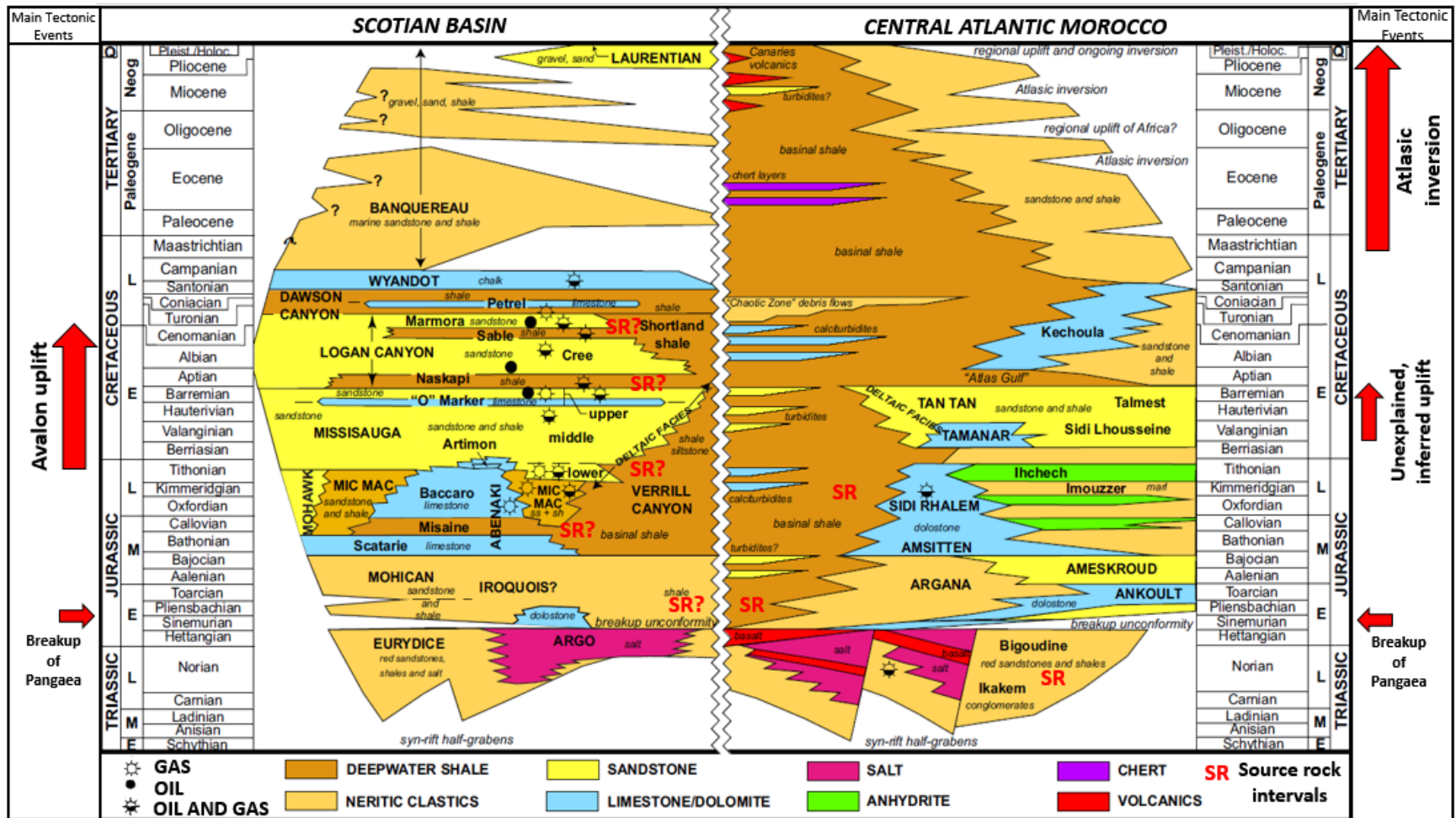


Figure 2.3: Simplified lithostratigraphic charts of the conjugate margins of offshore Nova Scotia and Atlantic Morocco (Central Nova Scotia chart modified from Wade and MacLean 1990 by Tari et al. 2012). The Triassic within the Scotian Basin has been modified from the original figure in Tari et al. 2012 based on Weston et al. 2012. Central Atlantic Morocco chart modified from Tari and Molnar 2005, in Tari et al. 2012).

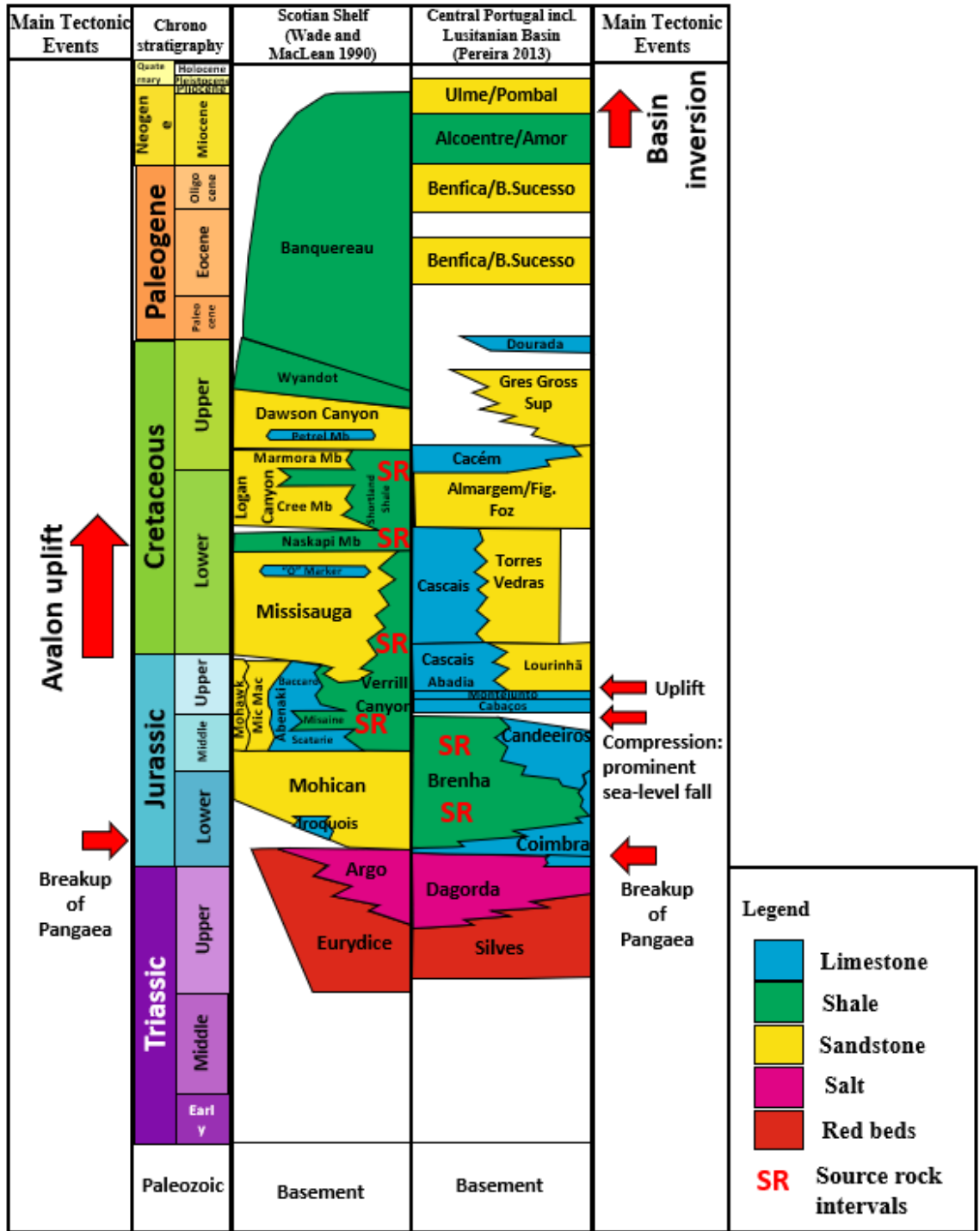


Figure 2.4: Simplified lithostratigraphic charts of the Scotian shelf (modified from Wade and MacLean 1990) and the Lusitanian Basin (modified from Wach et al. 2014, from Azerêdo 2003, Rey 2006).

Figures 2.5 - 2.8 are paleogeographic maps of the Early Jurassic (Sinemurian 190 Ma), Middle Jurassic (middle Bajocian, 170 Ma), Late Jurassic (Tithonian, 150 Ma), and the

Early Cretaceous (Valanginian, 136 Ma), all created by Sibuet et al. 2011 with formation names annotated for this study. These maps will be referenced within in chapter to compare the depositional environments at each margin.

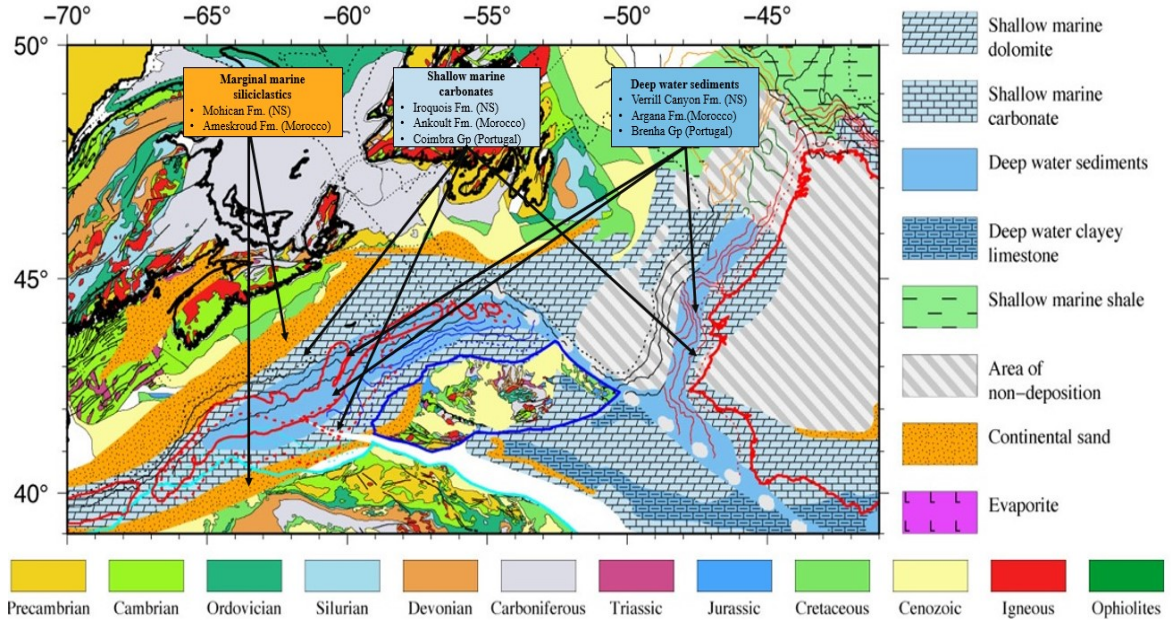


Figure 2.5: Paleogeographic map of the Early Jurassic (Sinemurian – Toarcian) end Sinemurian 190 Ma. Modified from Sibuet et al. 2011 with annotated formation names.

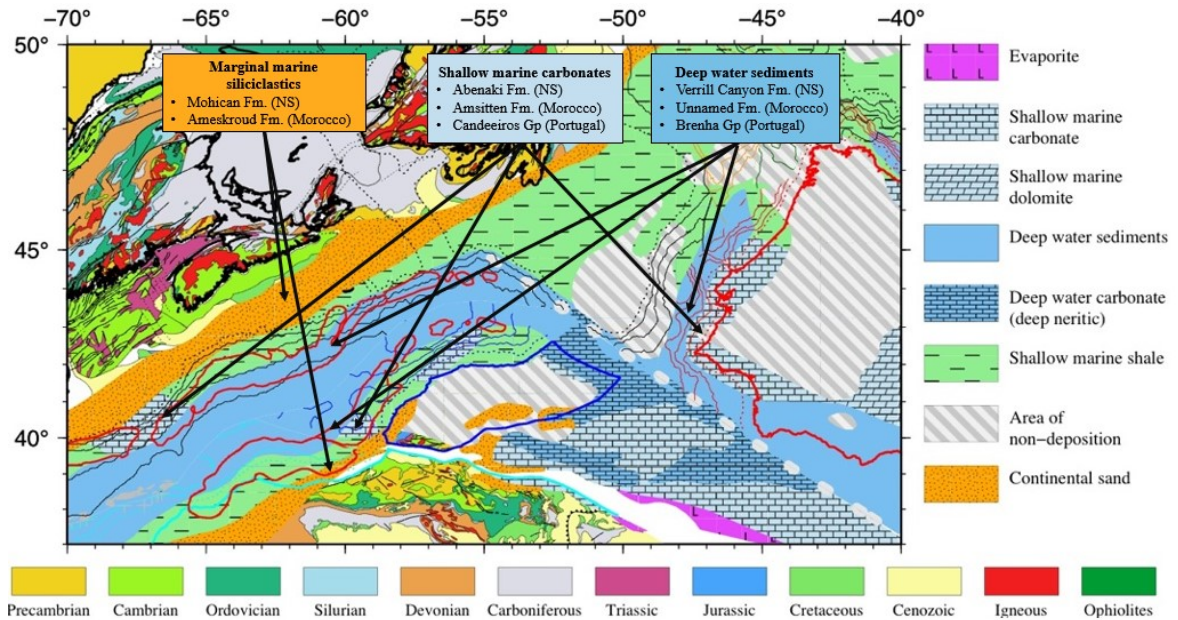


Figure 2.6: Paleogeographic map of the Middle Jurassic at Middle Bajocian, 170 Ma. Map modified from Sibuet et al. 2011 with annotated formation names for the Scotian and Moroccan margins and the Lusitanian Basin.

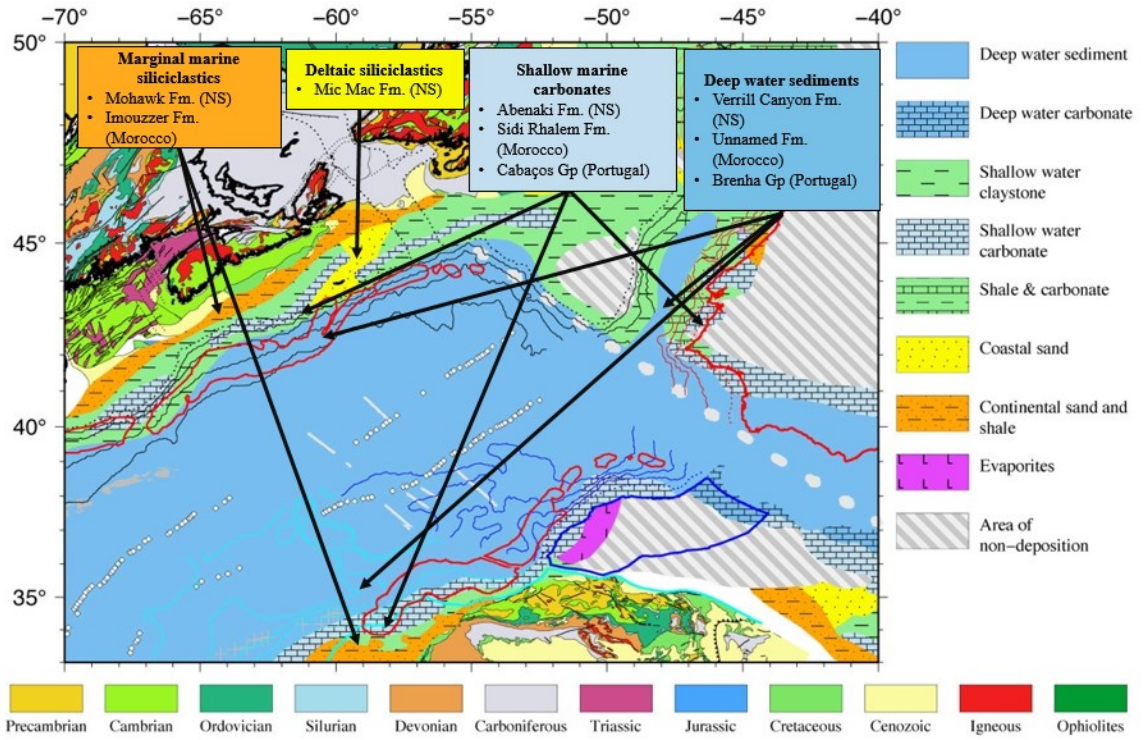


Figure 2.7: Paleogeographic map at Late Jurassic, Tithonian 150 Ma. Map modified from Sibuet et al. 2011 with annotated formation names for the Scotian and Moroccan margins and the Lusitanian Basin.

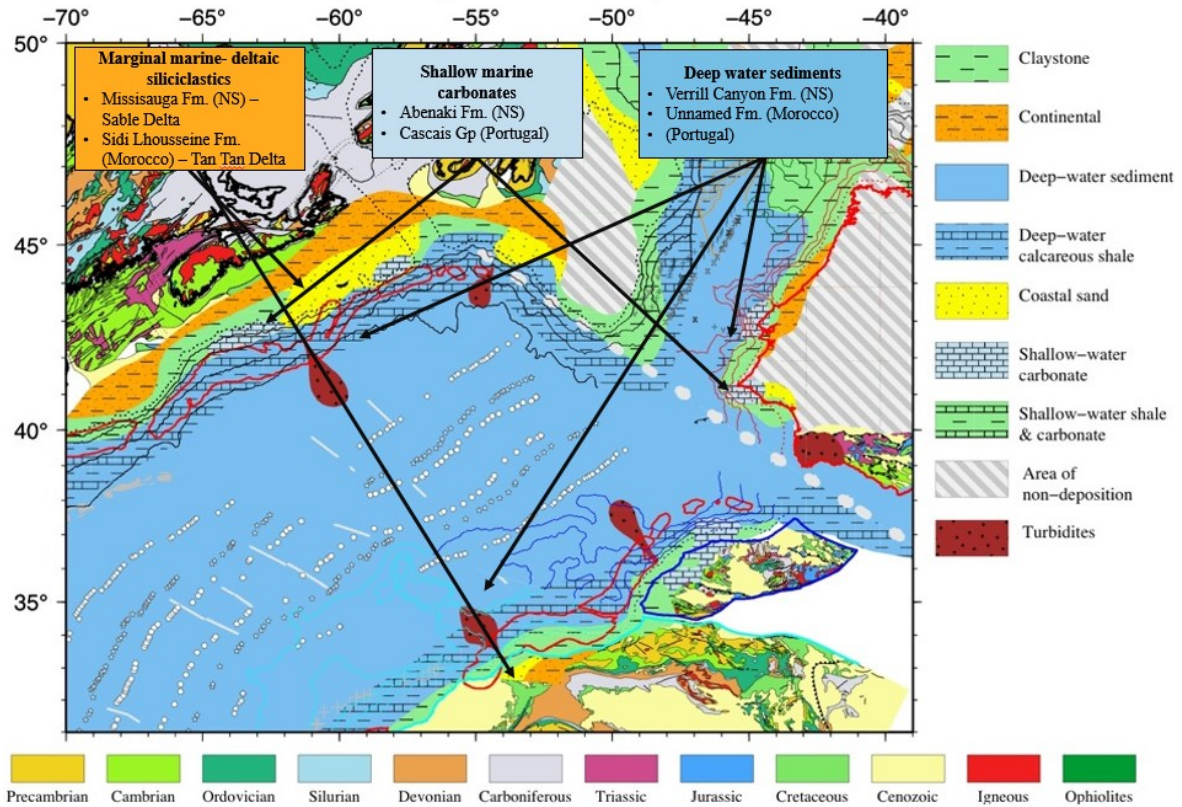


Figure 2.8: *Paleogeographic map of the Early Cretaceous (Berriasian-Barremian) at Valanginian, 136 Ma. Map modified from Sibuet et al. 2011 with annotated formation names for the Scotian and Moroccan margins and the Lusitanian Basin.*

2.3 Scotian Basin

The Scotian Basin is part of the Mesozoic to Quaternary passive margin along the length of offshore Nova Scotia extending 1200 km from the Yarmouth Arch/ United States border in the southwest to the Avalon Uplift on the Grand Banks of Newfoundland in the northeast. The total area of the basin is approximately 300,000 km², with half the basin on the present-day continental shelf in water depths less than 200 m and the other half on the continental slope, in water depths from 200 to 4000 m (Kidston et al. 2005) (Fig. 1.1). The Scotian Basin has several sub-basins, which are interconnected depocenters resulting from rifting and subsequent formation of the North Atlantic. From southwest to northeast, they are the Shelburne Sub-basin, Sable Sub-basin, Abenaki Sub-basin, Laurentian Sub-basin, and South Whale Sub-basin (Wade and MacLean 1990).

Deposition in the Scotian Basin began in the Middle Triassic during the break-up of Pangaea when the North American plate began to rift from the African plate (e.g. Wade

and MacLean 1990; Wade et al. 1995). At that time, the Scotian Basin was located near the centre of Pangea, accumulating continental sediments in a hot and arid environment (Fig. 2.1).

2.3.1 Geological Background of the Scotian Basin

Pre-rift (Early-mid Triassic)

Tensional forces in the Early Triassic created northeast-trending troughs on the eastern side of the Appalachian Mountains before seafloor spreading began in the Early Jurassic (Albertz et al. 2010). Red beds, dolomite and halite were the dominant deposits within the Scotian Basin during the late pre-rift phase, depositing in rift valleys that formed before the break-up of the continental mass (e.g. Given 1977; Wade and MacLean 1990; CNSOPB 2008).

Syn-rift (Late Triassic-Early Jurassic)

During this syn-rift phase of opening of the North Atlantic, grabens and half grabens developed progressively from the Middle to Late Triassic. This structuring is shown schematically on the Moroccan and Scotian margins stratigraphic chart (Fig.2.3) but is not illustrated on the Lusitanian Basin stratigraphic chart (Fig. 2.4). Progressive breaching of topographic barriers allowed marine waters from the eastern Tethys paleo-ocean to flood the interconnected syn-rift basins in each of these areas (e.g. Wade and MacLean 1990; Wade et al. 1995; Olsen et al. 2000, 2003; Shimeld 2004).

On the Scotian margin, terrestrial, and restricted shallow marine conditions, arid climate, and varying subsidence resulted in deposition of mixed clastics, minor carbonates and minor evaporites in the upper part of the Eurydice Formation, coeval with deposition of massive salt and anhydrite beds of the Argo Formation (Wade and MacLean 1990) (Fig. 2.3).

Early-Middle Jurassic post-rift (Sinemurian - Bajocian)

After the break-up of the Scotian and Moroccan margins, a shallow marine sea flooded the Scotian Basin resulting in the deposition of carbonates, dolomites and clastics of the Iroquois Formation (Fig. 2.3 and Fig 2.5). The Iroquois Formation transitions laterally and

upwards into terrestrial and marine siliciclastics of the Mohican Formation and distal shales (unnamed in Fig. 2.3).

Middle – Late Jurassic post-rift

Over much of the Scotian Basin, a prograding wedge of Middle and Late Jurassic clastics (Mohawk and Mic Mac formations), carbonates (Abenaki Formation) and basinal shales (Verrill Canyon Formation) overlies the Mohican Formation (Figs. 2.3 and 2.7), forming a mixed siliciclastic-carbonate system. This arrangement of proximal siliciclastics transitioning to a large-scale shelf-edge carbonate system, to basinal shale (on both the Scotian and Moroccan margins) is the sedimentary response to progressive opening of the Atlantic Ocean followed by thermal subsidence of each margin.

On the Scotian Margin, a basement controlled structural hinge line (Fig. 2.2) between the LaHave Platform and the Sable Sub-basin controls the seaward limit of shallow marine carbonates of the Abenaki Formation (Fig. 2.3.) (e.g. Eliuk 1978; Wade and MacLean 1990; Wade 2000; Kidston et al. 2005).

The development of the Abenaki carbonate bank began with deposition of the Scatarie Member of the Abenaki Formation, as a broad carbonate ramp comprising outer-ramp fossil wackestone to packstones and inner-ramp oolitic and oncolitic facies (Weissenberger et al. 2000). The Scatarie Member has been interpreted to be subsequently transgressed in the Callovian with deposition of the Misaine Member, which comprises dark grey, slightly calcareous shale with minor interbeds of siltstones and very fine sandstone (Wade and MacLean 1990). From the Middle to end of Jurassic, the Baccaro Member of the Abenaki Formation developed in carbonate reef and peri-reefal environments with a predominant aggrading pattern, organized into a series of third-order depositional sequences. The developing Baccaro carbonate member was in competition with an influx of clastic sediments and mixed siliciclastic-carbonate settings developed towards the northeast (Sable Delta complex) (Wade and MacLean 1990).

The landward equivalents to the Abenaki Formation include the Mohawk (feldspathic sandstones and siltstones with interbedded shale and limestones), and Mic Mac (sandstones, siltstones and shales) formations (McIver 1972). All formations grade

basinward into the shales of the Verrill Canyon Formation (distal shales and mudstones). These formations are defined lithostratigraphically.

Cretaceous post-rift

The Verrill Canyon Formation extends from Callovian to Barremian (Fig. 2.3). In the Cretaceous it interfingers with the overlying Missisauga Formation (Fig. 2.8), formed by a series of transgressive and regressive episodes. The contact between the Mic Mac and Missisauga formations is generally conformable (Wade and MacLean 1990). The sands of the Missisauga Formation were deposited by the paleo-St Lawrence River into a variety of transitioning environments, from fluvial-deltaic to shallow marine (Cummings et al. 2005). The Lower Member of the Missisauga Formation consists of sandstone and thin limestones. Sediments in the lower member were transported via local distributary systems to small clastic fans or active fault zones. Fluvio-deltaic sedimentation continued into the Early Cretaceous, depositing the Middle and Upper members of the Missisauga Formation. In the upper part of the Missisauga Formation, the “O” Marker was deposited as a series of thin oolitic to skeletal and sandy limestone beds of Hauterivian to Barremian age (Fig. 2.3) (Wade and MacLean 1990).

Deltaic sedimentation continued throughout the Aptian-Cenomanian, depositing the Logan Canyon Formation, sub-divided into four members, two of which are shale dominated: the Naskapi and Sable members (Jansa and Wade 1975). Transgression continued with deposition of the Dawson Canyon Formation, dominated by marine shale and culminated in the Late Cretaceous with the deposition of the Wyandot Formation (Fig. 2.3) chalk.

Cenozoic post-rift

Cenozoic sediments above the Wyandot Formation in the Scotian Basin comprise the Banquereau Formation, deposited as a progradational system of mudstones, marls and sandstones (McIver 1972). The Banquereau Formation is overlain by the Quaternary Laurentian Formation, which comprises glacial drift and stratified proglacial material (Jansa and Wade 1975) (Fig. 2.3).

2.4 Comparison of the Scotian and Moroccan Margins and the Lusitanian Basin

A detailed description on the geological background of the Moroccan Margin and Lusitanian Basin can be found in Appendix A.

Comparing the stratigraphic charts of the Scotian Basin, Moroccan Margin and the Lusitanian Basin, it is evident that similar depositional processes were taking place on all three margins from the Late Triassic to Early Cretaceous. All three margins developed grabens and half grabens during syn-rifting from the Middle to Late Triassic that were flooded with marine waters from the Tethys paleo-ocean. Terrestrial, and restricted shallow marine conditions deposited syn-rift red beds and salt on all three margins in the Late Triassic (Eurydice and Argo Formation within the Scotian Basin (Fig.2.3); Ikakem and Bigoudine formations on the Moroccan Margin (Fig. 2.3) (Tixeront 1973; Brown 1980); and Silves Group and Dagorda Formation within the Lusitanian Basin (Fig. 2.4) (Wilson et al. 1989).

From the Early to Middle Jurassic on all three margins there was deposition of marginal marine clastics prograding into carbonates and transitioning basinward into distal shales (Mohican and Iroquois formations within the Scotian Basin (Fig. 2.3); Ankoult, Argana and Ameskrout formations on the Moroccan Margin (Figs. 2.3 and 2.5); Coimbra and Brenha groups within the Lusitanian Basin (Figs 2.3 and 2.5)).

From the Middle to Late Jurassic on the Scotian and Moroccan margins, another basinward transitioning facies progression of clastics to carbonates to distal shales was deposited (Mohawk, Mic Mic, Abenaki and Verrill Canyon formations within the Scotian Basin (Figs. 2.3 and 2.6); Imouzzer and Amsitten formations and unnamed shales of Morocco on Figure 2.3 (e.g. Brown 1980; Jansa and Weidmann 1982; Broughton and Trepaniér 1993; Davison 2005). Within the Lusitanian Basin, there is considerably fewer siliciclastics as compared to the other two margins, due to inferred sediment starvation. Carbonates were deposited until the late Oxfordian (Montejunto Formation, Fig. 2.4). An abrupt rise in relative sea-level, accompanied by uplift of margin basement highs generated an influx of siliciclastics (Abadia Formation, Fig. 2.4) (Ellis et al. 1990) and continued into the Tithonian (Lourinhã Formation) (Pena dos Reis and Pimental 2010). The uplift may have been a result of thermal expansion of the upper crust due to rapid crustal thinning produced by the preceding stretching episode, it also could have been a result of a rapid eustatic sea-level drop (Ellis et al. 1990).

The depositional systems differ between the Scotian and Moroccan margins within the Cretaceous. The Avalon uplift on the Scotian Margin (Fig. 2.3) is a Late Jurassic rift flank uplift, associated with the initiation of seafloor spreading between the Grand Banks and Western Europe (Iberia) (Wade and MacLean 1990). As consequence of the Avalon uplift, a large influx of siliciclastics were deposited Early-Middle Cretaceous, designated as the Missisauga Formation. Deposition of carbonates of the Abenaki Formation ceased in the Early Cretaceous as they could not keep up with sea-levelrise. On the Moroccan Margin, the Atlantic orogeny during the latest Cretaceous and Tertiary allowed deposition of siliciclastic sediments to continue (Louden et al. 2013) (Fig. 2.8).

2.5 Study area

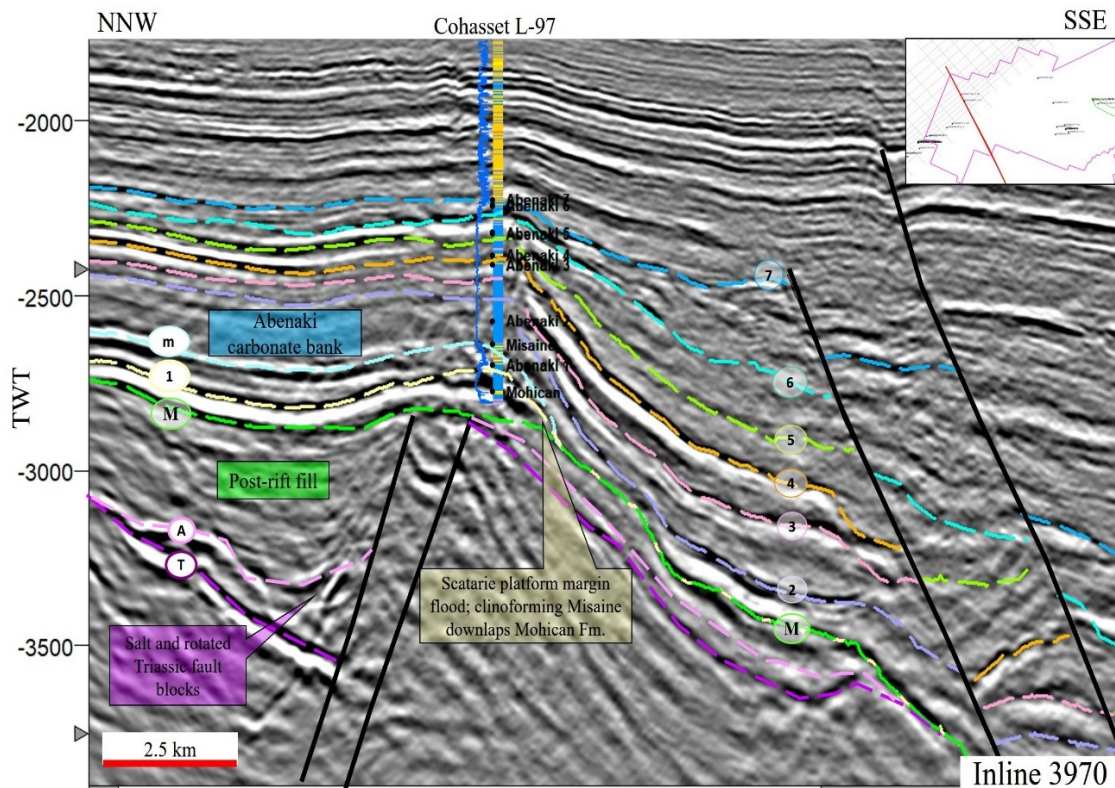


Figure 2.9: Seismic inline 3970 from the 3-D Sable MegaMerge dataset. Yellow horizon (1) to blue horizon (7) interval contain the interpreted seven third-order sequences Abenaki 1-7, deposited over approximately 20 million years, e.g. Weissenberger et al. 2000. Abenaki 4 (orange) is the most regressive of these sequences and can be mapped distally. These limestone seismic markers can be mapped confidently basin wards. Third-order sequences are labelled 1-7, the top of the Misaine Member is marked as “m” the top of the Triassic is marked by Tm the top of the Argo salt is marked by A, and the top of the Mohican is marked by M.

The study area is identified in Figure 1.1, situated within the Sable Sub-basin. Key seismic lines from this study illustrates the horizons correlated throughout the western area of the Sable MegaMerge (and beyond via 2D and 3D composite lines). Figure 2.9 illustrates the syn-rift and post-rift sections described above and the geometry of the carbonate bank to basin transition above the basement hinge line (LaHave Platform to Sable Sub-basin). The colored lines represent interpreted seismic horizons from the base of the Triassic salt to the top of Abenaki Formation. For this study, only the study interval (Middle Triassic to Early Cretaceous) was interpreted using seismic.

Figure 2.9 shows the Middle Triassic half-grabens within the Sable Sub-basin as rotated fault blocks (outlined in dark purple) which were then infilled by Argo salt (light purple). The top of the Mohican Formation is marked by an angular unconformity (green seismic horizon, Fig. 2.9), interpreted to be attributable to salt movement within the half grabens within the project study area, and does not represent the break-up unconformity. Regionally, the Mohican Formation overlies the break-up unconformity (Wade and MacLean 1990). The top of the Mohican Formation was easy to correlate throughout the seismic where the Scatarie Member of the Abenaki Formation (as seen in Fig. 2.9) is a well developed, high acoustic impedance limestone at the base of the Abenaki bank. The top of the Mohican Formation became difficult to correlate basinward, due to less of an acoustic impedance contrast between basinal mudstones of the Verrill Canyon Formation and clastics of the Mohican Formation. The Abenaki carbonate bank developed on the post-rift fill of the Mohican Formation until the Early Cretaceous (Fig. 2.9, pale yellow horizon to blue horizon). A series of major synsedimentary normal faults can be correlated within the study area bounding an expansion trend (e.g. Pe-Piper and Piper, 2011), which developed as consequence of sediment loading and movement of salt substrate and post-date the Abenaki carbonate bank.

2.5.1 Abenaki Formation

The focus of this study is on the Abenaki Formation from the Middle Jurassic to Early Cretaceous. Within the Middle Jurassic, the widening of the Atlantic Ocean allowed carbonate development to occur along a passive margin with the Scatarie Member of the Abenaki Formation, being drowned by the transgressive event during the Callovian

(Misaine Member). From the Middle to end of Jurassic, the Baccaro Member of the Abenaki Formation developed as a carbonate reef and peri-reefal environments with a predominant aggrading pattern, organized into a series of third-order depositional sequences. The developing Baccaro carbonate member was in competition with an influx of clastic sediments and mixed siliciclastic-carbonate settings developed towards the northeast (Sable Delta complex) (Wade and MacLean 1990).

The carbonate platform can be subdivided into two second-order depositional sequences, approximately 30 and 50 Ma respectively (e.g. Weissenberger et al. 2000; Encana 2006). The older sequence comprises the Argo/Eurydice, Iroquois and Mohican formations, extending from the Hettangian to the Aalenian. The sequence varies between hundreds and some places over a thousand metres thick, depending on the local accommodation space. The younger, second-order sequence comprises a part of the Mohican Formation, the Abenaki and Mic Mac formations. The Misaine Member of the Abenaki Formation represents the time of maximum flooding of this sequence. In the Cohasset area, the sequence is more than 1000 m thick, reflecting a time of high accommodation (Weissenberger et al. 2006). There are currently no defined formal third-order sequences in the older of the second-order sequence. The younger second-order sequence consists of seven third-order depositional sequences (Fig. 3.6). Weissenberger et al. (2000) and Encana (2006) interpreted the seven third-order depositional sequences on the carbonate bank. Using the depositional model proposed by Encana (2006), this study interprets the depositional sequences basinward to understand how these carbonate sequences interacted with the deposition of the Sable Delta and if there is potential for organic matter deposition in the distal facies of the carbonate bank.

Each third-order depositional sequence comprises a facies transition from proximal and distal siliciclastics that transition to the shelf margin carbonates (Fig. 3.7) (e.g. Weissenberger et al. 2000; Kidston et al. 2005; Wierzbicki et al. 2006; Eliuk 2016). The platform limestones of the Scatarie Member are defined as Abenaki 1. The base of this sequence overlies clastics of the upper part of the Mohican Formation. The overlying Misaine Member and the lowermost limestones of the Baccaro Member are characterized as Abenaki 2. This sequence has a poorly developed lowstand and can only be seen as

thin sands and silts at the base of the Misaine Member. Abenaki 3, 4 and 5 make up much of the Baccaro Member (Weissenberger et al. 2000). The cycles record several shallowing upwards successions of progradation and aggradation of the Abenaki platform margin during the Late Jurassic (Harvey and Macdonald 2013). Abenaki 6 and 7 show successions of progradation and aggradation on the carbonate platform until the early Berriasian.

The distinction of second, third and fourth order cycles for the model proposed by Weissenberger et al. (2000) and Encana (2006) is described in Section 3.4.1.

2.6 Source Rocks

Organic matter (OM) originates from photosynthesis by autotrophic organisms. The four factors that control and influence the production, accumulation and preservation of sedimentary OM are: biological, physical, chemical and geological.

Source rocks are the fundamental element in a petroleum system, and a key risk factor in many basins around the world. Source rocks are fine-grained sediments rich in organic matter (generally >2% Total Organic Carbon (TOC)), that when sufficiently heated (>60°C), will expel hydrocarbons via biogenic or thermogenic processes (Tissot and Welte 1984). Source rocks can develop in various sedimentary environments such as deep marine, deltaic, and lacustrine (e.g. Suárez-Ruiz et al. 2012). A source rock can be classified as oil-prone or gas-prone depending on the type of kerogen (insoluble sedimentary organic matter) it contains (Tissot and Welte 1984). It is necessary to define the origin, history and geochemistry of the organic-rich material within these source rocks and analyze their properties to determine the potential products that were or can be thermally generated (Suárez-Ruiz et al. 2012). Source rocks can be classified by four major categories: potential: contains organic matter (OM) in sufficient quantity to generate and expel hydrocarbons when subjected to adequate thermal maturation; effective: efficiently generating and/or expelling hydrocarbons; relic: a once effective source, that now has ceased generation and expulsion of hydrocarbons due to thermal cooling before exhaustion of its organic matter; and spent: an over mature source rock. The organic matter in the rock is divided into either kerogen (dispersed OM of ancient sediments insoluble in the usual organic solvents (Forsman and Hunt 1958) or bitumen (low molecular weight and soluble in organic solvents) (e.g. Suárez-Ruiz et al. 2012; Tissot and Welte 1984). The properties

of source rocks must be characterized by the amount of organic matter in the rock, quality and type of organic matter and maturity.

Figure 2.10 shows approximate water depths for depositional environments in a continental margin setting. This model is used during this study to approximate water depths in which the depositional sequences of the Abenaki carbonate bank were deposited in conjunction with Figure 3.8 to aid in determining if the potential organic-rich shales were deposited in sufficient water depths to have formed a successful source rock interval.

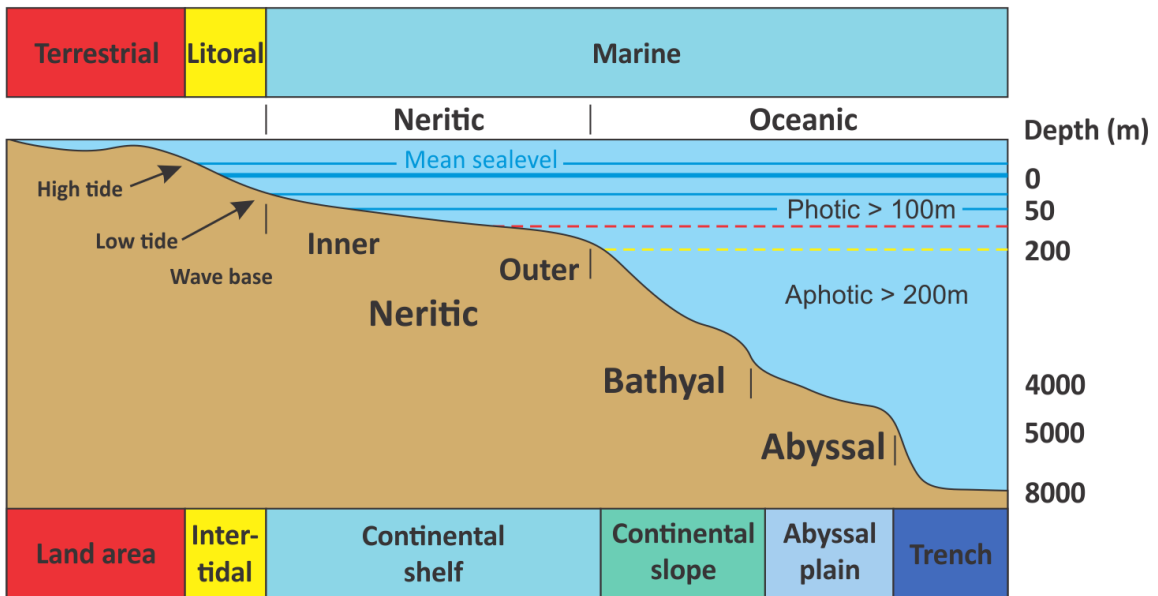


Figure 2.10: Zonation depositional environments for a continental margin setting (modified from Veeken et al. 2013).

Kerogen classifications

Kerogen can be classified into four separate types, type I to type IV. Type I has the highest hydrogen to carbon (H/C) and oxygen to carbon (O/C) ratios and type IV the least. The pseudo-Van Krevelen diagram is commonly used with RockEval pyrolysis oxygen index (OI= mg HC/g TOC), plotted against hydrogen index (HI= mg HC/g TOC). These ratios approximate the H/C and O/C elemental ratios. Van Krevelen (1993) noticed a relationship between kerogen type and the environment in which it was deposited. Type I is oil-prone and is typically linked with lacustrine depositional environments with algal dominance. Type II is both oil- and gas-prone and is associated with an open marine source with plankton preserved in sediment. Type III has a potential for only gas and is linked with a

terrestrial environment with abundant plant matter and could be deposited in a proximal to shoreline environment. Finally, type IV contains mostly decomposed organic matter that has already been oxidized or carbonized and has no hydrocarbon potential (Tissot and Welte 1984).

Chapter 3: Methods

3.1 Introduction

This chapter outlines the datasets (seismic and wells), project workflow, and techniques and methods. The methods are described in the order they were completed, beginning with geological interpretation methods including the understanding of depositional models (carbonate and siliciclastic), and the use of core and microfacies analysis. Petrophysical methods and the use of wireline logs are explained. Methods of tying well logs to seismic data, seismic interpretation (seismic facies analysis, and seismic stratigraphy) and the construction of a geocellular framework and model, all using 2D and 3D seismic data are described. The results of the geocellular framework and model are shown in Chapter 4 and discussed in Chapter 5.

3.2 Project workflow

The workflow of this study is outlined in Figure 3.1 and began with research of the Scotian Margin, modern analogs, depositional models and of the techniques and methods that were used throughout the study. Core analysis from specific wells within the study area, that reached the Middle-Late Jurassic of the Abenaki Formation, was then performed, as well as microfacies analysis from the cored intervals that had thin sections to determine the lithofacies present. Field work was then done in Eastern and Central Portugal to analyse and compare ancient analogs to the Scotian Basin during a similar time interval. The majority of analysis for this study (as outlined in Figure 3.1) was done in Petrel, an integrated suite of software that enables: well log correlations, seismic inversion and attribute analysis, 3D geocellular modelling and visualisation, and time to depth conversion.

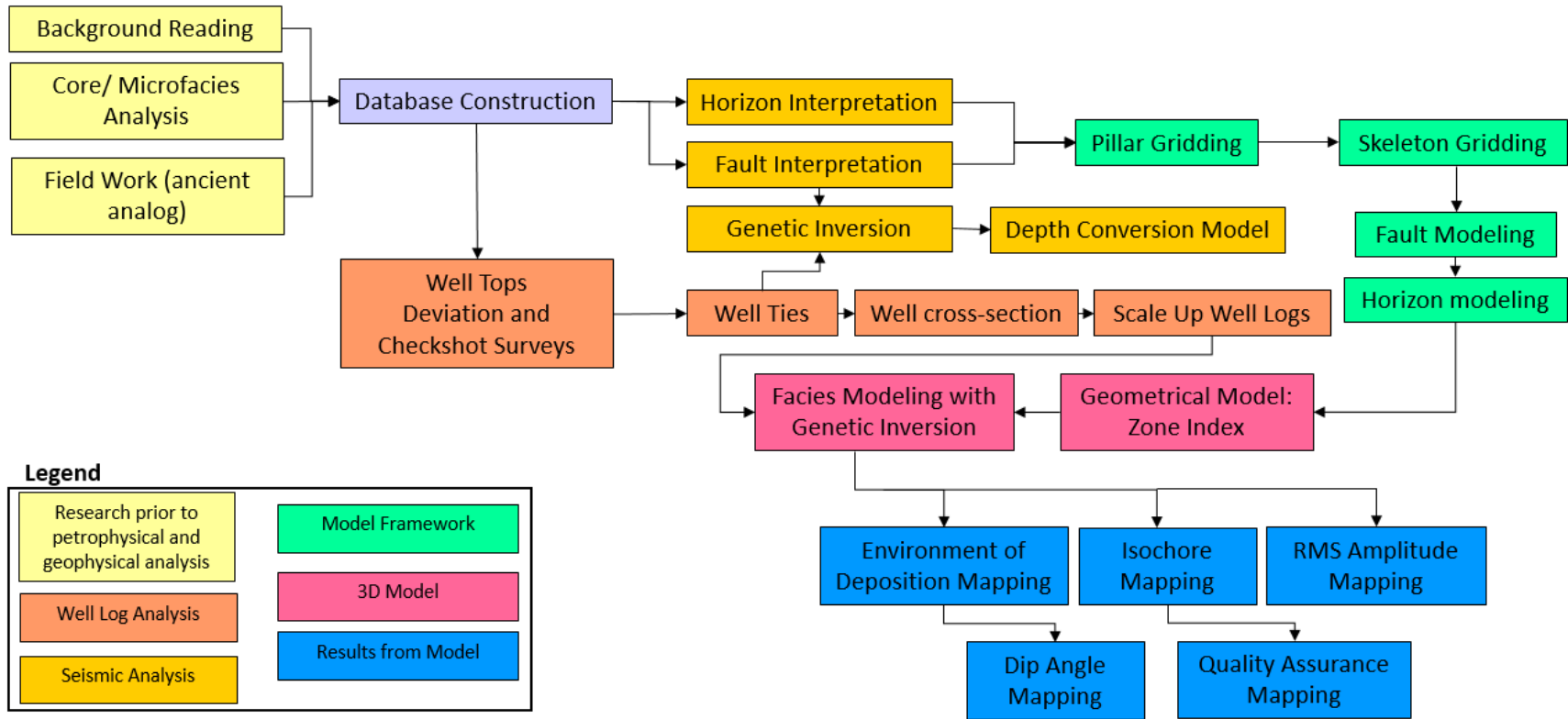


Figure 3.1: Project workflow outlining the integration of well logs and seismic to perform a depositional system analysis of the Middle Jurassic to Early Cretaceous interval. Much of the model framework, 3D Model, and results from the model are discussed in Chapters 4 and 5. The colors of the boxes within the legend correspond to the type of work performed within the workflow.

3.3 Datasets

Three seismic datasets were used for this study, one 3D seismic survey and two 2D seismic datasets. The thirteen key wells and their associated well logs, located across the study area are listed below.

3D MegaMerge

The 3D seismic used for this study is the Sable MegaMerge, courtesy of ExxonMobil, operator of SOEP and made available to Professor Grant Wach, principal investigator, Dalhousie University. The MegaMerge is a poststack merge of seven 3D seismic surveys acquired in the Scotian Basin from 1996 to 1999 (Fig. 3.2). The MegaMerge provides excellent imaging of the Mesozoic and Cenozoic section. It has a high signal-to-noise ratio, stable zero phase; and bandwidth is ~10-60 Hz. Ricker wavelets with 20-25 Hz peak frequency were used for well ties. The 3D volume was provided post-processing; therefore, the original data was not available and so the processing methods are not known, and there are no descriptions available of the processing stream or pre-stack or pre-migration data.

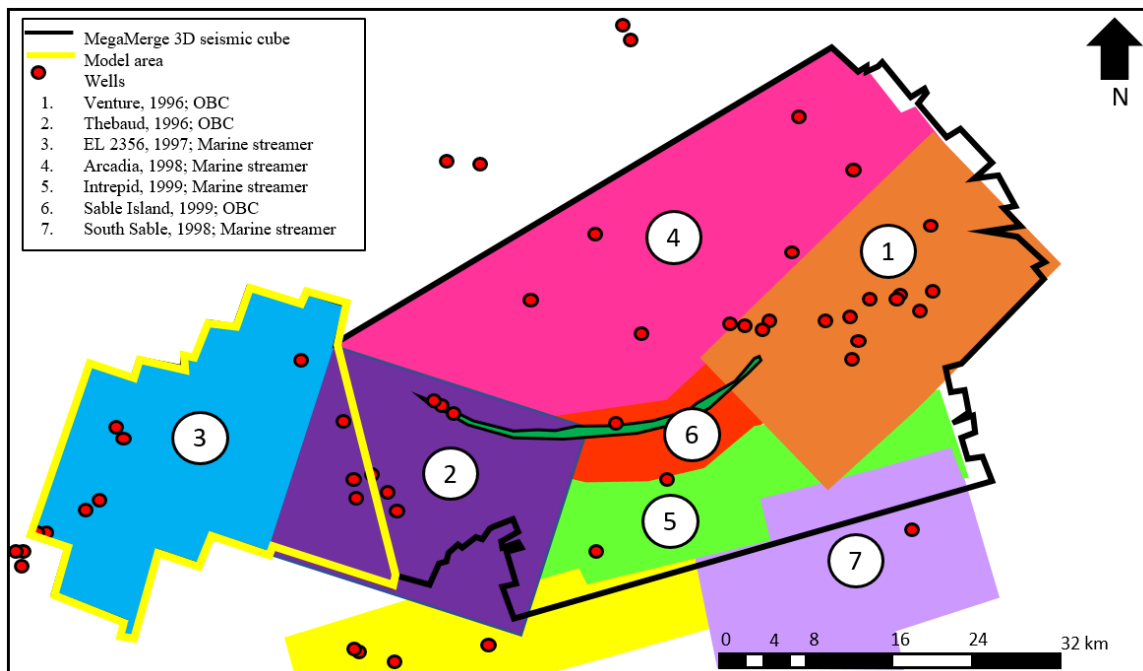


Figure 3.2: Location of the seven 3D seismic surveys included in the Sable MegaMerge survey (modified from Morrison 2017).

2D Seismic

One line of the 2D NovaSpan dataset was used in this study (line 1600) to determine how the third-order depositional sequences behave from shelf to basin adjacent to the 3D study area. The nine regional 2D NovaSpan lines were acquired and donated by ION (GX Technology Corporation) to Dalhousie University Basin and Reservoir Lab, Professor Grant Wach, principle investigator. The NovaSpan data provide a regional 2D seismic framework that spans the area from Georges Bank through Sable Island to the western edge of the Laurentian Channel (Fig. 3.3). In addition, 64 2D seismic lines (Fig. 3.4) were downloaded from the Data Management Centre, housed in the Canada-Nova Scotia Offshore Petroleum Board's Geoscience Research Centre and imported into Petrel™. These 2D data were acquired from 1977 to 1985 by Petro-Canada. These 2D seismic data enable well ties to Jurassic penetrations outside the Sable MegaMerge area. Horizons were interpreted on these 2D seismic lines and then correlated into the 3D Sable MegaMerge.

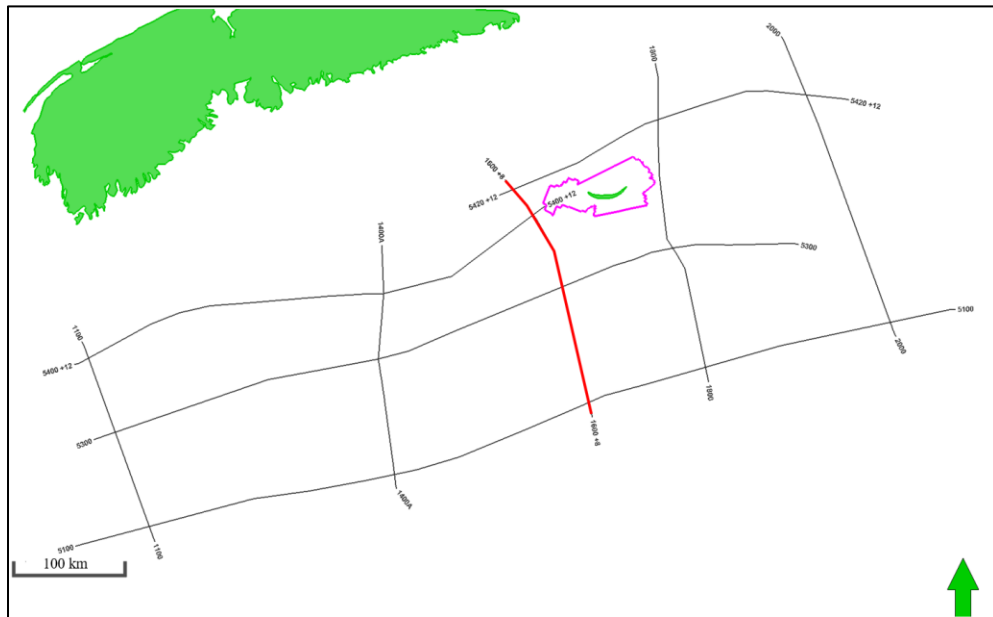


Figure 3.3: Location of the regional 2D NovaSpan seismic lines in relation to Nova Scotia (green landmass to the North) and to the Sable MegaMerge study area (pink polygon). Line 1600, the NovaSpan line used for this study, is highlighted by the red line.



Figure 3.4: Location of 2D seismic (grey lines) in relation to the 3D Sable MegaMerge (purple polygon) and the 2D regional NovaSpan line 1600 (longer black line).

Wells

The 13 key wells used for this study are summarized in Table 3.1 and are discussed further in Chapter 4 and 5. Ten of these wells were used for well log analysis and seismic interpretation and three additional wells were used for core and microfacies analysis. The locations of the ten key wells are shown in Figure 3.5. These wells penetrate Early to Middle Jurassic formations. They were used to create time-to-depth relationships, and sub-regional well log cross sections on which cored intervals, TOC analyses (from the Government of Canada BASIN Database) and lithologies (via digital Canstrat logs) are displayed. These cross sections were key in correlating well tops within the study area (Figs. 4.2 and 4.10).

Table 3.1: Information on the 13 key wells used for this study. Information from BASIN database, Natural Resources Canada, 2018.

Well Name	Spud Year	Operator	Area	Sub-basin	Measured depth (MD)
Arcadia J-16	1983	Mobil et al.	Scotian Shelf	Sable Sub-basin	6005
Citnalta I-59	1974	Mobil-Tetco-Texaco	Scotian Shelf	Sable Sub-basin	4575
Cohasset L-97	1978	Mobil-Tetco-PEX	Scotian Shelf	LaHave Platform	4872

Well Name	Spud Year	Operator	Area	Sub-basin	Total Depth (m)
Dominion J-14	2005	Encana-Marauder	Scotian Shelf	LaHave Platform	3700
Kegeshook G-67	1985	Shell PCI et al.	Scotian Shelf	LaHave Platform	3539
Migrant N-20	1977	Mobil-Tetco-PEX	Scotian Shelf	Sable Sub-basin	4468.7
Panuke H-08	2000	PanCanadian	Scotian Shelf	LaHave Platform	3682
Panuke M-79	2000	PanCanadian	Scotian Shelf	LaHave Platform	4598.3
Panuke PI1 J99	1991	Lasmo NSRL	Scotian Shelf	LaHave Platform	1585
Penobscot L-30	1976	Shell Petro Canada	Scotian Shelf	Abenaki Sub-basin	4267.2
South Desbarres O-76	1984	Shell Petrocan et al.	Scotian Shelf	Sable Sub-basin	6041
Uniacke G-72	1983	Shell Petrocan et al.	Scotian Shelf	Sable Sub-basin	5740
Venture B-13	1980	Mobil-Texaco-PEX	Scotian Shelf	Sable Sub-basin	5368

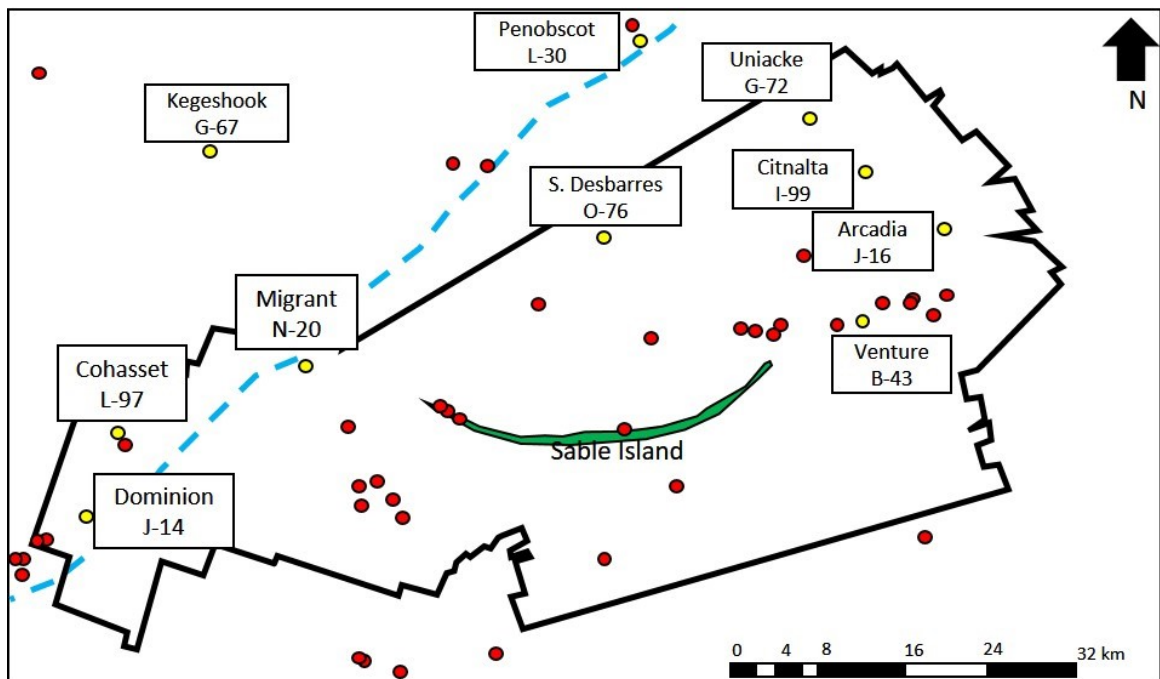


Figure 3.5: Location of 10 key wells (yellow points) across the study area. Pink polygon is the outline of the 3D Sable MegaMerge, black lines are 64, 2D seismic lines across the Scotian Shelf. Blue dashed line is the Abenaki bank margin.

Database construction

The construction of the Petrel database used in this study was a collaborative effort done by multiple people in the Basin and Reservoir Lab at Dalhousie University. The Sable MegaMerge 3D seismic survey and the NovaSpan 2D seismic lines were imported into Petrel by Carlos Wong, additional 2D seismic data northeast of the MegaMerge were imported by Carla Skinner. Many of the well logs and checkshot surveys within the study area were imported from Divestco by Carlos Wong. Canstrat data for the wells were imported into Petrel by Carlos Wong and Carla Skinner. Other well logs and well tops were imported by Bill Richards from the BASIN Database (Natural Resources Canada provided in Excel format by Paul Lake of the Geological Society of Canada). The wells were tied to the seismic data by multiple workers using synthetic seismograms with 20- 25 Hz Ricker wavelets. Several independent but overlapping fault and horizon frameworks within different regions of the Sable MegaMerge were created by Taylor Campbell, Natasha Morrison, Carla Skinner and Bill Richards and are largely consistent.

3.4 Geology

3.4.1 Carbonate geology (models)

The Abenaki carbonate bank offshore Nova Scotia within the Scotian Basin has been interpreted here to comprise seven depositional sequences, aging from the Bajocian to the Berriasian (e.g. Weissenberger et al. 2000; Encana 2006) (Fig. 3.6). The boundaries between the depositional sequences are defined by major flooding surfaces mapped throughout the study area, where foreslope and basinal microbial limestones are overlain by basinal mudstones. The sequence stratigraphic framework for the Mesozoic carbonates proposed by Encana (2006) was based on logs, sample descriptions and very limited core data. To build the sequence stratigraphic framework, the authors used several key assumptions and methods. The Jurassic carbonate facies model (Fig. 3.7) derived from core descriptions and literature (e.g. Eliuk 1978; Eliuk and Levesque 1988) was used with shoaling upward cycles (parasequence) identified from logs and any key facies indicators in samples or core; siliciclastic influxes on the platform that were observed in samples and logs were interpreted to represent hiatuses in carbonate deposition, suggesting the carbonate factory was shut down (Weissenberger et al. 2000).

The Encana (2006) sequence stratigraphic model was used in this study for the nomenclature of the third-order depositional cycles that were observed and mapped within the Sable MegaMerge, age control is provided from biostratigraphic analysis that was done by Van Helden's dating of the Panuke M-79 well, presented in Weissenberger et al. (2006), of each cycle within the interval.

In the carbonate model proposed by Weissenberger et al. 2000, the second-order depositional sequences are on the order of 30-50 million years duration for the Abenaki carbonate bank, related to sea-level change caused by global tectonics (Vail et al. 1991). Third-order depositional sequences are on the order of 0.5 to 3 million years in duration (Vail et al. 1991). However, the model from Weissenberger et al. (2000) has seven, third-order depositional sequences over approximately 50 Ma (averaging 7 million years per sequence). Weissenberger et al. (2000) used the Vail et al. 1977 model, which claims third-order sequences are on the order of 1 to 10 Ma, and not the refined model of Vail et al. 1991, which states 0.5 to 3 Ma. Fourth-order depositional sequences are interpreted to be 0.08- 0.5 Ma in duration (Vail et al. 1991). All sequences were interpreted from one bounding flooding surface to the next throughout the 2D and 3D seismic.

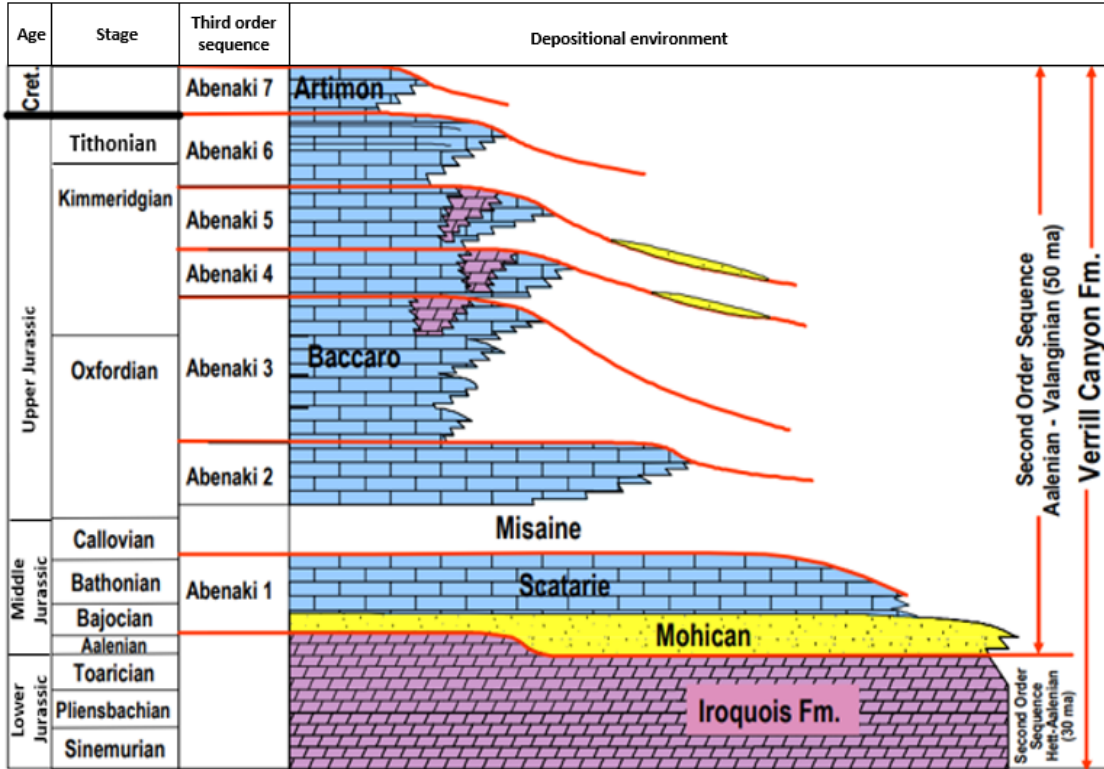


Figure 3.6: Schematic sequence stratigraphic chart of the Iroquois through Abenaki formations. Blue=carbonates, purple=evaporites/dolomites, yellow=siliciclastics. Modified from interpretations from the Deep Panuke Development Plan by Encana in 2006, representing the seven interpreted third-order depositional sequences of the Abenaki carbonate bank (Encana 2006).

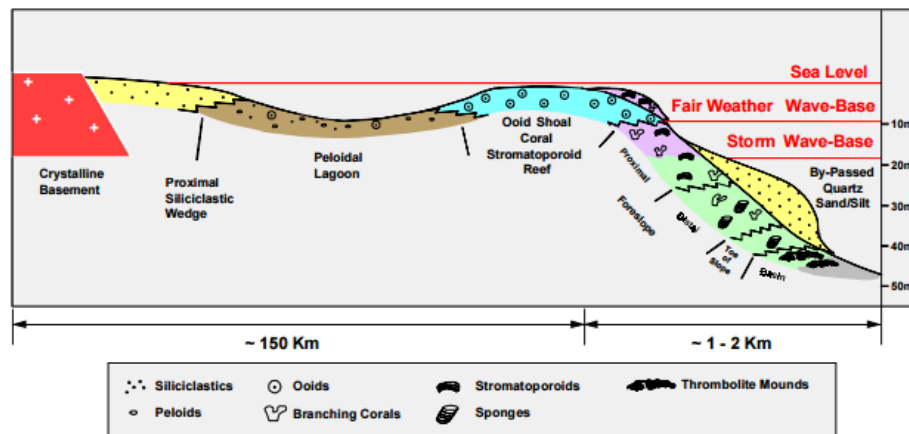


Figure 3.7: Simplified facies model of the Abenaki Formation, offshore Nova Scotia (modified from Weissenberger et al. 2000). A similar succession was examined in the field within the Lusitanian Basin and can be seen in Figure A-1.

The J.L. Wilson carbonate sequence stratigraphic model presented by Kidston et al. 2005 (Fig. 3.8) is also used for this study. Since there are no deep well penetrations in the study area which sample the basinal equivalents of the Abenaki carbonate bank, this sequence stratigraphic model is applied to the distal facies of the third-order depositional sequences, (Middle Jurassic to Early Cretaceous). From this model, the assumption is made that there is potential for organic-rich facies within the distal shales of the Abenaki carbonate bank.

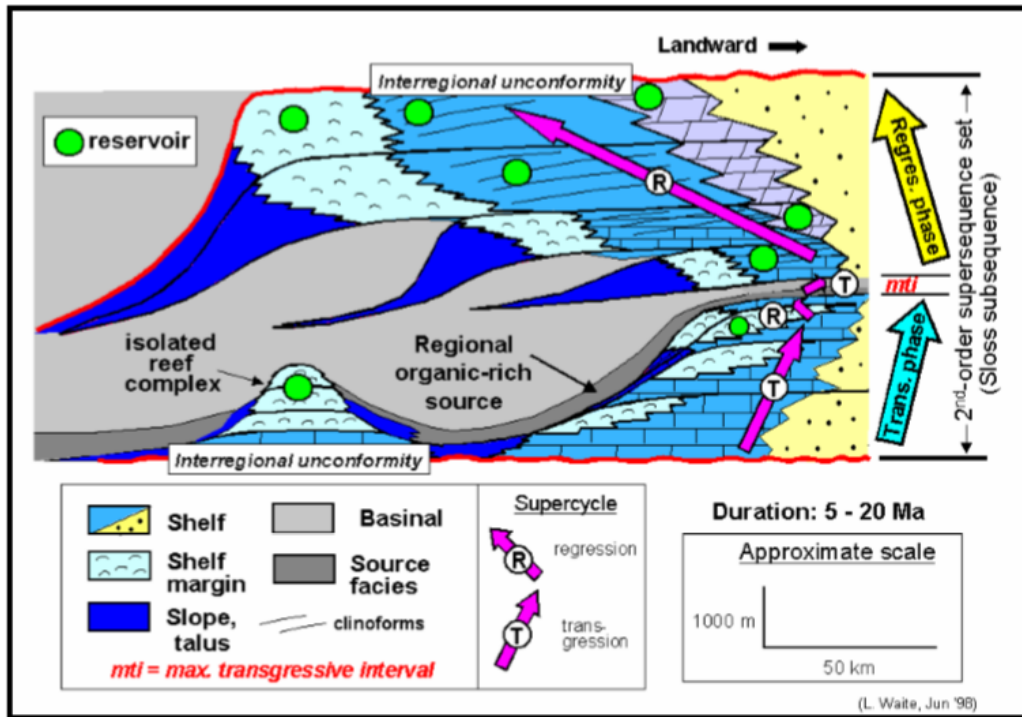


Figure 3.8: Schematic of J.L. Wilson carbonate sequence stratigraphic model from Kidston et al. (2005) modified from Waite (1998), also identifying where potential organic-rich materials can be deposited within a carbonate ramp depositional system.

3.4.2 Siliciclastic geology

A prograding siliciclastic model (Fig. 3.9) was used to understand the depositional processes of the Sable Delta of the Missisauga Formation and how that affected the growth of the Abenaki carbonate bank. Figure 3.9 shows a normal progression of a deltaic environment with coarser siliciclastics being deposited in the foreshore environment close to the river's mouth and becoming finer distally. Typically sandstones are deposited within delta front environment, and shales/mudstones are deposited within the prodeltaic environment. The progradation of deltas leads to coarsening-upwards successions,

typically exhibiting a transition from prodelta offshore muds through silty to sandy mouth bar deposits (Bhattacharya et al. 2010).

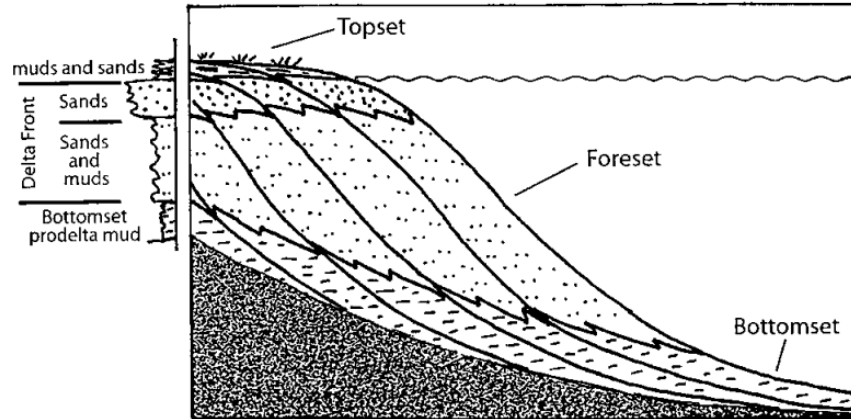


Figure 3.9: Basinward progradation of a delta, which builds a coarsening upwards facies succession that transition from marine into non-marine top set deposits (modified from Scruton 1960).

Throughout the 3D Sable MegaMerge, knowledge on how deltaic deposits prograded into the basin was useful to differentiate between the transgressive shales deposited within the distal foreslope of the carbonate depositional system and the onlapping shales deposited within the prodelta of the Sable Delta.

3.4.3 Core analysis

Typically, conventional coring is only done within proven hydrocarbon-bearing reservoir intervals. For this reason, the wells in this area containing cored intervals of the Middle to Late Jurassic are sparse. Seven wells that contain core of the Abenaki Formation were examined. There were 10 cored intervals of the Abenaki Formation from seven wells. The cores are stored at the Canada-Nova Scotia Offshore Petroleum Board (CNSOPB) Research Centre in Dartmouth, Nova Scotia. These core intervals were described and interpreted to obtain an overall understanding of facies changes within the Abenaki Formation. Of these 10 cores, only four (Cohasset L-97, PanCanadian Panuke H-08, PanCanadian M-79 and PanCanadian PI-1A) are discussed within this study due to the cored intervals of the Abenaki Formation exhibiting similar depositional environments on the shelf and/or shelf margin. The cores were used to examine the different minerals and lithologies that help determine the type of environment in which they were deposited.

Samples were taken for each significant facies change to create thin sections. Other cored intervals from the Jurassic that were previously interpreted by Eliuk in 1978 and 2016 and by Weissenberger et al. in 2006, were also used for this study. The wells from which the cores were taken, and the cored intervals, are shown in Table 3.2.

Table 3.2: *Well names of the cored intervals of the Abenaki Formation along with depth of the cored intervals and the member it belongs to.*

Well	Cored interval (m)	Total recovered core (m)	Abenaki Formation Member
Cohasset L-97	3406.0 - 3424.8	17.7	Baccaro
PanCanadian Panuke H-08	3445.0 - 3459.0	2.96	Baccaro
PanCanadian Panuke M-79	4532.7 - 4540 .0	5.2	Scatarie
Panuke PI-1A-J-99	4029.3 - 4032. 8	1.4	Baccaro

3.4.4 Microfacies analysis

Microfacies analysis is described as the total of all sedimentological and paleontological data which can be described and classified from thin sections, peels, polished slabs or rock samples (Flügel 2010). For this project, the focus of microfacies analysis was using thin sections and rock samples from cored intervals from the Abenaki Formation to determine the key lithofacies present. Microfacies analysis aided in interpreting the depositional model for downdip facies prediction. Figure 3.10 is the Dunham classification for subdividing limestones on the basis of matrix content, which was used in naming the interpreted lithofacies (Sections 4.2.1 and 5.2.1).




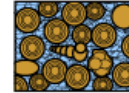
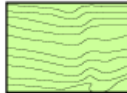
Original components not bound together at deposition				Original components bound together at deposition. Intergrown skeletal material, lamination contrary to gravity, or cavities floored by sediment, roofed over by organic material but too large to be interstices
Contains mud (particles of clay and fine silt size)		Lacks Mud		
Mud-supported		Grain-supported		
Less than 10% Grains	More than 10% Grains			
Mudstone 	Wackestone 	Packstone 	Grainstone 	Boundstone 

Figure 3.10: *Dunham classification of the subdivision of limestones based on their matrix content (modified by Kendall 2005 after Dunham 1962).*

3.5 Petrophysics

Three key wells within the western portion of the Sable MegaMerge were used in this study for petrophysical analysis: Dominion J-14 and Cohasset L-97 (penetrated approximately 1000m of Jurassic Abenaki carbonates); and Migrant N-20 (penetrated depth equivalent siliciclastics). Other wells, to the east within the MegaMerge and to the west and north of the MegaMerge, were used to aid in the interpretation of depositional environments (discussed further in Chapters 4 and 5). Wireline logs for these wells were donated to Dalhousie University (Professor Grant Wach, principal investigator) by Canstrat and Divestco. Canstrat data from cuttings include: lithology, color, fossil content, hydrocarbon occurrences and porosity. The Divestco wireline logs used for this study include gamma ray, sonic, resistivity and density logs acquired from drilling operations. Deviation and checkshot surveys were acquired from the Canada-Nova Scotia Offshore Petroleum Board's Data Management Centre, and were used to specify well surveys and time to depth relationships. Well logs were loaded and updated from the collective project (e.g. Skinner 2016, among others) in the Basin and Reservoir Lab at Dalhousie University.

Regional formation tops interpreted by Wade and MacLean at the Geological Survey of Canada were used to begin horizon correlation. These formation tops were based on their regional well log correlations and are persistent markers on regional 2D seismic data. The

associated formations are described by Wade and MacLean (1990) and the data are publicly available in the BASIN Database.

3.5.1 Well ties

Well ties were done using checkshot surveys previously loaded to a collective project in the Basin and Reservoir Lab at Dalhousie University. Wells were also tied using synthetic seismograms by several different workers. A synthetic seismogram is generated by convolving the reflectivity derived from acoustic and density logs with a Ricker wavelet derived from the seismic data. For the Cohasset L-97 well, Figure 3.11 from the Deep Panuke Offshore Gas Development Plan (2006) was used to aid in identifying and tying the Abenaki 1-7 carbonate cycles. The image was loaded into Petrel™ in a well section window and depth corrected to fit the wireline logs. Well tops were then picked from the image and used in seismic interpretation.

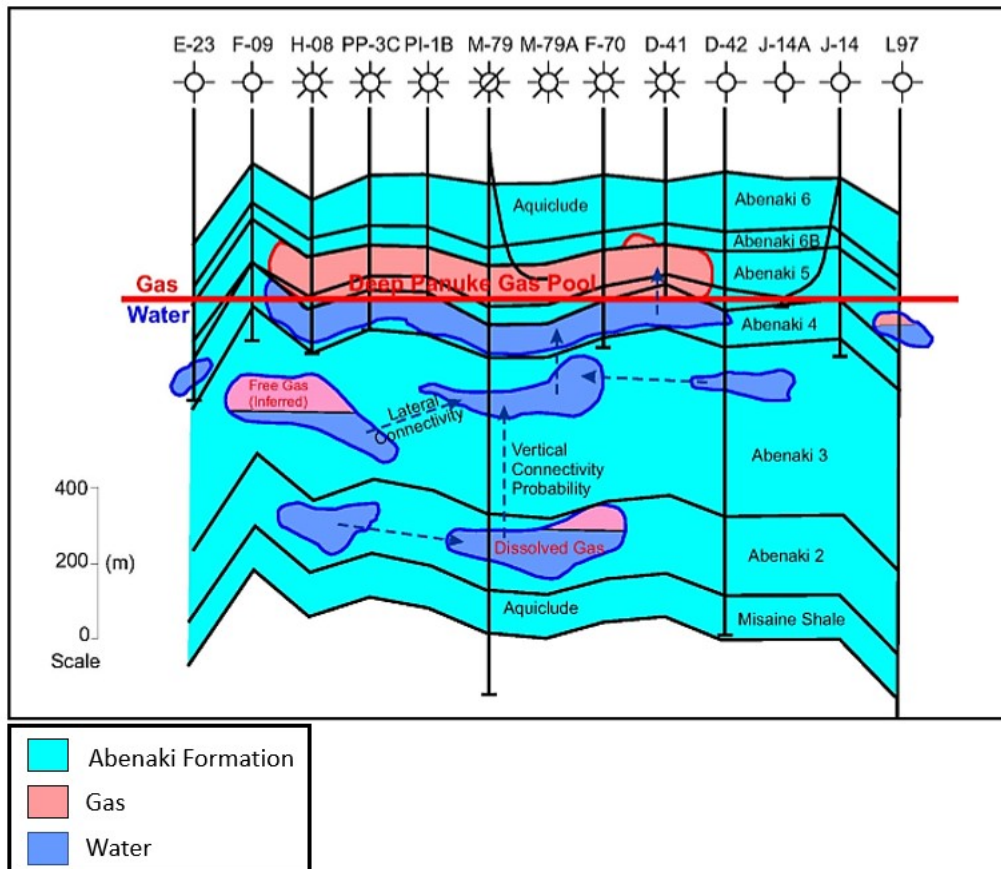


Figure 3.11: Well cross section from the Encana Deep Panuke Offshore Gas Development Plan (2006). This image was used to aid in tying the Cohasset L-97 well (last well on the right) in the Middle-Late Jurassic carbonates of the Abenaki Formation.

Checkshot surveys

A checkshot survey is designed to measure the seismic travel time from the surface to a known depth. The P-wave velocity of formations in a wellbore can be measured directly by lowering a string of hydrophones down the borehole and travel times are recorded at regular intervals. Trigonometrical corrections are then applied to convert non-vertical source-to-hydrophone travel times to vertical travel times, which establishes a time-depth relationship between well and seismic data. A synthetic seismogram generated from sonic and density logs can then be overlain on seismic data through any given well and matched to the seismic data to identify specific seismic reflections.

3.5.2 Wireline logs

A combination of wireline logs and mudlogs (logs created from examining mud and cuttings brought to the surface by circulating drilling mud) are used to determine lithology, porosity, fluid content, and permeability in each well. A detailed description of each wireline log can be found in Appendix B.

Lithology

Lithology is estimated from a combination of gamma ray, neutron, density, and sonic logs. Gamma ray logs typically show low radioactivity in clean sandstones and carbonates, and high radioactivity (high Uranium, Thorium and Potassium) in shales. Organic-rich shales show very high radioactivity readings. Lithologies estimated from well logs can then be ground-truthed against cuttings and core. Lithology can also be estimated from neutron, density and sonic logs that measure hydrogen ion density, bulk density and P-wave or S-wave velocity respectively. Typical lithologies have characteristic ranges of velocity and density which are partially dependent on porosity and fluid fill.

Porosity

The porosity of a rock can be determined from a neutron log, a density log or a sonic log. The bulk density is a function of matrix density, porosity and fluid density, therefore can be converted to porosity by using equation 3.1 or by using a log interpretation chart. The neutron log measures the hydrogen concentration in a formation, and by using logging charts specific to the neutron log, a porosity can be determined. Neutron energy loss is related to energy loss due to hydrogen being concentrated in the fluid filling the pores and

porous formation. If a reservoir is gas (or light oil) filled, it may appear to have lower sonic or density porosity than the same pores filled with oil or water, due to gas having a considerably lower density than oil or water (Alberly 1994).

$$\text{Equation 3.1: } \Phi = \frac{\rho_{ma} - \rho_b}{\rho_{ma} - \rho_f},$$

Where, Φ = porosity, ρ_{ma} = matrix density, ρ_b = formation bulk density (log value), ρ_f = density of the fluid saturating the rock immediately surrounding the borehole.

Fluid content

Fluid content can be estimated by resistivity, density and neutron logs. Salt water is more conductive (low resistivity) than either oil or gas and this formed the basis for the Archie saturation calculation (Equation 3.2) (Archie 1952). Oil and gas are both relatively high resistivity and are typically discriminated using neutron-porosity or density/porosity crossover and/or fluid gradients on pressure-depth plots.

$$\text{Equation 3.2: } S_w^n = \frac{R_w}{(\Phi^m \times R_t)},$$

Where, S_w = water saturation of uninvaded zone, n = saturation component, R_w = formation water resistivity at formation temperature, Φ = porosity, m = cementation exponent, R_t = true resistivity of the formation, corrected for invasion, borehole, thin bed, and other effects (Archie 1952).

Permeability

Permeability can be estimated qualitatively by examining the separation of the shallow, medium and deep resistivity logs, or by filter-cake build up indicated on a caliper log. The depth of investigation of resistivity logs is related to source-receiver spacing. Measured values vary, depending on permeability, as a function of how far drilling fluid invades reservoir rocks beyond the borehole wall. The separation of the curves takes place in the more porous and permeable sandstones (Asquith and Krygowski 2004).

3.6 Geophysics

Background information on seismic acquisition, processing and seismic display methods can be found in the Appendix C.

3.6.1 Seismic facies analysis

Seismic facies are recognized based on a combination of reflection configuration (geometry), strength, continuity, amplitude, frequency and interval velocity (Mitchum et al. 1977). Seismic facies analysis is used to determine the relative age and geometry of depositional units, and to interpret lithology, depositional environment and processes. Reflection amplitude contains information on the velocity and density contrasts at individual interfaces (Mitchum et al. 1977). Frequency is primarily a characteristic of the seismic pulse, although it is also related to the spacing of reflectors or lateral changes in interval velocity, both which correspond to geological responses (Sangree and Widmier 1979). Reflection continuity is interpreted to closely correspond to the continuity of strata, and reflection amplitude indicates contrasts in lithology and/or the reflector spacing (Mitchum et al. 1977). Reflection geometry can be described as parallel (concordant), sub-parallel, divergent, progradational, reflection-free, wavy, chaotic, hummocky, or contorted (Fig. 3.12). The three-dimensional character of deposits is important to consider due to the possibility of reflection configuration being different of dip-parallel sections and strike-parallel sections. Seismic facies were used to interpret lithology and depositional environments from 2D and 3D seismic in this study and this enabled mapping and understanding of depositional trends, and the architecture of third-order depositional sequences.

3.6.2 Seismic stratigraphy

Seismic stratigraphic analysis is used to analyze seismic reflection data within a context of basin systems that uses reflection geometry and acoustic character of seismic reflection data. The technique applies concepts developed from established stratigraphic and depositional models. Recognizing that primary seismic reflections approximate chronostratigraphic surfaces; the method involves the correlation of erosional and unconformable surfaces and their conformable equivalents throughout the study area (Vail et al. 1977).

Seismic stratigraphy involves the recognition of patterns (seismic facies) and requires the ability to identify important surfaces (bounding discontinuities) (Vail et al. 1977). Recognition of reflection terminations such as: onlap, downlap, toplap, concordance and erosional truncation are important for the identification of important surfaces that are necessary for subdividing the seismically imaged stratigraphic record (Fig. 3.13) (Mitchum et al. 1977). Reflection termination patterns and reflection configuration were used to identify the shelf, shelf-break, slope and basin floor at various intervals in the Sable Sub-basin. Seismic stratigraphy was used to correlate sequence boundaries representing the tops of the depositional sequences throughout the 2D and 3D seismic. For this study, seismic stratigraphy was used to interpret depositional environments and structural architectures based on reflector terminations, and is discussed further in Chapter 5.

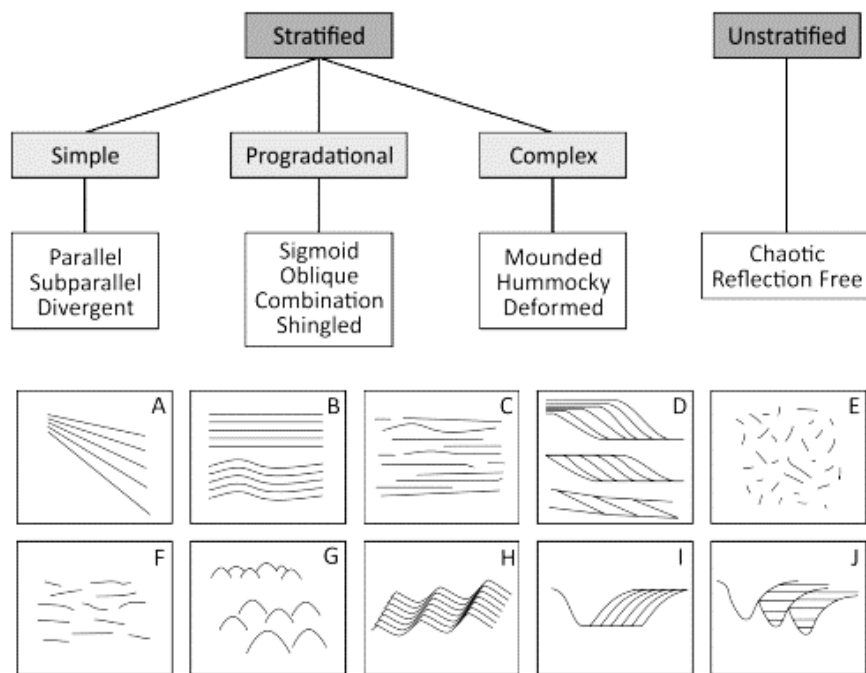


Figure 3.12: Reflection configurations (A) divergent, (B) concordant, (C) sub-parallel, (D) sigmoid, oblique and shingled, (E) chaotic (F) hummocky, (G) hyperbolic, (H) climbing waves, (I) accretionary channel, (J) cut-and-fill channel (modified from Mitchum et al. 1977).

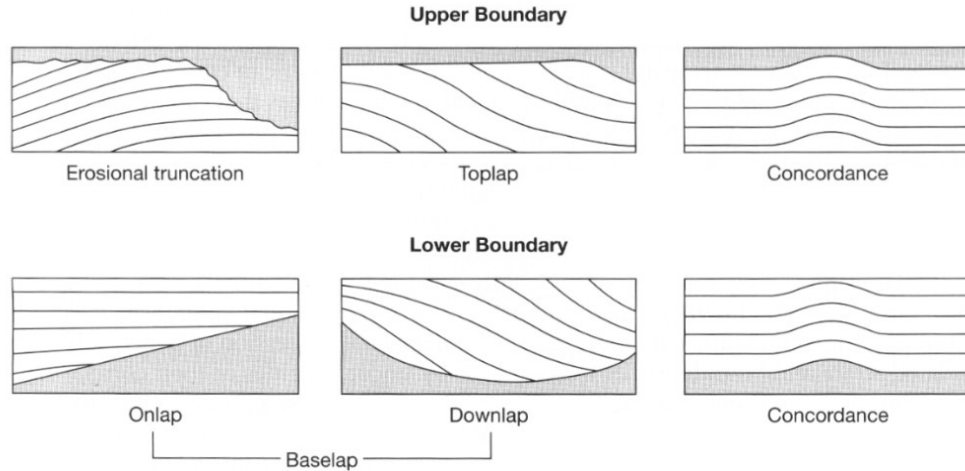


Figure 3.13: Relationship of strata to the upper and lower boundaries of a depositional sequence (Mitchum et al. 1977).

3.6.3 Seismic interpretation

Schlumberger Petrel™ E&P Software Platform

The software used in this study is Schlumberger's Petrel™ E&P Software Platform. Petrel™ was used to perform structural, stratigraphic and seismic attribute interpretations on reflection data. Petrel™ was used throughout this study for seismic interpretation, well correlation and analysis, and geocellular modeling.

Horizon interpretation

Seismic interpretations were done on the western portion of the Sable MegaMerge (some interpretations made in the eastern portion to correlate to South Desbarres O-76), the NovaSpan 1600 regional 2D seismic line, and multiple 2D seismic lines. For this study, seismic data files in SEG-Y format were loaded into Petrel™ and seismic stratigraphic analysis was conducted to establish a robust seismic stratigraphic framework. Wells with formation tops were tied into the 3D seismic survey using synthetic seismograms and wells outside the immediate study area were similarly tied to 3D data and 2D data. Horizon and fault interpretation were done progressively area by area and was done using a grid of lines (every 20 inlines and every 40 cross-lines). The focus of seismic interpretation in this study was to map the seven distinct third-order depositional sequences of the Abenaki Formation (e.g. Weissenberger et al. 2000; Encana 2006), distally into the Sable Sub-basin to create a stratigraphic framework.

Fault interpretation

The faults imaged within the 3D seismic were identified by vertical offsets between the laterally continuous carbonate reflections on inline and cross-line sections.

3.6.4 Seismic attributes

Seismic attributes are measurements extracted or derived from seismic data such as: time, amplitude, frequency, and attenuation; that can be analysed to enhance information that may be more subtle in a traditional seismic reflection image. The seismic attributes that were used in this study include reflection amplitude, reflection strength (magnitude) and two-way travel time (both time-thickness and time-structure) (e.g. Brown 1999).

Root Mean Square amplitude

Root mean square (RMS) amplitude is the square root of the arithmetic mean of the squares of a set of values within a given window. RMS amplitude emphasizes the variations in acoustic impedance over a selected time interval (e.g. Cartwright 2007) and mapping this attribute spatially can provide evidence of lithology and environment of deposition variations. In this study, RMS amplitude extractions were taken for each carbonate-clastic cycle to map where the carbonate bank ended (high amplitudes) and where the distal clastics began (low amplitudes). Generally, the higher the acoustic impedance variation of stacked lithologies, the higher the RMS amplitude values will be. RMS amplitude maps created to aid in determining the depositional environments can be found in Appendix C.

3.6.5 Genetic seismic inversion

Within Petrel™, multi-layer neural networks as well as a genetic algorithm are combined to provide a straightforward seismic inversion from reflection amplitude to any property selected from the well data. For the genetic inversion undertaken here, the inputs were reflection amplitude and the lithology logs, provided by Canstrat. Results from the genetic seismic inversion can be seen in Section 4.4.3.

The resultant lithologies from the genetic inversion are extracted from the seismic data (Fig. 4.21) and the lithology logs calculated from V-shale logs, with editing from the Canstrat logs (cuttings) to discriminate between limestones and sandstones. The extracted 3D attribute volume of log property was calculated using genetic algorithm and neural networks. The genetic algorithm allowed the neural net to find the global minimum of the

function and gave an optimal solution. The genetic inversion inverted the seismic data into the desired lithology log, producing a best fit from the given well data (Veeken et al. 2009).

3.6.6 Geocellular framework (initial model with no properties)

After a model was defined from the seismic and fault correlations, a boundary was set for the geocellular model and can be seen in Figure 4.23 as the red polygon. The geocellular model was then built progressively by inputting the seismically correlated faults and creating a fault model. The results of the geocellular framework can be seen in Section 4.4.5.

Fault modeling

The fault modeling tool was used to convert the seismic fault interpretations into a fault model within the defined Petrel model. The faults in this fault model were first conditioned to ensure that the ensuing pillar grid would not have unnecessary contortions. Faults were extended to a top limit of -2250 ms and to a bottom limit of -4500 ms, based on where most the faults terminated, by extending all the pillars within the fault. The faults were then individually examined in a 3D window to make corrections where some of the faults crossed one another and some of the pillars of the faults were distorted (Fig. 4.23).

Pillar gridding

Pillar gridding was done once a satisfactory fault model was created. Pillar gridding uses the faults in the fault model as the initial basis for a non-Cartesian 'i.j.k' 3D grid in which the faults define grid cell boundaries (Fig.4.24).

Horizon modeling

After a satisfactory fault-based pillar grid was completed, the 18 interpreted seismic horizons were input to the model using the "make horizon" tool. Each horizon was given a horizon type of either conformable, erosional, discontinuous or base. The i'j'k geocellular grid is further modified so that grid cell boundaries parallel the horizons and zones are defined between horizons.

The distance to faults was set to 250 m, which signifies the distance that will be ignored between the horizons and the faults, in case any of the horizons were interpreted over the fault plane which would skew the horizon model.

Time-to-depth conversion

The time-to-depth conversion was completed using Petrel “Geophysics: Advanced Velocity Model” after the time horizons were interpreted from the 3D seismic volume and gridded in a 3D geocellular framework model. The shallowest and the deepest interpreted horizons from the framework model (Abenaki 7 and Mohican Formation) and two horizons above them (Wyandot Formation and O Marker) were input into a velocity model together with interval velocities based on the Cohasset L-97 well. The lithologies that were calculated by genetic inversion were input into the two-way-time model and this was then converted to depth using the velocity model. An example of the result of the depth model can be seen in Section 4.4.4.

3.6.7 Geocellular modeling (with properties)

The results of the geocellular model can be seen in Section 4.4.6.

Zone index

The interval between each pair of horizons is termed a zone in Petrel, and the geometrical modeling tool enables a number (index) and color (loosely based on lithology) to be assigned as a property to each zone. This zone index can then be displayed (Fig. 4.25) on top of seismic data and inspected in 3D as the first step in quality checking the 3D grid.

Cell Height (Cell thickness)

Cell height is another geometrical property that was generated using the geometrical modeling tool, which like zone index, creates a discrete property for each cell and then assigns a specific value for each cell (Fig. 4.26). Cell height is useful to determine the thickness of the intervals of interest.

Genetic seismic inversion within geocellular model

First, layers were added to the modeled zones to give a more detailed result. The lithology attribute resulting from the genetic inversion was input into the geocellular model using geometrical modeling. The genetic seismic data was resampled into the geocellular model using the horizons and faults previously modeled. Two separate geocellular models were created to represent the lithologies associated with a mud-rich, distal carbonate depositional system (Fig. 4.27) and a mixed sand-rich deltaic depositional system with a carbonate depositional system (Fig. 4.28). This will be explained further in Chapter 5.

Chapter 4: Results

4.1 Introduction

This chapter shows examples of the results of the methods described in Chapter 3. They are presented beginning with geological results, progressing to petrophysical and geophysical results (which includes geophysically-driven geocellular modeling results). The interpretation of lithofacies from core and microfacies analysis is first described. These results helped in understanding depositional environments (Table 5.1) on the carbonate platform (where the cores were taken). Adjacent depositional environments were then interpreted downdip using the seismic data. A cross section of the 10 key wells across the study area (discussed further in Chapter 5) shows the results of wireline log interpretation of the lithology and architecture of the third-order depositional sequences in the study area. Examples of the results from the 2D and 3D seismic interpretation are shown as a series of seismic traverses from the shelf-to-basin. Each traverse shows the interpreted seismic horizons and faults that were used to analyse the stratigraphic architecture of the third-order depositional sequences (discussed in Chapter 5). The seismic traverses also show the interpreted depositional environments (summarized in Table 5.2) based on seismic character and facies within the specific intervals, and from an understanding of the geological model, core and well log analysis. Geophysical results including examples from the geocellular model that are used to show perspective views of seismically derived lithologies that are then interpreted in terms of environments of deposition and source rock potential are discussed in Chapter 5.

4.2 Geology

4.2.1 Core Analysis

Core analysis was completed on 11 cored intervals of the Abenaki Formation at the Canada-Nova Scotia Offshore Petroleum Board's Geoscience Research Centre (CNSOPB GRC) in Dartmouth, Nova Scotia. Only four of these cored intervals will be discussed due to the others having a similar depositional environment on the shelf and/or shelf margin (Fig. 4.1). The location of the four cored intervals can be seen as black dots within Figure 4.1 and are: one core from the Cohasset L-97 well, 17.7 m was recovered of the Upper Jurassic, from a depth of 3406-3424.79 m. One core from the PanCanadian Panuke H-08 well, 2.96 m of Late Jurassic was recovered from 3445 m-3459 m depth. One core from

PanCanadian M-79 well, 5.2 m of Middle Jurassic was recovered from 4532.7 m-4540.3 m depth. The fourth core is from the Panuke PI-1A J-99 well and recovered only 1.4 m of core from the Late Jurassic (Kimmeridgian) from a depth of 4029.28 m-4032.8 m. The locations of the four core can be seen in Figure 4.1 and in cross section Figure 4.2.

Penobscot L-30 and Penobscot B-41 cores were described by Eliuk (1978 and 2016) and by Campbell (2014). Other cored intervals of predominantly siliciclastics from the Early-Late Jurassic were previously described by Eliuk in 2016.

The Cohasset L-97 well was drilled of the western edge of the Sable salt basin (A' within Sable MegaMerge of Figure 4.1), approximately 31 km west of Sable Island. The well itself penetrated the entire Abenaki Formation from 3158 m – 4768 m. Kidston et al. 2005 referred to the target of this well as back reef, slightly away from the margin. The core was taken 200 m below the top Abenaki. The core is predominantly a mudstone-wackestone with large coral frame builders. There is minor pyritization throughout the core. Most of the core is difficult to interpret due to complicated dolomitic diagenesis.

4.2.2 Cored wells cross section

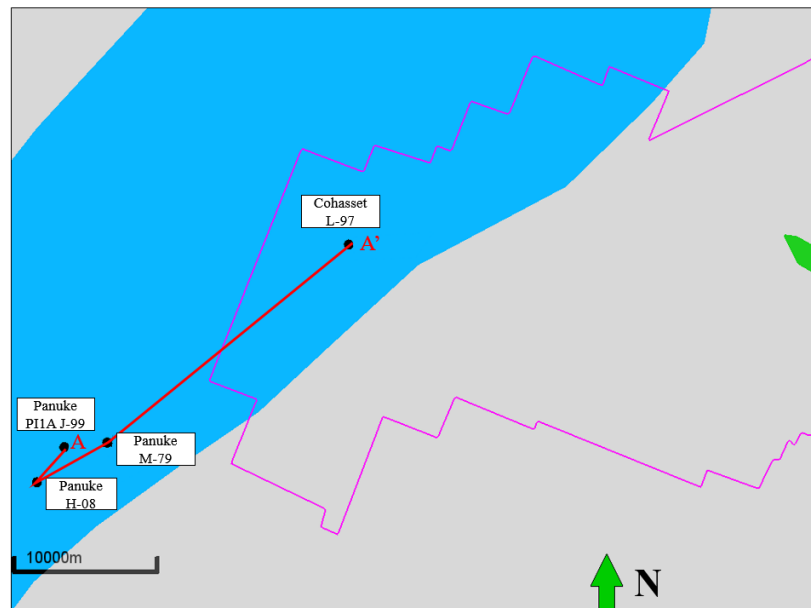


Figure 4.1: Location of the four wells (L-97, M-79, H-08 and PI-1A- J-99) with cored intervals of the Abenaki Formation (four black dots) from the Middle-Late Jurassic that were analyzed and described for this study. The pink polygon is the outline of the 3D Sable MegaMerge, the blue are carbonates on the shelf and on the shelf margin and the grey are predominately shale rich/ siliciclastics. A to A' is the cross section shown in Figure 4.2.

The three cored intervals that were described from the Deep Panuke Field just west of the 3D Sable MegaMerge were drilled by Encana. Deep Panuke was discovered by Encana (PanCanadian) in 1998 by deepening the well from the depleted overlying Panuke oil reservoir that was discovered in 1986 by Shell Panuke B-90 (Eliuk 2016).

Panuke H-08 was drilled in 2000. The cored interval was very broken up and heavily sampled making interpretation difficult. The core comprises an upper section, approximately 2 m of sponge-rich limestone, and a lower section of limestone, rich in crinoids, bryozoans and large bivalves. A brecciated textured interval separates the two sections. Both limestone sections are highly porous. This core was also affected heavily by dolomitic diagenesis.

Panuke M-79 was also drilled in 2000 by Encana (PanCanadian). It is the deepest well in the Deep Panuke gas field and drilled on the Abenaki bank edge. The core comprises oolitic-mudstone with abundant lithoclast intervals (predominantly quartz, 1-2 cm, sub-rounded, well sorted) and very fine, disarticulated shell fragments.

Panuke PI-1A J-99 was drilled in 1999 by Encana (PanCanadian). The cored interval was quite broken up, making interpretation difficult. It was also heavily affected by diagenesis, making the interpretation of microfossils difficult since they were all overprinted. The core is comprised of vuggy, reefal boundstone of dolomite creating a very porous texture.

Full core descriptions for these wells can be found in Appendix D. The core logs for the cored intervals can be found in the supplementary files.

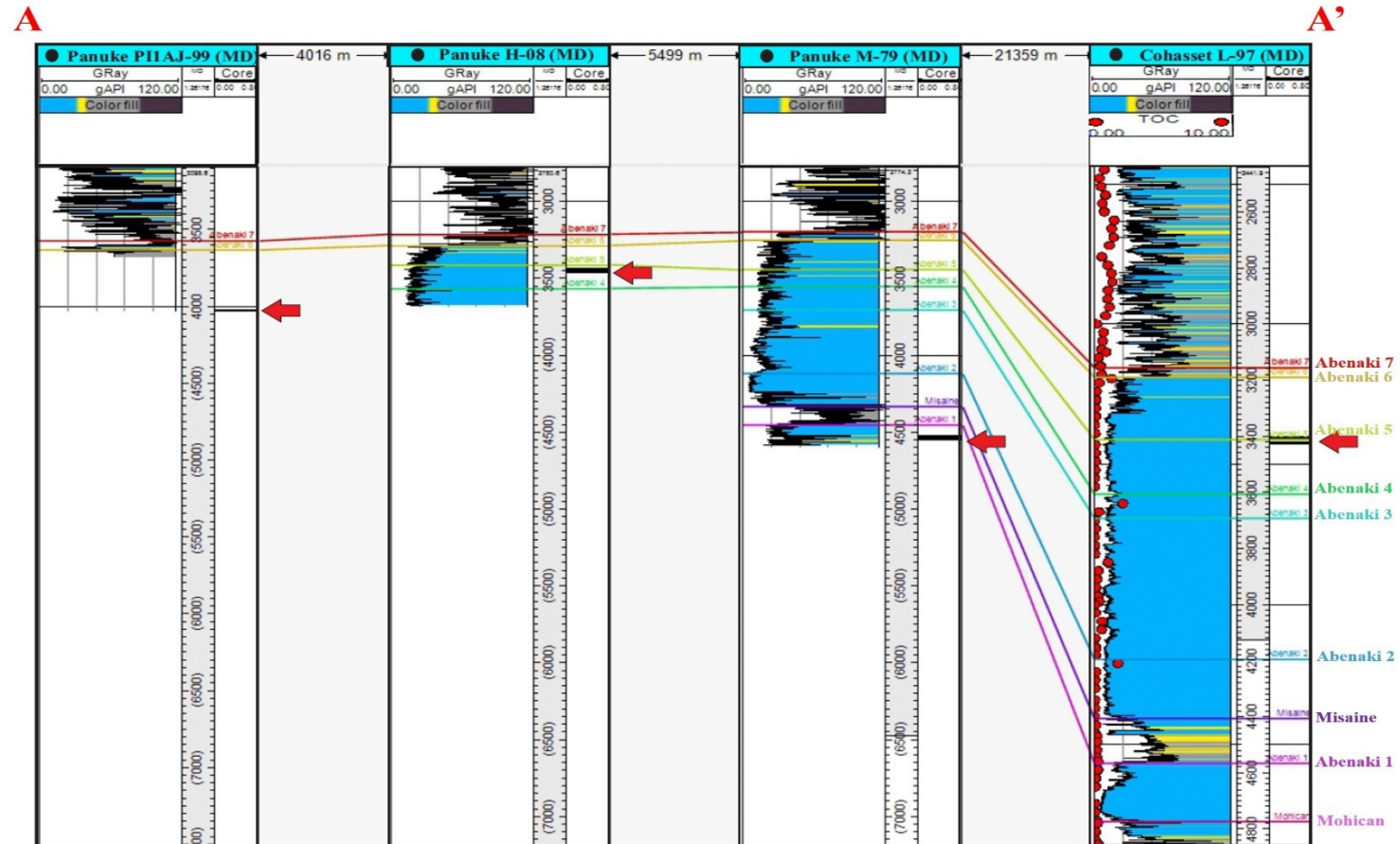


Figure 4.2: Cross section of wells used for core description of the Abenaki Formation for this study. Red arrows point to cored intervals of wells. The colored log is a gamma-ray log which is infilled with lithological values from Constat and the red points at TOC values. The blue=carbonates, yellow=sandstones and grey=mudstones. The colored lines across all of the wells are the well tops for the seven depositional sequences of the Abenaki carbonate bank that were correlated across all the wells using data from BASIN Database and by correlating the well tops with the seismic data.

4.2.3 Lithofacies

Seven lithofacies (Lithofacies 1-7) were examined through petrographic and microfacies analysis from the four cored wells of the Abenaki Formation. Table 5.1 in Chapter 5 is a summary table of all seven lithofacies with interpreted depositional environment. Seven thin sections from Cohasset L-97 were previously prepared and borrowed from the CNSOPB GRC, and three thin sections from Panuke H-08, four thin sections from Panuke M-79, and one thin section from Panuke PI-1A were prepared at Dalhousie University.

Microfacies analysis was done to confirm fossil assemblages, textures and rock types that were determined from core analysis, however most cored intervals were affected by diagenesis making interpretation and determination of fossils assemblages sometimes difficult using the naked eye. In some cases, a polarising microscope aided in the determination of some fossils, however for other thin sections, the fossils were indistinguishable. The polarising microscope was also used to try to distinguish which lithoclasts were present, if any at all, in the thin sections, potentially giving some indication as to the proximity to siliciclastic influence.

The thin sections from the Cohasset L-97 well had been stained with Alizarin Red S, which produces a pink to red stain on any carbonate that reacts with dilute acid. Therefore, the more reactive minerals like calcite and aragonite get stained red, whereas the less reactive minerals like dolomite remain unstained. The epoxy of the Cohasset L-97 thin sections was also stained blue to facilitate observation of porosity.

Lithofacies 1: Mudstone-wackestone

Lithofacies 1 (Table 5.1) (Fig. 4.3 A, B and C) is classified as a mudstone-wackestone (Dunham 1962), and is present in Cohasset L-97. It is medium to dark grey in color with sparite cement. There are peloids, microbes and sponges, crinoids, bivalves and stromatolites present within this lithofacies. Calcite is also present, which has infilled vugs and veins and has also formed as a cement within some intervals. There are clasts throughout which are unidentifiable, however they appear to be comprised of the main sparite matrix. Within the Cohasset L-97 core, there is approximately 7.9 6m of lithofacies 1, from depths of 3414 m – 3406.04 m. There is no visible porosity in core, or thin sections. Microfacies analysis determined there are fragmented scleractinian corals, abundant

bryozoans, and other various benthic foraminifera. This facies has blocky, subhedral calcite with many crystal face junctions (Fig. 4.3 B and C).

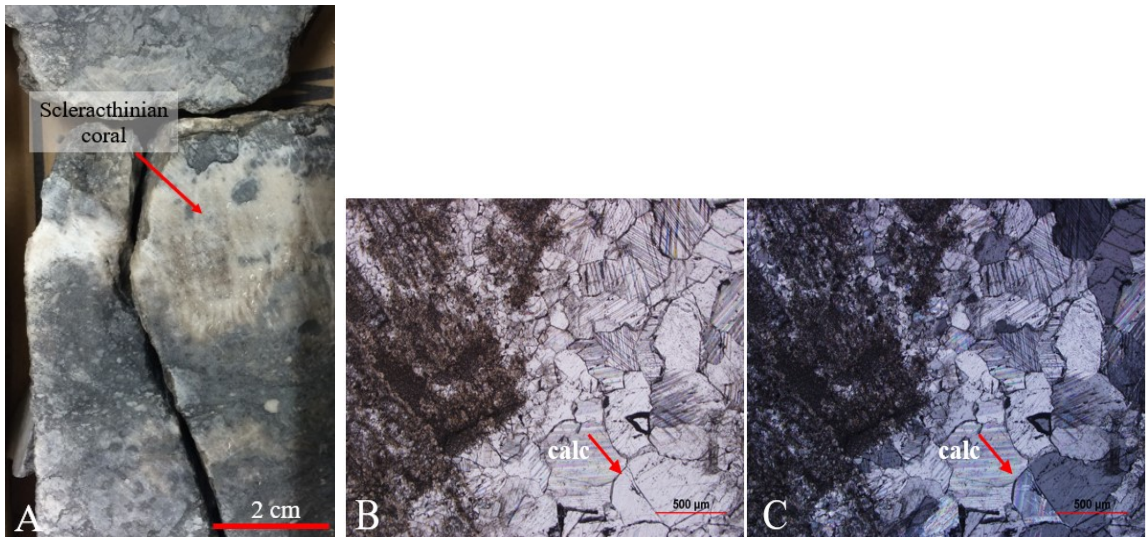


Figure 4.3 A, B and C: *A: Cohasset L-97 Core 1, at approximately 3407m depth. Large (6cm) scleractinian corals within a brecciated interval. There are also bivalves, and small stylolites within a sparry matrix. B and C: Thin section from Cohasset L-97 representing lithofacies 1, TSBF627, 3418 m MD 5x magnification, B: Plane polarized light (PPL) C: Cross polarized light (XPL). C2: XPL calc=calcite. There is no visible porosity.*

Lithofacies 2: Brecciated Wackestone-packstone

Lithofacies 2 (Table 5.1) (Fig. 4.4 A, B and C) is characterized as a brecciated wackestone-packstone (Dunham 1962), medium to light grey in color. It is present throughout the Cohasset L-97 core, from approximately 3419 m – 3414 m (~5 m). It has sparry calcite cement. There are abundant fragmented skeletal particles of bivalves, crinoids and foraminifera. There are peloids scattered throughout this lithofacies. Sponges and branching coral are also abundant. The branching coral interval is approximately 30 cm, then becomes brecciated. Some intervals are grain-supported with grains of matrix which has been brecciated, with nodule clasts from mixing and decompaction, although it is predominately wackestone. Stylolites are common because of pressure solution after burial, lithification and dolomitization. There is no visible porosity. Pyrite is visible within this lithofacies, formed in the muddier intervals of the wackestone. From microfacies analysis, fragmented scleractinian corals, bryozoans, and other benthic foraminifera can be seen. There is also evidence of silicisponges, encrusting foraminifera and annelid tubes. Seen within Figure 4.4 B and C, sparite filled a moldic cavity in a scleractinian

coral. A bivalve visible in B1 has a geopetal structure, while the rest of the bivalves have been replaced with blocky calcite.

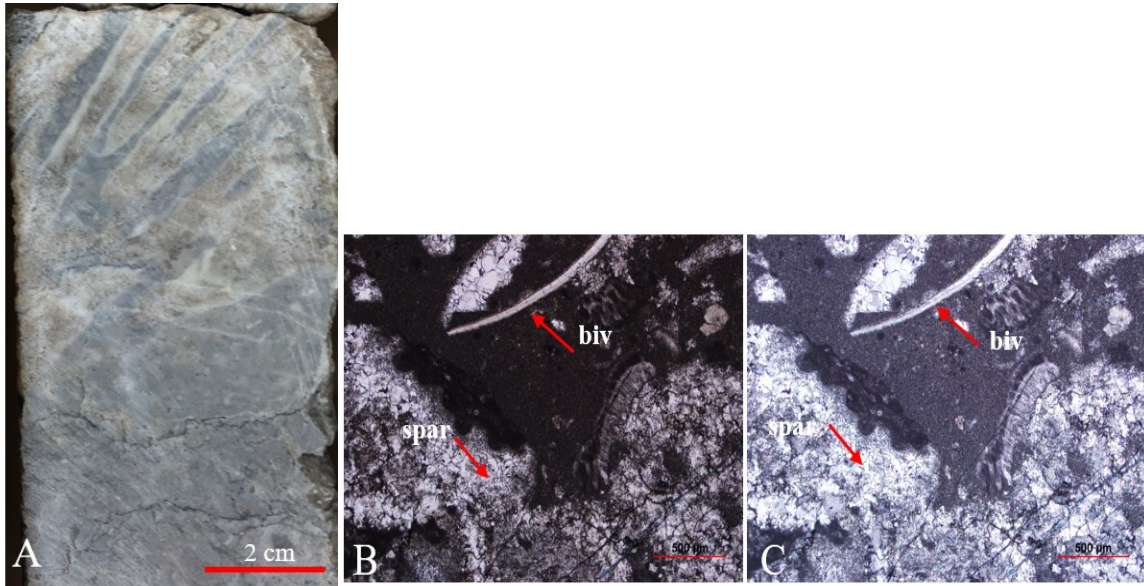


Figure 4.4 A, B and C: *A: Cohasset L-97 core 1, at approximately 3417.5m depth. Base of branching coral growth framework with minor stylolites. B and C: Thin section from Cohasset L-97 representing lithofacies 2, TSBF626, 3414 m MD, 5x magnification, B: PPL, C: XPL. spar=sparite, biv=bivalve. No visible porosity.*

Lithofacies 3: Crystalline mudstone

Lithofacies 3 (Table 5.1) (Fig. 4.5 A, B and C) comprises crystalline mudstone (Dunham 1962) present within the Cohasset L-97 core from approximately 3425 m – 3419 m (6 m), it is also present within the top of the core at approximately 3410 m, intermixed with lithofacies 1. It is light grey in color with no apparent grains throughout due to complex dolomite diagenesis. It is also difficult to distinguish fossil assemblages due to the dolomite. Porosity is <2%, however it is not fabric selective and appears as vugs. Most vugs however, are infilled with calcite. The lithofacies is brecciated with an abundance of stylolites. From microfacies analysis, this facies exhibits scleractinian coral fragments, all which have been replaced with dolomite. There is an abundance of bryozoans, bivalves and other benthic foraminifera that have mostly been replaced by dolomite or calcite. In Figure 4.5 B and C, a scleractinian coral has been slightly encrusted by microbialites. The coral fragment has been replaced by blocky, elongated calcite crystals and minor amounts of blocky dolomite.

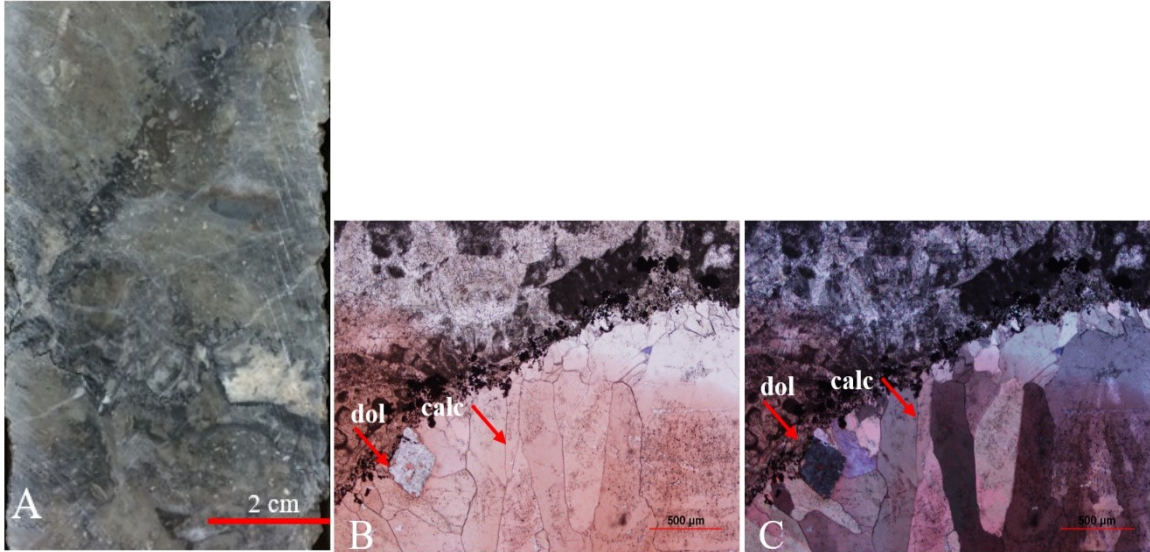


Figure 4.5 A, B and C: A: Cohasset L-97 core 1, at approximately 3424m depth. Indistinguishable fossil assemblages, predominately calcite and dolomite with some calcite filled vugs. Exhibits a brecciated fabric. B and C: Thin section from Cohasset L-97 representing lithofacies 3, TSEC467, 3410 m MD, 5x magnification. Pink is from Alizarin Red S staining, differentiating between dolomite and calcite (calcite will react and stain pink, dolomite remains unstained). B: PPL, C: XPL. dol=dolomite, calc=calcite. The red arrows are pointing to the dolomite and calcite which has replaced a scleractinian coral. There is no visible porosity.

Lithofacies 4: Sponge reefal Floatstone-grainstone

Lithofacies 4 (Table 5.1) (Fig. 4.6 A, B and C) is classified as a sponge reefal floatstone-grainstone (Dunham 1962). It is present within the Panuke H-08 core from approximately 3452 m – 3446 m (6 m), however that measured depth of core is inaccurate due to the core being very broken and sampled. There is only less than 1 m of cored interval of lithofacies 4. This limestone lithofacies is light brown/beige in color and has abundant bivalves, bryozoans, brachiopods and crinoids, as well as stromatoporids. The intervals that are closer to a floatstone, have very coarse grains (1cm – 5cm), comprised of predominantly oncoids. There are large coral fragments (~20cm) throughout. There are brecciated intervals. Calcite is also present within this lithofacies, commonly infilling vugs, there are also calcite veins. The vugs were most likely a result of the dissolution of the non-replaced limestone, or by the dissolution of more soluble particles. The thin sections from Panuke H-08 have been cut slightly thicker (~50 μm) and do not have a cover on the thin section, skewing some of the optical properties. From microfacies analysis (Fig. 4.6 B and C), this

lithofacies exhibits predominately silicisponges and a large scleractinian coral. From thin section alone, this lithofacies would appear to have more of a boundstone texture (large sponge section was sampled), however when compared to the core, the lithofacies has more grainstone characteristics.

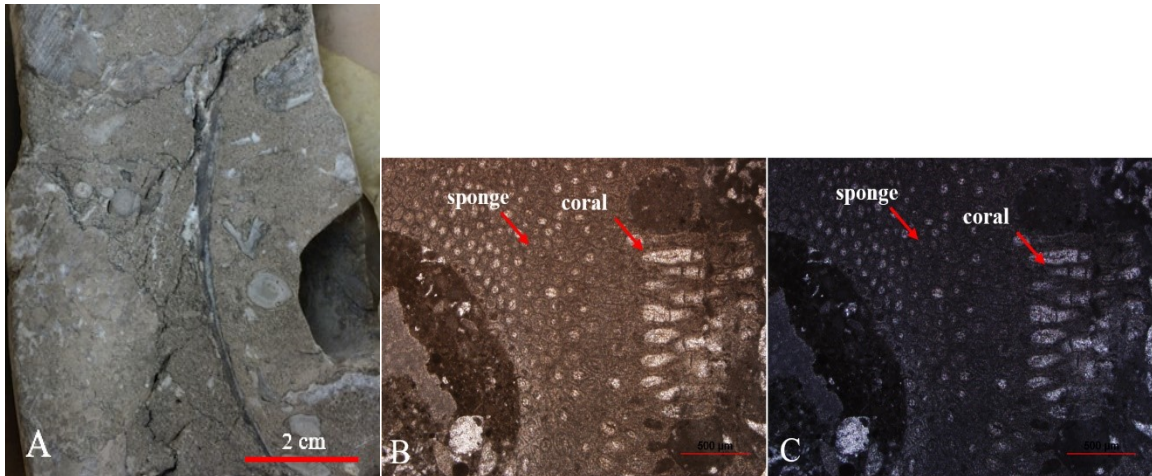


Figure 4.6 A, B and C: *A: Panuke H-08 core 1, at approximately 3450.7m depth. Coral, bivalve, and brachiopod fragments. Argillaceous material within a micritic matrix. Thin sections from Panuke H-08 representing lithofacies 4, TCH08-3, 3446m MD, 2.5x magnification. B: PPL, C: XPL.*

Lithofacies 5: Echinoderm Grainstone

Lithofacies 5 (Table 5.1) (Fig. 4.7 A, B and C) comprises echinoderm grainstone (Dunham 1962) and is present within the Panuke H-08 core from approximately 3460 m – 3452 m. However, like lithofacies 4, there is only less than 1 m of cored interval of lithofacies 5. Compared to lithofacies 4, lithofacies 5 has fine-medium grains (<1 mm) of predominantly echinoderm fragments, however, there are abundant disarticulated bivalves and brachiopods. The grains are all in contact. The matrix is composed of micrite. There are oncoids and ooids present as well as calcite appearing in veins and vugs. The sections had an abundance of disarticulated brachiopods and bivalves. Echinoderms and crinoids were also abundant, with minor amounts of bryozoans, and various benthic foraminifera. The sampled interval had a micritic matrix and shows little evidence of dolomitic diagenesis.

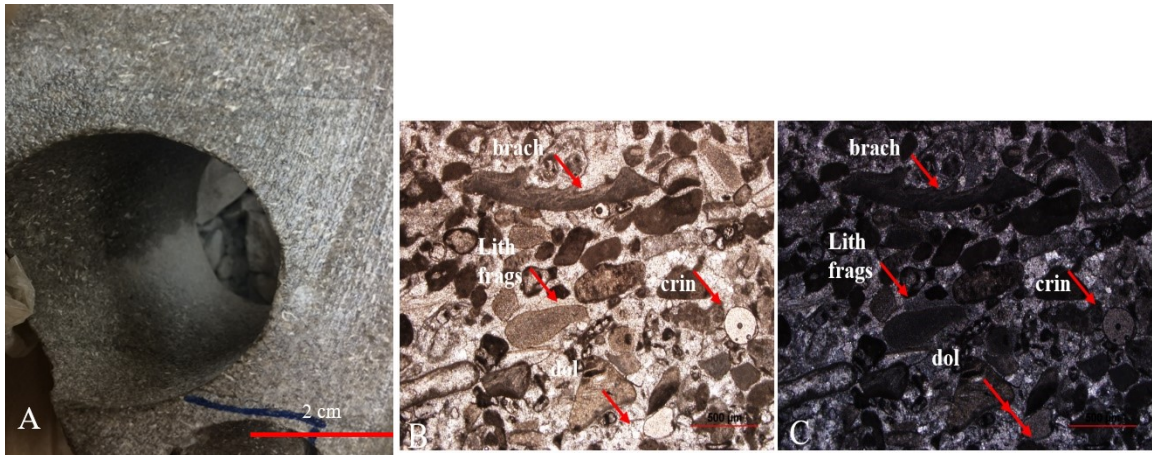


Figure 4.7 A, B and C: *A: Panuke H-08 Core 1, at approximately 3457.5m depth. Fine, broken up bivalves and brachiopods. There is calcite throughout. Thin section from Panuke H-08 representing lithofacies 5, TCH08-1, 3457.5m MD, 2.5x magnification. B: PPL, C: XPL. lith frag= lithics fragment (lithic clasts), dol=dolomite, brach= brachiopod, crin=crinoid.*

Lithofacies 6: Oolitic Mudstone

Lithofacies 6 (Table 5.1) (Fig. 4.8 A, B and C) is a oolitic mudstone (Dunham 1962) present within the Panuke M-79 cored interval from approximately 4537.8 m – 4532.7 m (5.1 m). This limestone lithofacies is dark grey to black in areas, with approximately 20% argillaceous materials. There are abundant ooids, representing approximately 70% of the fossil assemblage. There are also crinoids, bivalves and lithoclasts, which are interpreted to be quartz. The quartz lithoclasts are sub-rounded and poorly sorted, and appear in small laminations (<1 cm thick). These intervals can contain lithoclasts of approximately 6 cm in length, are considered to be more of a packstone than a mudstone. There are small carbonaceous laminations, sometimes wavy and lenticular. The thin sections for Panuke M-79 has been cut slightly thicker (~50 µm) and do not have a cover on the individual thin section, skewing some of the optical properties. From microfacies analysis, this lithofacies has a micritic matrix, with abundant intraclasts, mixed with assumed very fine detrital quartz grains, rounded and well sorted with larger (250 µm) quartz clasts, angular-sub angular and poorly sorted. Minor micritized ooids occur throughout section. Also contains brachiopod fragments that have been replaced by calcite.

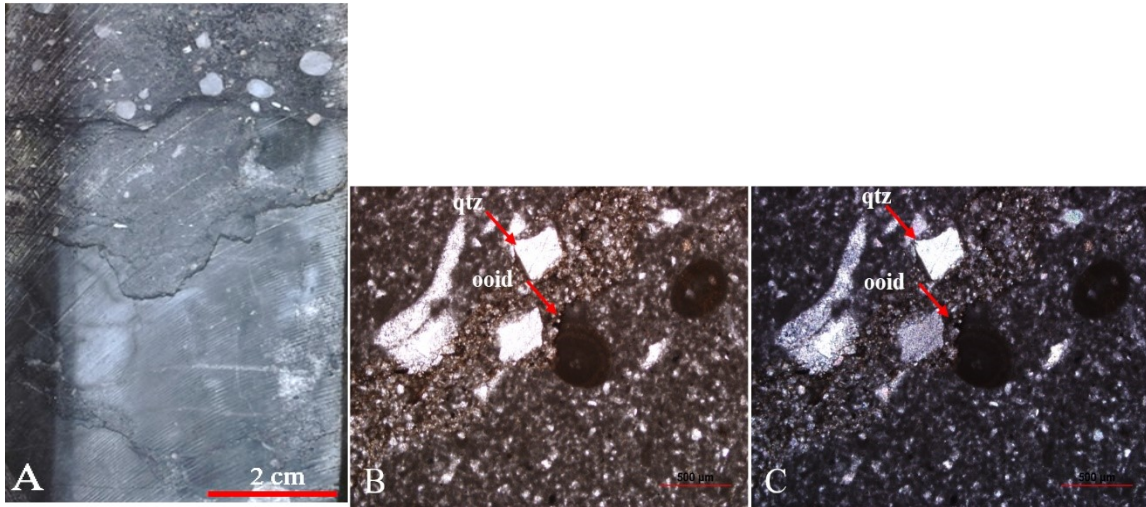


Figure 4.8 A, B and C: *A: Panuke M-79 core 1, at approximately 4532m depth. Dark grey mudstone with stylolites and quartz and calcite clasts, sub-rounded and poorly sorted, very fine to coarse grained. B and C: Thin section from Panuke M-79. Representing lithofacies 6, TCM79-4, 4532.5m MD, 2.5x magnification. B: PPL, C: XPL. brach=brachiopod, qtz=quartz.*

Lithofacies 7: Vuggy boundstone

Lithofacies 7 (Table 5.1) (Fig. 4.9 A, B and C) is characterized by vuggy boundstone (Dunham 1962) that can be found from approximately 4032.8 m – 4029.28 m within the Panuke PI-1A cored interval. Lithofacies 7 is light beige to white in color. Vugs are the main identifier of this lithofacies. It also has a crystalline cement. The skeletal fragments are difficult to identify due to complex dolomitic diagenesis, however it is interpreted to comprise stromatoporids and sponges. Porosity is estimated at approximately 5%, with predominately vuggy porosity. The thin section for Panuke PI-1A J-99 has been cut slightly thicker (~50 µm) and does not have a cover, skewing some of the optical properties. Only one facies was sampled for the Panuke PI-1A J-99 core, since it primarily comprised one lithofacies. This section has boundstone (Dunham 1962) textures, however it is affected heavily by diagenesis and is difficult to distinguish fossil materials and primarily comprises of dolomite. Little to no visible porosity throughout this section.

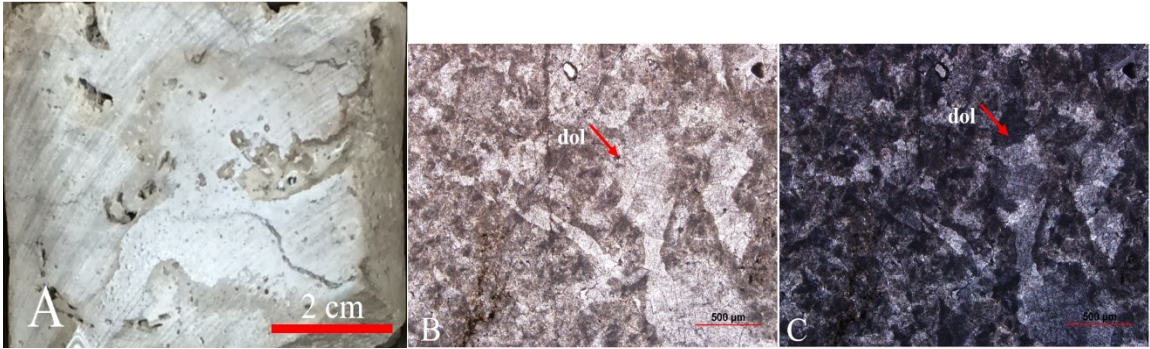


Figure 4.9 A, B and C: *A: Panuke PI-1A core 1, at approximately 4031.9 m depth. Predominately vugs with a crystalline matrix. Fossil assemblage is undistinguishable. B and C: Thin section from Panuke PI-1A J-99 representing lithofacies 7, TCPI1A-1, 4030.16m, 2.5x magnification. B: PPL, C2: XPL. dol=dolomite.*

4.3 Petrophysics

4.3.1 Well log Analysis

The ten main Jurassic well penetrations used for this study are summarized in Table 3.1, Section 3.3. These wells were used to tie seismic reflectors within the 3D MegaMerge and interpret the depositional environments and architecture of the depositional sequences of the Abenaki carbonate bank and the Sable Delta. A cross section of these ten key wells can be seen in Figure 4.10. The cross section is discussed further in Chapter 5, along with descriptions of the wells with TOC values.

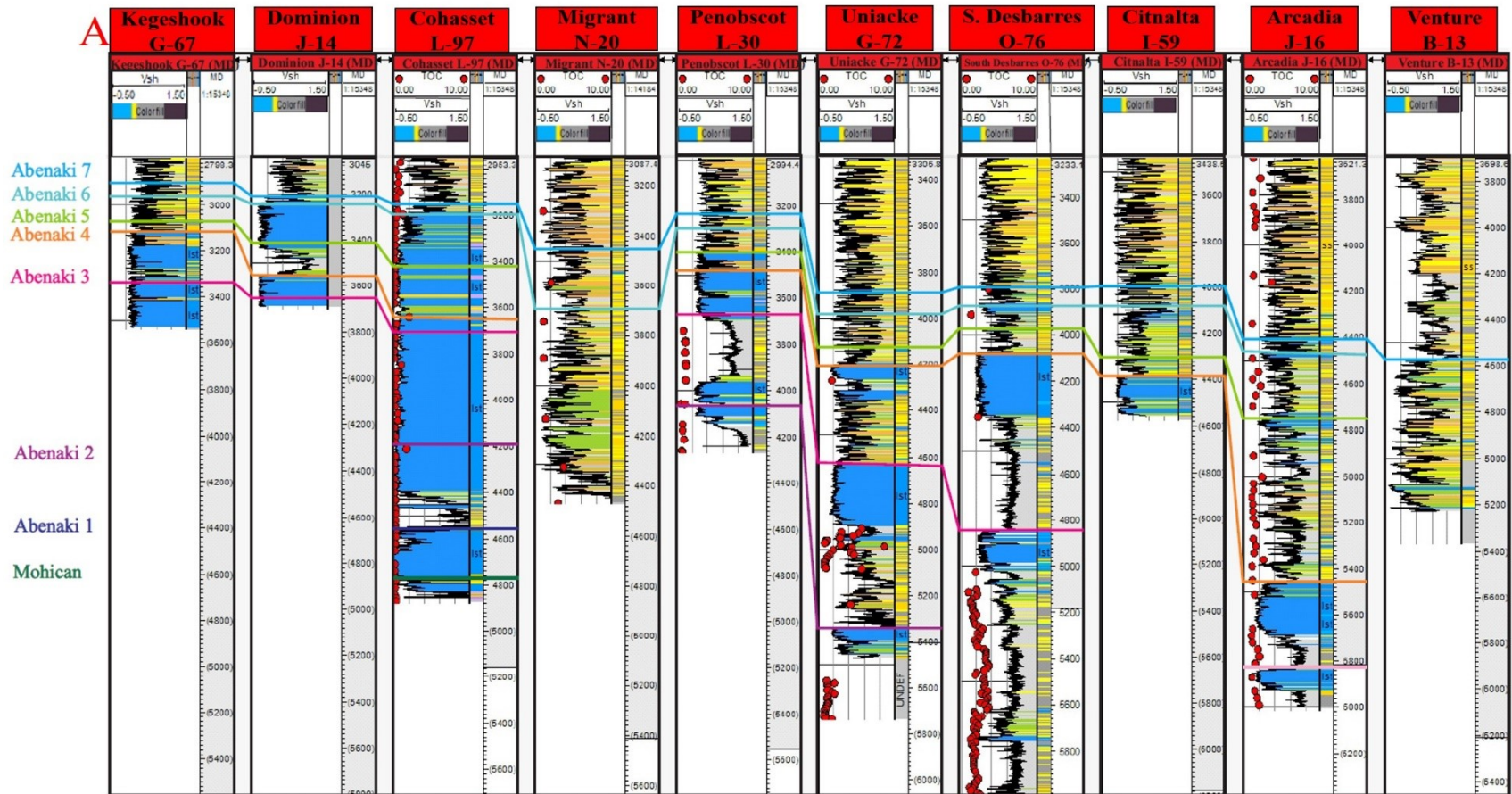


Figure 4.10: Key well log cross section. Blue, yellow and grey colored log are V-shale logs calculated from gamma ray logs. The color fill is from the Canstrat lithology log (based on cuttings). Blue=carbonates, yellow/green=sandier siliciclastics, grey=muddier siliciclastics. The red dots represent TOC measurements Cohasset L-97, Migrant N-20, Penobscot L-30, Uniacke G-72, South Desbarres O-76 and Arcadia J-16 (from the BASIN data base). The colored lines correlated across the wells represent the well tops of the seven third-order depositional sequences of the Abenaki carbonate bank and the top of the Mohican Formation, which can be seen at the base of the Cohasset L-97 well.

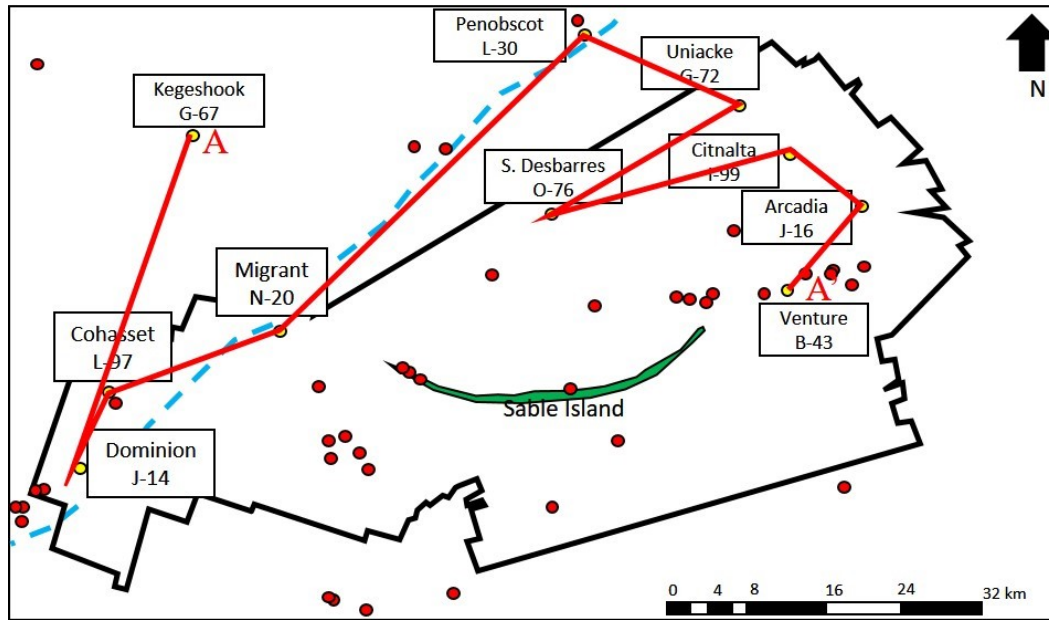


Figure 4.11: Location of wells for the cross section in Figure 4.10 (A-A').

4.4 Geophysics

4.4.1 Seismic interpretation: seismic facies

Ten distinct seismic facies were identified throughout the 2D and 3D seismic data from the basement to the top of the Abenaki carbonate bank and are summarized in Table 5.2 and shown in Figures 4.13 to 4.18. Figures 4.13 to 4.18 are seismic traverses from the west to east of the study area and show the transition from shelf, to shelf margin, to basin. Their orientation can be seen in Figure 4.12, A-A' to F-F'. The seismic traverses were chosen to show most of the key wells and seismic characteristics that aided in interpreting the depositional history of the Abenaki carbonate bank in relation to the growth of the Sable Delta (discussed further in Section 5.4.2). The seismic facies are intervals on the seismic data (Figs. 4.13-4.18) that share a suite of characteristics that represent similar signal-to-noise ratios, structural similarities, seismic reflection configuration, continuity, amplitude and frequency. The seismic facies were used to determine the variations of seismic parameters within the third-order depositional sequences, to infer lateral lithofacies changes. Seismic facies interpretations were calibrated from the lithofacies determined from well logs, core and cuttings.

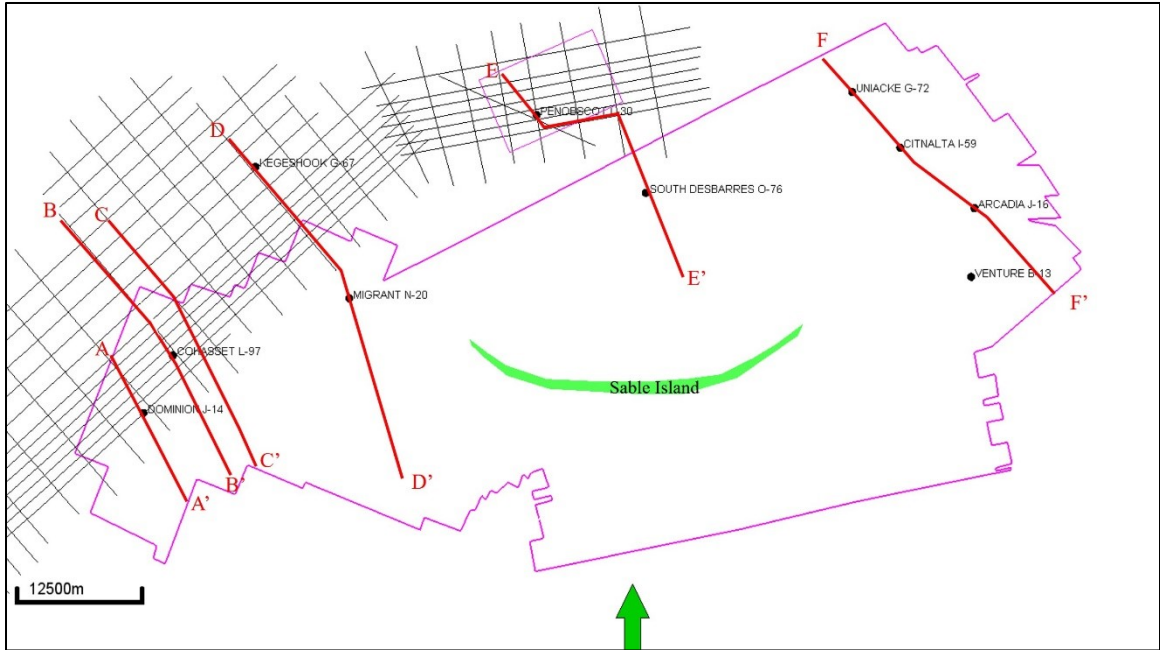


Figure 4.12 Location of the six seismic traverses seen in Figures 4.13 to 4.18. The seismic traverses were chosen to show the transition from shelf to basin (north to south and across the study (west to east). This was done to show the carbonate-dominated depositional system of the Abenaki carbonate bank within the western region of the Sable MegaMerge, transition to the mixed carbonate-siliciclastic depositional system in the east.

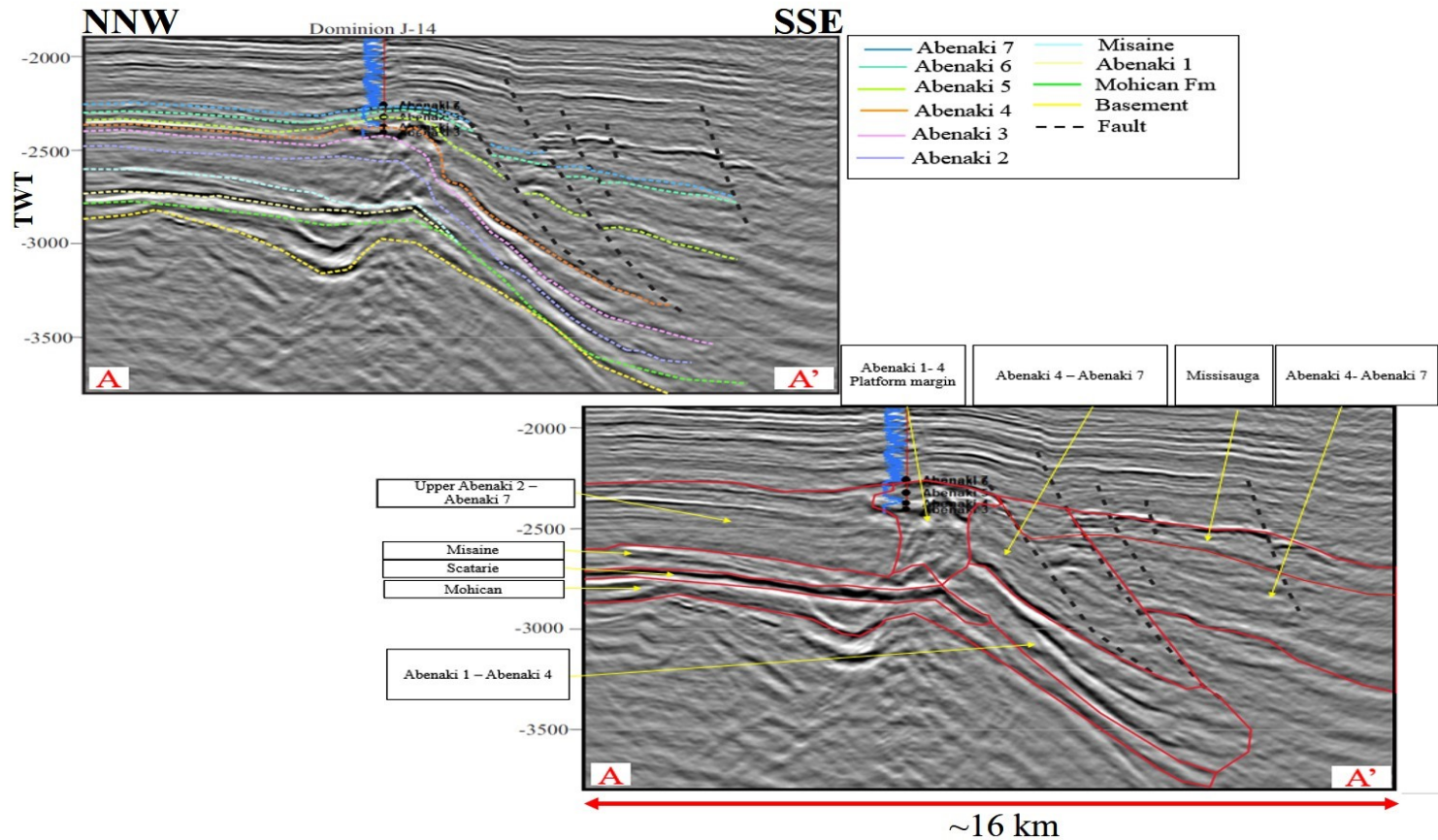


Figure 4.13: Seismic traverse showing the transition from the continental shelf margin where the carbonate platform grew, to the slope on the eastern edge of the study area. This line shows that this area was predominately carbonate dominated, even after the influx of siliciclastics from the Sable Delta, because the Dominion J-14 well is distal from the initial deltaic siliciclastic source in the northeast. Abenaki 5, 6 and 7 were able to grow on the bank margin and prograde onto the proximal foreslope. Bottom figure shows distribution of seismic facies and how they aided in interpreting depositional environments. Y-axis is TWT with a 5X vertical exaggeration. See Figure 4.12 for location.

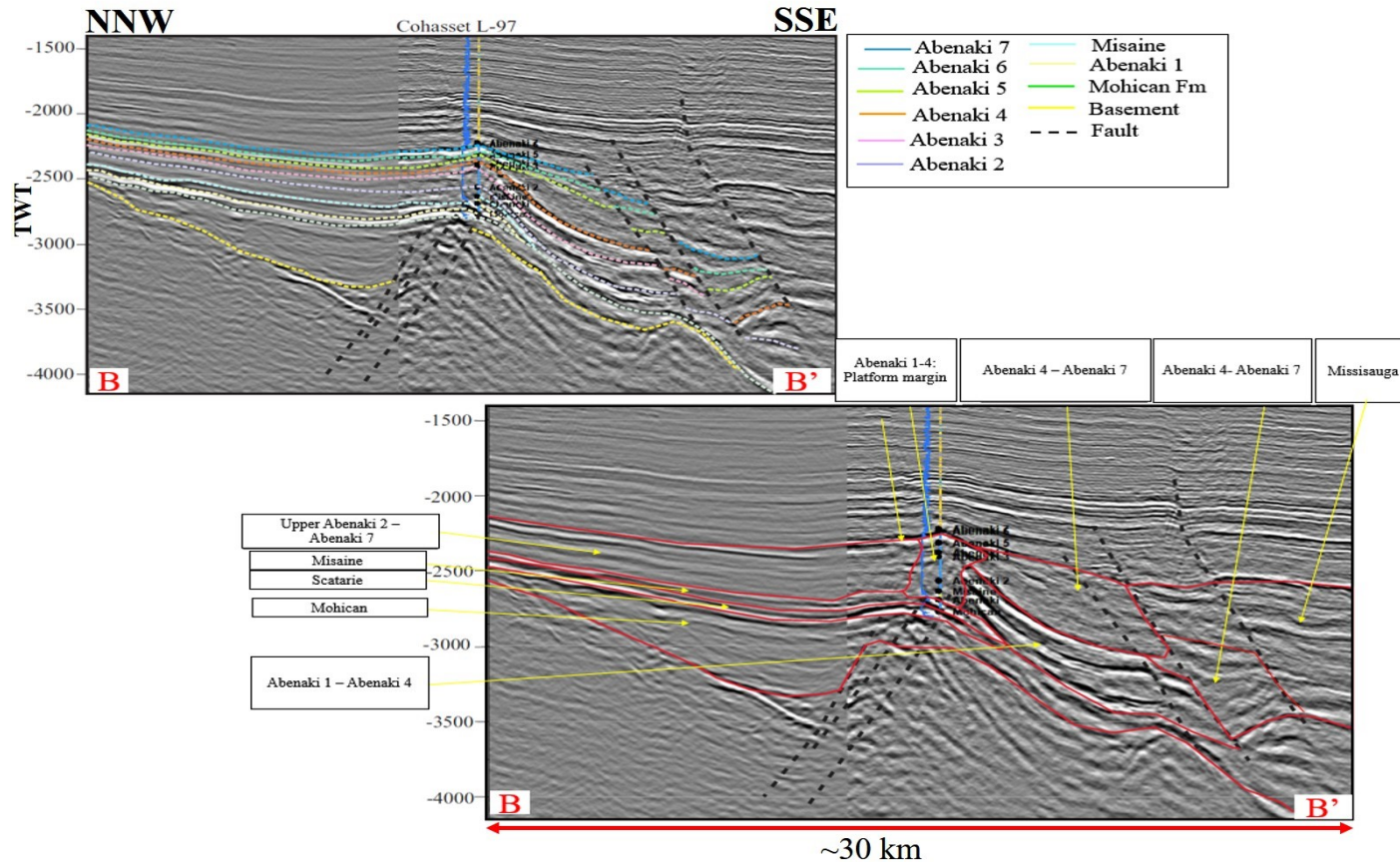


Figure 4.14: Seismic traverse showing the transition from continental shelf margin where the carbonate platform grew, to slope, to distal foreslope/deep basin within the east-central region of the study area. Carbonates were also predominately deposited within this region from the Middle Jurassic to Early Cretaceous, however there is more of a siliciclastic influence in Abenaki 5, 6 and 7 sequences interpreted by the lack of strong amplitude peak-troughs, and the sequences becoming thicker off the bank margin. Bottom figure shows distribution of seismic facies within the stratigraphic intervals. Y-axis is TWT with a 5X vertical exaggeration. See Figure 4.12 for location.

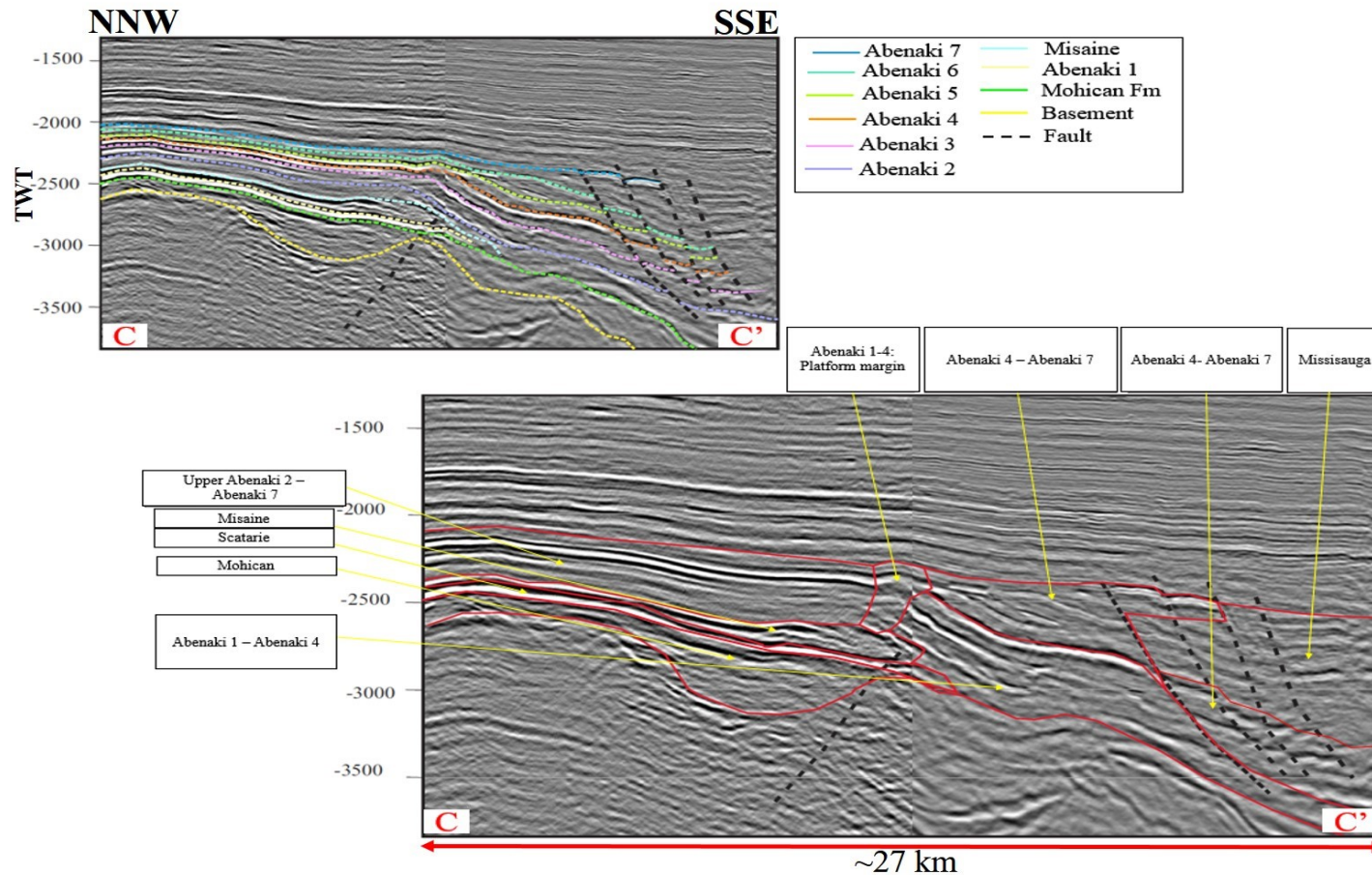


Figure 4.15: Seismic traverse close to the Cohasset L-97 well. This line shows the carbonates growing on the platform margin, becoming more influenced by siliciclastics on the slope, transitioning to mainly siliciclastics distally. The bottom figure shows the distribution of seismic facies within the stratigraphic intervals. Within the Abenaki 4 to Abenaki 7 mixed carbonate and siliciclastic seismic facies, small high amplitude carbonate reflections can be identified prograding distally as carbonate deposition kept up with sea-level. Y-axis is TWT with a 5X vertical exaggeration. See Figure 4.12 for location.

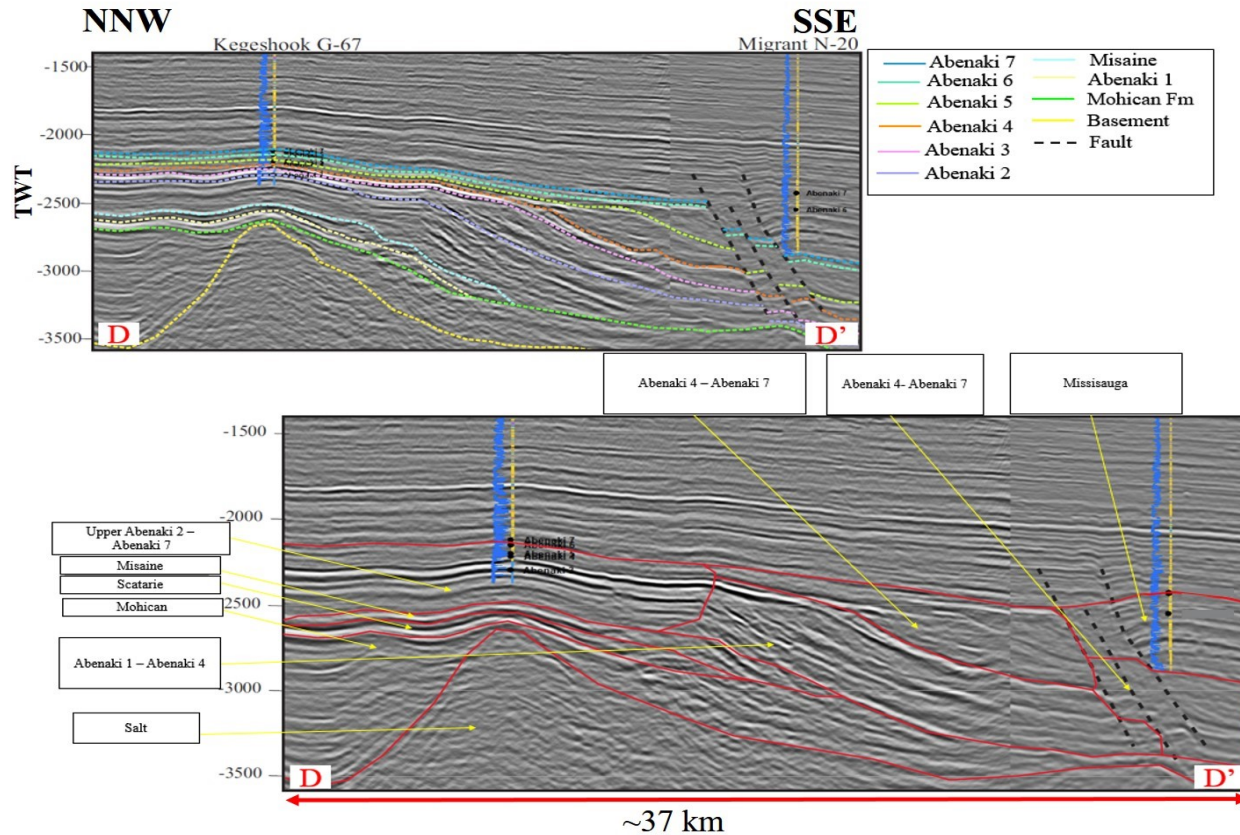


Figure 4.16: Seismic traverse showing the transition from continental shelf margin where the carbonate platform grew, through to the slope, to distal foreslope/deep basin within the central region of the study area. This line demonstrates the extent of the carbonate cycles basinward, and how the carbonate growth of Abenaki 5, 6 and 7 were all affected by the influx of siliciclastics. Migrant N-20 penetrated 1000 m siliciclastics, representing the beginning of the expansion trend as consequence of the influx of siliciclastics, causing sediment loading and salt withdrawal. It can also be observed that within the proximal platform interior, carbonates only grew until Abenaki 4 and it is not until the bank margin that Abenaki 5, 6 and 7 develop. Bottom figure shows distribution of seismic facies throughout the stratigraphic intervals. Y-axis is TWT with a 5X vertical exaggeration. See Figure 4.12 for location.

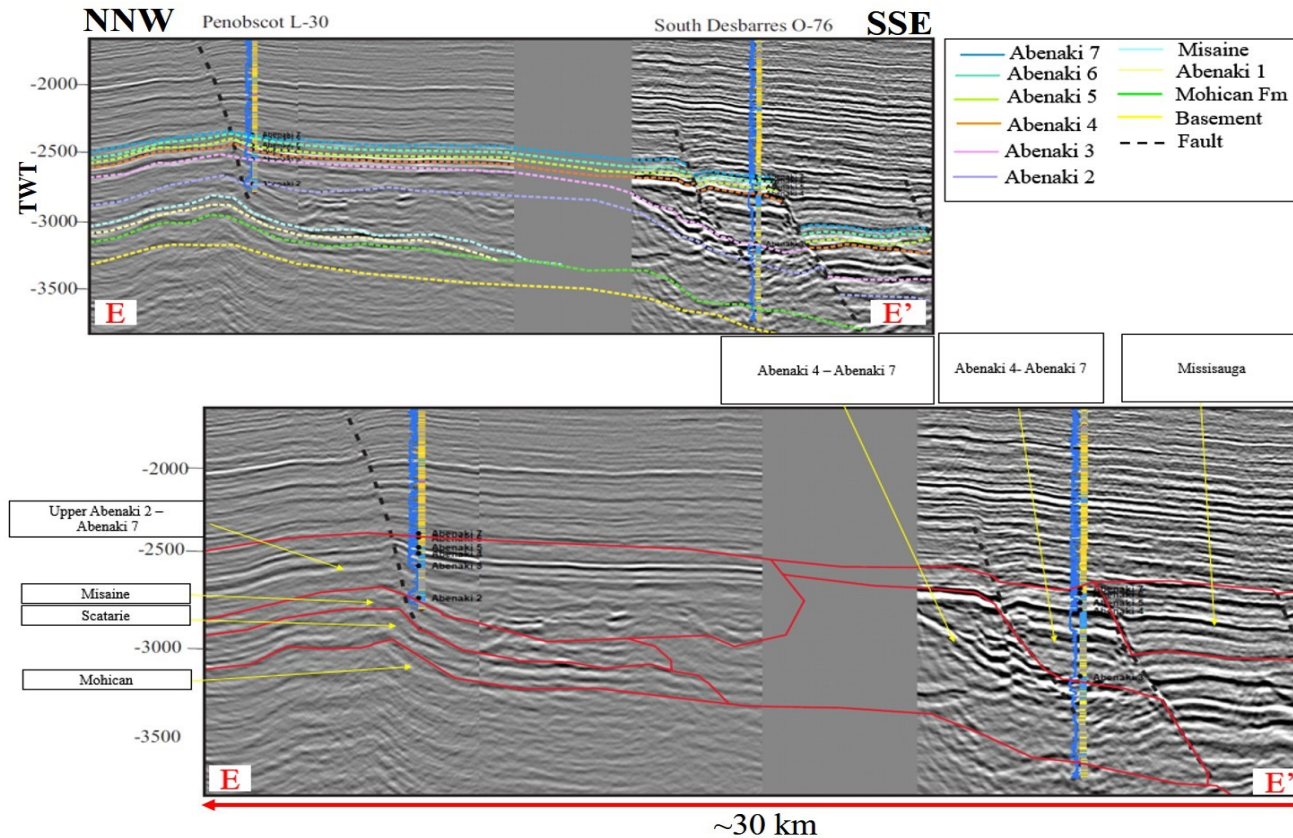


Figure 4.17: Seismic traverse showing the transition from continental shelf margin where the carbonate platform grew, to slope, to distal foreslope/deep basin within the western region of the study area. The grey area between the two wells represent a gap between the seismic surveys. This line shows that in the eastern region of the study area, near Penobscot L-30, the Abenaki bank only grew until the mid Kimmeridgian (Abenaki 4), and carbonates of Abenaki 5, 6 and 7 were only able to develop on the foreslope of the platform. South Desbarres O-76 penetrates the basinal Jurassic sediments, which has relatively high TOC values (discussed in Section 5.3.1). Bottom figure shows distribution of seismic facies throughout the stratigraphic intervals. Y-axis is TWT with a 5X vertical exaggeration. See Figure 4.12 for location.

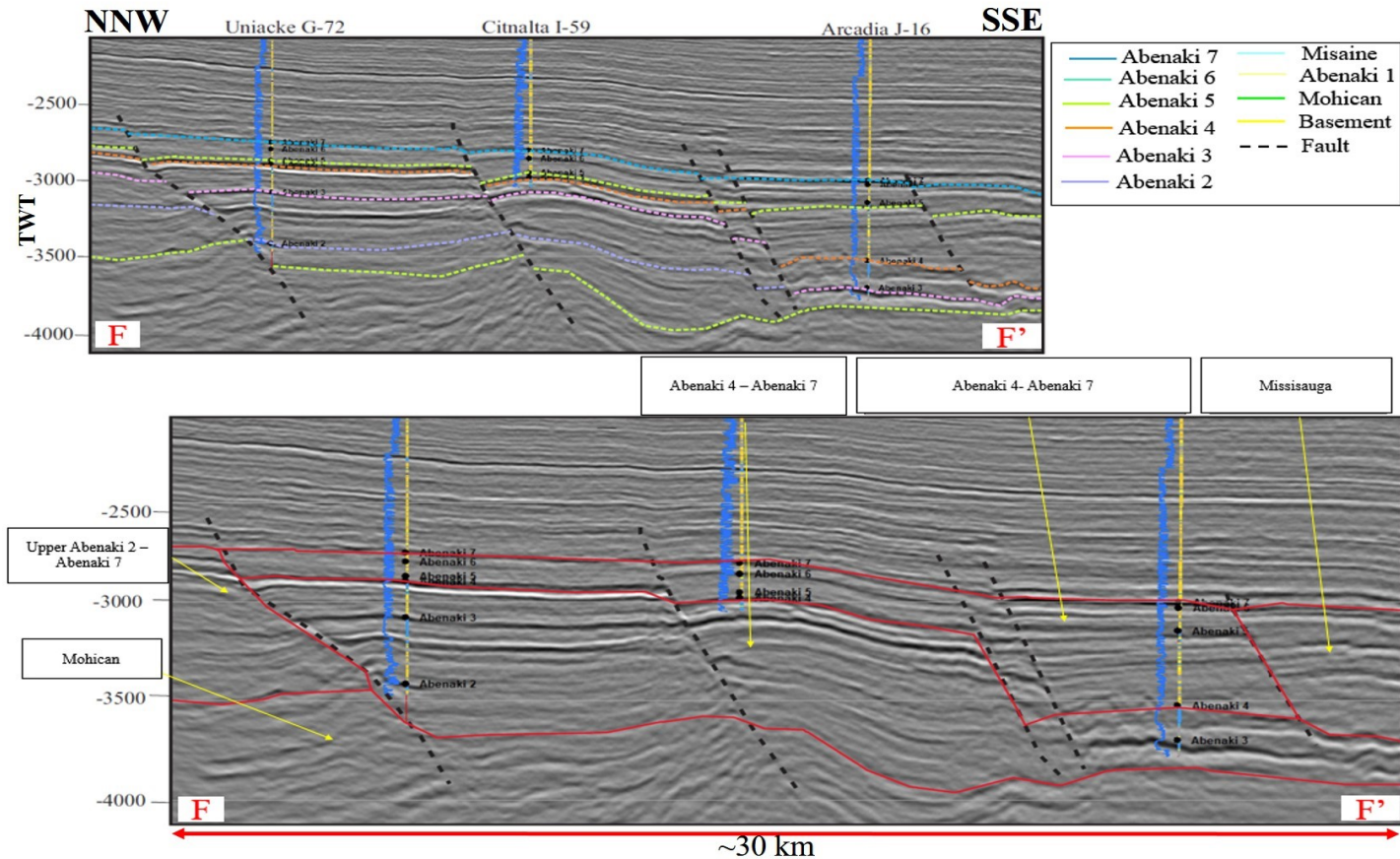


Figure 4.18: Seismic traverse showing the third-order depositional sequences of the Abenaki carbonate bank distally. This line in the southeast of the study area shows more siliciclastic influence amongst the sequences. All sequences have mudstones/shales at the base and prograde into carbonates at the top. Abenaki 5 to 7 are solely siliciclastic dominated with no carbonate growth. Both Uniacke G-72 and Arcadia J-16 have basinal penetrations of Jurassic sediment and have measured TOC values as discussed in Section 5.3.1. Bottom figure shows distribution of seismic facies throughout the stratigraphic intervals. Y-axis is TWT with a 5X vertical exaggeration. See Figure 4.12 for location.

4.4.2 Seismic interpretation: Horizons and faults

Seven third-order depositional sequences were mapped throughout the 2D and 3D seismic data. This was done primarily using the bright amplitude peak-trough pairs representing the top and bottom of a foreslope-basinal limestone interbedded with basinal mudstone (Fig. 2.9).

The majority of the seismic horizons are chronostratigraphic picks, however minor lithostratigraphic picks were correlated to map out the evolving carbonate bank edge within the study region, that were not included in the geocellular model. The top of the Misaine Member was also a lithostratigraphic pick. Eighteen seismic horizons were correlated from the Bajocian to the early Berriasian, throughout the northwest region of the Sable MegaMerge.

Within the west region of the Sable MegaMerge, 14 faults were interpreted and used in the subsequent geocellular model (Fig 4.19). The faults mapped within the Triassic-aged sediments were not used within the fault model due to being antithetic faults, which created major distortions of the pillar grid.

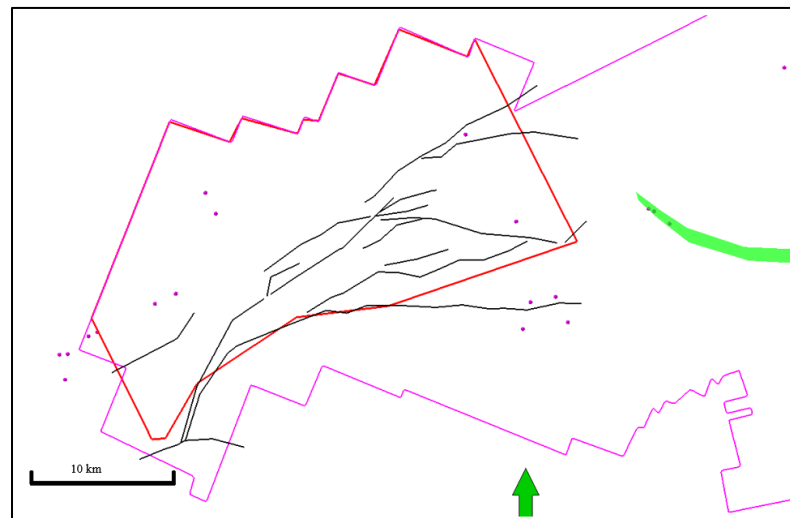


Figure 4.19: *Fourteen faults interpreted in the west region of the Sable MegaMerge within the Jurassic. The pink border is the boundary of the Sable MegaMerge and the red polygon is the geocellular model area.*

There is a lack of faults in the bank-to-basin transition, with the first major down-to-basin fault occurring approximately 10 km basinward of the reef front.

4.4.3 Genetic seismic inversion

The result of the genetic seismic inversion is a seismic cube in which each sample is a number representing a lithology (based upon Canstrat log) (Fig. 4.21), instead of a reflection amplitude.

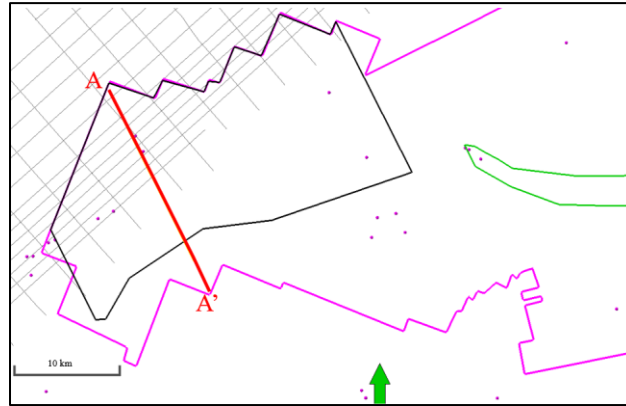


Figure 4.20: Location of A-A', which is the inline 3960, used for cross sections in Figures 4.21 and 4.22 and 4.25 and 4.26. Pink polygon is the 3D Sable MegaMerge area, the black polygon is the geocellular model area and the pink dots represent all the Jurassic well penetrations.

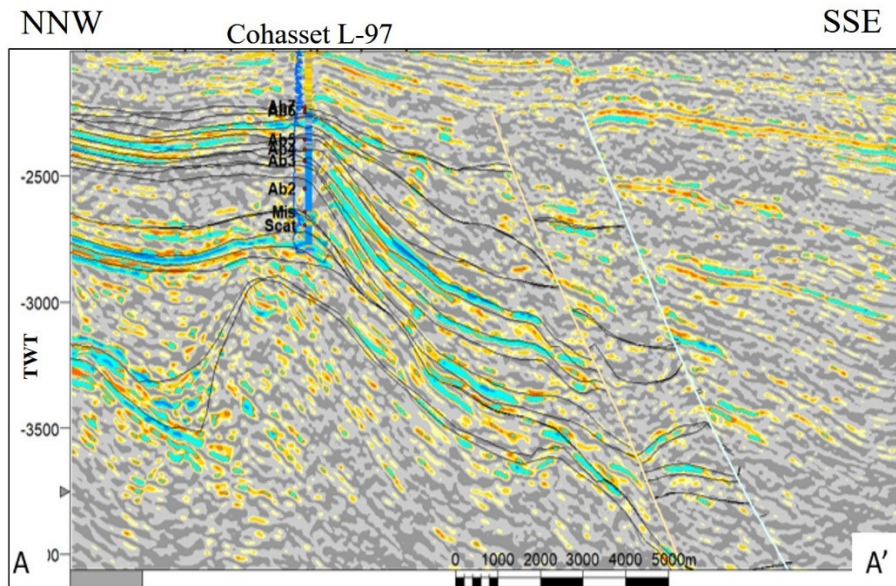


Figure 4.21: Vertical section (inline 3960, Fig. 4.20, 5X vertical exaggeration) showing the results of the genetic inversion. The genetic inversion matched the previously interpreted horizons quite accurately, giving confidence in the interpretations. The pale blue-to-dark blue are the carbonates, the yellow are the sandier siliciclastic intervals and the grey is the muddier siliciclastic intervals. The well on this inline is Cohasset L-97 with the gamma-ray and Canstrat lithology logs. Y-axis is TWT.

The genetic inversion results accurately matched the manually correlated horizons for the depositional sequences. The carbonates are represented by a pale-dark blue color, the sandier siliciclastics as a pale-dark yellow, and the muddier siliciclastics intervals as a pale-dark grey, using the color table that was created specifically for the genetic inversion. The siliciclastic intervals may have some uncertainties due to the inversion modeling of the seismic amplitudes from the lithological log. There is potential for a sand-rich interval to have lower, more chaotic reflections like the muddier intervals due to depositional conditions, therefore the inversion could model some sand-rich intervals as mud-rich and vice versa.

4.4.4 Depth model

An example of the depth model created from the velocity model that was described in Section 3.6.6 can be seen in Figure 4.22. From this model, approximate interval thicknesses can be estimated. For example, the approximate thickness of the interpreted proximal interval within the carbonate dominated shelf margin from Abenaki 7 (Early Berriasian) to the top of the Mohican Formation (Late Bajocian) is 2 km (purple arrow on Fig. 4.22). Distally, in the basinal equivalents, the thickness ranges from 2.5- 4 km (blue arrow on Fig. 4.22).

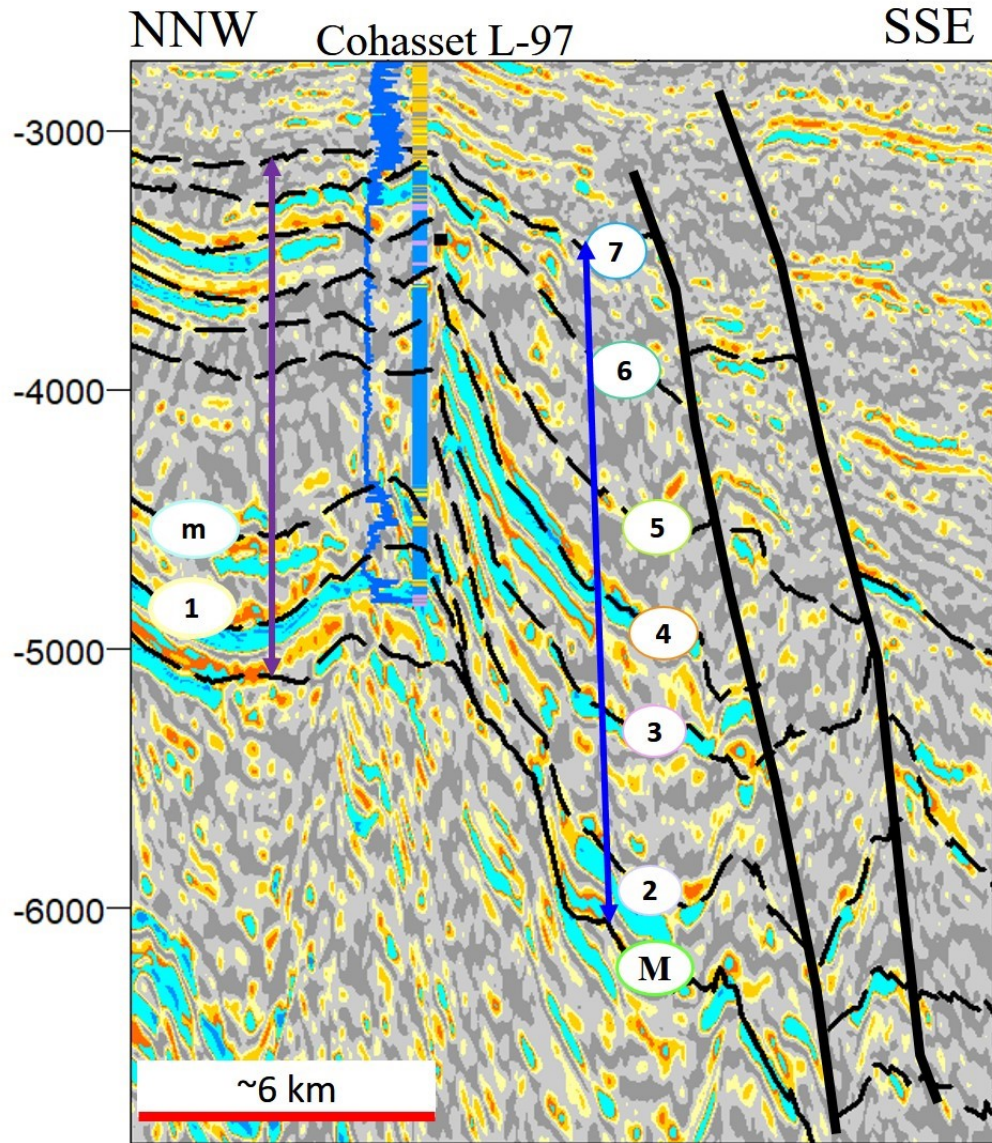


Figure 4.22: Vertical section (inline 3960, Fig. 4.20) showing the depth converted seismic from the genetic inversion. Red vertical lines represent two faults, and the black lines represent the tops of the interpreted carbonate cycles. The colors of the genetic inversion are the same as represented in Fig. 4.21. The Y-axis is depth in meters. The well is Cohasset L-97 with the gamma-ray (blue) and Canstrat lithology log. Y-axis has a 5X vertical exaggeration. Third-order depositional sequences labeled 1-7. Top of Misaine is marked as “m” and the top of the Mohican Formation is marked as “M”.

4.4.5 Geocellular framework results

Fault modeling results

Figure 4.23 shows the result of the fault modeling within the model area (red polygon).

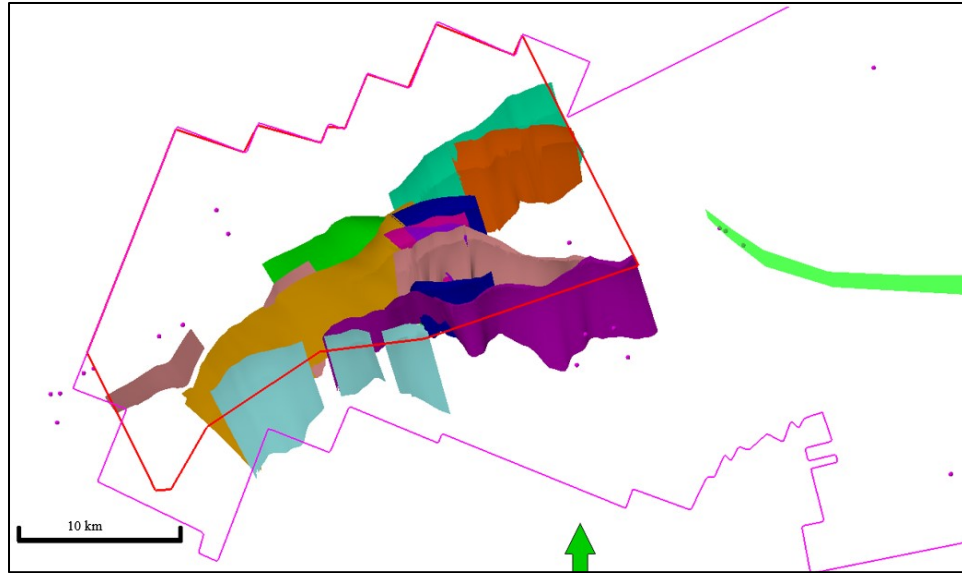


Figure 4.23: 3D display of fault interpretation model. The pink border is the boundary of the Sable MegaMerge and the red polygon is the model area. The faults generally trend northwest-southeast to west-east. 5X vertical exaggeration has been applied.

Pillar gridding results

Figure 4.24 shows the result of the skeleton grid from pillar gridding within the model area (red polygon).

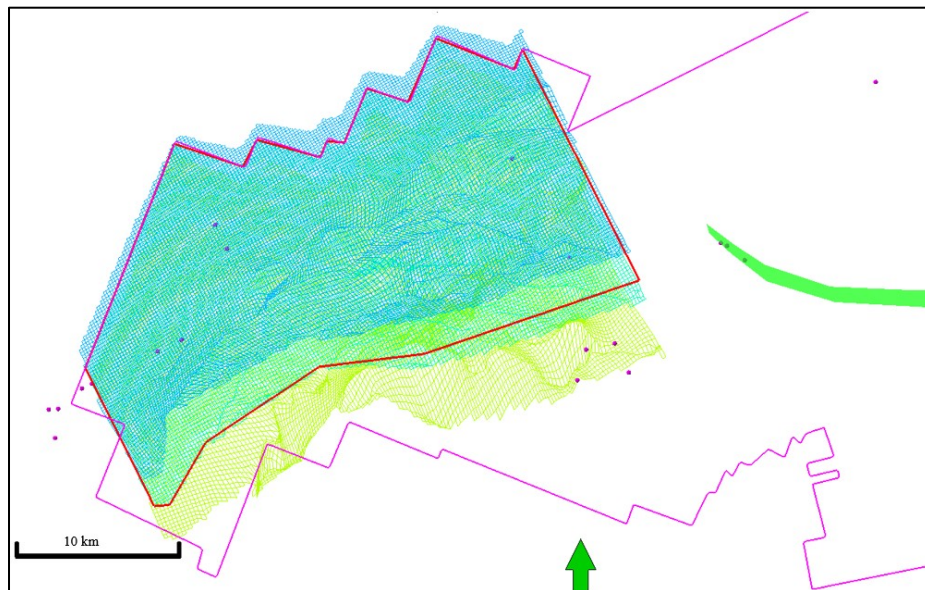


Figure 4.24: 3D display of pillar gridding. Top (blue), Mid (green), Base (yellow-green) skeleton grids. The red border is the boundary of the Sable MegaMerge and the purple polygon is the model area.

4.4.6 Geocellular model results

Zone index

Figure 4.20 shows the location of the seismic traverse used for Figures 4.25 and 4.26.

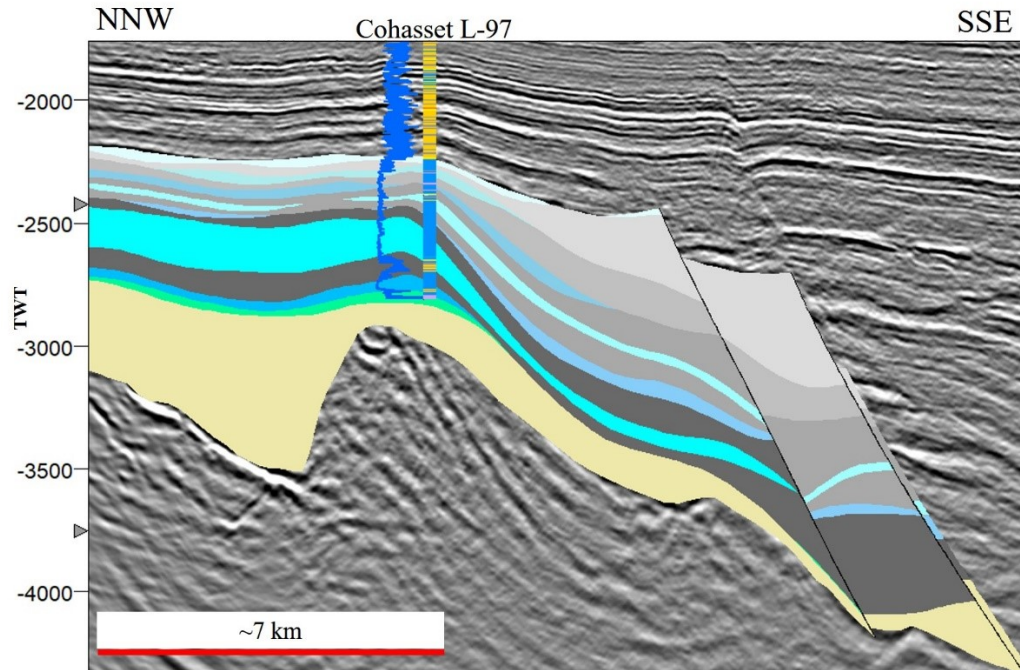


Figure 4.25: *Vertical section (inline 3970, Fig. 4.20, 5X vertical exaggeration) demonstrating the use of the zone index. Blue and grey colors are the chosen zones based on the horizons input into the model. The blues are the carbonates, whereas the greys are the clastics. The green is the Mohican Formation to the top of Argo Formation (salt=yellow) and the base of the yellow is the top of the basement. The well on this inline is Cohasset L-97, which drilled through most of the Abenaki carbonate bank. The logs are the gamma-ray (blue) and the Canstrat lithology. Y-axis is TWT.*

The zone index allows easy recognition of the interpreted carbonate cycles where the cycles transition from carbonates to siliciclastics, based on manual interpretation. It also aids in finding errors in the horizon and fault interpretations, which were corrected before extracting further information from the model.

Cell Height (Cell thickness)

Proximal to the Abenaki carbonate bank edge, the carbonate cycles all averaged approximately 15-40 m in thickness, when moving distally Abenaki 4 averages approximately 35 m thick within the study area. Abenaki 5-7 range from 0 m – 5 m thick, and Abenaki 1-3 range from 0 m – 25 m thick. The siliciclastic intervals thicken basinward, becoming over 1000 m thick.

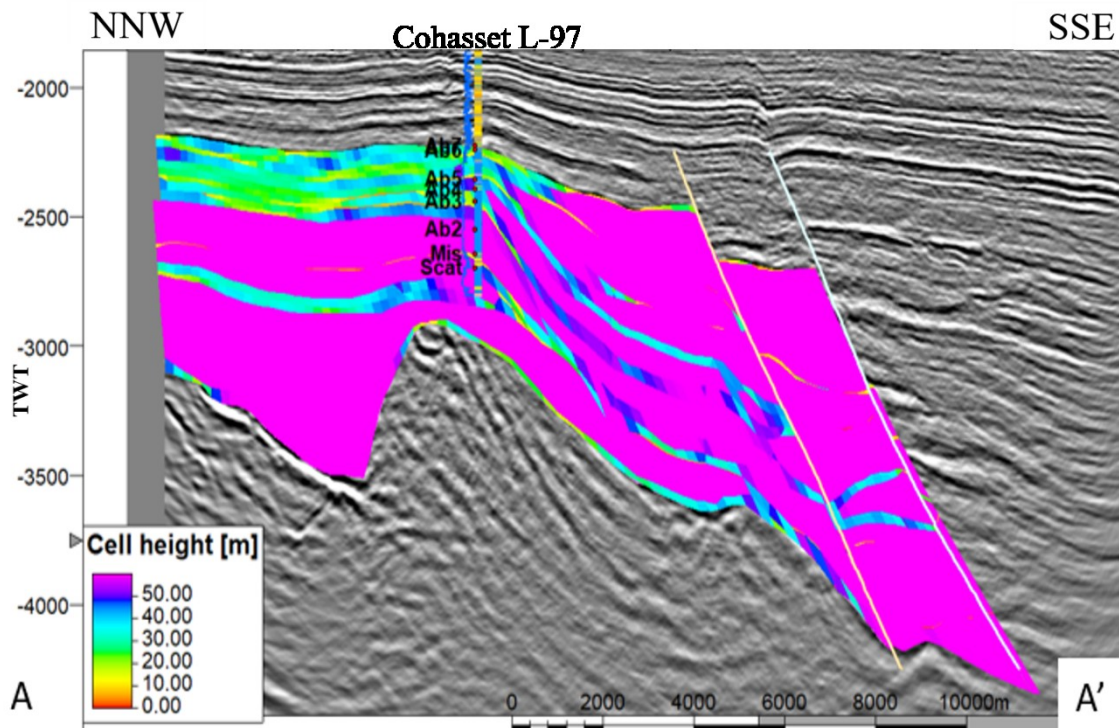


Figure 4.26: *Vertical section (inline 3970, Fig. 4.20, 5X vertical exaggeration) demonstrating the sequence thicknesses based from cell heights. The third-order depositional sequences are represented by the green-to-dark purple color, representing approximate thicknesses of 15 m -45 m. The light purple are the siliciclastic intervals, which range from 0 m – 1200 m in thickness. The well on this inline is Cohasset L-97 with the gamma-ray and Canstrat lithology logs. Y-axis is TWT.*

Genetic seismic inversion within geocellular model

The results of the geocellular depth model populated with lithologies are shown in Figures 4.27 and 4.28. These models show the proportions of carbonates to mudstones, within the carbonate dominated depositional system (Fig. 4.27) and the proportions of sandstone to carbonates and shales within the mixed siliciclastic, and carbonate depositional system (Fig. 4.28). From these models, depositional environments were interpreted down dip of the shelf margin and approximate water depths in which the sediments were deposited were estimated. The results from the geocellular model and how they were used to interpret the stratigraphic architecture, depositional environments and potential for source rocks are discussed in Chapter 5.

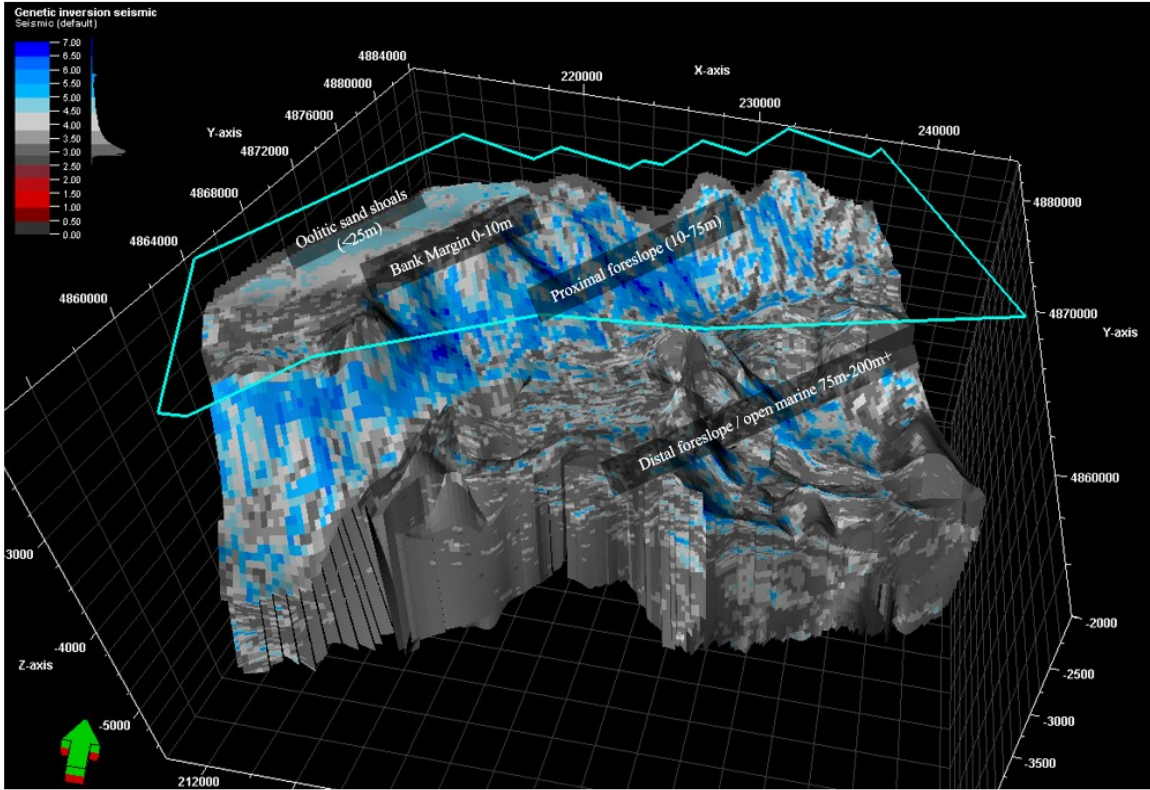


Figure 4.27: Geocellular model of the genetically inverted seismic data for the carbonate depositional system. The model bounded by the top of Abenaki 4, and by the top of the Mohican Formation. The blue polygon is the model area within the western region of the Sable MegaMerge. The color scale was manually created specifically for this geocellular model to represent the more mud-rich siliciclastic depositional system (pale-dark grey) and the carbonate cycles (pale-dark blue). Depositional environments and approximate water depths at time of deposition are labelled. 3D view to the north.

There are some uncertainties with the color tables of the resampled seismic that could vary the results of the model. The color tables were created separately for each model per depositional environment, however there may be more mud in the deltaic depositional system and more sand in the carbonate depositional system, however it was difficult to create a color table that represented both depositional environments in one model.

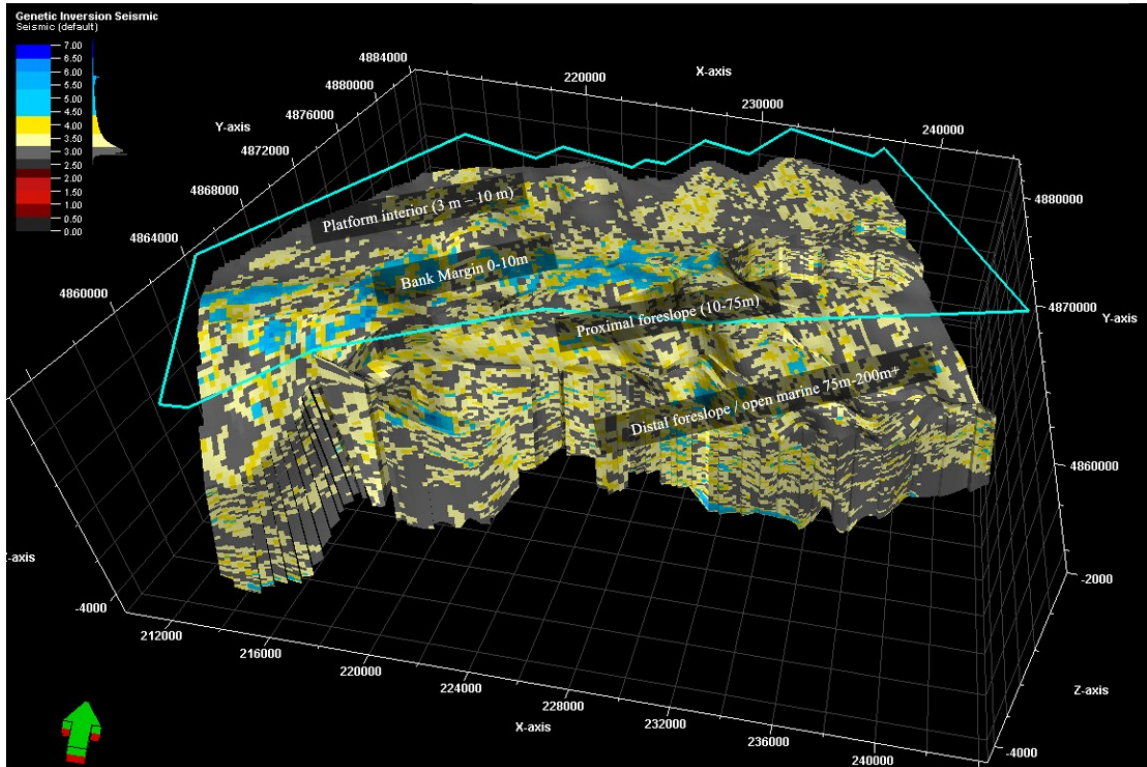


Figure 4.28: Geocellular model of the genetically inverted seismic data for the mixed siliciclastic and carbonate depositional system. The model bounded by the top of Abenaki 7, and by the top of Abenaki 4 third-order depositional sequence mapped throughout the study area. The blue polygon is the model area within the western region of the Sable MegaMerge. The color scale was manually created specifically for this geocellular model to represent the more sand-rich siliciclastic depositional system (yellow-dark grey) and the carbonate cycles (pale-dark blue). Depositional environments and approximate water depths at time of deposition are labelled. 3D view to the north.

Chapter 5: Discussion

5.1 Introduction

This chapter discusses the results presented in Chapter 4 and how interpretation of these results meets the study's objectives. It summarizes the geological interpretations made from the analysis of lithofacies in Table 5.1. These are incorporated into the discussion on the depositional environments basinward of the cored intervals. Chapter 5 also discusses the modern analog of the Fly River Delta in Papua New Guinea and the Great Barrier Reef offshore Australia to understand the mechanisms of a mixed carbonate-siliciclastic depositional system and demonstrates how this type of mixed environment has occurred in the past. Ancient analogs of the Moroccan Margin and the Lusitanian Basin are also discussed in terms of source rock potential.

The cross section of the ten key well logs is discussed with the TOC values for each well to determine if there is source rock potential within intervals down dip of the wells. This well cross section was crucial to understand the stratigraphic and lithologic changes of the third-order depositional sequences of the Abenaki Formation across the study area.

Table 5.2 discusses the characteristics of the seismic facies and how they were used to interpret the depositional environments across the study area. The intervals summarized in Table 5.2 correspond to the seismic traverses in Chapter 4 (Figs. 4.13-4.18). All the results from analogs, well logs, core, and seismic are then discussed in terms of the stratigraphic architecture of third-order depositional sequences of the Abenaki carbonate bank. Chapter 5 discusses the source rock potential of the distal shales of the Abenaki carbonate bank based on depositional models, analogs and seismic interpretation. This chapter also discusses a suggested revision to recently published stratigraphic charts in the Late Jurassic-Early Cretaceous (comparing Wade and MacLean 1990, Wach et al 2014 and Tari et al. 2012 to PFA 2011, Weston et al 2012, CNSOPB 2008). It also examines the multiple controlling factors on the growth of the Abenaki carbonate bank including; basement structures and an influx of siliciclastics from the Sable Delta. Uncertainties in seismic interpretation and source rock potential are reviewed at the end of this chapter.

5.2 Geology

5.2.1 Summary of lithofacies from core analysis

Table 5.1 is a summary of the lithofacies interpreted from core and microfacies analysis with their interpreted depositional environment.

Table 5.1: *Summary of lithofacies examined from core and petrographic examination.*

Lithofacies	Cored Intervals (m)	Texture and color	Fossil Assemblage	Diagenetic Alterations	Interpretation
Mudstone-wackestone	Cohasset L-97 (3414-3406)	Medium-dark grey color, massive, blocky subhedral calcite.	Scleractinian corals, bryozoans, benthic foraminifera.	Cementation by calcite overgrowth, some dolomite.	Lagoonal/shoal environment.
Brecciated wackestone-packstone	Cohasset L-97 (3419-3414)	Light-medium grey color, sparry calcite cement, massive and brecciated, vuggy.	Bivalves, crinoids, benthic foraminifera, peloids, sponges and branching scleractinian corals, bryozoans, annelid tubes.	Cementation by calcite overgrowth, some dolomite.	Proximal foreslope of an open marine carbonate bank. Brecciated from faulting after coral reef grew.
Crystalline mudstone	Cohasset L-97 (3425-3419)	Light grey color. Massive, vuggy with stylolites.	Scleractinian corals, bryozoans, bivalves, benthic foraminifera.	Cementation by calcite overgrowth, dolomite diagenesis. Stylolites formed from compaction calcite replacement of fossils.	Proximal foreslope of an open marine carbonate bank. Heavily faulted.
Sponge reefal floatstone-grainstone	Panuke H-08 (3452-3446)	Light brown/beige color, massive, vuggy.	Bivalves, bryozoans, brachiopods, crinoids, stromatoporids, oncoids, silicisponges, scleractinian coral.	Cementation by calcite overgrowth calcite replacement of fossils.	Shallow, back-reef environment rich in siliceous sponges and corals.
Echinoderm grainstone	Panuke H-08 (3460-3452)	Light brown/beige color, massive, vuggy.	Echinoderms, bivalves and brachiopods, oncoids, ooids.	Dolomitic diagenesis, micritization and calcite overgrowth.	Open marine carbonate bank, rich in coralgal sponge reefs.
Oolitic mudstone	Panuke M-79 (4537.9-4532.7)	dark grey to black color, small carbonaceous laminations (wavy and lenticular), massive in other intervals.	Ooids, crinoids, bivalves, lithoclasts (quartz), brachiopods.	Micritization and calcite overgrowth.	Open marine carbonate bank, back-reef, lagoon with sporadic influxes of siliciclastic debris.
Vuggy boundstone	Panuke PI-1A (4032.8-4029.3)	Light beige to white color, vuggy, massive, crystalline cement.	Stromatoporids and sponges.	Cementation by calcite overgrowth and calcite replacement of fossils.	Shallow, back-reef, open marine carbonate bank rich in skeletal debris.

5.2.2 Modern Analog: Great Barrier Reef and Fly River Delta

A modern analog was used in this study to understand the co-existence of a carbonate depositional system and a deltaic depositional system in close proximity. Australia's Great

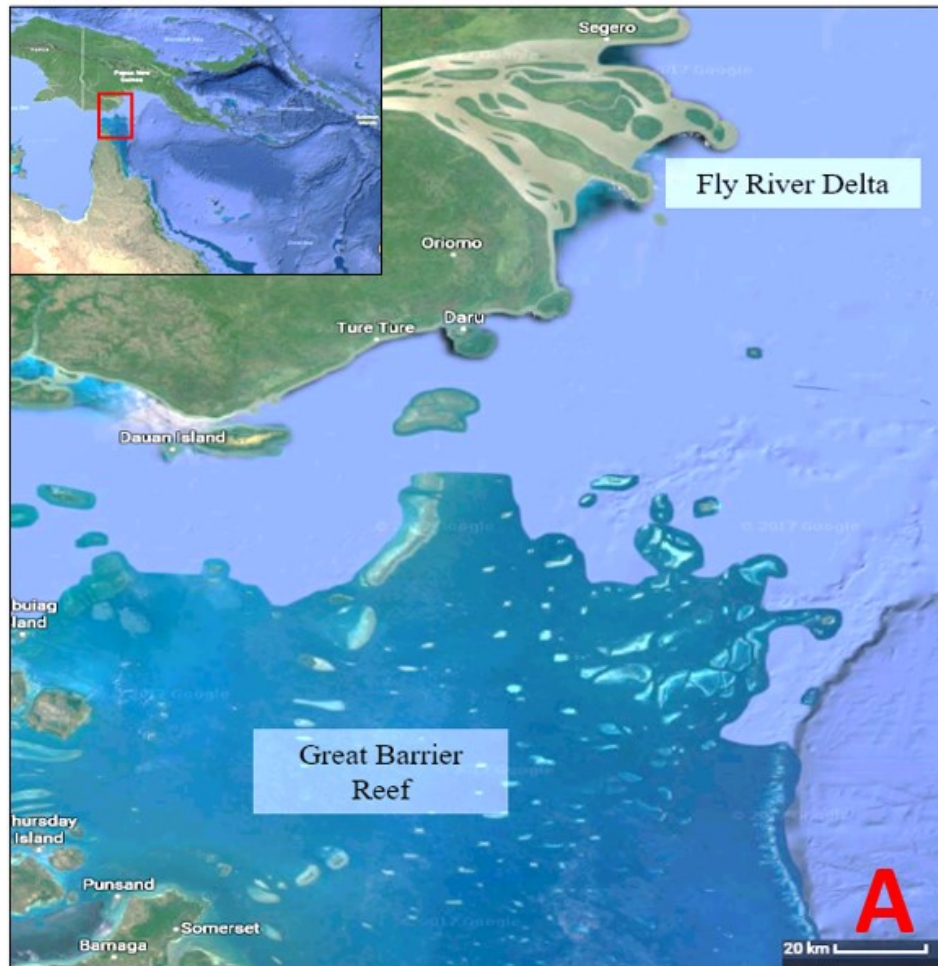
Barrier Reef system is the longest modern coral reef in the world. It terminates to the north in the large Fly River Delta in the Gulf of Guinea. The Fly River is the second longest river in Papua New Guinea at 1,050 km long. The delta of the Fly River is over 100 km wide at the entrance and 11 km wide at the apex (Canestrelli et al. 2010).

The Great Barrier Reef comprises over 2,900 individual reefs and 900 islands stretching 2300 km over an area of 344,400 km² (De'ath et al. 2012). The northern Great Barrier Reef is made up of carbonate banks (approximately 20-30 km long), atolls and pinnacle reefs making up small reefal islands (ranging from approximately 1-10 km long). The delta discharges sediment up to 30-40 km beyond the present-day shoreline limiting the northward development of carbonate banks and creating a mixed carbonate-siliciclastic depositional system basinward. This analog is similar to the interbedded carbonates and siliciclastics ramp packages interpreted within the Sable Sub-basin study area, as well as closer to the Sable Delta where thin carbonates are developed amongst the siliciclastic intervals.

It has been estimated that the total amount of sediment supply to the Gulf of Papua from all its rivers is 365 Mt yr⁻¹(metric tonne per year) (Milliman 1995), nearly six times the sediment yield of the rest of the continent of Australia (62 Mt yr⁻¹) (Milliman and Meade 1983). Given such a large regional supply of terrigenous sediment into the coastal ocean, it is surprising that many small reefs develop in the highly turbid waters south of the Fly River Delta mouth (Woolfe and Larcombe 1997). However it's been interpreted that the clockwise current gyre aids the deposition of small reefs (Francis 2008). The existence of these small reefs signifies that over a period of centuries to millennia, significant local accumulations of terrigenous sediment have not formed and that the water quality has been able to maintain at a level appropriate to allow reef formation and growth (Woolfe and Larcombe 1997).

Both the Fly River Delta/Great Barrier Reef and the Abenaki/Sable Delta comprise a mixed siliciclastic and carbonate depositional system. Within the Fly River Delta/ Great Barrier Reef system, a clockwise current along the shelf is capable of moving sediment to the northeast, extending the clinoforms to the shelf edge (Francis 2008). For the Abenaki/Sable Delta system, it is postulated that the direction of the ancestral Gulf Stream, caused currents

to drive prodelta shales northeast, away from the Abenaki carbonate bank, and transport basinal muds along the shelf slope from the southwest to northeast outboard of the carbonate bank (Eliuk 2014). The evolution of passive margins from rifting, development and termination of carbonate systems, and the burial of carbonates by prograding siliciclastics, is not unique to the Fly River/Great Barrier Reef and can be observed in other low-latitude regions over geological time (Tcherepanov et al. 2006).



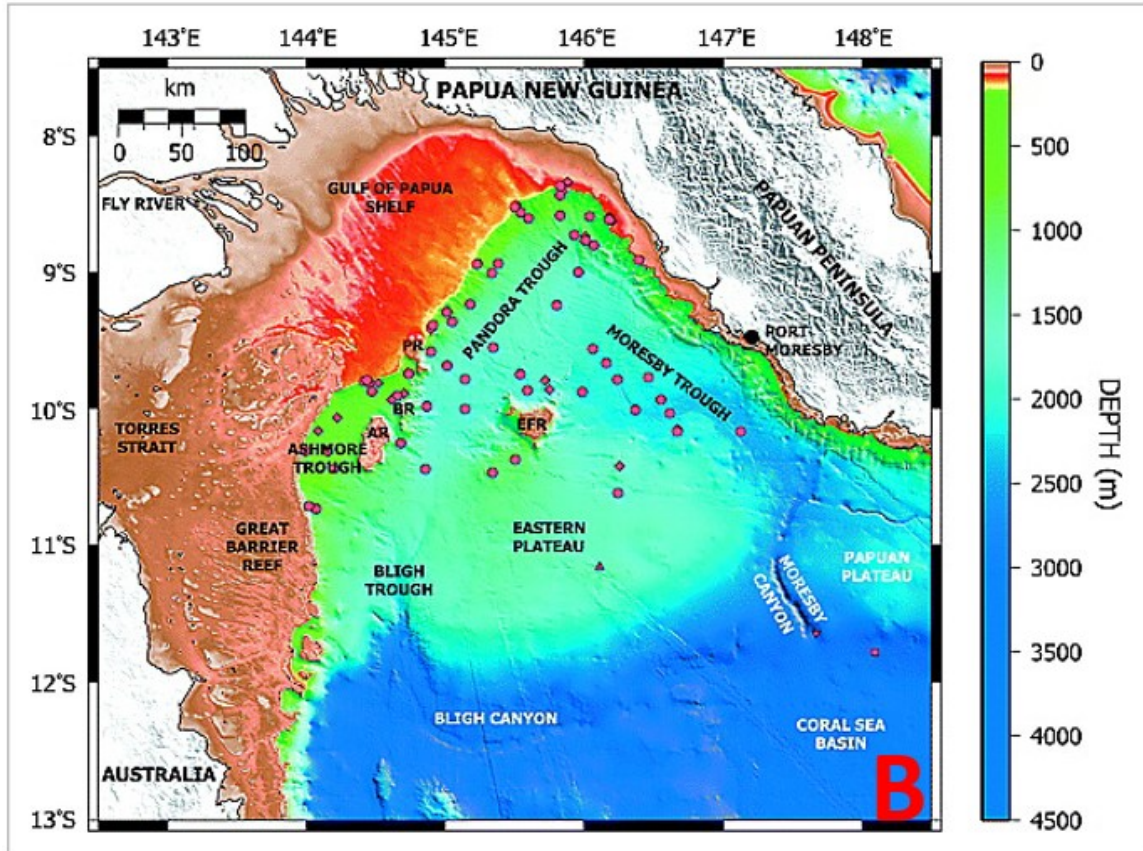


Figure 5.1 A and B: Both show the locations of the northern extent of the Great Barrier Reef, offshore Queensland, Australia in relation to the Fly River Delta located on the southeastern region of Papua New Guinea. A: The top left inset is the location of the zoomed in area (red rectangle) represented by the larger image (Google Earth, 2017). B: Similar location shown as in Figure 3.17 A, however larger scale and depth in meters (Francis et al. 2008).

5.2.3 Ancient analogs: Lusitanian Basin and Moroccan Margin

As discussed in Chapter 2, The Lusitanian Basin and the Moroccan Margin have many stratigraphic similarities within the Triassic and Jurassic to that of the Scotian Basin. The Essaouira Basin is the most important onshore, hydrocarbon-generating basin in western Morocco. Seven producing or shut-in oil and gas fields have been discovered, six produce from the Jurassic and one from Triassic reservoirs (Broughton and Trepaniér 1993). Modeling of the basin and geochemical analysis suggests that hydrocarbons were generated from at least two source rocks, one within the Jurassic (Oxfordian) shale accumulated in the Neknafa syncline, and the second being a deeply buried Carboniferous coal underlying the eastern area of the basin (Broughton and Trepaniér 1993). The Oxfordian shale was

buried deeply in western Essaouira and generated abundant gas and condensate liquids, and expelled them into structurally close reservoirs in the Jurassic strata. There has also been an oil show within one well (Guettatta) in the onshore Essaouira Basin, with an uncertain source origin, although it has been suggested that it is sourced from a Jurassic (Toarcian) carbonate source rock (e.g. Sachse et al. 2012). Further description of the Moroccan Margin can be found in Chapter 2 and Appendix A.

The Lusitanian Basin is known for the remarkable quantity and quality of its outcrops. Field work was conducted on the Jurassic carbonates of the Lusitanian Basin. Large scale depositional patterns were interpreted through outcrop description. Field work also allowed hands-on experience in carbonate sedimentology, which was central to interpreting the carbonate deposits offshore Nova Scotia properly through seismic and core.

The outcrops studied within the Lusitanian Basin are highlighted (Fig. 5.2). Outcrops from the Jurassic along the western coast of Portugal included; Cabo Mondego, Figueira da Foz, Pedrógão, São Pedro de Moel, Nazaré and Peniche. Middle-Late Jurassic successions were also analyzed around Macico Calcario Estremenho. Outcrops around Coimbra, located in central Portugal, from the Late Triassic to Early Jurassic, were also studied.

Four locations with potential source rock intervals from the Early–Middle Jurassic were studied within the Lusitanian Basin. A detailed literature review of the organic-rich intervals that were studied can be found in Appendix A.

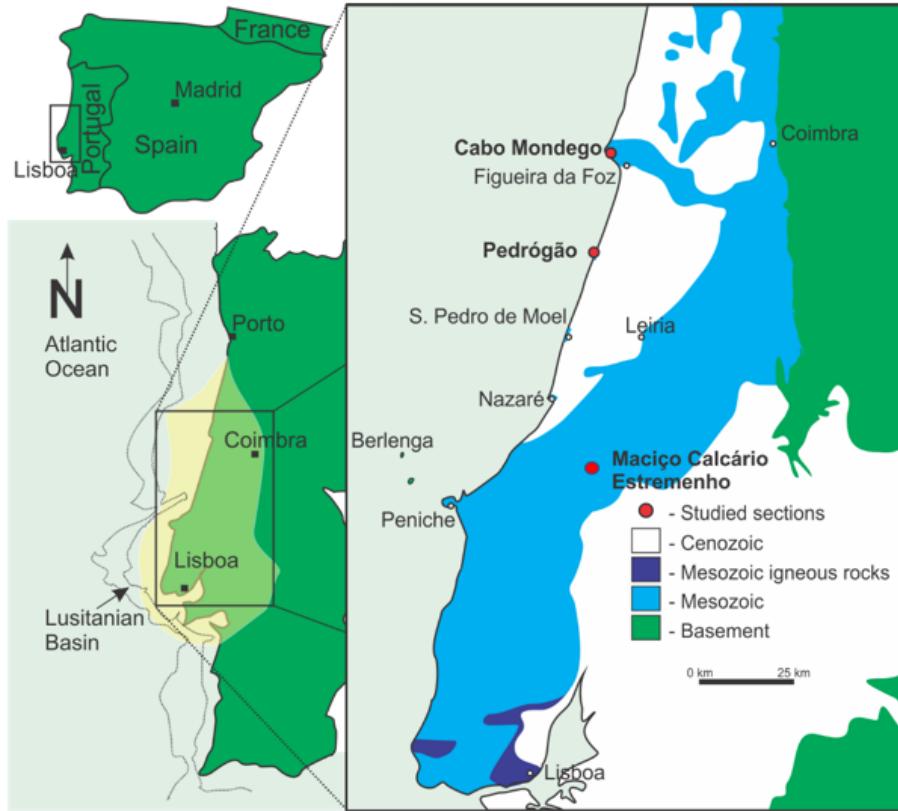


Figure 5.2: *Simplified geological map of the Lusitanian Basin, highlighting the locations of interest (Silva et al. 2014).*

5.3 Well log correlation and source rock sampling

5.3.1 Key well log cross section

The key well cross section in Chapter 4 (Fig. 4.10) is designed to show the progression of shelf to proximal foreslope to distal foreslope from west – east (A to A’): with the Migrant N-20 well located in a normal fault-bounded ‘expansion trend’ (e.g. Pe-Piper and Piper 2011) (Fig. 4.16).

Core from Cohasset L-97 and the gamma-ray log show that this well penetrates the entire Abenaki carbonate bank. The third-order depositional sequences of the Abenaki are difficult to distinguish from the well logs for this well due a succession of shallow water limestones with only minor incursions of basinal mudstones. Therefore, Cohasset L-97 shows little variations in radioactivity, velocity, density, etc. for the Abenaki Formation. Moving east and basinward from Cohasset L-97, the third-order depositional sequences of the Abenaki become more evident and shale-to-carbonate cycles can be observed. The

lithologies were confirmed from well logs, cuttings and core, and then mapped seismically throughout the study area.

Based on seismic correlations, the siliciclastics penetrated at Migrant N-20 are younger than Abenaki 6 sequence age (Fig. 4.16) (interpreted reflection correlated below the well) and are time equivalent to either the very last stages of carbonate growth, or post-date them (i.e., late Tithonian, early Berriasian). However, in the BASIN database; Ascoli (1979) has Valanginian to Oxfordian dating between 3200 m and 4203 m (total depth of well) in the Migrant N-20 well, which is inconsistent with seismic correlations. The same situation arises at Venture; Wade and MacLean (1990) made similar seismic correlations of the Abenaki 4 sequence post-dating the siliciclastics and carbonates above (Fig. 5.11), however faced a similar biostratigraphic discrepancy. The siliciclastics are re-worked by fluvio-deltaic processes in the Early Cretaceous eroding and redepositing Late Jurassic fluvio-deltaics (e.g. Weston et al. 2012).

Siliciclastics dominate the sequences above Abenaki 4 beyond the Cohasset L-97 well, signifying the Sable Delta limited the growth of the Abenaki carbonates to the east.

Total Organic Carbon values from key wells

Several studies regarding source rock potential within the Scotian Basin have been published by Mukhopadhyay (1991; 1994). Geochemical analysis, including RockEval pyrolysis and kerogen typing were completed by Mukhopadhyay (1994) on the Lower Missisauga Member, and the Mic Mac and Verrill Canyon formations on both core and cuttings. Mukhopadhyay (1990a) stated that TOC values measured from cutting samples were often contaminated from drilling mud additives, such as oil-based muds or lignites, which skew the RockEval data. Intervals which were turbo-drilled also show skewed results from producing smaller rock fragments, allowing additional contaminants from other intervals to be included, which would skew the weight percent calculations of the RockEval method (Mukhopadhyay and Wade 1990).

Well reports for the key wells in Figure 4.10, containing TOC measurements, were examined to understand if the TOC readings could indicate a potential source rock interval within the Middle to Late Jurassic or if the RockEval pyrolysis results could have been skewed due to the above-mentioned problems. A summary of each well containing TOC

data is below. Additional, detailed descriptions of the uncertainties of the RockEval results for the wells which penetrate to the Middle Jurassic within the Sable MegaMerge are discussed in Morrison 2017.

Cohasset L-97

TOC values for Cohasset L-97, seen on Figure 4.10, do not show any prospective source rock intervals within the Abenaki carbonate bank. Most of the TOC values are below 1%, except for two outliers (3620 m MD and 4220 m MD) that have TOC values of 2%. The occasional minor intervals with 2% TOC are unlikely to constitute a significant source, due to not being able to generate a continuous hydrocarbon phase.

Migrant N-20

The Migrant N-20 penetrated siliciclastics within the expansion trend, and not the Abenaki carbonate bank, it shows TOC values of 3.5% - 4% from 4200 m MD – 4500 m MD. From analysis of the well log report, there were no additives to the drilling fluids that would skew the TOC results, nor was the well turbo-drilled. If these TOC levels were present in sufficient quantity, this section could be a potential source rock.

Penobscot L-30

TOC values (<1%) for Penobscot L-30 seen on Figure 4.10 do not show any prospective source rock intervals for the Middle – Late Jurassic.

Uniacke G-72

TOC values for Uniacke G-72 in Figure 4.10, range from 1% - 8% within Abenaki 3. The well was turbo-drilled from 4832 m MD to 5142 m MD, potentially skewing the TOC values (Sine et al. 1984a). Numerous drilling fluids were also added throughout the drilling history of this well, including chrome lignite with cromex, lignosol, tannathin, weikseal, nutpluf, pilphase and pipelax, all of which could yield higher than actual TOC values. Since this well was turbo drilled and the samples were contaminated with drilling mud additives, it cannot be considered a reliable data point.

South Desbarres O-76

South Desbarres O-76 shows TOC values of 2-4% within Abenaki 3 in Figure 4.10. From 5343 m MD to 6006 m MD, the well was turbo-drilled (Sine et al. 1984a), potentially

adding contaminants into the cuttings. An oil-based drilling mud was also used for this well, which made geochemical analysis difficult, and is the possibly cause of higher TOC values. Since the well was turbo-drilled through the interval of interest, and an oil-based drilled mud was used, the TOC values are not considered to be reliable.

Arcadia J-16

The interval of interest on Figure 4.10 shows some TOC values of approximately 2-2.5%. However, this interval, from approximately 4400 m MD and ~6000 m MD was turbo-drilled, which likely introduced contaminants to the samples (Geochem Laboratories 1983a; Creybohm et al. 1983). Freshwater polymer with chrome lignite mud was used as the drilling fluid from 3023 m MD to 5904 m MD, which could have given skewed TOC values. The TOC values within the intervals of interest are not reliable due to the bit design (turbo-drilled).

5.4 Geophysics

5.4.1 Seismic facies

Descriptions of the seismic facies (described in Section 3.6.1 from Mitchum et al. 1977) and their geological interpretations are summarized in Table 5.2. Seismic traverses showing examples of the seismic facies can be seen in Section 4.4.1 in Figures 4.13 to 4.18. The seismic facies were used to interpret stratigraphic intervals of similar depositional environments, which are labeled in column three of Table 5.2.

Table 5.2: Summary of the ten seismic facies used for interpreting the seismic structural and stratigraphic framework. For examples of seismic facies from stratigraphic intervals see Figures 4.13 to 4.18. Table E-1 shows examples of the seismic facies from the 3D Sable MegaMerge.

Seismic Facies Characteristics	Geologic Interpretation	Stratigraphic Intervals
Low to high amplitude throughout study area. Parallel to sub-parallel, sometimes chaotic.	Lagoonal, platform interior, High amplitude bursts are low impedance, porous clastics, or dolomitized limestone.	Upper Abenaki 2 - Abenaki 7
Structural bump, contractional drape. Noisy, chaotic high amplitudes in low impedance zones.	Reef margin and basinal shale incursions. Transition between the reef margin and proximal foreslope. Typically resistant frame builders creating a raised rim. Diagenesis at the reef margin creates sporadic low impedance porosity which adds to the chaotic signature.	Abenaki 1-7: Platform margin
High amplitude peak-trough pairs. Divergent to concordant, parallel, good continuity.	Carbonate dominated proximal-distal foreslope. Clean microbial limestones on calcareous mudstone pairs (section 5.4.2 Abenaki 4).	Abenaki 1 - Abenaki 4
Medium to high amplitudes, generally peak-trough pairs. Displays increasingly more chaotic, discontinuous reflections moving east. Parallel to sub-parallel, some sigmoidal reflections.	Mixed carbonate and siliciclastics. Siliciclastics are interpreted to be the Mic Mac Formation sands which bypassed the carbonate bank and deposited on the proximal foreslope amongst the carbonates of the Abenaki bank (section 5.4.3).	Abenaki 4 - Abenaki 7
Low to medium amplitudes, poor continuity. Some high amplitude peak-trough pairs, although generally trough-peak pairs. Mainly sub-parallel, or deformed reflections, some chaotic.	Mixed carbonate and increasing siliciclastics. Proximal to distal foreslope transition. Moving west, more siliciclastics are interpreted from more trough-peak pairs, due to the Sable Delta depositing into the Sable Sub-basin.	Distal Abenaki 4 - Abenaki 7
High amplitude trough-peak pairs. Sometimes chaotic, parallel to sub-parallel reflectors.	Prodelta siliciclastics infilling expansion trend (Fig. 4.16, section 5.4.3).	Missisauga
Downlapping clinofolds, low to medium amplitudes, sub-parallel, relatively continuous (Fig. 5.5).	Proximal to distal foreslope of Abenaki 2 carbonates. Distal toe of Abenaki 2 (section 5.4.2 Abenaki 2).	Misaine
High amplitude peak-trough pair. Downlaps onto Mohican. Continuous (Fig. 5.5).	Shelf limestone which grew amongst the platform interior (Figs. 4.13-4.17).	Scatarie
Angular unconformity. Low to high amplitudes. High amplitudes on the shelf margin, changing to low amplitudes basinward. Mainly chaotic, or deformed reflections.	Angular unconformity interpreted to be due to salt movement. High amplitudes on the shelf due to impedance changes between shelf carbonates and Mohican siliciclastics. Low amplitudes basinward due to little impedance changes between Mohican Formation and Verrill Canyon formations siliciclastics (section 5.4.2).	Mohican
Chaotic, low amplitude, poor continuity.	Salt diapirs which moved due to a large influx of siliciclastics from the Sable Delta.	Salt

5.4.2 Stratigraphic architecture of third-order depositional sequences of the Abenaki carbonate bank

Six seismic traverses (A-F) (Fig. 4.12) were generated to show how the third-order depositional sequences were correlated, bounded by seismic horizons throughout the study area. These traverses were also interpreted to identify when the Sable Delta began affecting the growth of the carbonate sequences. Key well logs and tops were used to help determine the approximate timing of the influx of siliciclastics within the seismic survey. They were chosen to show how the architecture of depositional sequences change from west to east in the study area.

Interpretation of the third-order depositional sequences began on the shelf, where there is a greater 2D seismic coverage that contain well ties. The regional 2D NovaSpan seismic lines were also used to interpret the overall pattern of how these depositional sequences were deposited. Figure 5.3 is the regional 2D NovaSpan 1600 line. This line illustrates the main horizon picks for the stratigraphic framework. The green horizon representing the top of the Mohican Formation was the most challenging correlation from shelf to basin. It was easy on the shelf due to a strong impedance change between the limestone of the Scatarie Member and the siliciclastics of the Mohican Formation and an angular unconformity interpreted to be caused due to salt movement. However, correlating the Mohican distally was challenging due to weak impedance contrasts between the Mohican Formation and the shales of the Verrill Canyon Formation. In Figure 5.3, distinctive, high amplitude clinoform reflections (Abenaki 1, 2, and 3) appear to distally downlap the top Mohican reflection, or may continue distally as very thin, condensed mudstones. Based on this criterion, the Mohican top was interpreted higher than in previous studies (e.g. Wade and MacLean 1990; PFA 2011; 2016).

Above the top of the Abenaki 4 seismic horizon (orange horizon), the downlap pattern of the third-order depositional sequences is no longer observed. The expansion between the top Abenaki 4 and the top of Abenaki 5, along with an abrupt change in seismic facies, is interpreted to be caused by the influx of fine-grained, distal, pro-delta siliciclastics coming from the Sable Delta in the northeast. This is coeval with the termination of carbonate growth at Penobscot to the north, and therefore dates the time at which the Sable Delta

began influencing the Abenaki carbonate bank in this area to be approximately 155 Ma, in the middle Kimmeridgian. The thickness of the sediment package between Abenaki 4 and Abenaki 5 expands from approximately 25-30 m on the carbonate platform, to approximately 140-190 m south of Moheida Ridge on the distal slope. The beginning of the expansion trend, a consequence of sediment loading from the Sable Delta and from salt withdrawal can then be observed after the second fault in Figure 4.16. Abenaki 5, 6 and 7 developed as intermittently dispersed patch reefs basinward of the carbonate platform in some intervals within the study area, signifying a mixed carbonate and siliciclastic depositional environment, whereas in other areas, Abenaki 5, 6 and 7 are not present at all as carbonates, and occur solely as siliciclastics.

Abenaki 1 (Scatarie Member)

The third-order depositional sequence of Abenaki 1 corresponds to the Scatarie Member of the Abenaki Formation. The Scatarie Member is a single high amplitude peak-trough pair in the southwest and west extremities of the 3D Sable MegaMerge where it is a high impedance shelf carbonate. Everywhere else within the MegaMerge, (basinward of where it downlaps), the time equivalent reflection is difficult to interpret. Abenaki 1 occurs predominately as a carbonate platform which prograded out across the shelf to the outer shelf hinge zone. It can be seen as the pale-yellow horizon (top of Scatarie Member) in Figures 4.13-4.17 and 5.3, downlaps onto the top of the Mohican Formation, and is bounded at the top with deeper marine shales of the Misaine Member. If Abenaki 1 prograded basinward into distal shales and marls, they are presumably very thin, therefore there is very poor source rock potential of this third-order depositional sequence beyond the platform margin. The lowstand component of Abenaki 1 cannot be identified on seismic.

The Abenaki 1 (Scatarie Member) horizon pick depends on the horizon pick of the top of the Mohican Formation. If the Mohican horizon was moved slightly lower, the Scatarie Member could then be interpreted to continue basinward throughout the entire basin (e.g. Wade and MacLean 1990; PFA 2011; 2016). Figure 5.4 denotes the reasoning for the picks of Abenaki 1 and the Mohican.

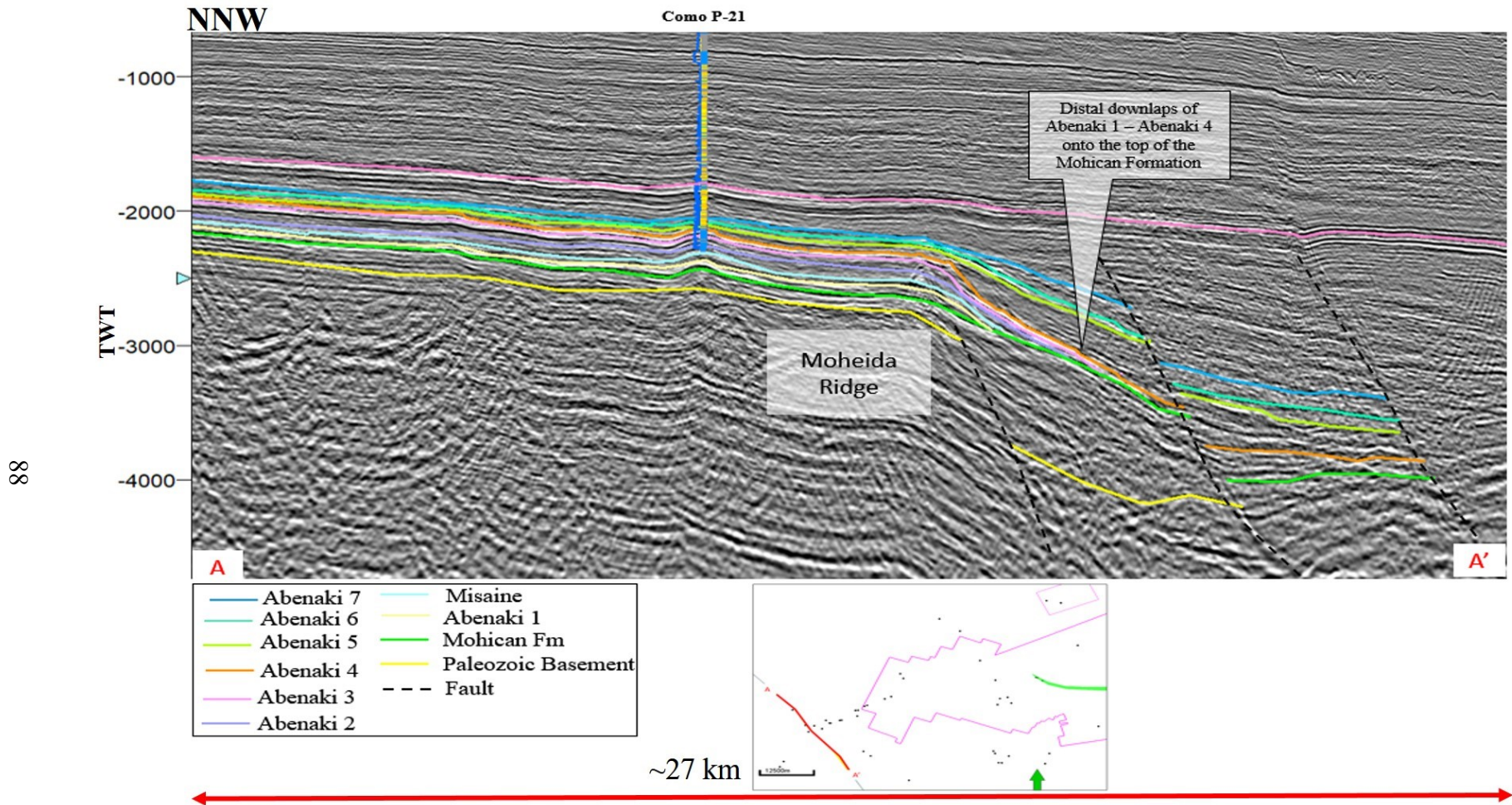


Figure 5.3: Regional 2D NovaSpan seismic line. This seismic line was used to understand the seismic stratigraphic framework of the Middle Jurassic to Early Cretaceous time interval in the Sable Sub-basin, which was then loop-tied into the 3D Sable MegaMerge. Y-axis is in TWT with a 5X vertical exaggeration.

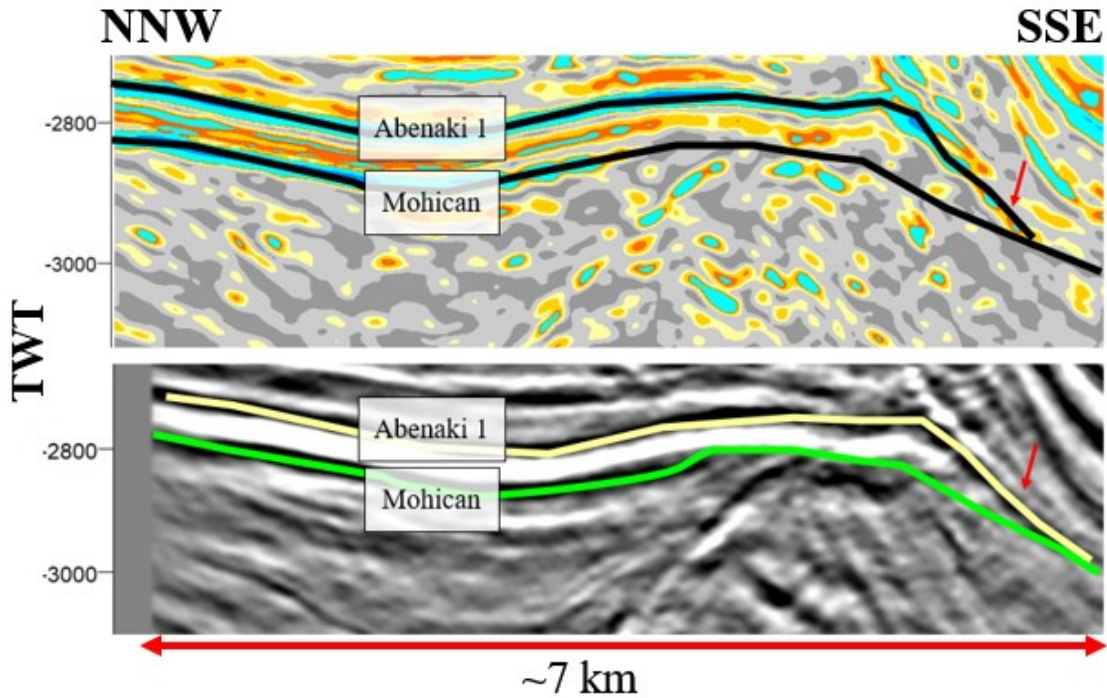


Figure 5.4: *Inline 3920 from the Sable MegaMerge. Top of Abenaki 1 (pale-yellow) downlaps onto the top of the Mohican Formation (green). The top figure shows the genetic inverted seismic data, the blue are carbonate-rich lithologies; grey are siliciclastic-rich lithologies. The Scatarie marker is a very distinct, strong amplitude peak-trough, easily recognized where it is a shelf carbonate in the study area. The top of the Mohican Formation is easily identified on the shelf and somewhat on the slope, as a strong peak with truncations below due to the angular unconformity. When these horizons are correlated off the shelf, it becomes evident that the strong amplitude of the Scatarie Member terminates on the Mohican Formation. A factor affecting the continuation of the Scatarie reflection could be the interaction of salt in this area, which can be seen on seismic. However this downlapping of the Scatarie Member can also be seen within the 2D seismic on the shelf where salt interaction is not as evident. Y-axis is in TWT with a 5X vertical exaggeration.*

Abenaki 2

The Misaine Member is interpreted by Weissenberger et al. (2000) and Encana (2006) to be the transgressive systems tract of the Abenaki 2 sequence. The top of the Misaine was interpreted as a lithostratigraphic surface and shown on seismic traverses 4.13-4.17 and 5.3 as the light-blue horizon on the landward (left-hand side) of the lines, similar to Abenaki 1. The lithostratigraphic top of the Misaine Member is interpreted to also terminate at the platform edge as it can also be seen downlapping onto the Mohican Formation. However, the mudstones of the Misaine Member should be included in the distal highstand component of Abenaki 2 and can be correlated chronostratigraphically off the platform

edge and into the basin as the “base” of Abenaki 2. Therefore, on the seismic traverses, the top of the Misaine Member is interpreted as a horizon of its own just to observe how the shales of this member interacted on the platform, although the entirety of the Misaine Member is a part of the Abenaki 2 third-order depositional sequence. The clinoforms of the Misaine shales can be seen in Figure 5.5 coming from the north northwest.

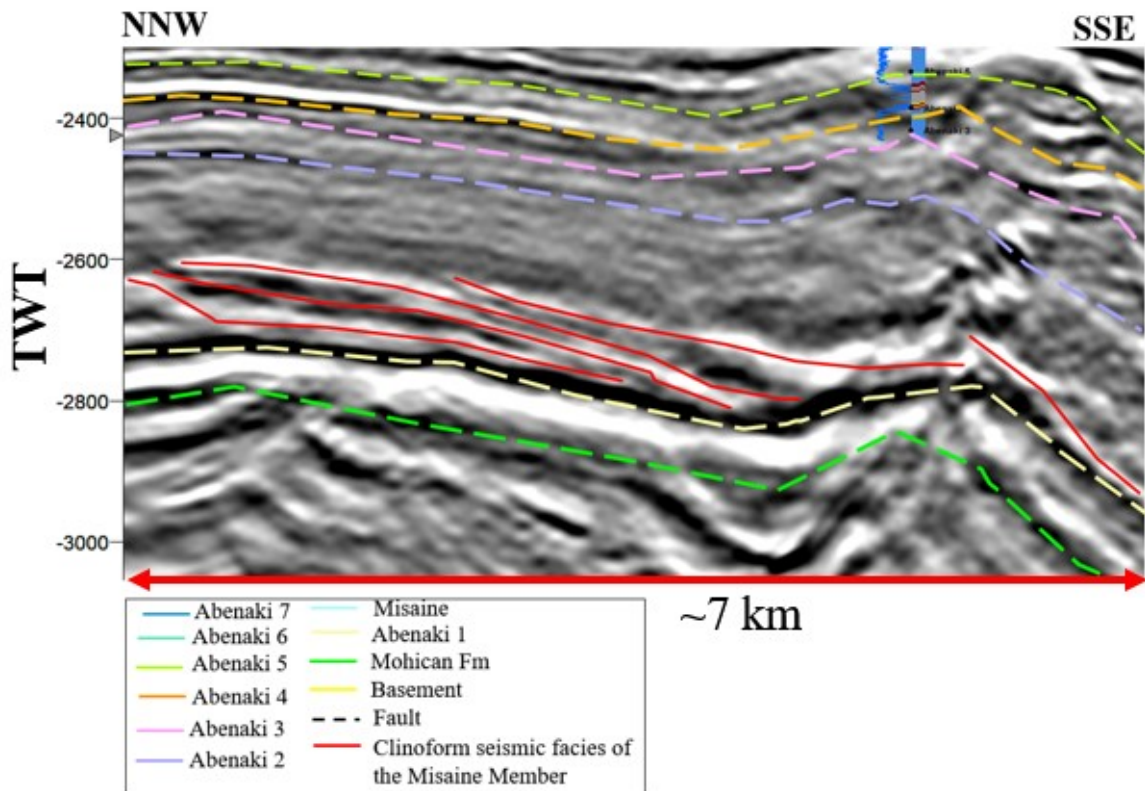


Figure 5.5: Zoom in of seismic traverse 4.13 near the Dominion J-14 well. The red lines mark the tops of the prograding clinoform from the northwest of the Misaine Member. This is the reasoning of why the Misaine Member is interpreted to be the distal shales of the Abenaki 2 depositional sequence. It also shows the high amplitude peak-trough pair of the Scatarie as well as the angular unconformity of the Mohican Formation. Y-axis is TWT in milliseconds with a 5x vertical exaggeration.

The distal mudstones of Abenaki 2 deposited in a highstand systems tract prograded basinward almost to Thebaud C-74 (Appendix E, Fig. E-2). The carbonates of Abenaki 2 deposited during the highstand systems tract, prograded basinward almost to Migrant N-20 (Fig.4.16; purple is the top of the Abenaki 2 depositional sequence). The third-order depositional sequence of Abenaki 2 is then assumed to downlap onto the Mohican Formation like Abenaki 1 (Scatarie Member) or be present as a very thin mudstone,

unidentifiable on seismic (Figs. 5.3). On the platform, the thickness of Abenaki 2 ranges from 100-200 m thick from the top of the sequence to the base of the Misaine Member.

Abenaki 3

The third-order depositional sequence of Abenaki 3 is similar to Abenaki 2. The lowstand systems tract cannot be seen on the platform due to sea-level dropping below the shelf margin. This would allow the platform to become subaerially exposed, causing cementation by the interaction with meteoric water, making the interval less prone to erosion. However, some allochthonous material derived from erosion on the slope could have been deposited distally on the foreslope. Thin, condensed deposits may have occurred atop the platform during maximum transgression (Wendt 1988). Eventually, shallow-marine sedimentation rates exceeded subsidence and the eustatic rise, which lead to deposition of aggradational to progradational shelf, shelf-edge and slope strata of a highstand systems tract. Aggradation and progradation in this carbonate dominated environment took place as a result of in situ carbonate sedimentation and accumulation. The carbonates of Abenaki 3 prograded basinward into water depths of approximately 200 m to around the Migrant N-20 area (see Fig. 4.16, pink horizon is the top of Abenaki 3, where it then prograded into mudstones across the rest of the study area (Fig.4.18)). The highstand systems tract of Abenaki 3 lead to higher rates of re-sedimentation on the slope and in the basin, where large amounts of platform-derived, fine grained sediments could have been transported off the bank by storm waves and currents. These sediments settled slowly from suspension and accumulated on the foreslope and basin floor (Loucks and Sarg 1993).

Like Abenaki 1 and Abenaki 2, Abenaki 3 is inferred to downlap the cycle below (Abenaki 2) basinward, however it is difficult to interpret on seismic due to the distal shales of the Abenaki Formation becoming shales of the Verrill Canyon Formation, therefore not giving strong impedance contrasts. Carbonates of Abenaki 3 can also be interpreted eastward, to the Emma N-03 well (Appendix E, Fig. E-3), however not further basinward than that. Abenaki 3 aggraded on the shelf to approximately 30-50 m thick. Basinward, where carbonates were deposited with basinal mudstones, Abenaki 3 grew to a thickness of approximately 70-90 m.

Abenaki 4

As seen in all seismic traverses (Figs. 4.13-4.18), the orange horizon is the top of Abenaki 4 which prograded the furthest into the basin as a carbonate. Abenaki 4 can be interpreted as a carbonate basinward until approximately Adamant N-97 (Appendix E Figure E-2), where it then transitions into a basinal mudstone. Abenaki 4 can be correlated basinward under the Venture Field as the Citnalta limestone (Wade and MacLean 1990), which can be seen schematically in Figure 5.11. Salt diapirism also heavily influenced this region making interpretation around the Adamant N-97 well difficult. Like the sequences below, the lowstand systems tract of Abenaki 4 cannot be seen. Some allochthonous debris from the platform is interpreted to have been pushed out over the carbonate margin and deposited on the slope or in the basin as mudstones. The transgressive systems tract of Abenaki 4 is seen on the platform as being slightly more siliciclastic-rich within restricted lagoons as sea-level was increasing, creating lower amplitude, more discontinuous, chaotic reflections in the interior region of the platform. The reef margin within the Dominion J-14 and Cohasset L-97 area (Figs. 4.13 and 4.14) is very dolomitized (Section 4.2.1) making interpretations of the top and base of these sequences difficult. Carbonates of Abenaki 4 aggraded and prograded approximately 40 km into the basin during sea-level highstand. Abenaki 4 is interpreted to have been deposited as a keep-up carbonate highstand, which signifies that there was a relatively rapid rate of accumulation that could keep pace with periodic rises in relative sea-level. Abenaki 4 did not aggrade as thickly as the previously deposited sequences below, however it prograded the furthest, signifying faster carbonate deposition rates as eustatic sea-level rose within the basin. On the shelf, Abenaki 4 accumulated to approximately 30 – 40 m thick, whereas basinward, Abenaki 4 achieves thicknesses of up to 200 m.

Abenaki 4 represents the upper limit of continuous carbonate deposition on the platform at the northern end of the carbonate bank. In Figures 4.16 and 4.17, in the Penobscot L-30, Kegeshook G-67 wells, it can be observed that carbonate deposition did not continue past the middle Kimmeridgian (Abenaki 4) within the platform interior or the shelf. After the deposition of Abenaki 4 on the margin, the shelf margin system did not continue as a dominantly carbonate depositional system like the sequences below (Abenaki 1, 2 and 3). Within the South Desbarres O-76 well in Figure 4.17, fourth-order depositional cycles can

be interpreted within the third-order depositional sequence of Abenaki 4. These can be interpreted as episodic parasequences and as shoaling-upward successions of siliciclastics to carbonates from early prodelta to lower delta front clastics of the Sable Delta coming in from the north, around the northern extent of the carbonate bank. This signifies that there was a large siliciclastic influx happening in the northeast that did not quite reach the extent of the Abenaki margin, however began affecting the growth of the Abenaki carbonate bank during intervals of sea-level fall.

Abenaki 5, 6 and 7

The third-order depositional sequence of Abenaki 5 is interpreted to represent the change from a carbonate dominated depositional sequence to a mixed carbonate-siliciclastic depositional sequence. This mixed depositional environment continued during the deposition of Abenaki 6 and 7, becoming more siliciclastic-rich through time. Carbonates of Abenaki 5 and 6 developed during a sea-level highstand on the platform and reef margin, and where penetrated at Dominion J-14 (Fig. 4.13) and at Cohasset L-97 (Figs. 4.14 and 4.15). Basinward of Cohasset L-97, carbonates interfinger with siliciclastics of the Mic Mac Formation (Figs. 4.14 and 4.15). The thickness of Abenaki 5 grew from approximately 30 m thick on the platform, to approximately 100 m thick on the slope and in the basin due to the influx of siliciclastics (Figs. 4.14, 4.16 and 5.3 light green is the top of Abenaki 5). Siliciclastics interbedded with carbonates in the platform interior and on the slope of these depositional sequences are interpreted to have come from the north-northeast from the prodelta of the Sable Delta, after it had blanketed the Penobscot area to the north, as well as from continental siliciclastics being eroded from present-day Nova Scotia. During sea-level lowstands, these siliciclastics were able to bypass the Abenaki carbonate bank and accumulate within the foreslope environments.

Using the 3D Sable MegaMerge, it is interpreted that Abenaki 7 did not develop as part of the carbonate platform in this area. Instead, it was deposited as patch reefs on the shelf margin, as carbonate deposition kept up with a rise in sea-level. The patch reefs tended to accumulate on the basinward edge of the shelf margin as it prograded further into the basin (Figs. 4.15 and 4.20, blue is the top of Abenaki 7). Fourth-order depositional sequences (as discussed in Section 3.4.1) can be interpreted within the third-order depositional sequence

of Abenaki 7 as episodic, shoaling upwards parasequences from mudstones to carbonate patch reefs, which prograde basinward with the carbonate bank margin (Fig. 4.15).

Figure 5.6 is a refined schematic of the third-order depositional sequences of the Abenaki Formation using the seismic stratigraphic framework interpreted from this study. It is based upon the schematic made by Encana (2006) (Fig. 3.6), which only represented the Abenaki Formation on the bank near Panuke and inferred basinward slightly. The new schematic summarizes the extents to which the carbonate sequences prograde in relation to one another. It also recognizes that the first four third-order depositional sequences of the Abenaki carbonate bank were deposited in a predominately prograding carbonate depositional system, where the distal mudstones of the sequences, basinward of the carbonate bank margin, are the mudstones of the Verrill Canyon Formation. Above the fourth, third-order depositional sequence, the Sable Delta of the Missisauga Formation influenced the distal growth of the fifth, sixth and seventh third-order sequences, and siliciclastics of the Mic Mac Formation interfinger with the carbonates just outboard of the carbonate bank. Basinward of the Missisauga Formation, the laterally equivalent mudstones of the Verrill Canyon Formation become prevalent.

All third-order depositional sequences represent marine regression, defined by a basinward progradation when the rate of sediment flux exceeds the rate of new space added. This allows the sequences to transition from siliciclastics/carbonates on the shelf, to carbonates on the margin/slope, prograding basinward into distal mudstones.

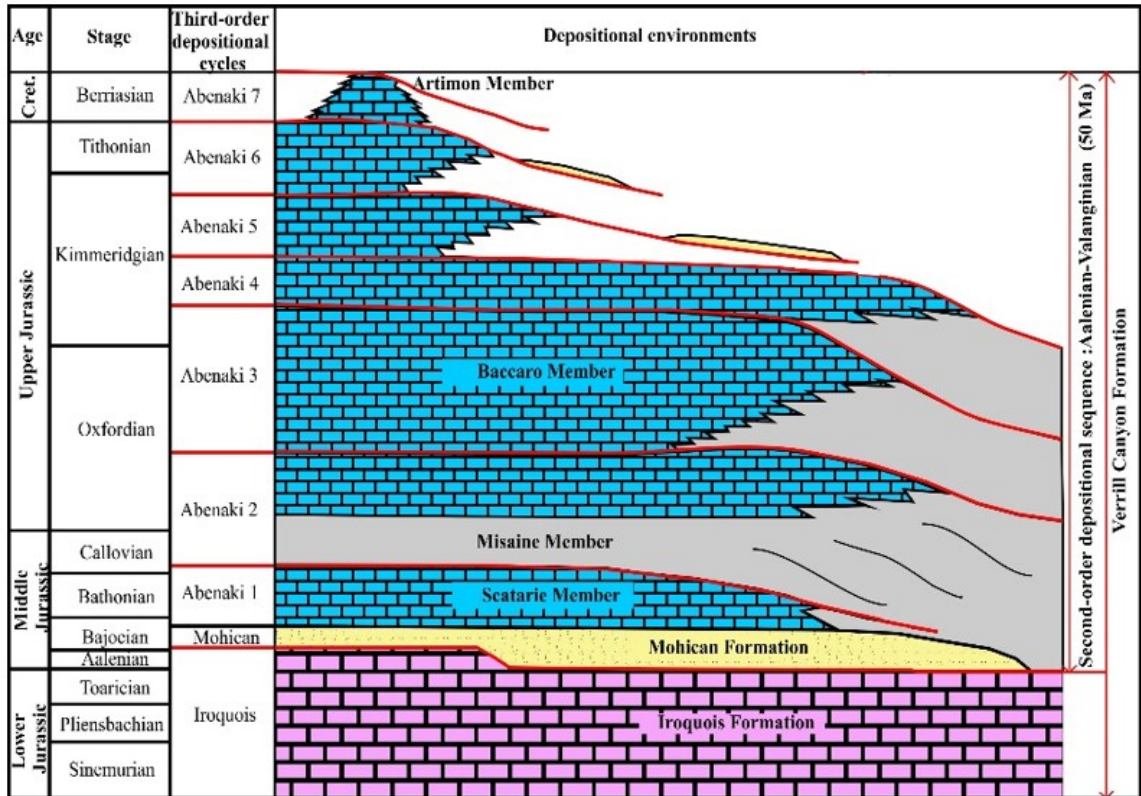


Figure 5.6: Refined schematic of the third-order depositional sequences of the Abenaki Formation modified from Weissenberger et al. 2000 and Encana 2006.

5.4.3 Discussion of the Late Jurassic-Early Cretaceous siliciclastics on published stratigraphic charts

Some recent interpretations have inferred that Lower Missisauga Formation shallow water clastics interfinger with distal shales of the Verrill Canyon Formation in a basinal setting. (CNSOPB 2008; PFA 2011, 2016; Weston et al. 2012) (Fig. 5.7 A). These recent interpretations differ from the interpretation made by Wade and MacLean (1990) (Fig. 5.7 B) that the siliciclastics directly outboard of the carbonate bank are designated Mic Mac Formation, which interfingers with the carbonates of the Abenaki Formation, and the siliciclastics of the Missisauga Formation distally.

Based on seismic correlation from well logs, cuttings reports, and seismic facies analysis of 2D and 3D seismic data, a revised stratigraphic chart of the Late Jurassic to Early Cretaceous was made for the siliciclastics outboard of the Abenaki carbonate bank (Fig. 5.7 C). It is interpreted that directly outboard of the carbonate bank, the carbonates interfinger with siliciclastics of the Mic Mac Formation, which could have bypassed the

carbonate bank or siliciclastics could have come in around the carbonate bank from the north. Figure 4.16 shows the beginning of the expansion trend (Migrant N-20) (Section 2.4), interpreted to be a result of the siliciclastic influx from the northeast causing loading and consequent normal faulting and salt movement. The carbonates and distal carbonate facies of the third-order sequences are correlated below the Migrant N-20 well (Fig. 4.16), signifying that the siliciclastics within the expansion trend do not interfinger with the carbonate bank and are separate and younger, designated Missisauga Formation. Figure 5.7 C shows the revised stratigraphic chart, where a fault is placed between the siliciclastics of the Mic Mac Formation and the siliciclastics of the Missisauga Formation.

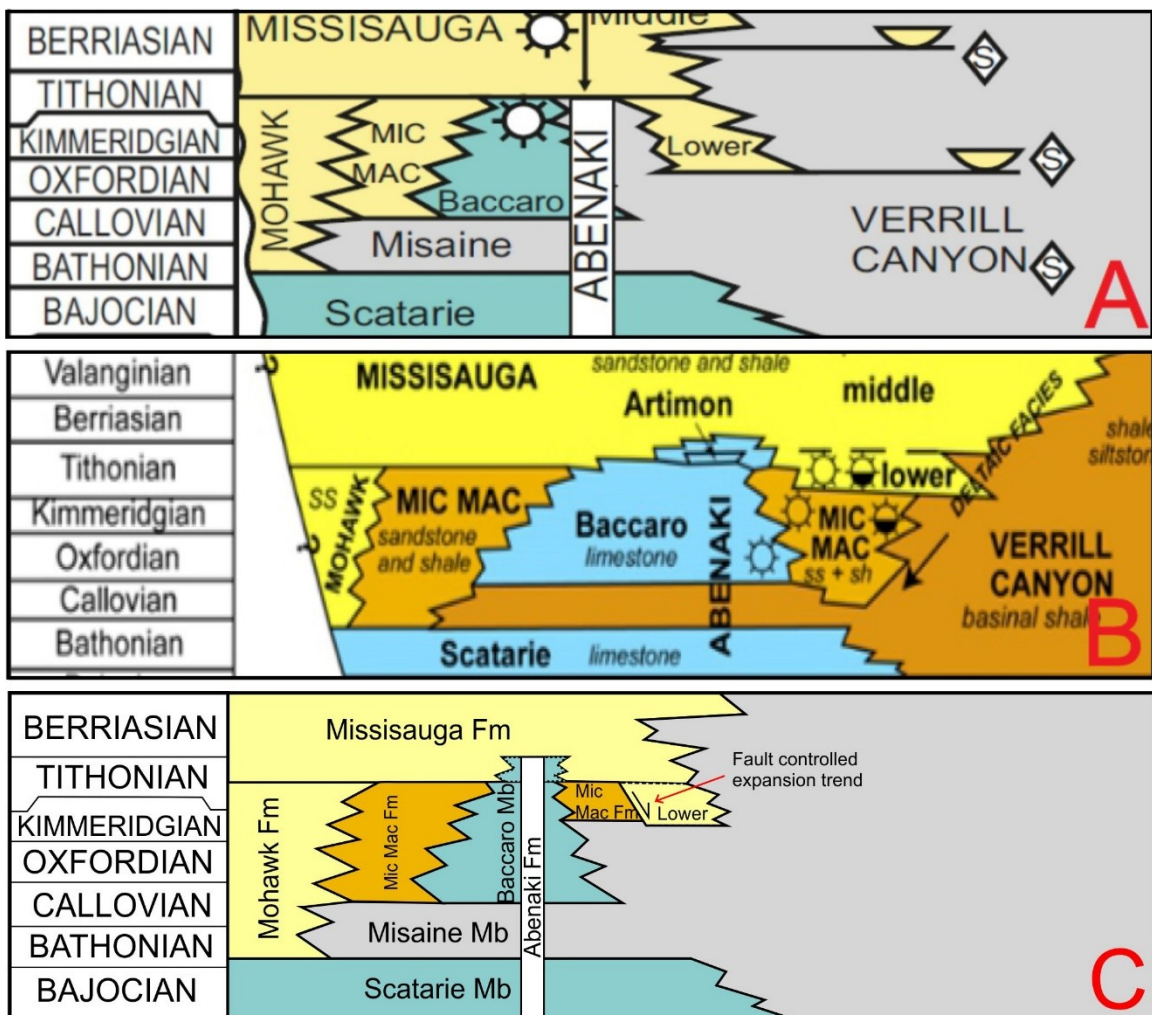


Figure 5.7: A and B are stratigraphic charts of the Late Jurassic to Early Cretaceous of the Scotian Basin. A is from Weston et al. 2012. The authors interpreted the siliciclastics outboard of the Abenaki carbonate bank to be sourced from the Missisauga Formation and to interfinger with the distal shales of the Abenaki carbonate bank. B is a stratigraphic

chart created by Tari et al. 2012 from Wade and MacLean 1990. The authors interpreted the siliciclastics just outboard of the carbonate bank to be part of the Mic Mac Formation, which interfingers with both the Missisauga Formation and the Verrill Canyon Formation distally. C is a revised stratigraphic chart created from interpretations from this study. The siliciclastics just outboard of the carbonate bank are interpreted to be from the Mic Mac Formation, which interfinger with the carbonates, which are then juxtaposed against siliciclastics of the Missisauga Formation due to faulting, creating the expansion trend around Migrant N-20 (Fig. 4.16). Dashed lines in C are uncertainties in age due to not being able to distinguish between siliciclastics of the Mic Mac and Missisauga formations, and not having exact age dates for the carbonates within the distal section of the Sable-Sub-basin.

5.5 Source rock potential of distal third-order depositional sequences of the Abenaki carbonate bank

Deposition of Abenaki 1, 2, 3 and 4 (Fig. 5.9, A-E) took place during the Middle to Late Jurassic (middle Bajocian to middle Kimmeridgian (e.g. Weissenberger et al. 2000)) in a predominately carbonate depositional environment. The growth of Abenaki 1 was influenced by the transgressive event of the Misaine Member and was unable to prograde basinward into distal shales and marls, therefore is unlikely to host organic-rich materials beyond the platform margin. Abenaki 2 contains the Misaine shale, which was interpreted to have been deposited in an inner to outer neritic environment on the continental shelf (Fig. 2.10) at Cohasset L-97 (Ascoli 2013; PFA 2011). Although there are many potential uncertainties in the TOC values recorded in the well logs (as discussed in Section 5.3.1), the intervals with the most potential to contain organic-rich facies are the distal shales of the Abenaki 2 to 4 depositional sequences.

The distal shales of Abenaki 2 (Fig.5.9 B), associated with the transgressive event of the middle Callovian has the greatest potential for organic-rich material. During the lowermost Callovian, carbonate platforms were restricted to the tropical zones, and the Middle Callovian witnessed a widespread and pronounced decline of carbonate across all latitudes (Dromart et al. 2003). The lack of carbonates during this time interval is consistent with a cooling event lasting approximately one million years (Dromart et al. 2003). The decline in carbonates during this time interval enabled significant deposition of marine shales from sea-level rising and blanketing the carbonate platform. Carbonate deposition started again in the early Oxfordian and continued steadily in the study area until the middle Kimmeridgian.

Similarly, on the Moroccan Margin, Oxfordian shales present in the onshore fields of the Essaouira Basin have type 2 sapropelic kerogen, reaching up to 4.3% TOC in an approximate 10 m thick interval. This is a good indication that anoxic conditions could also prevail at a similar water depth on the Scotian Margin due to both margins hosting similar depositional environments from the Early Triassic to Early Cretaceous.

The condensed sections of marine mudstones (Section 3.4.1 Figure 3.8) and argillaceous deep-water carbonates that were deposited in the distal foreslope to deep shelf environments during the middle Oxfordian and the middle to early Kimmeridgian (Abenaki 2, 3 and 4), would have been starved of terrigenous materials during a period of maximum relative sea-level rise. This would result in deposition of sediments that primarily comprise skeletal remains of pelagic fauna. These sediments deposit in water depths of approximately 200 – 500 m (Tyson 1987). Water depth is an important control on the TOC content of marine sediments because the proportion of organic matter surviving sedimentation decreases with increasing residence time in the water column (Tyson 1987). If anoxia and high organic activity prevailed during times of organic deposition, these intervals have potential to contain kerogen of predominately type 2 source.

Figure 5.8 shows the geocellular models for both depositional systems; the carbonate depositional system from Abenaki 1 to Abenaki 4 (grey and blue colours) and the mixed siliciclastic-carbonate depositional environment from Abenaki 5 to Abenaki 7 (yellow, grey and blue colours). The models were used to create the environment of deposition maps in Figures 5.9 and 5.10. The two models were created using the same method (explained in Section 3.6.7), however their colour tables were manually determined based on their interpreted depositional environments. This aided in seeing the proportions of carbonate to mudstone in the carbonate depositional environment, and in the proportions of carbonate to sand-rich siliciclastics in the mixed siliciclastic and carbonate depositional environment.

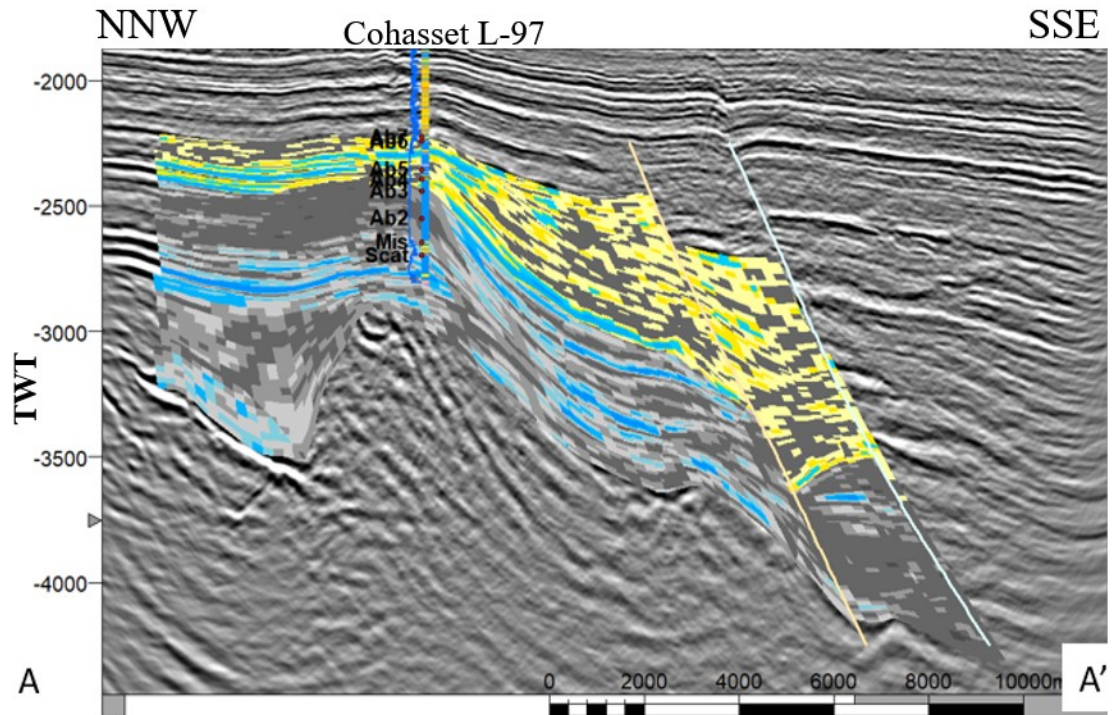
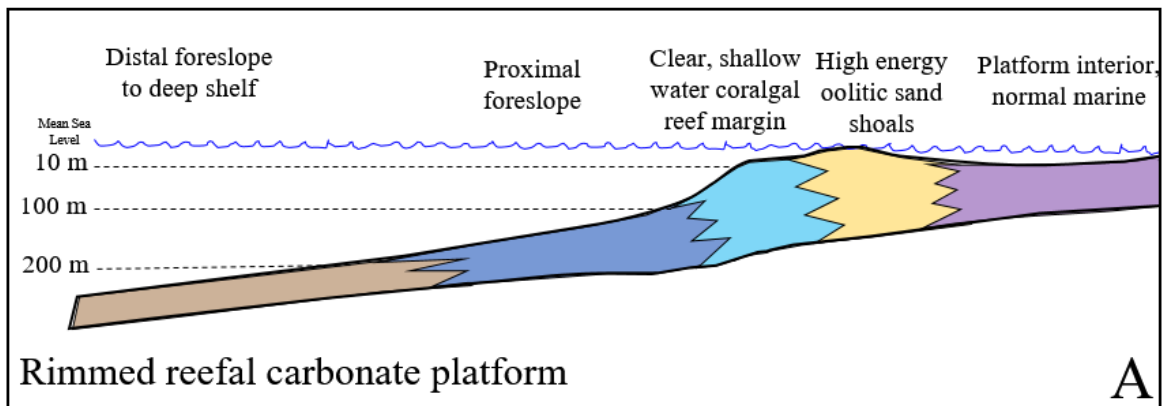
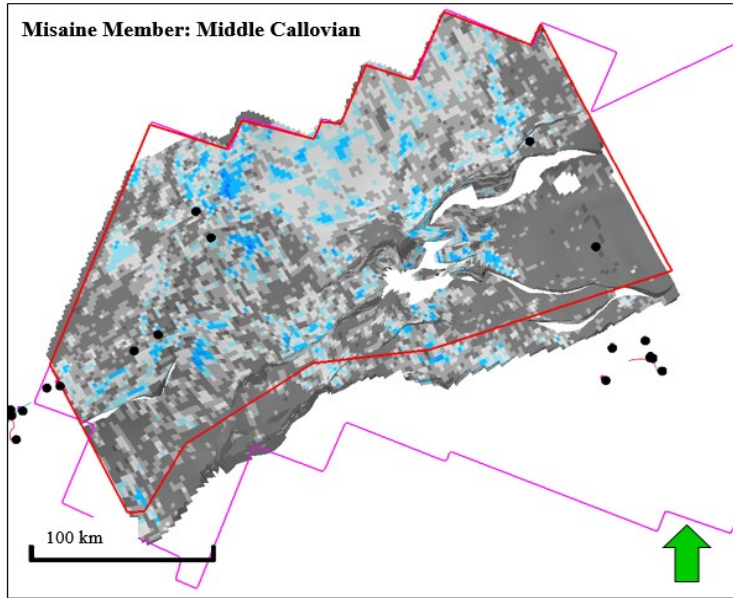


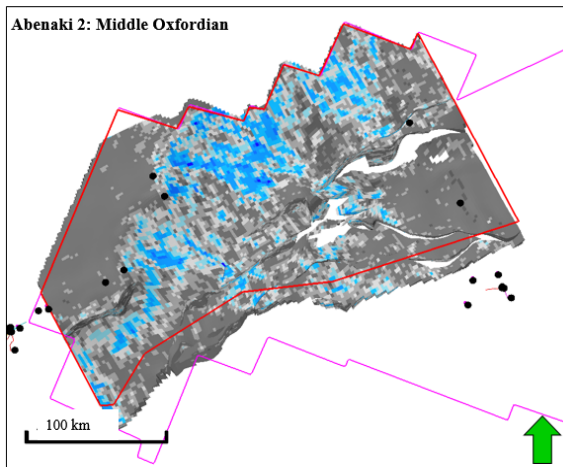
Figure 5.8: Vertical section (inline 3960, Fig. 4.20, 5X vertical exaggeration) showing both geocellular models (mud-rich and sand-rich depositional systems). Pale-dark blue=carbonate, yellow=sand, grey=mud. The well is Cohasset L-97 with the gamma-ray and the Canstrat lithology log.





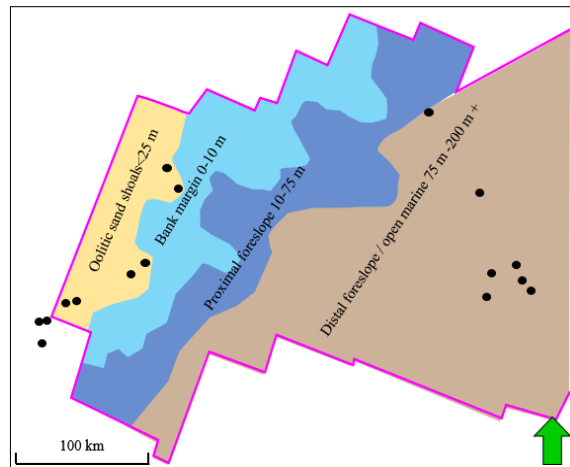
Carbonate
Shale

B



Carbonate
Shale

C



High energy oolitic sand shoals
Clear, shallow water coralgall reef margin
Proximal foreslope
Distal foreslope to deep shelf

C'

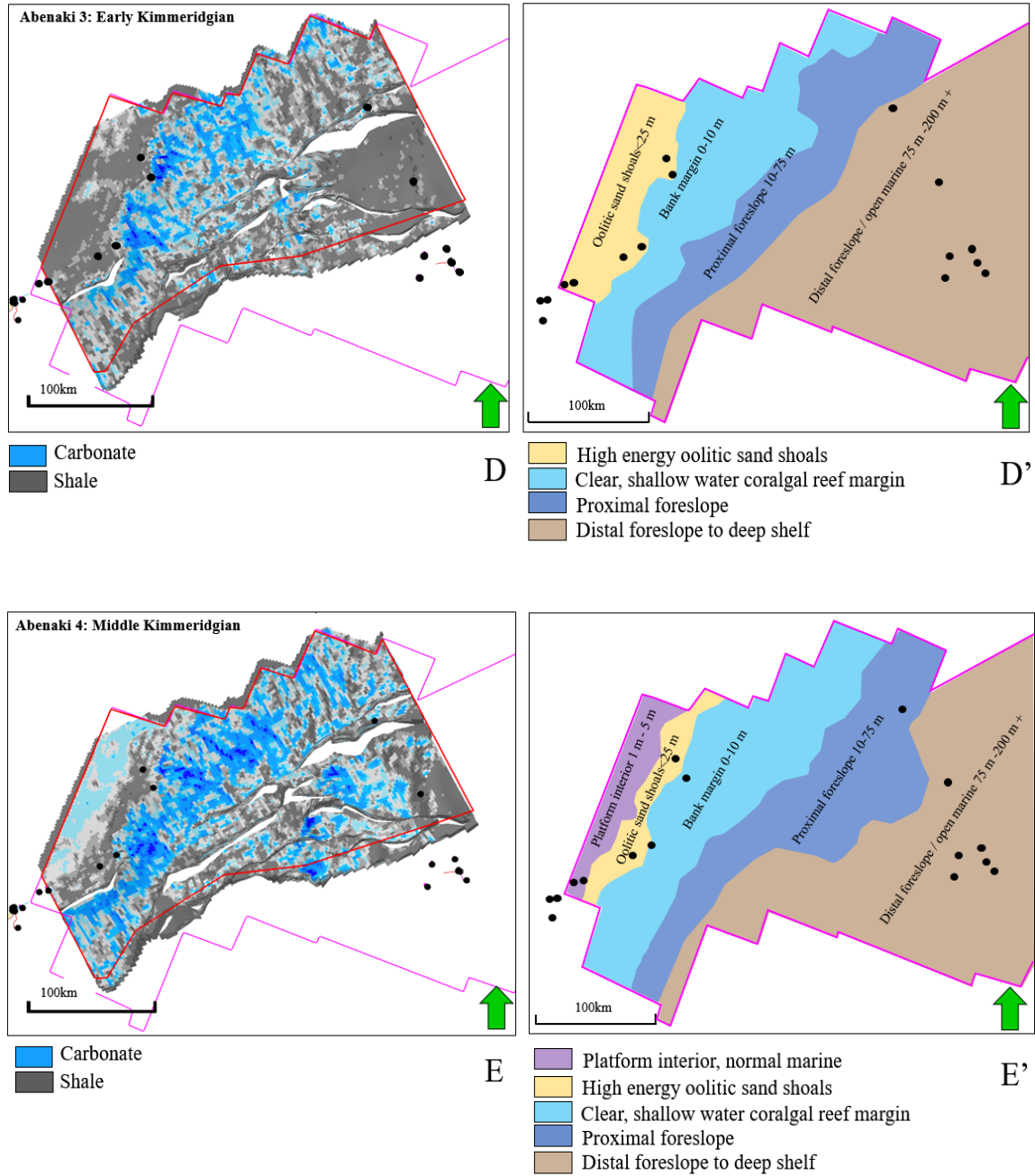


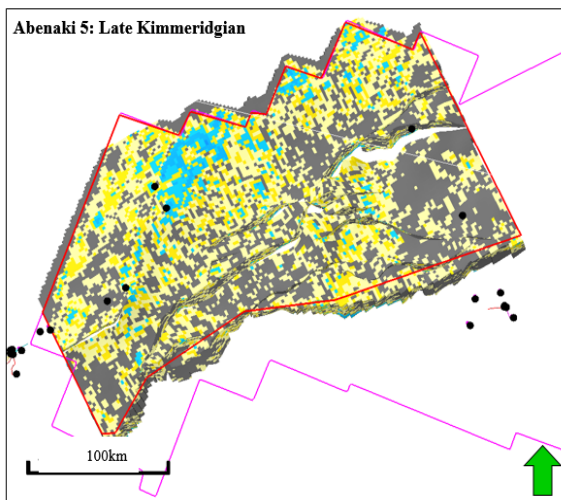
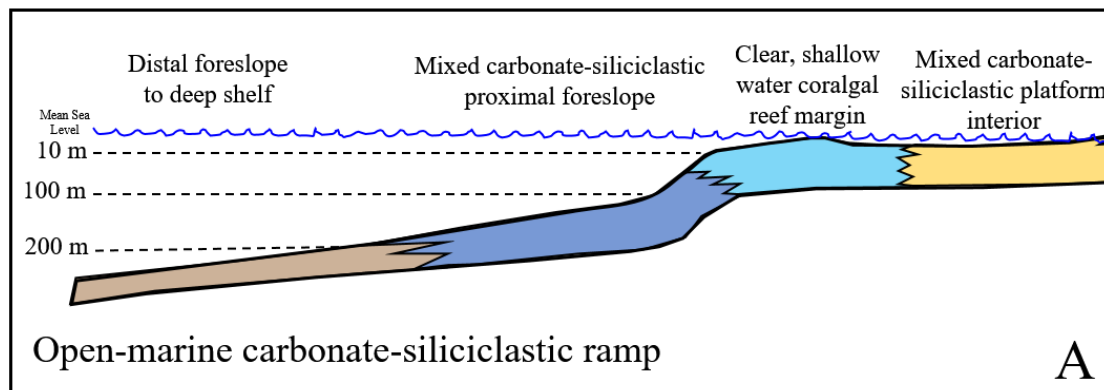
Figure 5.9 A-E: Figure A shows the carbonate depositional model in which the environment of deposition maps were created from for Abenaki 2, 3 and 4. The boundary between the distal foreslope to outer neritic was unable to be determined throughout the seismic, therefore it is just interpreted as being deposited in water depths greater than 200 m (modified from PFA 2016). 5.9 B is a map view of the middle Callovian from the geocellular model for the carbonate depositional system. It shows the approximate proportion of mudstones to carbonates that were deposited during this time interval. The middle Callovian represents a regional transgressive event; therefore, it is predominately mudstones. Figure 5.9 B and B' to Figure 5.9 E-E' all represent the map views of Abenaki 2, 3 and 4 during the middle Oxfordian, early Kimmeridgian and middle Kimmeridgian.

B, C, D and E represent the geocellular model view, and B', C', D' and E' represent environment of deposition maps interpreted from the geocellular model as well as from the seismic stratigraphic framework. The potential organic-rich intervals are interpreted to have been deposited on the distal foreslope to deep shelf (outer neritic) of these third-order depositional sequences. Black dots are the well locations. Depositional environments and approximate water depths at time of deposition are labelled.

The distal foreslope to deep shelf environments of Abenaki 5, 6 and 7 (Fig. 5.10 B-D) are less likely to contain type 2 kerogen due to having a mixed marine and terrigenous source. The distal foreslope of the carbonate platform was influenced by the prodelta of the Sable Delta. The sediments deposited in this mixed depositional environment are more likely to have coarser grained sediments due to their terrigenous source. Coarser grained sediments are more likely to be organic-poor since they typically occur in more highly oxidizing regimes, causing organic matter to degrade with better efficiency (Tyson 1987). The conditions normally associated with a marine petroleum source rock formation typically result from low contents of terrestrial organic matter except in the immediate proximity of fluvial sources. The source of the Sable Delta was approximately 10-20 km from the distal intervals (within the study area) in which Abenaki 5, 6 and 7 were deposited. This may have allowed terrestrial organic matter to be preserved, or organic matter could have degraded during transport. Terrestrial organic matter would decompose very slowly and is usually incapable of creating sufficient oxygen demand to result in significant oxygen deficiency in the bottom water (Tyson 1987). The depositional environment in which the mudstones of these third-order sequences were deposited was most likely of higher energy and in relatively shallower water depths compared to the older depositional sequences (Abenaki 1-4) which were interpreted to have been deposited in water depths of approximately 200-300 m. If anoxic conditions at this water depth prevailed, there may be potential to host a mixed type 2/type 3 kerogen source with the terrigenous detritus sourced from the Sable Delta having potential to provide significant organic content (Silva et al. 2015) basinward of the platform margin.

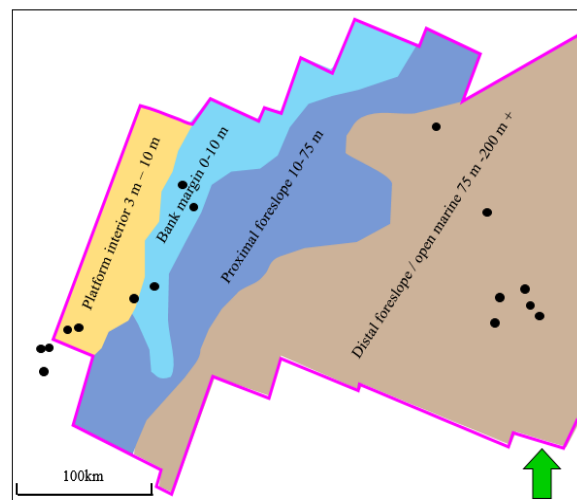
Within the Late Jurassic in the Lusitanian Basin onshore Portugal, the Cabaços Formation (see Appendix A) has kerogen assemblages of mostly continental origin, with minor bursts of marine influence and a TOC content up to 30.56 % at one location, however generally having approximately 4% TOC (Silva et al. 2014). The deposition of the source prone

intervals of the Cabaços Formation is interpreted to have been in calm and proximal environments, close to the source area. Similar continental sourced sediments have been interpreted to have deposited within the sequences of Abenaki 5 to 7 within the Sable Sub-basin, although further from the source than the Cabaços Formation. If anoxic conditions prevailed during this time in the Scotian Basin, the distal shales of Abenaki 5 to 7 have potential to host organic-rich facies with similar characteristics. Type 2 source rocks of the Early Jurassic Água de Madeiros Formation are also present outboard of the carbonate ramp within the Lusitanian Basin, and provide a further analog to having potential source rocks outboard the Abenaki carbonate bank.



- Carbonate
- Shale
- Sandstone

B



- Mixed carbonate-siliciclastic platform interior
- Clear, shallow water corallgal reef margin
- Mixed carbonate-siliciclastic proximal foreslope
- Distal foreslope to deep shelf

B'

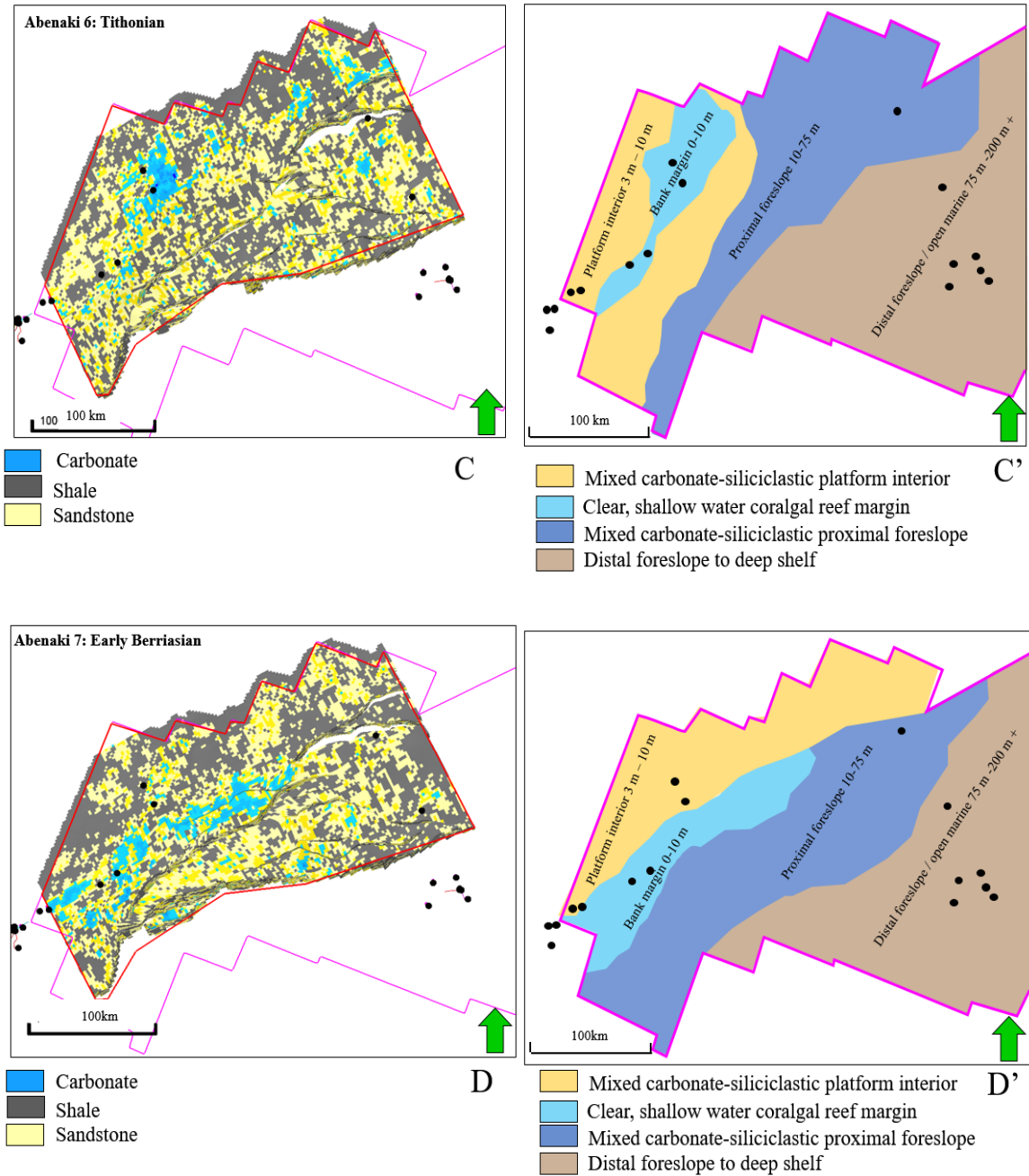


Figure 5.10 A-D: Figure A shows the carbonate depositional model from which the environment of deposition maps were created from for Abenaki 5, 6 and 7. The boundary between the distal foreslope to deep shelf was unable to be determined throughout the seismic, therefore it is just interpreted as being deposited in water depths greater than 200m. These maps show the approximate proportion of mudstone/siliciclastics to carbonates that were deposited during this time interval (modified from PFA 2016). Figure 5.10 B and B' to Figure 5.10 E-E' all represent the map views of Abenaki 5, 6 and 7 during the late Kimmeridgian, Tithonian and early Berriasian. B, C, and D represent the geocellular model view, and B', C', and D' represent environment of deposition maps

interpreted from the geocellular model as well as from the seismic stratigraphic framework. The potential source of intervals of these third-order depositional sequences are interpreted to have been deposited on the distal foreslope to deep shelf.

5.6 Controlling factors on the growth of the Abenaki carbonate bank

5.6.1 Influx of siliciclastics from the Sable Delta

Landward to seaward progression of siliciclastics of the Mohawk and Mic Mac formations to the back-reef of the Abenaki Bank with reciprocal sedimentation, occasional bypass and eventual over-running and extinction of the reef near the Jurassic-Cretaceous boundary were described by Weissenberger et al. 2000 and 2006 (Fig. 3.7) and Qayyum et al. 2014. These are considered normal facies progressions and are consistent with this study. Wade and MacLean (1990) and Cumming and Arnott (2005) addressed the presence of Late Jurassic deltaic siliciclastics at the Venture Field approximately 30 km basinward of the Abenaki carbonate bank. Wade and MacLean's 2D seismic correlations are shown schematically (Fig.5.11), and indicate that siliciclastics interpreted as deltaic deposits penetrated at that field are considerably younger than the Abenaki Bank. This is consistent with the results of this study at Migrant. Weston et al. (2012) express concern that reworking of fossil assemblages is a pervasive issue in prodelta settings on this margin and this provides an explanation for Oxfordian to Tithonian age dates at Venture in the BASIN data base that are inconsistent with relative ages from seismic correlations.

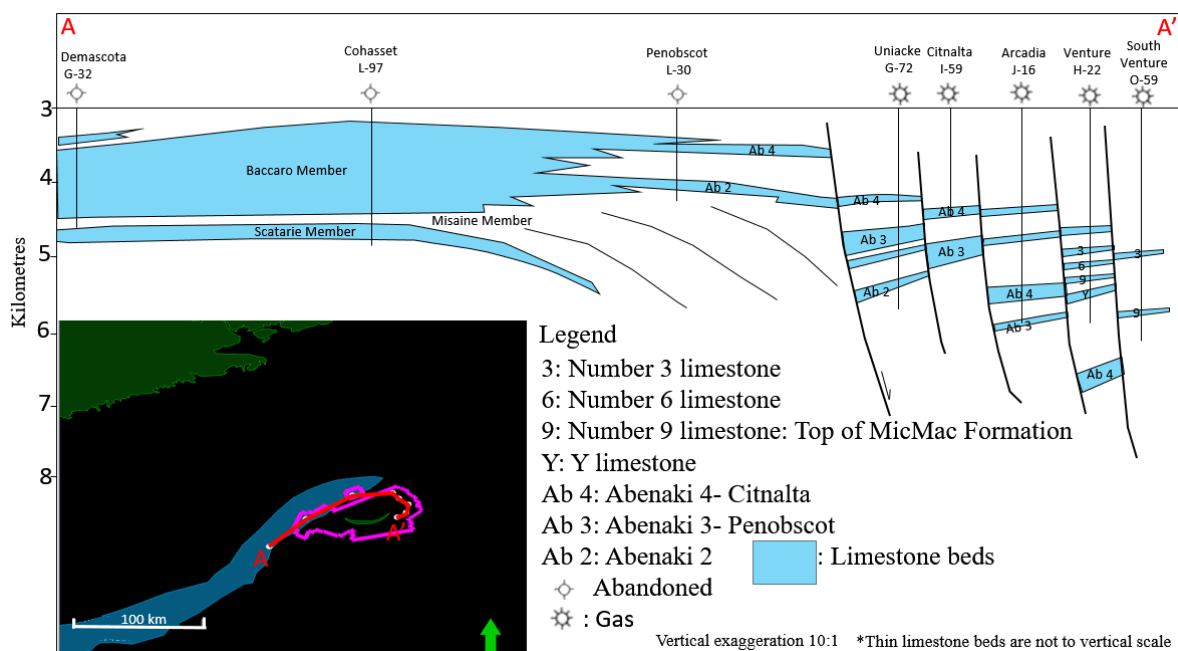


Figure 5.11 Schematic illustrating faulting of the Abenaki Formation in the Sable sub-basin interpreted from 2D seismic modified from Wade and MacLean (1990). The limestones penetrated in the Venture H-22 well are interpreted to be younger than the Abenaki Formation at Penobscot L-30 based on seismic horizon correlation of limestone markers.

Weston et al. (2012) suggested that reworking of microfossils caused from gravity-flow processes on the paleo-delta slope during the Early Cretaceous and Late Jurassic made determining the age and distribution of the microfossils quite difficult. They also state that the most widespread carbonate deposition generally occurs in the Late Jurassic, however age relationships in this time interval are complicated due to the occurrence of discontinuous, younger carbonate units of the Artimon Member (Abenaki 7). This unit is interpreted to have been deposited in the Early Cretaceous and coeval with the Missisauga and Logan Canyon formations in the northeast. Within the Cohasset L-97 well, the Artimon Member is absent, and the age equivalent interval is occupied by clastics of the Missisauga Formation (Weston et al. 2012) with minor carbonate reefs (<1km) developing on the seaward edge of the carbonate bank, showing that carbonate growth kept up with sea-level at this time. Moving down-section in the Cohasset L-97 well, thick carbonates of the Baccaro Member (Abenaki 6 to Abenaki 2) lie below the maximum flooding surface (MFS) of the Tithonian (Fig. 5.12), implying that the main carbonate bank deposition ceased slightly before the end of the Jurassic (Weston et al. 2012) in this region.

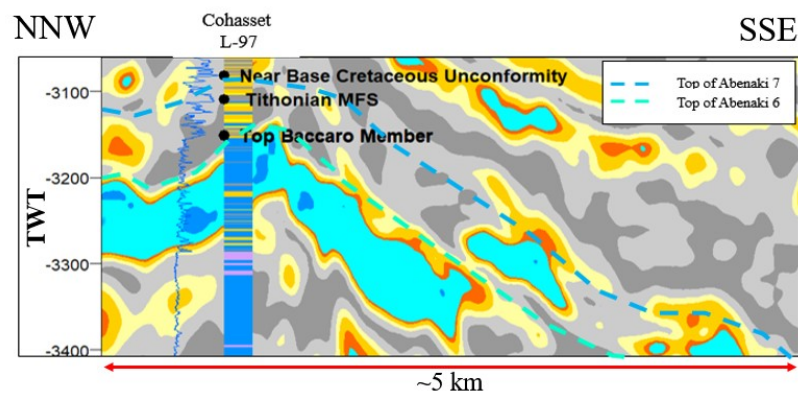


Figure 5.12: Cohasset L-97 lithological and gamma ray logs with lithostratigraphic picks from the Play Fairway Analysis from the Nova Scotia Department of Energy in 2011. The seismic was converted to genetic seismic data and depth converted to match the lithostratigraphic picks. Light blue of the genetic seismic data are limestones, the grey are shales whereas yellow are more sand-dominated intervals. The color scaling is not exact as it was chosen manually, however its main purpose is to distinguish between carbonates and siliciclastics.

In South Desbarres O-76 and Uniacke G-72, the interval between the base of the Early Cretaceous unconformity (age equivalent to the base of Abenaki 7) and the MFS of the Tithonian is expanded to hundreds of metres due to increased siliciclastic deposition and accommodation, interpreted to be due to subsidence from sediment loading causing salt withdrawal (e.g. Weston et al. 2012). There are also thin limestones layers interbedded with siliciclastics at South Desbarres O-76, signifying that while the delta was being deposited, the depositional environment was still suitable for minor carbonate deposition. This could be because temporary waning of clastic influx (during highstands or intervals of reduced sediment supply) enabled carbonate deposition to re-establish.

5.6.2 Northern termination

The cessation of carbonate sedimentation in the Abenaki carbonate bank is related to the subsequent influx of siliciclastics associated with the Sable Delta that is interpreted to result from the Avalon uplift, which is an Atlantic margin rift-flank uplift (Jansa and Wade 1975; Jansa 1981; Wade and MacLean 1990). The pre-Sable Delta northern termination, morphology and orientation of the Abenaki carbonate bank appears to be controlled by the northern extent of a basement hinge line between the LaHave Platform and the Sable Sub-basin, shown via magnetic data in Figure 5.15.

Figure 5.13 A and B show the approximate location of the Abenaki carbonate bank, relative to the Sable Delta in the middle Kimmeridgian and the early Berriasian. In the middle Kimmeridgian, the Sable Delta was close enough to the carbonate bank for prodelta sedimentation to affect the carbonate bank, ceasing the deposition of the carbonate platform. By the early Berriasian, siliciclastics sourced from Sable Delta dominated the region and arrested carbonate deposition northward of Cohasset L-97.

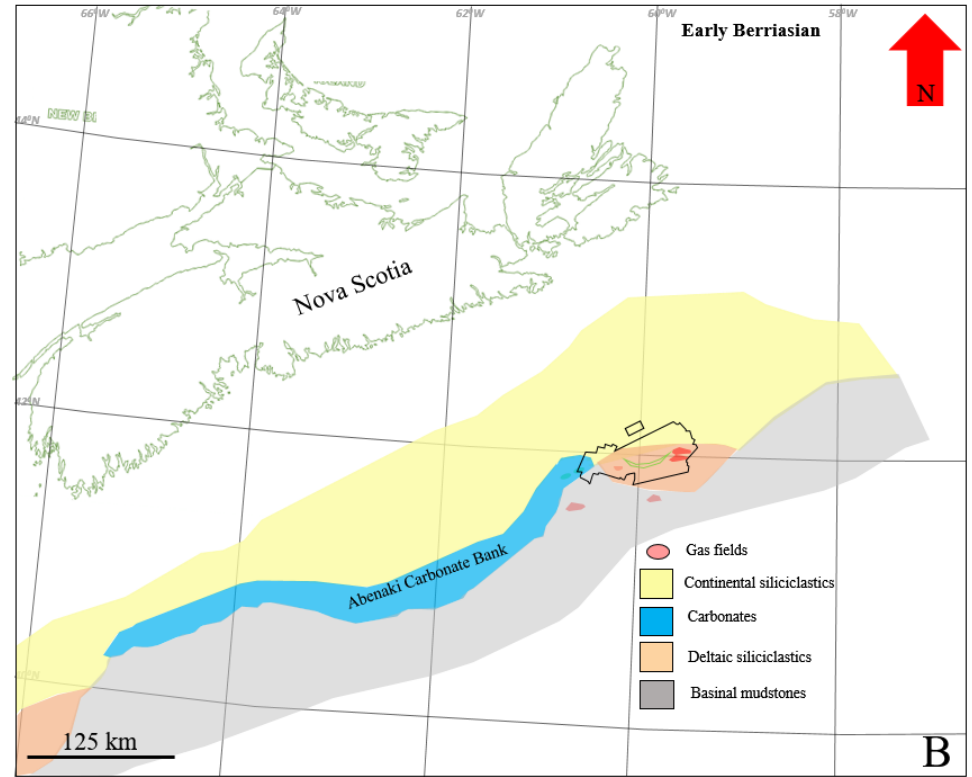
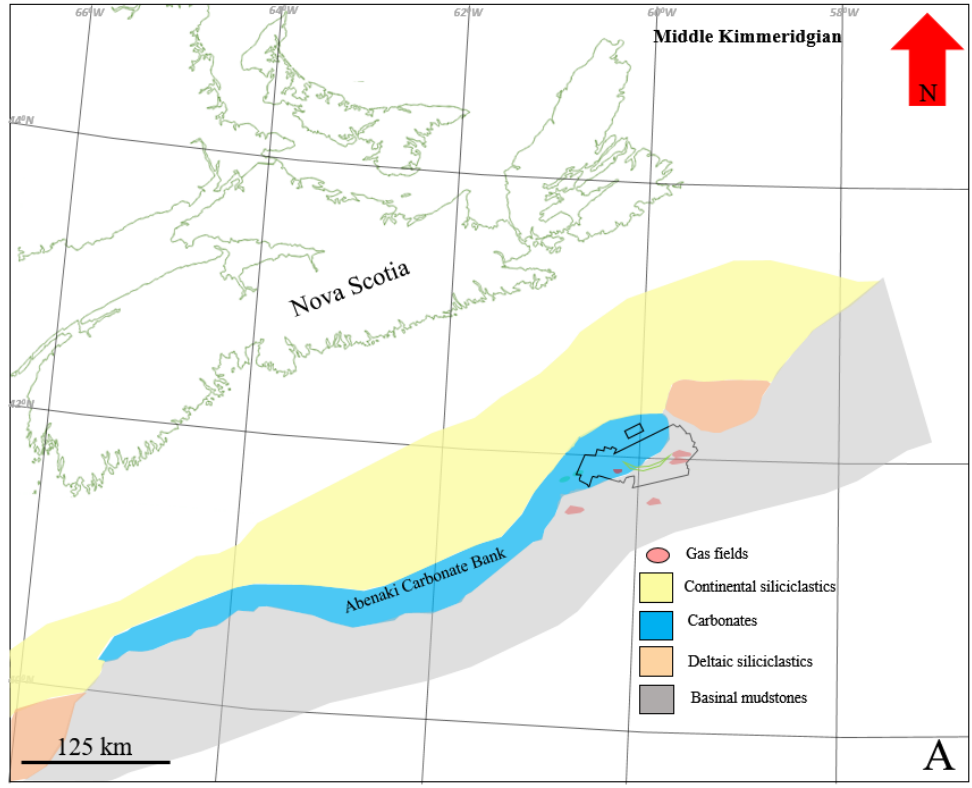


Figure 5.13 A and B: Generalized facies distribution of the Abenaki Formation (blue) the Verrill Canyon Formation (grey), Lower Missisauga Formation (orange) and the Mic

Mac- Mohawk Formation (yellow). 6.14A shows the facies distribution during the middle Kimmeridgian. The Abenaki carbonate bank prograded the furthest into the basin at this time, although the Sable Delta must have been relatively close to the bank due to minor siliciclastic influence being interpreted throughout the western region of Abenaki 4 as siliciclastics were able to bypass the bank margin and be deposited on the slope. Figure 5.11 B shows the facies distribution during the early Berriasian. Initially, the northeastern extent of the Abenaki carbonate bank was controlled by the extent of the basement hinge line and was then progressively suppressed from the influx of siliciclastics from the Sable Delta. These maps were based upon the original interpretation of the facies distribution for these time intervals by Wade and MacLean, 1990.

5.6.3 Steep slope to shallow ramp transition

From correlating the seismic horizons within the western-most region of the Sable MegaMerge, it was interpreted that the bank margin transitions northward from a steep margin dipping at approximately 30°-40° (coincident with a small offset fault that extends upwards into the Cretaceous) to a low angle ramp, dipping at approximately 12°.

Present structural dip angles were calculated from the depth surfaces created from the seismic horizons. Figure 5.14 shows the dip angles calculated for the Top of Abenaki 4 and how the angle changes quite drastically between the locations of the two red arrows. There is a steeply dipping slope in western part of the model area, dipping at approximately 40°, and less than 200 m away it transitions to a shallow dipping ramp at approximately 12°. The other high valued dip angles (~20°-35°) in the model area in Figure 5.16 represent the dips associated with fault offsets.

The basement hinge line is interpreted to play a role in the significant change in dip over a relatively short distance. Upon close examination of the magnetic grid map (Fig. 5.15) edited from Verhoef et al. (1996) and Dehler (2010), it was observed that in the northwest region of the Sable MegaMerge, there is a basement high related to the LaHave Platform that shallows to the southeast and north-northeast into the top western corner of the Sable MegaMerge. This change in carbonate bank morphology is important to understand the structural architecture of the third-order depositional sequences and how they changed throughout the study area.

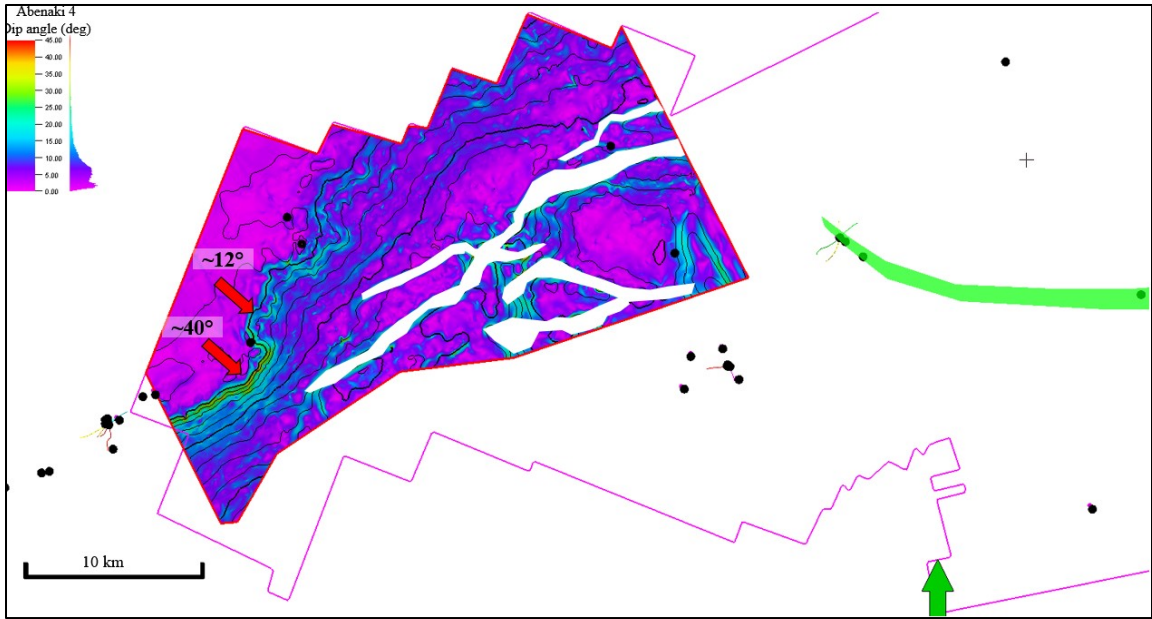


Figure 5.14: Dip angle map for Abenaki 4. The shelf margin transitions from a steeply dipping ramp at approximately 40° (as indicated on map) to a gentle dipping slope at approximately 12° (as indicated on map) within approximately 200 m laterally. White areas are fault gaps. Other areas with relatively high dip angles are caused from other minor faulting within the area.

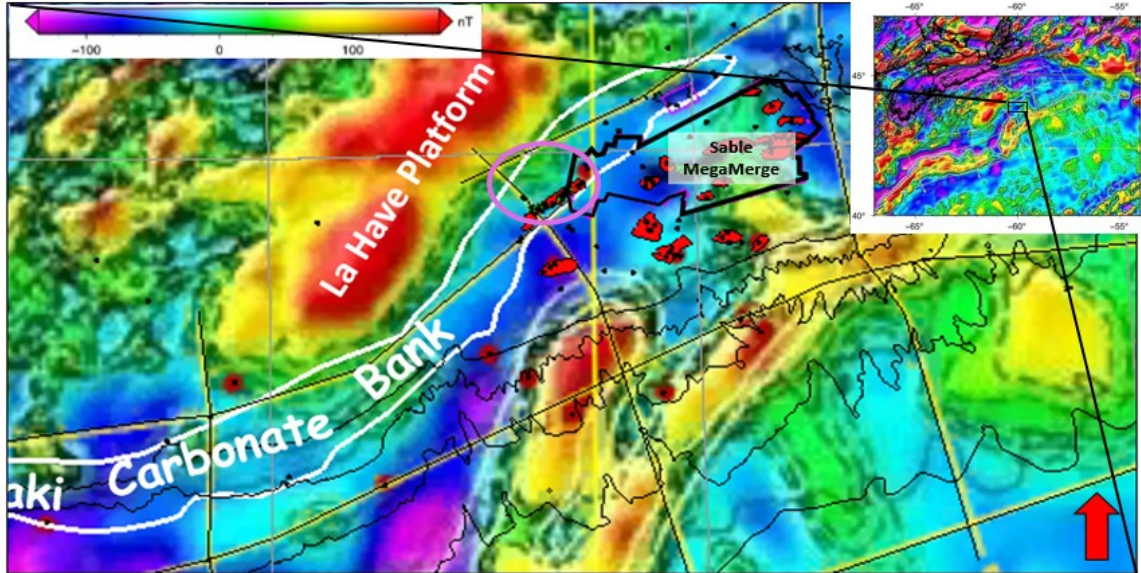


Figure 5.15: Updated magnetic anomalies map along the Scotian margin, overlain with an outline of the approximate boundaries of the Abenaki carbonate bank (white) and the outline of the Sable MegaMerge (black) showing how the Abenaki carbonate bank developed on the basement hinge zone (modified from Verhoef et al. 1996 and Dehler, 2010). The location of the basement high discussed in Section 4.78 can be seen in the top

left corner of the Sable MegaMerge outlined by a pink circle. Red patches represent gas fields.

In this area, it is interpreted that the Abenaki carbonate bank grew on the edge of this basement high, causing reefal debris to form a steep angle foreslope. There is evidence of early faulting at the hinge line on some of the seismic lines in the western region, however the faults due to compaction over the basinal edge of the basement high are interpreted to have formed prior to the carbonates being deposited (faults shown on Fig. 5.16 A and B). Figure 5.16 A shows the seismic horizons of the Abenaki carbonate bank that were correlated within the western area, deposited on the basement high and prograded off the shelf at a steep angle. Figure 5.16 B shows how the seismic horizons of the Abenaki carbonate bank were correlated only ~8 km to the east, having a much shallower (~10°) dipping carbonate ramp.

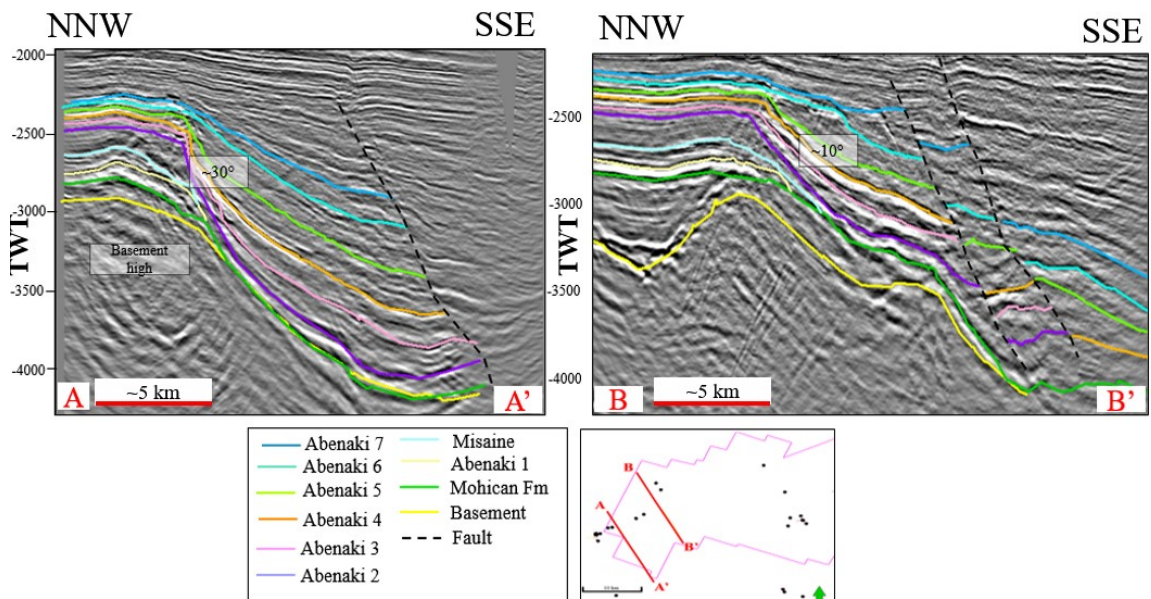


Figure 5.16 A: Inline 3440 from the Sable MegaMerge showing the steep slope angle of the Abenaki carbonate bank within the western region (A-A') caused by the carbonate bank being deposited on a basement high. B: Inline 3880 from the Sable MegaMerge, approximately 7.5 km from inline 3440, the carbonate ramp has a much shallower dip. The dip of the carbonate cycles in the western region become shallower (~10°) around the Upper Kimmeridgian (approximately during the deposition of Abenaki 6) due to siliciclastic influx from the northeast. Y-axis is TWT in milliseconds and has a vertical exaggeration of 5x.

5.7 Uncertainties

5.7.1 Seismic uncertainties

Sources of error for this study include interpretive error and spatial error. Interpretive error may be due to the misinterpretation of the seismic reflection data. Picking stratigraphic horizons via seismic reflection data is a manual process that depends on the available well tops (which are limited) and knowledge of the geology in the study area. The uncertainty of human bias has not been quantified (Bond et al. 2007). The interpretive error was minimized by researching published references on the study interval and discussing with other interpreters who also have knowledge of the study interval. Errors were also minimized by using an iterative interpretation process (Fig. 3.1).

Spatial errors may be due to the techniques used to gather the seismic reflection data, through errors in how well natural surfaces were modeled by the interpolation algorithm in Petrel™, and errors introduced in converting data from time to depth. The data acquisition and processing for the Sable MegaMerge was performed by the data owners and no knowledge of either was provided for this study. The errors that could be introduced at the seismic data acquisition and processing stage are generally only within the quality control of the survey.

5.7.2 Source rock potential uncertainties

Due to lack of well penetrations into the sediments of the Middle to Late Jurassic off the platform margin, there are several uncertainties in quantifying the potential of source rocks in the distal shales of the third-order depositional sequences. According to Tyson (1987), TOC content of marine sediments is controlled by the interplay of six main parameters: 1. Sediment texture (especially grain size); 2. Water depth; 3. Primary productivity; 4. Rate of allochthonous organic matter supply; 5. Rate of sediment accumulation and, 6. Bottom water oxygenation. These parameters have been interpreted for this study based on seismic stratigraphy and from knowledge of the depositional environments from core, thin sections and well log analysis, however the parameters were assumed for ideal conditions, and cannot be proven until there is more data from these time intervals in the Sable Sub-basin. There is no way to confidently predict whether there was high organic activity at the time of organic matter deposition from the Bajocian to the Mid-Kimmeridgian, and whether

anoxic conditions prevailed during these times intervals (Armstrong et al. 2016). It is also difficult to predict the rate of sediment accumulation; however, it can be assumed the sediment accumulation had a slower rate from the Bajocian to the Mid-Kimmeridgian in a carbonate-dominated depositional environment and a relatively faster rate from the Mid-Kimmeridgian to the Early Berriasian based on the thicker seismic units caused by the siliciclastic influx of the Sable Delta.

Chapter 6: Conclusions and recommendations for future work

6.1 Conclusions

This study provides a detailed stratigraphic framework of the Middle Jurassic to the Early Cretaceous, for the Abenaki carbonate bank region of the Sable Sub-basin. The study utilized 2D and 3D seismic data, analog studies and well information to interpret 17 seismic horizons and 14 faults, correlated throughout the western region of the 3D Sable MegaMerge. This seismic stratigraphic framework was correlated to the 2D seismic lines on the shelf, and the regional 2D NovaSpan 1600 line. Two-way-time and depth geocellular models were produced and populated with lithological information.

The primary objectives of this study were to:

1. Investigate structural, stratigraphic and depositional relationships between the two different depositional systems;
2. Interpret the interplay of the growth and cessation of the carbonates of the Abenaki Formation as a result of the influx of siliciclastics from the Sable Delta in the north;
3. Investigate the source rock potential of Middle Jurassic basinal mudstones (Verrill Canyon Formation) that preceded the deltaic influx;
4. Determine why the Abenaki carbonate bank transitions from a steeply dipping ramp ($\sim 30^\circ$) to a gently dipping slope ($\sim 10^\circ$) in the 10 km north of the Cohasset L-97 well.

It was hypothesized that the stratigraphic architecture and framework developed at Deep Panuke by Weissenberger (2000) and Encana (2006) could be extended basinward sub-regionally using modern, high quality 3D seismic data; and low impedance calcareous shales can be interpreted outboard of the carbonate platform margin. With favorable oceanic circulation and climatic conditions, these calcareous shales could have been deposited at a time of high organic productivity and there may have been subsequent preservation.

This study was successful in extending the Deep Panuke stratigraphic framework basinward and, as a consequence, deep water calcareous shales were interpreted with considerable confidence.

The stratigraphic architecture of the Middle Jurassic – Early Cretaceous was investigated using the seismic stratigraphic framework interpreted here. It was determined that the depositional environments, interpreted in each third-order depositional sequences, support the conclusion that the Sable Delta sourced from the northeast began influencing the growth of the Abenaki carbonate bank in the middle Kimmeridgian. The third-order depositional sequences below the middle Kimmeridgian (Abenaki 1-4) were deposited as a normal, shelf-margin carbonate system, outboard of siliciclastics of the Mic Mac and Mohican formations. The younger third-order depositional sequences, extending from the middle Kimmeridgian to the early Berriasian (Abenaki 5-7) were deposited as an increasingly mixed siliciclastic-carbonate depositional system in both the inboard and outboard settings. The carbonates in the Abenaki 5-7 sequences kept up with sea-level rise and grew predominately as patch reefs at the shelf margin, however they were not able to prograde as far into the basin as the sequences below. These upper sequences represent increasing influx of siliciclastics sourced from the Sable Delta.

The top and base horizons of each limestone and calcareous shale cycle were mapped and input into a 3D geocellular model. It is interpreted from this geological model and analog studies that the calcareous shales deposited on the distal foreslope/deep basin of the middle Callovian, middle Oxfordian and middle Kimmeridgian were in water depths potentially amenable to preservation of organic matter in anoxic conditions. If organic matter could be preserved, it would likely be type 2 kerogen.

It is less likely that there are potential source rocks in the late Kimmeridgian, the Tithonian and early Berriasian within the study area due to there being a mixed carbonate-siliciclastic depositional environment with shallower water, less anoxia and more dispersed organic matter. The depositional environment in which the mudstones of these third-order sequences were deposited was most likely of higher energy and in relatively shallower water depths compared to the older third-order depositional sequences of Abenaki 1-4 which were deposited in approximately 200-300 m water depths. If all conditions to produce a successful source rock were met, and anoxic conditions at this water depth prevailed, there may be potential to host a mixed type 2/type 3 kerogen source, with the terrigenous detritus sourced from the Sable Delta having potential to provide significant

organic content (Silva et al. 2015) basinward of the platform margin. Anoxic condition at this depth in the Scotian Margin may be inferred from analogous studies of the Moroccan Margin and the Lusitanian Basin, both of which have analogous source prone intervals within the Middle to Late Jurassic. However, this cannot be confirmed without well control.

From seismic correlations and the ensuing stratigraphic framework of the study area, it is interpreted that the siliciclastics that are interpreted directly outboard of the carbonate bank are Jurassic in age and therefore belong to the Mic Mac Formation, which interfingers with the carbonates and distal shales of the Abenaki Formation (Fig.5.7 C). At Migrant N-20, the siliciclastics within the interpreted expansion trend are interpreted to be younger, sourced from the Sable Delta of the Missisauga Formation and are juxtaposed against the clastics of the Mic Mac Formation and Verrill Canyon Formation at the faults. These siliciclastics do not interfinger with the distal shales of the Abenaki carbonate bank as stratigraphic charts (CNSOPB 2008; PFA 2011, 2016; Weston et al. 2012) suggest, based on seismic correlation of the third-order depositional sequences which are interpreted below the Migrant N-20 well (Fig.4.16), signifying the siliciclastics above are younger.

This study also concludes that the transition from a steep slope (~30 degrees) to a gentler dipping slope (~10 degrees) is due to positioning of the basement hinge line (between the LaHave Platform and Sable Sub-basin), determined from the magnetic grid created by Verhoef et al. (1996) and updated in 2010 by Dehler.

This project provides insight into the interactions between two separate depositional systems (carbonate depositional system of the Abenaki Formation and siliciclastic depositional system of the Missisauga and Mic Mac formations). Furthermore, it provides insight into how and when the influx of siliciclastics of the Sable Island Delta affected the growth of the third-order depositional sequences of the Abenaki carbonate bank, and how that may have affected the deposition and preservation of organic-rich material in the basal equivalents of the Abenaki carbonate bank.

The platform margin offshore Nova Scotia has been studied extensively for commercial reasons, but the interplay between the platform margin and associated basinal sediments

has received far less attention, due to lack of well penetrations and less direct commercial interest.

6.2 Recommendations for future work

The main uncertainty in this project, due to lack of well penetrations, is whether there was anoxia and high organic activity at the time of deposition of Middle to Late Jurassic basinal mudstones. To confirm the presence of source rock intervals within the distal mudstones of the Abenaki carbonate bank, a well would need to be drilled distal to the Jurassic shelf-slope break.

It is recommended that stratigraphic charts of the Scotian Basin (e.g. CNSOPB 2008; Weston et al. 2012; PFA 2011, 2016) be updated. They should not show the distal shales of the Abenaki carbonate bank (Verrill Canyon Formation) interfingering with younger sediments of the Missisauga Formation. These outboard clastics of the Missisauga Formation should be shown being separated by faulting.

$^{87}\text{Sr}/^{86}\text{Sr}$ isotope analysis is also recommended to be performed on in situ carbonates to test age relationships in the carbonates cored from the West Venture C-62 well. This analysis can also be useful to age date the third-order cycles more accurately.

References

- Alberty, M.W. 1994. Standard interpretation; part 4- wireline methods. *In*: Morton Thompson, D., and Woods, A.M (eds). Development Geology Reference Manual. AAPG Methods in Exploration Series, **10**. pp. 180-185.
- Albertz, M., Beaumont, C., Shimeld, J., Ings, S.J., and Gradmann, S. 2010. An investigation of salt tectonics structural styles in the Scotian Basin, offshore Atlantic Canada:1. Comparison of observations with geometrically simple numerical models. *Tectonic*, **29** (4): TC4017.
- Archie, G.E. 1952. Classification of carbonate reservoir rocks and petrophysical considerations. *AAPG Bulletin*, **36**(2): 218-298.
- Armstrong, H.A., Wagner, T., Herringshaw, L.G., Farnsworth, A.J., Lunt, D.J., Harland, M., Imber, J., Lopston, C., and Atar, E.F.L. 2016. Hadley circulation and precipitation changes controlling black shale deposition in the Late Jurassic Boreal Seaway. *Paleoceanography*, **31**: 1041-1053.
- Asquith, G., and Krygowski, D. 2004. *Basic Well Log Analysis*. 244.
- Azerêdo, A.C., Wright, V.P., Ramalho, M. 2002. The Middle-Late Jurassic forced regression and disconformity in central Portugal: eustatic, tectonic and climatic effects on a carbonate ramp system. *Sedimentology*, **49**: 1339-1370.
- Azerêdo, A.C., Duarte, L.V., Henriques, M.H., and Manupella, G. 2003. Da dinâmica continental no Triásico aos mares do Jurássico Inferior e Médio. *Cadernos de Geologia de Portugal*. Instituto Geológica e Mineiro, Lisboa (2003).
- Beicip-Franlab. 2011. Play Fairway Analysis. (PFA) offshore Nova Scotia Canada [online]. Halifax: Nova Scotia Department of Energy. Available from <http://energy.novascotia.ca/oil-and-gas/offshore/play-fairway-analysis/analysis>
- Beicip-Franlab. 2016. Central Scotian Slope Play Fairway Analysis (PFA) [online]. Halifax: Nova Scotia Department of Energy. Available from <http://www.oera.ca/offshore-energy-research/geoscience/central-scotian-slope-atlas-2016>
- Bhattacharya, J.P. 2010. Deltas. *In*: Facies Models 4 (eds). James. N.P and Dalrymple, R.W. Geological Association of Canada, St John's, Newfoundland.
- Bond, C.E., Gibbs, A.D., Shipton, Z.K., and Jones, S. 2007. What do you think this is? "Conceptual uncertainty" in geoscience interpretation. *GSA Today*, **17**: 4-10.

- Broughton P., and Trepaniér, A. 1993. Hydrocarbon generation in the Essaouira Basin of Western Morocco. *The American Association of Petroleum Geologist Bulletin*, **6**:999-1015.
- Brown, R.H. 1989. Triassic Rocks of Argana valley, Southern Morocco, and their structural implications. *American Association of Petroleum Geologists Bulletin*, **64**: 1988-2003.
- Brown, A.R. 1999. Interpretation of Three-Dimensional Seismic Data 5th ed. American Association of Petroleum Geologists Memoir, **42**. pp. 525.
- Campbell, T. 2014. Seismic stratigraphy and attribute analysis of the Mesozoic and Cenozoic of the Penobscot Area, offshore Nova Scotia. Honours Thesis, Department of Earth Sciences, Dalhousie University, Halifax, N.S.
- Campbell, T.J., Richards, F.W.B., Silva, R.L., Wach, G., and Eliuk, L. 2015. Interpretation of the Penobscot 3D seismic volume using constrained sparse spike inversion, Sable sub-Basin, offshore Nova Scotia. *Marine and Petroleum Geology*, **68**: 73-93.
- Canestrelli, A., Fagherazzi, S., Defina, A., and Lanzoni, S. 2010. Tidal hydrodynamics and erosional power in the Fly River delta, Papua New Guinea. *Journal of Geophysical Research*, **115**: 1-14.
- Cartwright, K.V. 2007. Determining the effective or RMS voltage of various waveforms without calculus. *The Technology Interface*, **8**(1): 1-20.
- CNSOPB. 2008. Canada- Nova Scotia Offshore Petroleum Board Call for Bids 2007 2008. Retrieved September 2013 from http://www.callforbids.cnsopb.ns.ca/2007/01/regional_geology.html
- Creybohm, J.R., Earley, K.M., Gunn, D., and Lackie, C. 1983. Well History Report. Mobil et al Arcadia J-16.
- Cummings D.C., and Arnott R.W.C. 2005. Growth-faulted shelf-margin deltas: a new (but old) play type, offshore Nova Scotia. *Bulletin of Canadian Petroleum Geology*, **53**(3): 211-236.
- Davison, I. 2005. Central Atlantic margin basins of North West Africa: Geology and hydrocarbon potential (Morocco to Guinea). *Journal of African Earth Sciences*, **43**: 254-274.
- Dromart, G., Garcia, J., Gaumet, F., Picard, S., Rousseau, M., Atrops, F., Lecuyer., and Sheppard, S.M.F. 2003. Perturbation of the carbon cycle at the Middle/Late Jurassic transition: Geological and geochemical evidence. *American Journal of Science*, **303**, 667-707.

- De'ath, G., Fabricius, K.E., Sweatman, H., and Puotinen, M. 2012. The 27-year decline of coral cover on the Great Barrier Reef and its causes. *Proceedings of the National Academy of Sciences of the United States of America*, **109(44)**: 17995-17999.
- Dehler, S.A. 2012. Initial rifting and breakup between nova Scotia and Morocco: insight from new magnetic models. *Canadian Journal of Earth Sciences*, **49**: 1385-1394.
- Deptuck, M.E. 2003. Post-rift geology of the Jeanne D'Arc Basin, with a focus on the architecture and evolution of early Paleogene submarine fans, and insights from modern deep-water systems. Ph.D. Thesis, Department of Earth Sciences, Dalhousie University, Halifax, N.S.
- Deptuck, M., and Kendell, K. 2012. Contrasting salt tectonic styles on the western versus central parts of the Scotian Margin, offshore Nova Scotia-Part 1 and Part 2. CNSOPB Geoscience Open File Poster 2012-001PF, 2 panels.
- Duarte, L.V. 1997. Facies analysis and sequential evolution of the Toarcian-Lower Aalenian series in Lusitanian Basin (Portugal). *Comunicações do Instituto Geológico e Mineiro*, **83**: 65-94.
- Duarte, L.V., and Soares, A.F. 2002. Litostratigrafia das séries margo-calcárias do Jurássico Inferior da Bacia Lusitânica (Portugal). *Commun. Inst. Geol. Min.*, **89**: 135–154.
- Duarte, L.V., Silva, R.L., Mendonça Filho, J.G., Poças Ribeiro, N., and Chagas, R.B.A. 2012. High resolution stratigraphy, palynofacies and source rock potential of the Água de Madeiros formation (Lower Jurassic), Lusitanian Basin, Portugal. *Journal of Petroleum Geology*, **35 (2)**: 105–126.
- Dunham. 1962. Dunham's Carbonate Rock Texture Classification. Modified by Embry & Klovan, 1971, and by Wright, (1992).
- Eliuk, L.S. 1978. The Abenaki Formation, Nova Scotia, Canada – a depositional and diagenetic model for a Mesozoic carbonate platform. *Bulletin of Canadian Petroleum Geology*, **26**: 424-514.
- Eliuk, L.S., and Levesque, R. 1988. Earliest Cretaceous sponge reef mound Nova Scotia shelf (Shell Demascota G-32). *In* Reefs, Canada and Adjacent Area. *Edited by* Geldsetzer, H.H.J., James, N.P., and Tebbutt, G.E. *Canadian Society of Petroleum Geologists Memoir 13*. pp. 713-720.
- Eliuk, L. and G. Wach. 2008, Carbonate and siliciclastic sequence stratigraphy examples from the Late Jurassic Abenaki limestone and West Venture deltaic beds, offshore Nova Scotia, Canada. *In*: Brown, D.E. (eds.) Program & Extended abstracts Central Atlantic Conjugate Margin Conference, CD and website. pp. 410-437.

- Eliuk, L.S. 2016. Abenaki carbonate platform in relation to the Jurassic-Cretaceous Sable Island Delta, offshore Nova Scotia, Canada. Ph. D Thesis, Department of Earth Sciences, Dalhousie University, Halifax, N.S.
- Ellis, P.M., Wilson, R.C.L., Leinfelder, R.R. 1990. Tectonic, palaeogeographic and eustatic controls on Upper Jurassic carbonate buildup development in the Lusitanian Basin, Portugal. *International Association of Sedimentologists Special Publication*, **9**: 169-202.
- Encana Corporation. 2006. Deep Panuke Offshore Gas Development. Development Plan, Volume 2. Halifax, NS. pp.2-65.
- Flügel, E. 2010. *Microfacies of carbonate rocks*. New York: Springer Heidelberg Dordrecht London New York.
- Forsman, J. P., and Hunt, J. M. 1958. Insoluble organic matter (kerogen) in sedimentary rocks. *Geochimica et Cosmochimica Acta*. **15**: 170-182.
- Fowler, M., Webb, J., Obermajer, M., Monnier, F., Mort, A., Luheshir, M., and MacDonald, A. 2016. Petroleum Systems of the Scotian Basin. *Search and Discovery Article*, **10871**.
- Francis, J.M., Daniell, J.J., Droxler, A.W., Dickens, G.R., Bentley, S.J., Peterson, L.C., Opdyke, B.N., and Beaufort, L. 2008. Deep water geomorphology of the mixed siliciclastic carbonate system, Gulf of Papua. *Journal of Geophysical Research*, **133**: F01S16.
- Frizon de Lamotte, D., Leturmy, P., Missenard, M., Khomsi, S., Ruiz, G., Saddiqi, O., et al. 2009. Mesozoic and Cenozoic vertical movements in the Atlas system (Algeria, Morocco, Tunisia): an overview. *Tectonophysics*, **475**: 9-28.
- GeoChem Laboratories (Canada) Ltd. 1983a. Hydrocarbon Source Facies Analysis: Mobil et al Arcadia J-16 Well. Prepared for Mobil Oil Canada Ltd.
- Given, M.M. 1977. Mesozoic and Early Cenozoic Geology of Offshore Nova Scotia. *Bulletin of Canadian Petroleum Geology*, **25**(1): 63-91.
- Hafid, M. 2000. Triassic-Early Liassic extensional systems and their Tertiary inversion, Essaouria Basin (Morocco). *Marine Petroleum Geology*, **17**: 409-429.
- Hafid, M., Zizi, M., Ait Salem, A., and Bally, A.W, 2006. Structural styles of the western onshore and offshore termination of the High Atlas, Morocco. *Comptes Rendus Geosci.*, **338**: 50-64.
- Hames, W. E., McHone, J. G., Ruppel, C., and Renne, P. (eds) 2002. The Central Atlantic Magmatic Province: Insights from Fragments of Pangea. *American Geophysical Union, Geophysical Monograph*, **136**: 267.

- Harvey, P.J., and Macdonald, D.J. 2013. Pre-discovery seismic modelling and prediction of the Deep Panuke Late Jurassic carbonate bank gas discovery, offshore Nova Scotia. Geological Society, London, Special Publications, **369**.
- Henry, S. 2004. Understanding Seismic Amplitudes. Search and Discovery Article 40135.
- Heyman, M.A.W. 1989. Tectonic and depositional history of the Moroccan continental margin. *In*: Tankard, A.J., Blankwill, H.R. (Eds.), *Extensional Tectonics and Stratigraphy of the North Atlantic Margins*. The American Association of Petroleum Geologists Memoir (**46**): 23-340.
- Ings, S.J., and Shimeld, J.W. 2006. A new conceptual model for the structural evolution of a regional salt detachment on the northeast Scotian margin, offshore eastern Canada. *American Association of Petroleum Geologists*. **90**(9): 1407-1423.
- Jabour, H., and Tari, G. 2007. Subsalt exploration potential of the Moroccan salt basin. *Leading Edge*, **26**: 1454-1460.
- Jansa, L.F., and Wade, J.A. 1975. Geology of the continental margin off Nova Scotia and Newfoundland. *In* *Offshore Geology of Eastern Canada, Regional Geology*. (Eds.) Vander Linden, W.J.M., Wade, J.A. Geological Survey of Canada, **2**: 51-106.
- Jansa, L.F. 1981. Mesozoic carbonate platforms and banks of the eastern North American margin. *Marine Geology*, **44**: 97-117.
- Jansa, L.F., and Weidmann, J. 1982. Comparison of northwest Africa and Canary and Cape Verde Islands. *In*: Von Rad, U., Hinz, K., Sarnthein, M., Seibold, E. (Eds.), *Geology of the Northwest African Continental Margin*. Springer Verlag, Berlin. pp. 215-269.
- Jenkyns, H.C. 1985. The early Toarcian and Cenomanian-Turonian anoxic events in Europe: comparisons and contrasts. *International Journal of Earth Sciences*, **74** (3): 505-518.
- Jenkyns, H.C. 1988. The early Toarcian (Jurassic) anoxic events: stratigraphic, sedimentary and geochemical evidence. *American Journal of Science*, **288**: 101-151.
- Kearey, P., and Brooks, M. 1991. *An Introduction to Geophysical Prospecting* (2nd ed.) Blackwell, Boston.
- Kendell, C.G.St.C., Alsharhan, A.S., Johnston, K., and Ryan, S.R. 2000. Can the sedimentary record be dated from a sea-level chart? Examples from the Aptain of the UAE and Alaska. *In*: Alsharhan, A.S and Scott, R.W. (eds). Society of Economic Petrologists and Mineralogists (SEPM) Special Publication 69 on the Jurassic-Cretaceous Platform-basin Systems; Middle East Models. pp. 65-76.

- Kenter, J.A.M., and Campbell, A.E. 1991. Sedimentation on a Lower Jurassic carbonate platform flank: geometry, sediment fabric and related depositional structures (Djebel Bou Dahar, High Atlas, Morocco). *Sedimentary Geology*, **72**: 1-34.
- Kidston, A.G., Brown, D.E., Smith B.M., and Altheim, B. 2005. The Upper Jurassic Abenaki Formation Offshore Nova Scotia: A Seismic and Geologic Perspective. Canada-Nova Scotia Offshore Petroleum Board, Halifax, NS.
- Klitgord, K.D., and Schouten, H. 1986. Plate kinematics of the Central Atlantic. *In*: Vogt, P.R., and Tucholke, B.E. (Eds). *The Western North Atlantic Region. The Geology of North America*. The Geological Society of America, **M**:351-377.
- Le Roy, P., and Pique, A. 2001. Triassic-Liassic Western Moroccan syn-rift basins in relation to the Central Atlantic opening. *Marine Geology*, **172**: 359-381.
- Loucks, R.G., and Sarg, J.F. 1993. Depositional Sequences and Systems Tracts Responses of Carbonate Platforms to Relative Sea-Level Changes. *In* *Memoir 57: Carbonate Sequence Stratigraphy: Recent Developments and Applications*. (Eds). K.T Biddle. AAPG, Tulsa, Oklahoma. pp. 19-40.
- Louden, K., Wu., Y., and Tari, G. 2013. Systematic variations in basement morphology and rifting geometry along the Nova Scotia and Morocco conjugate margins. Geological Society, London, Special Publications, **369**: 267-287.
- Marzoli, A., Renne, P.R., Piccirillo, E.M., Ernest, M., Bellieni, G., and De Min, A. 1999. Extensive 200 ma year old continental flood basalts of the Central Atlantic Magmatic Province. *Science*, **284**: 616-618.
- Mattis, A.F. 1977. Nonmarine Triassic sedimentation, central High Atlas Mountains, Morocco. *Journal of Sedimentary Petrology*, **47**: 107-119.
- McIver, N.I. 1972. Mesozoic and Cenozoic stratigraphy of the Nova Scotia Shelf. *Canadian Journal of Earth Sciences*, **9**: 54-70.
- Milliman, J.D., and Meade, R.H. 1983. World-wide delivery of river sediments to the oceans. *Journal of Geology*, **91**: 1-21.
- Milliman, J.D. 1995. Sediment discharge to the ocean from small mountainous rivers: The New Guinea example. *Geo-Marine Letter*, **15 (3-4)**:127-133.
- Mitchum, R., Vail, P., and Sangree, J. 1977. Seismic stratigraphy and global changes of sea level, part 6: stratigraphic interpretation of seismic reflection patterns in depositional sequences. *In* *Memoir 26: Seismic stratigraphy - applications to hydrocarbon exploration*. Edited by C. Peyton. AAPG, Tulsa. pp. 117-133.

- Mondol, N. 2010. Seismic Exploration. In Petroleum Geoscience. Springer Science, New York. pp. 375-402.
- Morrison, N, M. 2017. Seismic inversion and source rock evaluation on Jurassic organic rich intervals in the Scotian Basin, Nova Scotia. M.Sc. Thesis, Department of Earth Sciences, Dalhousie University, Halifax, N.S.
- Mosher, D.C., and Simpkin, P.G. 1999. Environmental marine geoscience 1. Status and trends of marine high-resolution seismic reflection profiling: Data acquisition. *Journal of the Geological Association of Canada*, **26(4)**: 174-187.
- Mukhopadhyay, P.K. 1990a. Characterization and maturation of selected Cretaceous and Jurassic source rocks and crude oil, Scotian Shelf. Geologic Survey of Canada, Open File #2621. Mukhopadhyay, P.K. 1990b. Characterization and Maturation of Selected Oil and Condensate Samples and Correlation with Source Beds, Scotian Shelf. Geologic Survey of Canada, Open File #2620.
- Mukhopadhyay, P.K. 1991. Evaluation of organic facies of the Verrill Canyon Formation, Sable Sub-Basin, Scotian Shelf. Geologic Survey of Canada, Open File #2435.
- Mukhopadhyay, P.K. 1994. Organic Petrography and Kinetics of Limestone and Shale Source Rocks in Wells Adjacent to Sable Island, Nova Scotia and the Interpretation on Oil-Oil or Oil-Source Rock Correlation and Basin Modeling. Geologic Survey of Canada, Open File #3167.
- Mukhopadhyay, P.K., and Wade, J.A. 1990. Organic facies and maturation of sediments from three Scotian Shelf wells. *Bulletin of Canadian Petroleum Geology*, **38(4)**:407-425.
- Neuweiler, F., Mehdi, M., and Wilmsen, M. 2001. Facies of Liassic sponge mounds, Central High Atlas, Morocco. *Facies*, **44**: 243-264.
- Newman, B.J. 1985. Deconvolution of noisy seismic data – A method for prestack wavelet extraction. *Geophysics*, **51**:34-44.
- Nunez-Betelu, L., and Baceta, J.L. 1994. Basics and application of Rock-Eval/TOC Pyrolysis: an example from the uppermost Paleocene/lowermost Eocene in the Basque Basin, western Pyrenees. *Munibe*, **46**: 43-62.
- Olsen, P.E., Kent, D.V., Fowell, S.J., Schlische, R.W., Jack M.O., and LeTourneau, P.M. 2000. Implication of a comparison of the stratigraphy and depositional environments of the Argana (Morocco) and Fundy (Nova Scotia) Permian Jurassic basin. *In*: Oujidi, M. and Et-Touhami, M., (eds), *Le Permien et le Trias du Maroc, Actes de la Premièr Réunion du Groupe Marocain du Permien et du Trias*: Oujda, Hilal Impression. pp. 165-183

- Olsen, P.E., Kent, D.V., Et-Touhami, M., and Puffer, J.H. 2003. Cyclo, magneto-and biostratigraphic constraints on the duration of the CAMP event and its relationship to the Triassic-Jurassic boundary. *In: Hames, W.E., McHone, J.G., Renne, P.R., Ruppel, C. (eds). The Central Atlantic Magmatic Province: Insights from Fragments of Pangea, Geophysical Monograph Series, 136:7-32.*
- Passey, Q. R., S. Creaney, J. B. Kulla, F. J. Moretti and J. D. Stroud. 1990. A practical model for organic richness from porosity and resistivity logs. *American Association of Petroleum Geologists Bulletin. 74: 1777-1794*
- Pena dos Reis, R., and Pimental, N. 2010. Analysis of the Petroleum Systems of the Lusitanian Basin (Western Iberian Margin)- A tool for deep offshore exploration. *In: Sedimentary Basin: Origin Depositional Histories and Petroleum Systems.*
- Péron-Pinvidic, G., and Manatschal, G. 2009. The final rifting evolution at deep magma poor passive margins from Iberia-Newfoundland: A new point of view. *International Journal of Earth Sciences, 98 (7): 1581-1597.*
- Pinheiro, L.M., Wilson, R.C.L., Pena dos Reis, R., Whitmarsh, R.B., and Ribeiro, A. 1996. The Western Iberia Margin: A geophysical overview. *In: Withmarsh, R.B., Sawyer, D.S., Klaus, A., and Masson, D.G. (Eds), Proceedings of the Ocean Drilling Program, Scientific Results, 149: 3-18.*
- Poças Ribeiro, N., Mendonça Filho, J.G., Duarte, L.V., Silva, R.L., Mendonça, J.O., and Silva, T.F., 2013. Palynofacies and organic geochemistry of the Sinemurian carbonate deposits in 708 the western Lusitanian Basin (Portugal): Coimbra and Água de Madeiros formations. *International Journal Coal Geology. 111: 37–52.*
- Posamentier, H.W., and Vail, P.R. 1988. Eustatic controls on clastic deposition I. Conceptual framework. *In: Wilgus, C.K., Hastings, B.S., Kendall, C.G.St.C., Posamentier, H.W., Ross, C.A., Van Wagoner, J.C. (eds). Sea-level changes-An integrated approach. SEPM Special Publication, 42:110-124.*
- Piper, D.J.W., Hiscott, R.N., and Normark, W.R. 1999. Outcrop-scale acoustic facies analysis and latest quaternary development of Hueneme and Dume submarine fans, offshore California. *Sedimentology, 46:47-78.*
- Rey, J. 1972. Recherches géologiques sur le Crétacé inférieur de l'Estremadura (Portugal) *Memórias dos Serviços Geológicos de Portugal, 21: 477*
- Rey, J., Dinis, J.L., Callapez, P., and Cunha, P.P. 2006. Da roturacontinental à margem passive. Composição e evolução do Cretácico de Portugal: *Cadernos de Geologia de Portugal. INETI, Lisbon, pp. 53*
- Sachse, V.F., Grobe, A., and Littke, R. 2012. Organic geochemistry and petrology of a lower Jurassic (Pliensbachian) petroleum source rock from AïT Moussa, Middle Atlas. *Journal of Petroleum Geology, 35(1):5-24.*

- Sangree, J.B., and Widmier, J.M. 1979. Interpretation of depositional facies from seismic data. *Geophysics*, **44**: 131-160.
- Sassen, R., and Post, P.J. 2007. Geochemical Evaluation of Condensate from Deep Panuke, Offshore Nova Scotia. Canada-Nova Scotia Offshore Petroleum Board Sample Report SR(E)2007-5. pp.1-7.
- Scholle, P.A., and Ulmer-Scholle, D.S. 2003. A Color Guide to the Petrography of Carbonate Rocks: Grains, textures, porosity and diagenesis. American Association of Petroleum Geologist Memoir 77. The American Association of Petroleum Geologists, Tulsa, Oklahoma, U.S.A.
- Schlager, W. 1980. Mesozoic calciturbidites of a drowned carbonate platform. *In*: Lancelot, Y., and Winterer, E.L. (Eds). Initial Reports of the Deep-Sea Drilling Project. US Government Printing Office, Washington, DC, **50**:733-749.
- Schlumberger Limited. 2015. Oil Field Glossary [online]. Available at <http://www.glossary.oilfield.slb.com> [Accessed February 8, 2016].
- Scotese, C. R. 2001. Atlas of Earth History, Volume 1, Paleogeography, PALEOMAP Project, Arlington, Texas. pp. 52
- Scruton, P.C. 1960. Delta building and the deltaic sequence. *In*: Shepard, F.P., Phleger, F.B., and van Andel, T.H. (eds.). Recent sediments Northwest Gulf of Mexico. American Association of Petroleum Geologist. pp. 82-102.
- Shimeld, J. 2004. A comparison of salt tectonic subprovinces beneath the Scotian slope and Laurentian Fan. Gulf Coast Section of the Society of Economic Paleontologists and Mineralogists Transactions, **24**: 502-532.
- Sheriff, R., and Geldart, L.P. 1995. Exploration seismology (2nd ed.). Cambridge, New = York. Cambridge University Press.
- Silva, R.L., Mendonça Filho, J.G., Azerêdo, A.C., and Duarte, L.V. 2014. Palynofacies and TOC analysis of marine and non-marine sediments across the Middle-Upper Jurassic boundary in the central northern Lusitanian Basin (Portugal). *Facies*, **60**: 255-276.
- Silva, R.L., Wach, G., and Wong, C. 2015 Source Rocks and Petroleum Systems of the Scotian Basin. *CSEG Recorder*, **40**: 22-27.
- Silva, R.L., Duarte, L.V., Wach, G., Morrison, N., and Campbell, T. Submitted. Accumulation of a large oceanic DOC pool during the Bathonian-Callovian. Submitted.

- Simm, R., and Bacon, M. 2014. *Seismic Amplitude: An Interpreter's Handbook*. Cambridge University Press, United Kingdom. pp. 30-37.
- Sine, G., Ellsworth, W., and Donnelly, D. 1984a. Well History Report. Shell Petrocan et al. South DesBarres O-76.
- Soares, A.F., Rocha, R.B., Elmi, S., Henriques, M.H., Mouterde, R., Almeras, Y., Ruget, C., Marques, J., Duarte, L.V., Carapito, C., and Kullberg, J.C. 1993. Le sous bassin nord 741 lusitanien (Portugal) du Trias au Jurassique moyen: Histoire d'un "rift avorté". *Comptes Rendus de L'Académie des Sciences*, **317**: 1659–1666.
- Suárez-Ruiz, I., Flores, D., Mendonça Filho, J.G., and Hackley, P. C. 2012. Review and update of the applications of organic petrology: Part 1, geological applications. *International Journal of Coal Geology*, **99**: 54-112.
- Tari, G., and Molnar, J. 2005. Correlation of syn-rift structures between Morocco and Nova Scotia, Canada. *Gulf Coast Section of the Society of Economic Paleontologist and Mineralogists Transactions*, **25**: 132-150.
- Tari, G., and Brown, D.E. 2012. The conjugate margins of Morocco and Nova Scotia. *In Regional Geology and Tectonics: Phanerozoic Passive Margins, Cratonic Basins and Global Tectonic Maps. Edited by Roberts, D.G and Bally, A.W.* pp. 285-318.
- Tari, G., and Jabour, H. 2013. Salt tectonics along the Atlantic margin of Morocco. *Geological Society of London Publications*, **369**: 337-353.
- Tissot, B., and Welte, D.H. 1984. *Petroleum formation and occurrence*. 2nd ed. Springer Verlag, Heidelberg.
- Tixeront, M. 1973. Lithostratigraphie et minéralisation cuprifères et uranifères syngénétiques et familiares des formations détritiques permo-triassique du couloir d'Argana (Haut Atlas occidental Maroc). *Notes du Service géologique du Maroc*, **33** (249):147-177.
- Tyson, R.V. 1987. The genesis and palynofacies characteristics of marine petroleum source rocks. *In: Brooks, J., and Fleet, A.J. (eds). Marine Petroleum Source Rocks. Geological Society Special Publication*, **26**: 47-67.
- Vail, P.R., Todd, R.G., and Sangree, J.B. 1977. Seismic Stratigraphy and Global Changes of Sea Level: Part 5. Chronostratigraphic Significance of Seismic Reflections: Section 2. *In Memoir 26: Application of Seismic Reflection Configuration to Stratigraphic Interpretation*. pp. 99-116.
- Van Krevelen, D.W. 1993. *Coal: typology–physics–chemistry–constitution*, 3rd edition. Elsevier Science Publishers, Amsterdam, NL.

- Van Wagoner, J.C., Posamentier, H.W., Mitchum, R.M., Vail, P.R., Sarg J.F., Lutit, T.S., and Hardenbol, J. 1988. An overview of sequence stratigraphy and key definitions. *In: Wilgus, C.K., Hastings, B.S., Kendall, C.G.St.C., Posamentier, H.W., Ross, C.A., and Van Wagoner, J.C. (eds). Sea-level changes-an integrated approach. SEPM Special Publication, 42:39-45.*
- Veeken, P.C.H., and van Moerkerken B. 2013. Seismic stratigraphic techniques. *In Seismic stratigraphy and Depositional Facies Models. Edited by EAGE Publications. Academic Press, The Nertherlands. pp 110.*
- Verhoef, J., R. Macnab, and Project Team. 1996. Compilation of magnetic data in the Arctic and north Atlantic oceans, Bedford Institute of Oceanography unpublished report. pp.1-13
- Wach, G.D., Pena dos Reis, R., and Pimental, N. 2014. Petroleum Systems of the Central Atlantic Margins, from outcrop and subsurface data. 2012 GCSSEPM Foundation Bob F. Perkins Research Conference, January 26-28, 2014, Houston, Texas.
- Wade, J.A., and MacLean, B.C. 1990. Chapter 5- the geology of the southeastern margi of Canada part 2: aspects of the geology of the Scotian Basin from recent seismic and well data. *In Geology of Canada No.2-Geology of the Continental Margin of Eastern Canada. Edited by Keen, M.J., Williams, G.I. Geological Survey of Canada, 2: 190-238.*
- Wade, J.A., MacLean, B.C., and Williams, G.L. 1995. Mesozoic and Cenozoic stratigraphy, eastern Scotian Shelf: new interpretations. *Canadian Journal of Earth Sciences, 32: 1462-1473.*
- Wade, J.A. 2000. Depth to pre-Mesozoic and Pre-Carboniferous basements. Geological Survey of Canada Open-File Report 3842.
- Weissenberger, J.A.W., Harland, N, Hogg, J., and Syhlonyk, G. 2000. Sequence Stratigraphy of Mesozoic Carbonates, Scotian Shelf, Canada. PanCanadian Petroleum Limited.
- Weissenberger, J.A.W., Wierzbicki, R.A., and Harland, N.J. 2006. Carbonate sequence stratigraphy and petroleum geology of the Jurassic Deep Panuke Field, offshore Nova Scotia, Canada. *In Giant Hydrocarbon reservoirs of the World: From rocks to reservoir characterization and modeling. Edited by Harris, P.M and Weber, L.J. American Association of Petroleum Geology Memoir 88/SEPM Special Publication, pp. 395-431.*

- Weston, J.F., MacRae, R.A., Ascoli, P., Cooper, M.K.E., Fensome, R.A., Shaw, D., and Williams, G.L. 2012. A revised biostratigraphic and well-log sequence stratigraphic framework for the Scotian Margin, offshore eastern Canada. *Canadian Journal of Earth Sciences*, **49**: 1478-1503.
- Wierzbicki, R., Dravis, J.J., Al-Aasm, I., and Harland, N. 2006. Burial dolomitization and dissolution of Upper Jurassic Abenaki platform carbonates, Deep Panuke reservoir, Nova Scotia, Canada. *American Association of Petroleum Geology Bulletin*, **90**: 1843-1861.
- Wilson, R.C.L., Hiscott, R.N., Willis, M.G., and Gradstein, F.M. 1989. The Lusitanian Basin of West-Central Portugal: Mesozoic and Tertiary Tectonic, Stratigraphic, and Subsidence History: Chapter 22: European-African Margins. *In* *Memoir 46: Extensional Tectonics and Stratigraphy of the North Atlantic Margins*. pp. 341-360.
- Woolfe, K., and Larcombe, P. 1997. Terrigenous sedimentation and coral reef growth: a conceptual framework. *Marine Geology*, **155 (3-4)**: 331-345.
- Yilmaz, O., and Doherty, S.M. 1987. Seismic data processing (Investigations in geophysics). Tulsa, OK, Society of Exploration Geophysicists.
- Yilmaz, O. 2001. Seismic data analysis: Processing, Inversion, and Interpretation of Seismic Data. Chapter 3: Velocity Analysis and statics corrections. Society of Exploration Geophysicist.

Appendix A: Ancient analogs: Moroccan Margin and Lusitanian Basin

Geological background of the Moroccan Margin and Lusitanian Basin

Pre-rift (Early-mid Triassic)

Tensional forces in the Early Triassic created northeast-trending troughs on the eastern side of the Appalachian Mountains before seafloor spreading began in the Early Jurassic (Albertz et al. 2010). Red beds, dolomite and halite were the dominant deposits during the late pre-rift phase, deposited in rift valleys formed before the break-up of the continental mass (e.g. Given 1977; Wade and MacLean 1990; CNSOPB 2008)

Syn-rift (Late Triassic-Early Jurassic)

Within the Essaouira Basin, Morocco, approximately 5 km of extensional syn-rift red beds (conglomerate, sandstone and claystone of the Ikakem and Bigoudine formations (Fig. 2.3)), disconformably overlie a metamorphic Paleozoic basement within the Argana graben (Tixeront 1973; Brown 1980).

In the Lusitanian Basin, Triassic red fluvial siliciclastics (Silves Group, Soares et al. 1993) are overlain by evaporites deposited during the Hettangian (Dagorda Formation) (Fig. 2.4). The depositional thickness of the Dagorda Formation controlled the distribution of halokinetic structures throughout the basin. Where this formation was thick, diapiric structures developed over reactivated Hercynian basement faults (reactivated during both the Mesozoic extensional and Tertiary compressional episodes), but where it was thin or absent, the faults propagated directly into younger sediments (e.g. Wilson et al. 1989). Sediments of Triassic and Hettangian age accumulated within grabens and half grabens.

Rifting continued until Early Jurassic, when sea-floor spreading initiated, separating North America and Africa, initiating the proto-Atlantic. Extension then became confined to the spreading centre, terminating rifting. This is marked by a break-up unconformity between syn-rift and post-rift sections.

Tectonism continued into the Late Triassic – Early Jurassic allowing for the complete separation of North America and Africa, forming the proto-Atlantic Ocean (McIver 1972).

Early-Middle Jurassic post-rift (Sinemurian - Bajocian)

After the break-up of the Scotian and Moroccan margins, a shallow marine sea flooded the Scotian Basin resulting in the deposition of carbonates, dolomites and clastics of the Iroquois Formation (Fig. 2.3 and Fig 2.5). The Iroquois Formation transitions laterally and upwards into terrestrial and marine siliciclastics of the Mohican Formation and distal shales (unnamed in Fig. 2.2).

On the Moroccan Margin, in a similar arrangement, carbonates of the Ankoult Formation transition from terrestrial and marginal marine clastics of the Argana Formation (Figs. 2.3 and 2.4) below, and upwards to marginal marine siliciclastics of the Ameskrout Formation. This mixed carbonate clastic system transitions laterally to unnamed distal shales (Fig. 2.6).

Within the Lusitanian Basin, the Coimbra and Brenha groups of the Early Jurassic blanketed the basin and show minor indications of contemporaneous faulting (e.g. Wilson

et al. 1989). The Coimbra Formation marks the first carbonate influence in the Lusitanian Basin. It was deposited from Lower Sinemurian to Toarcian and is broadly coeval with Iroquois carbonates in Nova Scotia. Time equivalent basinal shales are designated the Brenha Formation in the Lusitanian Basin but are not named on the Scotian Margin. The Coimbra Group comprises dolostones and dolomitic limestones. The fluvial clastics of the Mohican Formation (Middle Jurassic) on the Scotian Margin are time equivalent to the dolomitic limestones of the São Miguel Formation within the Coimbra Group, deposited during the Upper Sinemurian. Within the Lusitanian Basin, there are no equivalent aged clastics, like there are on the Scotian and Moroccan margins, due to the Lusitanian Basin being in a quiescent gulf stage from the Sinemurian to the Callovian (e.g. Soares et al. 1993; Azerêdo et al. 2003).

Middle – Late Jurassic post-rift

By the Middle Jurassic on the Moroccan margin, marine sedimentation dominated the proto-Atlantic, accumulating a thick sedimentary wedge until the Late Cretaceous. The wedge is bounded to the north and south by Hercynian structures. During the Middle to Late Jurassic, a carbonate platform (Amsitten Formation) approximately 800 m thick developed, which corresponds to the Abenaki Formation in the Scotian Basin. In the Late Jurassic, approximately 2000 m of regressive red beds and evaporites were deposited within the Neknafa syncline (Imouzzer Formation, Fig. 2.3 and 2.7) (e.g. Brown 1980; Jansa and Weidmann 1982; Broughton and Trepaniér 1993; Davison 2005). This influx of siliciclastics is attributed to the regional tectonic uplift of the Atlas (Davison 2005).

Within the Lusitanian Basin, the Middle-Late Jurassic transition corresponds to a basin-wide disconformity and stratigraphic gap that spans from the latest Callovian to early Oxfordian, followed by forced regression (Silva et al. 2014). The Middle Jurassic units are fully marine, whereas the Late Jurassic sediments are freshwater/brackish lacustrine, grading into brackish-restricted lagoonal and shallow-marine paleoenvironments (Silva et al. 2014). The Cabaços Formation contains the earliest Oxfordian sediments, consisting of lacustrine ostracod-charophyte lime mudstones (Ellis et al. 1990; Azerêdo et al. 2002). The Cabaços Formation also contains highly bituminous horizons and is hypothesized as the source for the numerous hydrocarbon shows in the southern part of the Lusitanian Basin (e.g. Silva et al. 2014). The Candeeiros Group was deposited basin-wide as marl-limestone alternations (dominated by limestones). The Candeeiros Group (Middle Jurassic) and the Cabaços Formation (Oxfordian) correspond to the Middle-Late Jurassic Abenaki Formation of the Scotian Basin.

Relative sea-level rise resulted in deposition of marine carbonates in most of the southern and central parts of the Lusitanian Basin in the late Oxfordian. This was the main carbonate buildup phase in the basin history, when the limestones of Montejunto Formation (Fig. A-1) were deposited.

During the early Kimmeridgian, an abrupt rise in relative sea-level, accompanied by uplift of marginal basement highs, ended the deposition of carbonates in most parts of the Lusitanian Basin generating a sudden influx of siliciclastics (Abadia Formation similar to the Missisauga Formation with the Sable Sub-basin). However, carbonate sedimentation did continue on structural highs into the Kimmeridgian, contemporaneous with the

deposition of shale and limestone breccia of the Tojeira member at the base of the clastic Abadia Formation in the central part of the basin (Ellis et al. 1990).

Prograding continental siliciclastics continued during the Tithonian, resulting in the accumulation of approximately 1 km of fluviodeltaic sands and clays of the Lourinhã Formation (Pena dos Reis and Pimental 2010).



Figure A-1: *Montejunto Formation, Middle Jurassic platform.*

2.3.5 Cretaceous post-rift

The Atlasic orogeny on the Moroccan Margin during the latest Cretaceous and Tertiary significantly modified the basin by uplifting the sediments and tilting them seaward, eroding much of the sediments in the process (Broughton and Trepaniér 1993). Uppermost Cretaceous to Tertiary sediments reflect the diminished influence of the Atlantic seafloor spreading on the passive continental margin as well as compressive Atlasic tectonics. This change in tectonics resulted in a shift from shale accumulation on the shelf and the deposition of limestone to widespread erosion, leaving coarser conglomeratic clastics in structural lows (Broughton and Trepaniér 1993). Fine-grained marine clastic sedimentation dominated the early Cretaceous associated with regional tectonic uplift of the Atlas, except for regressive red beds in the mid-Hauterivian (Fig. 2.3) (Davison 2005). Transgression took place in the Campanian to Maastrichtian with marls, dolomites, limestones and chalk (Aounine Formation, unnamed on Fig. 2.3) reaching 300 m in thickness (Davison 2005).

Within the Lusitanian Basin, the facies pattern of carbonates replacing siliciclastics southwards within the Berriasian time continued into the Valanginian. The Farta Pão Formation contains brackish fauna of Tithonian age at its top and is overlain conformably by a series of carbonate units, in the south grouped into the Cascais Formation. Rey (1972)

suggested that Berriasian strata are missing, therefore the siliciclastics of the Torres Vedras Formation (Fig. 2.4) rest unconformably on older strata.

2.3.6 Cenozoic post-rift

East of the present-day Essaouira Basin on the Moroccan margin, the Atlas trough was inverted during the Cenozoic, forming the Atlas Mountains (Broughton and Trepaniér 1993). A fold belt along the northern margin separates the Essaouira and Doukkala basins. The southern boundary of the basin has folded and faulted strata against the High Atlas Mountains, associated with the South Atlas Fault Zone (Heyman 1989). In the Essaouira Basin, Palaeocene and Eocene sedimentation is represented by marl and sandstone passing up into dolomite sandstone and red marl of Eocene age (Imi n'Tanout Formation, unnamed on Fig. 2.3). The Oligocene-Miocene uplift eroded as much as 3 km of Jurassic and Cretaceous section from the southern part of the basin. Pliocene, shallow-marine marl and sandstone complete the stratigraphic section (El Mhasseur Formation, unnamed on Fig. 2.3) (Davison 2005).

The main difference between the Scotian and Moroccan margins after the Barremian is the amount of siliciclastics delivered across their paleo-shelves. Several major deltas developed on the Canadian margin throughout most of the Cretaceous; whereas in Morocco, the last major pulse of siliciclastic sedimentation on the paleo-slope was deposited by the Neocomian Tan-Tan fan delta system in the Tarfaya and Agadir Basins (Louden et al. 2013). This is interpreted to be due to the Avalon uplift on the Scotian Margin, which is a Late Jurassic rift flank uplift, associated with the initiation of seafloor spreading between the Grand Banks and western Europe (Iberia) (Wade and MacLean 1990) causing the drowning of carbonates on the Scotian margin approximately mid Cretaceous; whereas on the Moroccan margin, the Atlasic orogeny during the latest Cretaceous and Tertiary allowed deposition of siliciclastic sediments to continue (Louden et al. 2013).

Within the Lusitanian Basin, as much as 1 km of siliciclastic sands were deposited throughout the basin during the Cenozoic (Wilson et al. 1989).

Figure A-2 is an interpreted petroleum systems chart of the Moroccan margin based upon literature review.

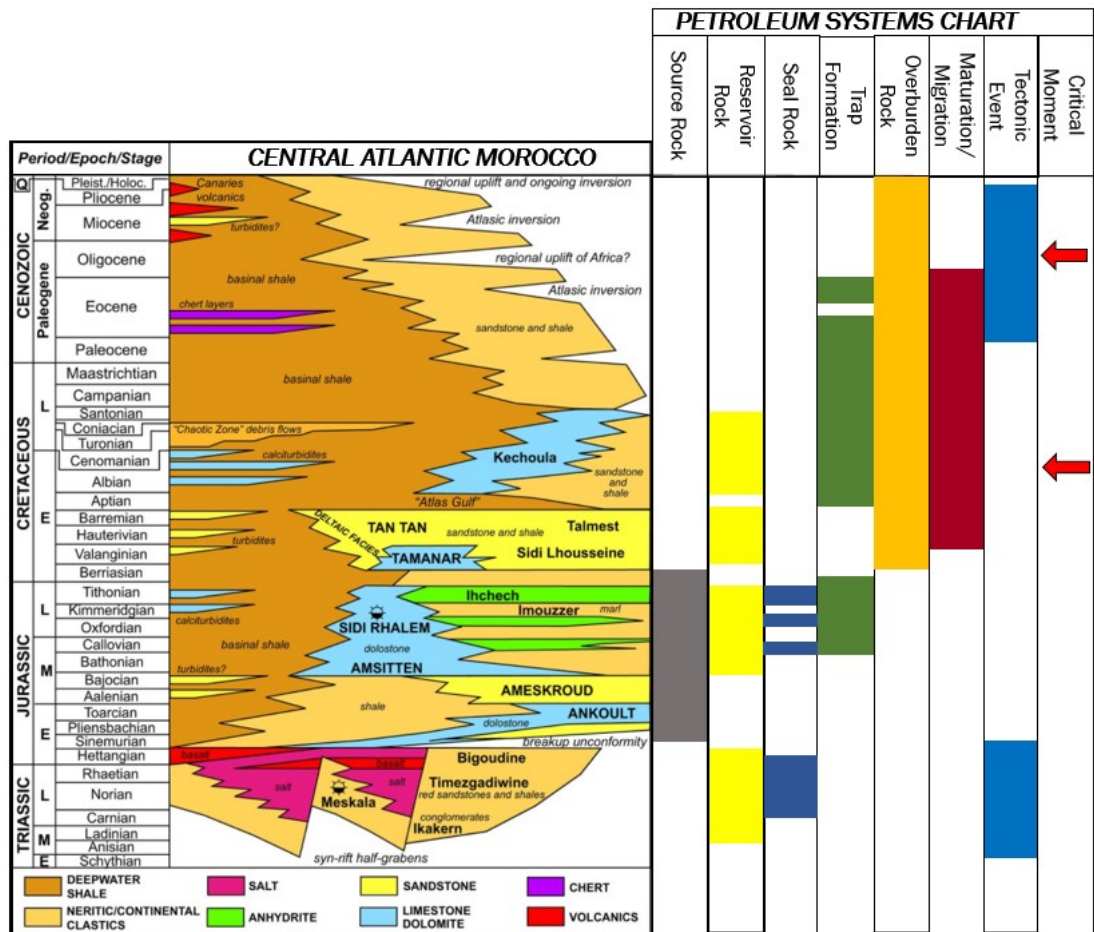


Figure A-2: Petroleum systems chart of the Moroccan Margin interpreted from literature review. Stratigraphic chart is from Tari et al. 2012.

Field work in the Lusitanian Basin: Organic-rich intervals

The organic-rich intervals studied throughout the Lusitanian Basin included Figueira da Foz site, Pedrógão site, Vale de Ventos (Maciço Calcário Estremenho) site, and S. Pedro de Moel site, where the Água de Madeiros Formation can be found.

Figueira da Foz

At Figueira da Foz, the Cabo Mondego Formation disconformably overlies the Cabaços Formation (Chapter 2). The Cabaços Formation starts with an association of sandstones with oyster-rich mudstones, and bioclastic limestones with coral (Silva et al. 2014). The marine influence in the Cabaços Formation gradually dissipates upwards, where dinosaur footprints were observed. At Figueira da Foz, the Cabo Mondego Formation comprises marl-limestone alternations with marine macrofossil assemblage including, brachiopods, bivalves and ammonites (Fig. A-3 A and B). Previously analyzed sections of the Cabo Mondego Formation at this locality by Silva et al. (2014) demonstrate that the basal deposits of the Upper Callovian have type 2 kerogen assemblages, containing vast array of marine palynomorphs such as acritarchs, dinoflagellate cysts, prasinophyte phycococci

and Amorphous Organic Matter derived from plankton. There is also an upward variation in kerogen assemblages at both Pedrógão and Figueira da Foz, suggesting evidence of an overall regressive trend, becoming less marine upwards (Silva et al. 2014), similar to the depositional trend observed within the Abenaki carbonate bank.

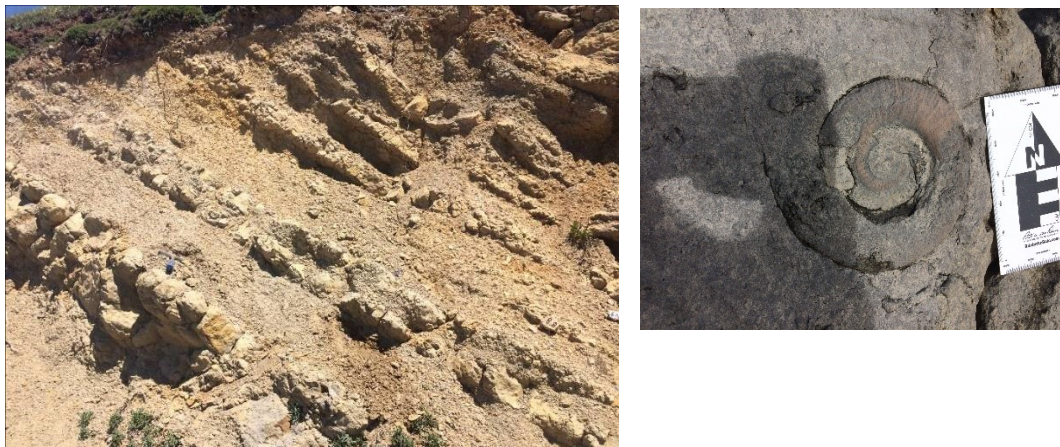


Figure A-3 A: *Cabo Mondego Formation at Figueira da Foz, demonstrating marl-limestone alternations.* B: *ammonite found within the Cabo Mondego Formation at Figueira da Foz.*

Pedrógão

Pedrógão is located approximately 30 km south of Figueira da Foz. At this location, the angular unconformity between the Middle-Late Jurassic can be seen, with the Cabaços Formation overlying the Uppermost Cabo Mondego Formation (Silva et al. 2014). The Cabo Mondego Formation is mostly marls with some limestone intercalations and includes a vast array of marine benthic and nektonic fauna including: brachiopods, bivalves, echinoderms, foraminifers, ostracods and ammonites (Silva et al. 2014). The faunal assemblages change to shallow-marine reworked with non-marine towards the top of the succession, hosting reptile teeth and fossil wood fragments. The top ferruginous limestone bed is irregular and corresponds to the disconformity surface (Azerêdo et al. 2002). Overlying the disconformity is a ferruginous charophyte coquina, which marks the beginning of the Cabaços Formation.

At this location, the Cabaços Formation is approximately 25m thick and is made up of marls, marly limestones and ferruginous limestones. Desiccation features (Fig. A-4A) and minor erosion surfaces are present throughout the section. The interval at this locality is characterized by the absence of marine fossils as well as the presence of non-marine bivalves (Fig. A-4B), gastropods, charophytes and ostracods (Silva et al. 2014). This succession was interpreted to be deposited in shallow, fresh to brackish water, paralic to marginal-marine restricted environments (Azerêdo et al. 2002).



Figure A-4 A: *Desiccation features (polygonal cracks) within the limestone of the Cabaços Formation. B: Serpulid colony amongst fresh water bivalves.*

Like the Cabo Mondego Formation at Figueira da Foz, at Pedrógão, this interval also showed type 2 kerogen. Palynofacies at Pedrógão indicates that the particulate organic matter is of continental origin, but also incorporates small marine events, indicated by the rare occurrence of dinoflagellate cysts. Palynofacies from the Cabo Mondego Formation also indicates that deposition happened in a calm, proximal environment close to the source area.

Maciço Calcário Estremenho

In the heart of the Maciço Calcário Estremenho is the Vale de Ventos section, where the Cabaços Formation angular unconformity overlies the Upper Bathonian limestones of the Serra de Aire Formation (Fig. A-5). Here, the Cabaços Formation is approximately 9 m thick comprised of pedogenic limestones, black-pebble conglomerates, lignitic clays and marls, and marly limestones (Silva et al. 2014). Here, the base of the Cabaços Formation does not contain marine fossils, as it does at Pedrógão. Silva et al. (2014) stated that fresh water ostracods, charophytes, porostromates and gastropods are abundant at this location, and interpreted this section to have been deposited in a very shallow, protected inland system, such as a pond or marsh, without marine influence.

At Vale de Ventos, kerogen assemblages are almost all from a terrestrial origin. As suggested by Silva et al. (2014), these palynofacies reflect an overall proximal to distal distribution, and the Cabaços Formation encompasses a broader range of depositional environments than the Cabo Mondego Formation.



Figure A-5: *Middle-Late Jurassic disconformity (red dashed line), with the Cabaços Formation of the Late Jurassic overlying the limestones of the Serra de Aire Formation of the Middle Jurassic.*

S. Pedro de Moel

The carbonate dominated succession of the Early Jurassic in the Lusitanian Basin has significant source rock potential. S. Pedro de Moel in western Portugal has the type locality of the Água de Madeiros Formation of the Upper Sinemurian-lowermost Pliensbachian, composed of alternating organic-rich marls and limestones, including black shale horizons, generally 10 cm thick, with the thickest being 50 cm thick (Duarte et al. 2012) (Fig. C-6).

The Água de Madeiros Formation comprises two members, Polvoeira and Praia da Pedra Lisa. Ammonites provide good biostratigraphic markers to separate these two members. On top of the Água de Madeiros Formation is the Vale das Fontes Formation, Pliensbachian in age, dominated by marlstones. At S. Pedro de Moel, a complete succession from the underlying Coimbra Formation to the overlying Vale das Fontes Formation is exposed, including the two members of the Água de Madeiros Formation. At this locality, the Água de Madeiros Formation has a total thickness of approximately 58m. The basal section of the Polvoeira Member is dominated by limestones with regular marl-limestones alternations. The carbonates and some marls contain abundant benthonic macrofauna including brachiopods, infaunal and epifaunal bivalves and the trace fossil *Rhizocorallium*. Also, within this member are organic-rich black shales, approximately 10 cm thick, the thickest being 50 cm thick (Duarte et al. 2012) and have type 2 kerogen assemblages.

The Praia da Pedra Lisa Member is a carbonate-dominated unit, approximately 16 m thick. At the base, it comprises decimeter-centimeter thick mudstones to wackestones rich in ostracods and radiolarians with ammonites, and trace fossils *Rhizocorallium* and *Thalassinoides* present in some layers. The upper part of this member is approximately 7 m thick and is marked by a gradual increase in dark grey marls and a thickening of limestone beds. Some of the marly intervals contain high amounts of organic matter (OM),

with type 2 kerogen, where limestone beds contain molluscs, ostracods, brachiopods, belemnites and ammonites (Duarte et al. 2012).



Figure A-6: *Transition between Sinemurian and Pliensbachian, Early Jurassic within the Água de Maderios Formation. TOC in this location ranges from 0-15% with 0.45 vitrinite reflectance. There are type 1 kerogen microbial mats present. Very fissile shale is rich in ammonites and bivalves as well as fish scales. Marl/limestone alterations, with predominately marls at this location.*

Overall, the Água de Madeiros Formation comprises three organic-rich lithofacies: dark grey marlstones, black shales and thin laminated limestones, which contains TOC <1 wt%. The Polvoeira Member has maximum TOC values of 22 wt.% and is the interval with the greatest amount of black shale layers. Kerogen assemblages in the Água de Madeiros Formation are dominated by Amorphous Organic Matter with some contribution by phytoclasts and palynomorphs, based on the geochemical evaluation of this formation done by Duarte et al. (2012). Organic geochemical data obtained by Duarte et al. in 2012 show that the Água de Madeiros Formation hosts some of the most organic-rich intervals in the basin. However it is immature or very early mature as a source for potential hydrocarbon systems, as determined by T_{max} values below 437°C and average vitrinite reflectance values of 0.43% R_o (Duarte et al. 2012).

Appendix B: Wireline logs used within the study area

Gamma ray

Gamma ray logs measure the natural radioactivity within the rock surrounding the well. The elements of interest that produce gamma radiation in typical sedimentary rocks include potassium, thorium and uranium. Generally, shale contains most of these elements and therefore the gamma ray reading of shale is typically greater than that of sandstone. Gamma ray logs can provide an indication of potential source rock intervals by examining the decay chain of the three elements: potassium, thorium and uranium, and the log response in which they form. Since these elements are found in shales, the higher log responses on a gamma ray log could potentially represent source rock intervals.

Sonic

A sonic log is an acoustic log that displays interval transit time (in microseconds per foot or microseconds per meter) of primary acoustic waves versus depth (Schlumberger 2015). Interval transit time is the inverse of the velocity, therefore the slower the velocity, the greater the interval transit time. The sonic log measures how fast sound travels through rocks and provides valuable information related to the porosity of a rock; a low porosity rock will have a faster interval transit time and will generate a low sonic reading and a high porosity rock will have a greater interval transit time due to the sound waves spending a longer amount of time in fluids, therefore will generate a high sonic reading (Passey et al. 1990). Sonic logs get recorded by sending out acoustic pulses from a source, that travel through the surrounding rock and the velocity of the sound of the rock gets recorded at the receiver at the other end of the logging tool (Asquith and Krygowski 2004).

Resistivity

A log of the resistivity of a rock formation is expressed in ohm-m. It measures the resistance to the electrical current within a volume of rock (Schlumberger 2015). Resistivity logs measure the resistance between two and four electrodes, which are in contact with the rocks surrounding the well. Measured resistivity is a function of water saturation, the percentage of the porosity that is filled with water. Resistivity logs help indicate the fluid present within a rock; water has a very low resistivity while hydrocarbons can have very high resistivity (Passey et al. 1990). Although, if the fluid comprises hydrocarbons the use of other well logs, such as gamma ray, are necessary.

Formation factor is important to determine the concentration of pores and their connectivity. Rocks that have a low permeability but a still quite porous will have a higher formation factor because the electrical current will be obstructed, giving an overall higher total rock resistivity (Asquith and Krygowski 2004).

Density

Density logging tools measure the bulk density of the combined matrix and pore-filling fluids. Density logs measure the density of the rocks and their pore fluid by measuring the electro density of a rock. A strong radioactive source emits high-energy gamma rays down the borehole, and with every collision with an electron the gamma rays loses energy and some eventually get absorbed when their energy gets too low (Asquith and Krygowski 2004). The gamma rays that get returned to the detectors are measured and the formation's density is determined. Formations with a high gamma ray count have lower densities than

those with a low gamma ray count (Asquith and Krygowski 2004). Densities typically increase with depth in a normal pressure regime due to pore water loss from compaction.

Lithology

Lithology logs are plotted versus depth and were created by the Canadian Stratigraphic Services (2000) Ltd. (Canstrat) from analyzing cuttings taken from wellbores using petrographic methods. Canstrat washed and dried cuttings, and these were examined and compared to the description completed by the wellsite geologist. From the cuttings, data on grain size, rounding and sorting of grains, rock type and percentage of minerals, porosity type, oil straining, fluorescence, mineral occurrence and fossil type were compiled. The data collected by Canstrat was digitized into .las files and was helpful in correlating formations from the wellbore to the seismic data.

RockEval pyrolysis well data

RockEval pyrolysis of cutting samples was performed on Cohasset L-97 by the Geological Survey of Canada (GSC) in 1986 and by Dr. Mukhopadhyay in 1991 and 1994. RockEval pyrolysis was also performed on cutting samples of South Desbarres O-76 by the GSC in 1991 and by Dr. Mukhopadhyay in 1991 and 1994. From the Cohasset L-97 well, samples were selected from the Abenaki Formation from 3100-4900 m and from the South Desbarres O-76 well, samples from the Logan Canyon, Missisauga, Verrill Canyon and Mic Mac formations from 2345-5705 m were chosen. For determination of kerogen type by organic petrography, three types of sample preparations were used by Mukhopadhyay: kerogen smear slide, whole rock polished pellet, and kerogen polished pellet. Vitrinite reflectance was measured using both whole rock and kerogen pellets. RockEval pyrolysis was carried out on selected washed/hand-picked cuttings.

Appendix C: Seismic acquisition and processing applied to the Sable Sub-basin

Seismic data acquisition and processing

Seismic acquisition and processing of the 3D Sable MegaMerge was all done prior to Dalhousie University receiving the data. This section discusses different acquisition and processing techniques to understand potential constraints on seismic interpretation.

The primary tool used in this study is reflection seismic data. Seismic data are acquired with acoustic sources and receivers. The acoustic energy propagates in different directions and gets reflected or refracted when it reaches boundaries between two geological layers of variable density (Mondol 2010). Seismic receivers, such as hydrophones are designed to detect seismic energy in the form of pressure changes in the water during marine acquisition, are placed near the surface of the water and measure the reflected or refracted acoustic energy (Mondol 2010). The receivers convert the acoustic energy into an electrical signal that typically consists of seismic frequencies in the range of 5-100 Hz (Mondol 2010). An individual seismic trace represents a time-series (in units of two-way travel time-TWTT) of reflection returns from subsurface interfaces, convolved with the input source, and recorded by hydrophones towed behind the vessel.

Seismic reflections are generated at surfaces where there are contrasts in acoustic impedance (AI), which is the product of density (ρ) and velocity (V),

$$\text{Equation 3.1: } AI = \rho \cdot V, \frac{\text{kg}}{\text{m}^3} \cdot \frac{\text{m}}{\text{s}}$$

If a low impedance layer (e.g. shale) overlies a high impedance layer (e.g. limestone) a positive reflection coefficient is generated; if the deeper layer has a lower impedance, a negative coefficient is generated. Reflection coefficients (RC) are caused by contrasts in AI between layers,

$$\text{Equation 3.2: } RC_1 = \frac{AI_2 - AI_1}{AI_2 + AI_1}$$

Ocean bottom cables

Venture (1996), Thebaud (1996), and Sable Island (1999) 3D seismic surveys within the Sable MegaMerge were collected using ocean bottom cables. Ocean bottom seismic (OBS) is collected by placing vertically oriented hydrophones connected by electrical wires and deployed on the seafloor to record and rely data to the seismic recording vessel (Fig. C-1).

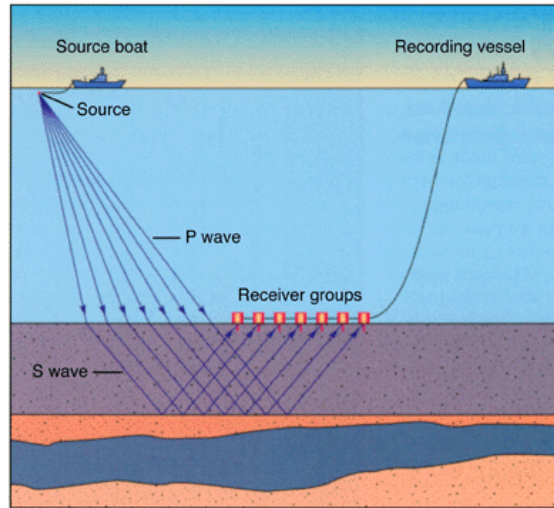


Figure C-1: General set up to collect OBS. A source boat sending out a source (a noise that creates a water pulse) to the receivers placed vertically in the subsurface, which then relay their information to a recording vessel (Peak Seismic Solutions Ltd 2017).

Marine Streamers

Another acquisition method, used for collecting 3D seismic data for the EL 2356 (1997), Arcadia (1998) and Intrepid (1999) surveys within the Sable MegaMerge, is recording via marine streamers. The hydrophones are combined to form streamers that trail behind the seismic acquisition vessel. Typically, the length of the steamer is about 4-6 km long with approximately 96 hydrophones along a 75 m long receiving section. A source is sent out of the acquisition vessel in the form of a shot, which creates a water pulse, typically from an airgun, in which high pressure air is stored in a chamber, and upon triggering this air is expelled in the water. The release of air generates a strong pressure pulse and forms an air bubble. The bubble oscillates, generating a sequence of decaying pressure variations that follow the initial pulse. The acoustic impulse response of the earth is then reflected up to the receivers being towed behind the acquisition vessel and the data is collected (Fig. C-2).

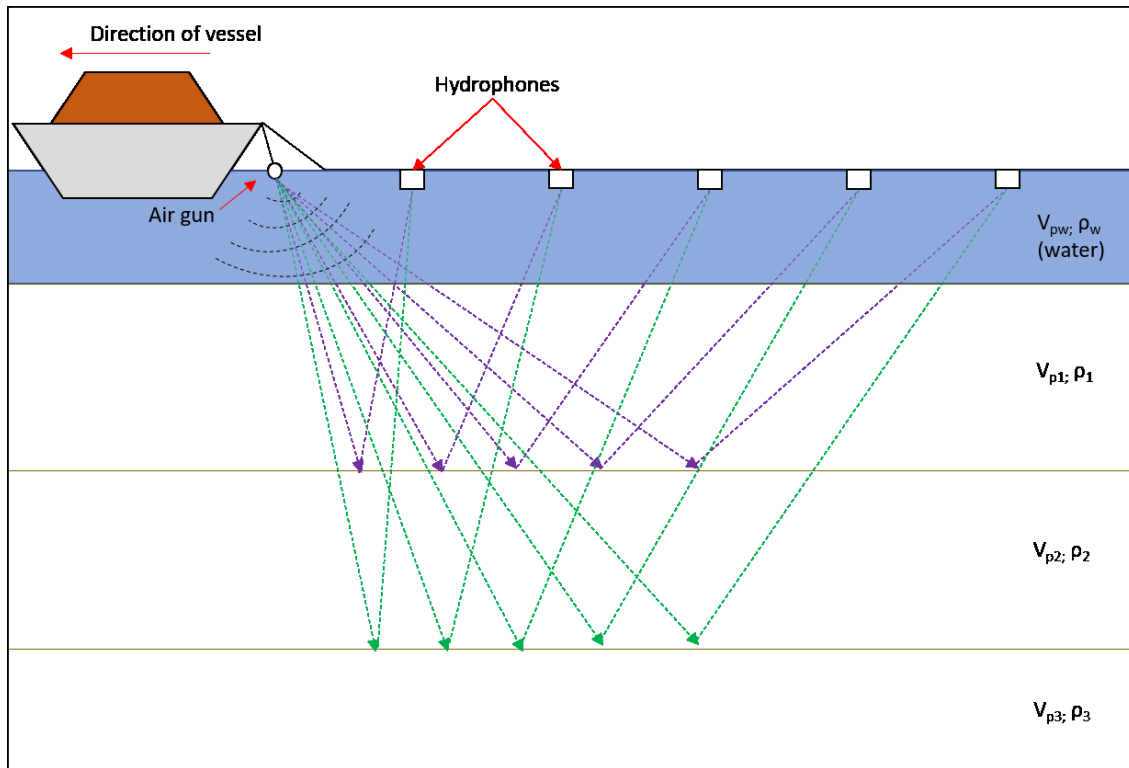


Figure C-2: Diagram of an acquisition vessel towing streamers (with hydrophones) and the ray paths that results from a single shot of an airgun. V =velocity, ρ =density (modified from Analytics Magazine 2018).

Exponential gain (spherical divergence)

Exponential gain is typically applied to prestack data before deconvolution to compensate for attenuation losses. Energy is lost due to the curved-ray spherical divergence and needs to be corrected for to obtain true amplitudes. The spherical divergence effect on amplitudes is often approximated by the inverse square of distance, which for a constant velocity is the inverse square of time. This factor is smaller for reflectors that are separated by less time, and minor for most lateral changes (Henry 2004).

Prestack deconvolution

Seismic data are normally deconvolved prior to stacking to force on each trace within a common midpoint gather to have the same bandwidth and phase. The purpose of prestack deconvolution is to remove the effects of varying source and receiver wavelets to enable a good common-midpoint (CMP) stacking over the entire seismic bandwidth (Newman 1985). Within offshore data, the source wavelet and attenuation pattern are often stable, therefore pulse compression (whitening deconvolution), phase control and short-period multiple removal are the main objectives in deconvolution (Newman 1985).

Multiple suppression

Multiples are reflected seismic energy, or any event in seismic data that has incurred more than one reflection in its travel path. Multiples can cause many issues for interpretation due to multiples creating features that do not reflect the true geology of a structure and therefore need to be suppressed (Yilmaz 2001). The two main types of multiples are water bottom

multiples and interbed multiples. Both types of multiples produce reflections from a second or more “bounce” within a layer. They are suppressed by predictive deconvolution and filtering techniques.

Filtering for noise

Removal of noise allows for all other signal processes to work more effectively. There are generally two categories for the source of noise: Coherent noise, which can be modeled and subtracted from the data, includes, ground roll, strum noise, and multiples. Random noise, which is any noise spikes or bursts which are not coherent in nature. The seismic trace is the combination of both signal (wanted data) and noise (unwanted data). To enhance the signal-noise ratio, different techniques are used to remove the noise including: frequency filtering, inverse filtering (deconvolution), and velocity filtering (Yilmaz 2001). Common midpoint gathering is the most effective way to enhance the signal-to-noise ratio.

Normal moveout correction (NMO)

Normal moveout describes the effect that the distance between a seismic source and a receiver (the offset) has on the arrival time of a reflection in the form of an increase of time with offset. Normal moveout correction is a function of time and offset that is used to compensate for the effects of the normal moveout, or the delay in reflection arrival times (Yilmaz 2001).

Common mid-point gathering (CMP)

Figure 3.2 and 3.3 show that each receiver is recording reflections from different subsurface locations. If the Earth is made up of relatively flat-lying layers, then the various traces relating to the source-receiver pairs which share a CMP will also share common subsurface reflection points. Once a CMP gather has been created and NMO corrected, the traces are then summed or stacked. This increases the signal-to-noise ratio considerably. If the geology is not horizontally bedded, data can still be stacked, however migration issues will occur either pre- stack or post stack, which is usually adequate in passive margin settings. (Fig. C-3). (Simm and Bacon 2014).

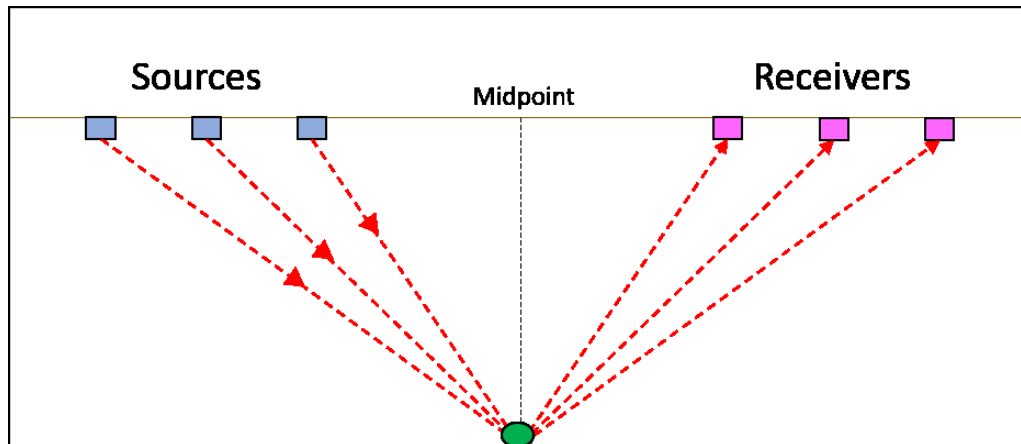


Figure C-3: *Common midpoint (CMP) gather method, if assumed that the Earth is relatively flat lying, the data can be arranged according to reflection location (modified from Agile Scientific 2017).*

Deconvolution

Deconvolution is a filtering process which attempts to remove a wavelet from the recorded seismic trace by stabilizing the bandwidth and phase of a data set, with some broadening of the amplitude spectrum (whitening). It also attenuates reverberations and short-period multiples, thus increases the temporal resolution and gives a good representation of the subsurface reflectivity. The most common way to perform deconvolution is to design a Wiener filter (best shapes a given wavelet to a desired wavelet in a least-squares sense). Predictive deconvolution suppresses multiple reflections and optionally alters the spectrum of the input data to increase resolution (Yilmaz 2001).

Gain (AGC)

An automatic gain control (AGC) is sometimes applied to seismic data to strengthen weak signals. It also has the possibility of destroying signal character. AGC is used to improve visibility of late-arriving events in which attenuation of wavefront divergence has caused amplitude decay (Yilmaz 2001).

Poststack migration

Migration of seismic data moves dipping events to their correct positions, collapses diffractions, and increases spatial resolution. While migration algorithms are capable of accurately imaging reflections from steep interfaces, CMP stacking can lead to destruction of such reflections before conventional poststack migration is applied. Poststack migration with the added step of dip moveout (DMO) applied after NMO correction can convert data recorded with separated sources and receivers to a close approximation to zero-offset data, preserving reflections from both gently dipping and steep reflectors (Yilmaz 2001).

Resolution

Seismic resolution refers to the ability to distinguish between objects, and in seismic is considered in the vertical and horizontal (x and y) directions. Units need to be sufficiently thick or laterally extensive to visualize the unit as a reflection. By varying the frequency content of the sound source, a wide range of resolution is possible. Frequencies that are absent from the input sound source, will also be absent from the resulting seismic traces, therefore the sound source is important (Mosher and Simpkin 1999). Higher resolution provides detailed information at approximately the bed scale, but the source has limited penetration due to lack of lower frequencies therefore only allowing the shallow strata to be well imaged (Piper et al. 1999). In comparison, typical 2D and 3D seismic data use an airgun source with a dominant frequency range of between 30 and 60 Hz. Such data have lower vertical resolution (6-20 m) but are capable of imaging deeply buried systems. Sheriff and Geldart (1995) classify seismic resolution as the minimum separation of two objects such that they can be distinguished as two separate entities rather than one.

Vertical resolution

Vertical resolution is a measure of the ability to distinguish individual closely spaced reflectors and depends strongly on the frequency content of the acoustic source (Kearey and Brooks 1991). Vertical resolution is typically taken as $\frac{1}{4}$ the dominant wavelength of the acoustic source, although a bed that is significantly thinner than $\frac{1}{4}$ wavelength can still produce a reflection, but the bed thickness cannot be determined from the wave shape (Yilmaz 1987). Vertical resolution of seismic data can be calculated using equation B-1b.

$$\text{Equation B-1a: } \lambda = v/f \text{ and}$$

$$\text{Equation B-1b: } \textit{vertical resolution} = (v/f)/4$$

Where λ represents wavelength, v is the velocity and f is the dominant frequency. Vertical resolution can be improved by increasing the dominant frequency of the input source and decreasing the unwanted noise (Yilmaz 1987). A common effect on seismic data is the decrease in frequency with depth, due to various effects of the earth filter. This change is frequency with depth and an overall increase in velocity with depth, has have an obvious effect on vertical resolution (Simm and Beacon 2014).

Horizontal resolution

Horizontal resolution refers to the ability to distinguish between features that are displaced horizontally with respect to one another (Sheriff and Geldart 1995). Horizontal resolution depends on the size of the Fresnel zone, a circular area on a reflector from which a reflection is generated (Sheriff and Geldart 1995). The width of the Fresnel zone depends on the dominant wavelength (hence frequency f) of the sound source, the distance from the source to the reflector (z), and the velocity (v) above the reflector (Yilmaz 1987). The Fresnel zone gets larger with increasing depth due to spherical divergence of the wavefront and attenuation of higher frequencies (Kearey and Brooks 1991).

Migration is the main tool for improving horizontal resolution and can be thought of as collapsing the Fresnel zone (Sheriff and Geldart 1995). The horizontal resolution of migrated seismic data is approximately equivalent to the dominant wavelength of the source.

Methods for viewing seismic data

Since 3D seismic surveys consist of a volume of data, there are various methods which allow interpreters to “slice” through the volume and extract specific information from a vast quantity of data (Deptuck 2003). Several methods were used in this study to enhance interpretation. Specific strategies were developed to investigate different aspects of carbonate and deep-water depositional systems. The most common methods used for viewing the data in this study include vertical seismic sections and time-slices.

A vertical seismic section can be taken in any orientation, parallel to 3D inlines or cross lines, diagonally, or multi-panel displays. These sections allow a cross sectional view of the subsurface. Vertical sections were used to determine the extent and morphology of the carbonate sequences and the internal seismic character (seismic facies) of the carbonate depositional system. Features that are too subtle to be detected using vertical sections are better imaged using horizontally oriented sections called time-slices (parallel to given TWTT, or depth, if seismic volume is depth converted). Time slices were used in this study to examine the seismic data for patterns in amplitude.

Seismic Traverses (composite lines)

Multiple composite lines (not an inline or crossline) of 2D and 3D data were generated to tie the 3D to wells outside the 3D survey area and to look at structural and stratigraphic relationships beyond the 3D area. Composites within the 3D survey were generated to observe and interpret specific structural and stratigraphic relationships.

Seismic Amplitudes

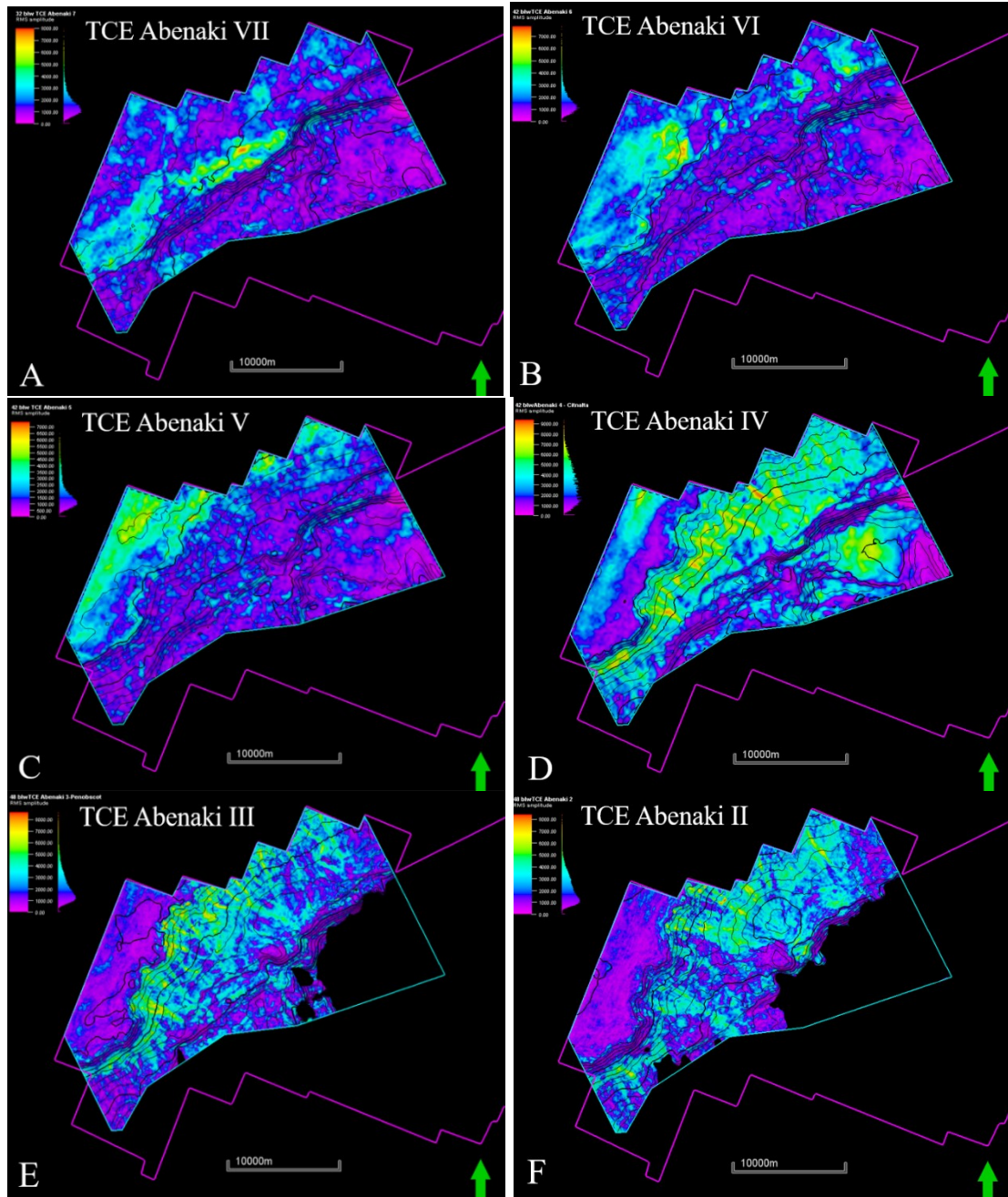
Reflection amplitude and strength

Reflection amplitude is the most commonly used attribute for vertical, horizontal and horizon-parallel slices. It is the measure of the strength and polarity (positive or negative) of a reflection and depends on the contrasts in acoustic impedance between the overlying and underlying lithologies. The amplitude attribute is non-unique and therefore different lithologies or geological situations can create similar amplitudes. Reflection strength is plotted independent of polarity, meaning that it is the absolute value of amplitude (Mitchum et al. 1977).

Time-structure and time-thickness (isochron)

Time-structure maps represent the structure of a seismic horizon in units of TWT. 2D seismic horizons were correlated using seismic-well ties and a “loop-tying” technique. This technique is done by correlation of one 2D line that crosses a well penetration with well tops. Those well tops are manually interpreted onto the 2D line. The location where the newly interpreted 2D line crosses another 2D line is then interpreted until all of the horizons on the 2D lines are confidently picked.

RMS amplitude maps



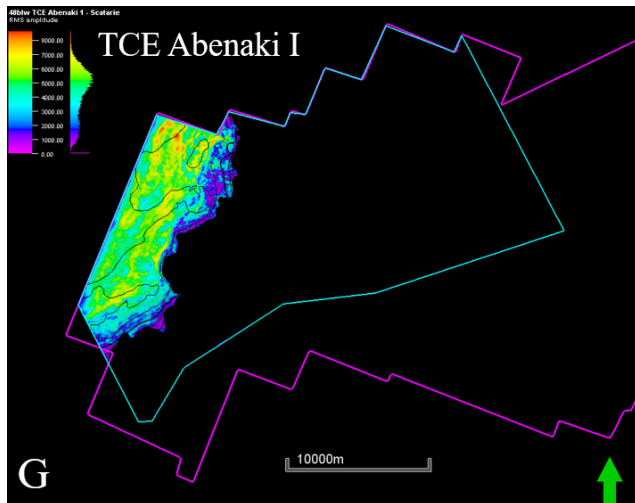


Figure C-4: A-G: RMS amplitude maps for all third-order depositional sequences. Maps were cropped to fit within the model area (blue polygon). The purple polygon is the 3D Sable MegaMerge area. High RMS amplitude (4000-7000, light blue-green-red) represent carbonate rocks. Low RMS amplitude (0-4000, purple-dark blue) represent siliciclastic rocks.

Root mean square (RMS) amplitude is a surface attribute calculated from the “Surface Attributes” tool within Petrel™. It was run for each interpreted carbonate cycle by creating three copies of the same horizon, and moving one above the original horizon by 12ms, and moving the other horizon below the original horizon by 48ms, this attribute can be run multiple ways within Petrel™, however this gave the most accurate results based from interpretations of the seismic data. The RMS amplitude was then computed between each “above 12ms” and “below 42ms” horizon to obtain the RMS amplitude for all the carbonate cycles. The result of the RMS amplitude mapping shows the growth of the carbonate cycles (i.e., how far they developed into the basin), where carbonate was most prevalent compared to siliciclastics, and therefore aided in creating environment of deposition maps discussed in Chapter 4.

RMS amplitude shows where high amplitudes and low amplitudes are located within a given time interval and emphasizes the variations in acoustic impedance over a selected time interval. Where there are high amplitudes (light blue-green-red), it is interpreted to be primarily carbonate rocks having a high velocity and density, producing a high acoustic impedance. Where there are low amplitudes (dark blue-purple), it is interpreted to be primarily siliciclastic rocks having a lower velocity and density, giving a low acoustic impedance.

Figure C-4 shows that carbonate growth prograded the furthest out into the basin during the middle Kimmeridgian with the Abenaki 4 (D) cycle. Abenaki 1 (G) is the Scatarie Member and has very strong amplitudes signifying predominantly carbonate growth during the Bajocian-Bathonian on the platform margin. The reflections representing the top of the Scatarie Member downlap onto the Mohican Formation terminating the carbonate growth of this member. Abenaki 7 (A) - Abenaki 5(C) sequences did not develop as far into the basin as carbonates, however transitioned to siliciclastics beyond the platform margin. The

carbonates for these cycles developed more sporadically as patch reefs and pinnacles, primarily on the depositional edge of the margin, as the Sable Delta influenced the growth of carbonates. Minor reefs developed on the siliciclastic edge, keeping up with sea-levelchange.

Appendix D: Core descriptions

Core logs for the core descriptions are available in supplementary data.

Mohican I-100 Core #3: 29.1ft Recovered

Box 8: 9318ft-9314ft

Dark grey/black fissile shale from 9318ft-9316.5ft then abruptly transitions back into lighter grey wackestone that is heavily bioturbated

Box 7: 9322ft-9318ft

Dark grey/black fissile shale (storm deposit?) (perhaps a grain-packstone) with abundant disarticulated shell frags (primarily bivalves). Silty to very fine-grained sand size with scattered and discontinuous wavy laminae. No bioturbation unit this interval. Grains are well sorted. Intraclasts with oncoids, serpulids, bivalves and have micritic envelopes. Minor amounts of echinoderms (Intraclast came from quieter setting).

Box 6: 9325ft-9322ft

Gradual transition into fissile shale (storm deposit?) (perhaps a grain-packstone) with abundant disarticulated shell frags (primarily bivalves). Silty to very fine-grained sand size with scattered and discontinuous wavy laminae. No bioturbation unit this interval. Grains are well sorted. Intraclasts with oncoids, serpulids, bivalves and have micritic envelopes. Minor amounts of echinoderms

Box 5: 9329ft-9325ft

Missing core from 9327ft-9325ft. Dark grey in color. Small black organic rich laminations. Abundant shell frags including mollusks, gastropods, brachiopods. Other fossils visible include serpulids and foraminifera. Heavily bioturbated ~3. Shell frags are all in the mud-wackestone, would have come from elsewhere (bivalves are filled with other sediments). Mud-wackestone is interbedded with small intervals (<3cm thick) of argillaceous siltstone). *Thalassinoid* trace fossil.

Box 4: 9333ft-9329ft

Dark grey in color. Small black organic rich laminations. Abundant shell frags including mollusks, gastropods, brachiopods. Other fossils visible include serpulids and foraminifera. Heavily bioturbated ~3. Shell frags are all in the mud-wackestone, would have come from elsewhere (bivalves are filled with other sediments). Mud-wackestone is interbedded with small intervals (<3cm thick) of argillaceous siltstone).

Box 3: 9335ft-9333ft

Dark grey in color. Small black organic rich laminations. Abundant shell frags including mollusks, gastropods, brachiopods. Other fossils visible include serpulids and foraminifera. Heavily bioturbated ~3. Shell frags are all in the mud-wackestone, would have come from elsewhere (bivalves are filled with other sediments). Mud-wackestone is interbedded with small intervals (<3cm thick) of argillaceous siltstone).

Box 2: 9339ft-9335ft

Dark grey in color. Small black organic rich laminations. Abundant shell frags including mollusks, gastropods, brachiopods. Other fossils visible include serpinlids and foraminifera. Heavily bioturbated ~3. Shell frags are all in the mud-wackestone, would have come from elsewhere (bivalves are filled with other sediments). *Rhizocorallium* trace fossil. Small <1cm microbial mud lamination. Mud-wackestone is interbedded with small intervals (<3cm thick) of argillaceous siltstone).

Box 1: 9344ft-9339ft

Dark grey in color. Small black organic-rich laminations. Abundant shell frags including mollusks, gastropods, brachiopods. Other fossils visible include serpinlids and foraminifera. Heavily bioturbated ~3. Shell frags are all in the mud-wackestone, would have come from elsewhere (bivalves are filled with other sediments).

Mohican I-100 Core #4: 29.8ft Recovered

Box 9: 10568ft-10565ft

Medium grey in color, with silty to medium grained framework grain component. Heavily bioturbated, however ooids and intraclasts return >20% clasts. Minor black mud laminations (almost stylolites).

Box 8: 10572ft-10568ft

Medium grey in color, with silty to medium grained framework grain component. Heavily bioturbated, not many structures to see.

Box 7: 10577ft-10572ft

Medium grey in color, with silty to medium grained framework grain component. Heavily bioturbated, not many structures to see. Minor black mud laminations (almost stylolites).

Box 6: 10579ft-10577ft

Medium grey in color, with silty to medium grained framework grain component. Heavily bioturbated, not many structures to see. Minor black mud laminations (almost stylolites).

Box 5: 10582ft-10579ft

Medium grey in color, with silty to medium grained framework grain component. Heavily bioturbated, not many structures to see. Minor black mud laminations (almost stylolites).

Box 4: 10585ft-10582ft

Medium grey in color, with silty to medium grained framework grain component. Heavily bioturbated, not many structures to see. Minor black mud laminations (almost stylolites).

Box 3: 10588ft-10585ft

Medium grey in color, with silty to medium grained framework grain component. Abundant black specs are primarily intraclasts with a micritic envelope (very minimal ooids). Intraclasts gradually disappear upwards (intra-oomicrite microbial mud). Ooids have a micritic envelope as well. The intervals with intraclasts are interbedded with intervals of no intraclasts (packstone and wackestone). Other shell frags include: disarticulated bivalve shells, crinoids. Bioturbation index ~3.

Box 2: 10591ft-10588ft

Medium grey in color, with silty to medium grained framework grain component. Abundant black specs are primarily intraclasts with a micritic envelope (very minimal ooids). The intervals with intraclasts are interbedded with intervals of no intraclasts (packstone and wackestone). Other shell frags include: disarticulated bivalve shells.

Box 1: 10595ft-10591ft

Medium grey in color, with silty to medium grained framework grain component. Micritic matrix with >10% grains. Abundant black specs are primarily intraclasts with a micritic envelope (very minimal ooids). Interval ~10592m has a brecciated fabric where medium grey wackestone is intermixed with dark grey laminations. The intervals with intraclasts are interbedded with intervals of no intraclasts (packstone and wackestone). Other shell frags include: disarticulated bivalve shells.

Mohican I-100 Core #5: 23ft Recovered

Box 7: 11364ft-11360ft

Darker grey in color with abundant ooids (<1cm), very densely packed ~90%. Variably argillaceous. Many shell frags are recrystallized to calcite. Minor randomly distributed, wavy discontinuous laminae. Some intervals with laminations have poorly defined cross-lamination. Interbedded with “mixed layers” of mudstone, carbonaceous and fine grained.

Box 6: 11367ft-11364ft

Dark grey in color with abundant coarser ooids (1-2cm), very densely packed ~90%. Variably argillaceous. Many shell frags are recrystallized to calcite. Minor randomly distributed, wavy discontinuous laminae. Some intervals with laminations have poorly defined cross-lamination. Interbedded with “mixed layers” of mudstone, carbonaceous and fine grained. Intervals of lighter grey mudstone with little fossil frags, only laminations and intervals (larger) of dark grey ooids rich-grainstone.

Box 5: 11370ft-11367ft

Darker grey in color with abundant ooids (<1cm), very densely packed ~90%. Variably argillaceous. Many shell frags are recrystallized to calcite. Minor randomly distributed, wavy discontinuous laminae. Some intervals with laminations have poorly defined cross-lamination. Interbedded with “mixed layers” of mudstone, carbonaceous and fine grained.

Box 4: 11373ft-11370ft

11370.5m-11370m missing core. Dark grey in color with abundant black specs (ooids and intraclasts with micritic envelope). Clasts are getting slightly coarser. Variably

argillaceous. Variable sorted grain size from very fine to very coarse and pebbly within a silty matrix. Abundant shell frags (bivalves, gastropods, echinoderms). Many shell frags are recrystallized to calcite. Minor randomly distributed, wavy discontinuous laminae. Some intervals with laminations have poorly defined cross-lamination. Interbedded with “mixed layers” of mudstone, carbonaceous and fine grained.

Box 3: 11376ft-11373ft

Dark grey in color with abundant black specs (ooids and intraclasts with micritic envelope). Variably argillaceous. Variable sorted grain size from very fine to very coarse and pebbly within a silty matrix. Abundant shell frags (bivalves, gastropods, echinoderms). Many shell frags are recrystallized to calcite. Minor randomly distributed, wavy discontinuous laminae. Some intervals with laminations have poorly defined cross-lamination. Interbedded with “mixed layers” of mudstone, carbonaceous and fine grained.

Box 2: 11379ft-11376ft

Dark grey in color with abundant black specs (ooids and intraclasts with micritic envelope). Variably argillaceous. Variable sorted grain size from very fine to very coarse and pebbly within a silty matrix. Abundant shell frags (bivalves, gastropods, echinoderms). Many shell frags are recrystallized to calcite. Minor randomly distributed, wavy discontinuous laminae. Interbedded with “mixed layers” of mudstone, carbonaceous and fine grained.

Box 1: 11383ft-11379ft

Dark grey in color with abundant black specs (ooids and intraclasts with micritic envelope). Variably argillaceous. Variable sorted grain size from very fine to very coarse and pebbly within a silty matrix. Abundant shell frags (bivalves, gastropods, echinoderms). Many shell frags are recrystallized to calcite. Minor randomly distributed, wavy discontinuous laminae.

Shell Acadia K-62 Core #4: 17.4m Recovered

Box 13: 3344m-3339m

Calcite cement, sparite matrix. Large fossil frags, including bivalves, coral, gastropods, bryozoans, oncoids and ooids. Minor fine-medium grained clasts, rounded and dark grey, brown or white in color. Perhaps calcite, mudstone. Isolated but common discontinuous, clay laminae. Fossils are primarily coral frags, although fossils are much smaller (<1cm-2cm). Color also changes slightly to darker beige/greenish tinge.

Box 12: 3349m-3344m

Light beige/peach color. Calcite cement, sparite matrix. Large fossil frags, including bivalves, coral, gastropods, bryozoans, oncoids and ooids. Minor fine-medium grained clasts, rounded and dark grey, brown or white in color. Perhaps calcite, mudstone. Isolated but common discontinuous, clay laminae. Fossils are primarily coral frags (<1cm-10cm) and oncoids (<1cm-10m). Oncoids are bordered by clay/silt laminae, brecciated fabric. Large coral fragments.

Box 11: 3353m-3349m

Light beige/peach color. Calcite cement, sparite matrix. Large fossil frags, including bivalves, coral, gastropods, bryozoans, oncoids and ooids. Minor fine-medium grained clasts, rounded and dark grey, brown or white in color. Perhaps calcite, mudstone. Isolated but common discontinuous, clay laminae. Fossils are primarily coral frags (<1cm-10cm) and oncoids (<1cm-10m). Oncoids are bordered by clay/silt laminae, brecciated fabric.

Box 10: 3358m-3353m

Light beige/peach color. Calcite cement, sparite matrix. Large fossil frags, including bivalves, coral, gastropods, bryozoans, oncoids and ooids. Minor fine-medium grained clasts, rounded and dark grey, brown or white in color. Perhaps calcite, mudstone. Isolated but common discontinuous, clay laminae. Fossils are primarily coral frags (<1cm-10cm) and oncoids (<1cm-10m). Oncoids are bordered by clay/silt laminae, brecciated fabric. As oncoids get larger, more mudstone is present, surrounding them.

Box 9: 3363m-3358m

Light beige/peach color. Calcite cement, sparite matrix. Large fossil frags, including bivalves, coral, gastropods, bryozoans, oncoids and ooids. Minor fine-medium grained clasts, rounded and dark grey, brown or white in color. Perhaps calcite, mudstone. Isolated but common discontinuous, clay laminae. Fossils are primarily coral frags (<1cm-10cm) and oncoids (<1cm-10m). Oncoids are bordered by clay/silt laminae, brecciated fabric. Large coral fragments. 30cm thick interval ~3357m is darker grey/green matrix with abundant oncoids, coral and shell frags. Abrupt transition above and below.

Box 8: 3368m-3363m

Light beige/peach color. Calcite cement, sparite matrix. Large fossil frags, including bivalves, coral, gastropods, bryozoans, oncoids and ooids. Minor fine-medium grained clasts, rounded and dark grey, brown or white in color. Perhaps calcite, mudstone. Isolated but common discontinuous, clay laminae. Fossils are primarily coral frags (<1cm-10cm) and oncoids (<1cm-10m). Oncoids are bordered by clay/silt laminae, brecciated fabric. Large coral fragments.

Box 7: 3374m-3368m

Light beige/peach color. Calcite cement, sparite matrix. Large fossil frags, including bivalves, coral, gastropods, bryozoans, oncoids and ooids. Minor fine-medium grained clasts, rounded and dark grey, brown or white in color. Perhaps calcite, mudstone. Isolated but common discontinuous, clay laminae. Fossils are primarily coral frags (<1cm-10cm) and oncoids (<1cm-10m). Oncoids are bordered by clay/silt laminae, brecciated fabric. Large coral fragments.

Box 6: 3378m-3374m

Light beige/peach color. Calcite cement, sparite matrix. Large fossil frags, including bivalves, coral, gastropods, bryozoans, oncoids and ooids. Minor fine-medium grained clasts, rounded and dark grey, brown or white in color. Perhaps calcite, mudstone. Isolated but common discontinuous, clay laminae. Two stylolites. Fossils are primarily coral frags (<1cm-10cm) and oncoids (<1cm-10m). Oncoids are bordered by clay/silt laminae, brecciated fabric. Most fossils have an envelope of pink/beige color (microbial?).

Box 5: 3382m-3378m

Not quite as interbedded as below, now is mostly grainstone (onkolitic grainstone). Light beige/peach color. Calcite cement, sparite matrix. Large fossil frags, including bivalves, coral, gastropods, bryozoans, oncoids and ooids. Minor fine-medium grained clasts, rounded and dark grey, brown or white in color. Perhaps calcite, mudstone. Isolated but common discontinuous, clay laminae. Two stylolites. Fossils are primarily coral frags (<1cm-5cm) and oncoids (<1cm-2cm). At ~3379m, erosional transition to ~10cm thick mudstone interval with shell frags and clay laminae. Erosional surface also at top. Transitions back into original grainstone.

Box 4: 3387m-3382m

Not quite as interbedded as below, now is mostly grainstone (onkolitic grainstone). Light beige/peach color. Calcite cement, sparite matrix. Large fossil frags, including bivalves, coral, gastropods, bryozoans, oncoids and ooids. Minor fine-medium grained clasts, rounded and dark grey, brown or white in color. Perhaps calcite, mudstone. Isolated but common discontinuous, clay laminae. Two stylolites. Fossils are primarily coral frags (<1cm-5cm) and oncoids (<1cm-2cm).

Box 3: 3391m-3387m

Light beige/peach color. Calcite cement, sparite matrix. Large fossil frags, including bivalves, coral, gastropods, bryozoans, oncoids and ooids. Largest fossils are coral and gastropods. Minor fine-medium grained clasts, rounded and dark grey, brown or white in color. Perhaps calcite, mudstone. Isolated but common discontinuous, clay laminae. Large coral fragments ~<2-10cm within grainstone interval. Abundant oncoids. Bivalve shell ~8cm across.

Box 2: 3395m-3391m

Light beige/peach color. Calcite cement, sparite matrix. Large fossil frags, including bivalves, coral, gastropods, bryozoans, oncoids and ooids. Not as many large fossils within this section. Minor fine-medium grained clasts, rounded and dark grey, brown or white in color. Perhaps calcite, mudstone. Isolated but common discontinuous, clay laminae. Wackestone interbedded with grainstone. Grainstone typically comprises shell-rich, clasts, poorly sorted grains (slightly darker beige). Wackestone comprises clay-silt size grains with scattered, discontinuous muddy laminae with minor fossil frags <10%.

Box 1: 3399.2m-3395m

Missing core from 3399.2m-3397m. Light beige/peach color. Calcite cement, sparite matrix. Stylolites abundant. Large fossil frags, including bivalves, coral, gastropods, bryozoans, oncoids and ooids. Largest fossils are coral and gastropods. Minor fine-medium grained clasts, rounded and dark grey, brown or white in color. Perhaps calcite, mudstone. Large calcite filled vugs, typically within fossil frags (coral). Intraclast porosity. Isolated but common discontinuous, clay laminae.

Shell Acadia K-62 Core #5: 15.5m Recovered

Box 11: 3738.2m-3736.2m

Light beige color, micritic matrix. Very brecciated fabric. Abundant stylolites throughout, core is fracturing along stylolites. Minor shell frags, mollusks although everything is very recrystallized (diagenesis). Wackestone clasts intermixed with mudstone (lighter beige vs slightly darker beige). Mottled appearance.

Box 10: 3739.6m-3738.2m

Light beige color, micritic matrix. Very brecciated fabric. Abundant stylolites throughout, core is fracturing along stylolites. Minor shell frags, mollusks although everything is very recrystallized (diagenesis). Wackestone clasts intermixed with mudstone (lighter beige vs slightly darker beige). Mottled appearance.

Box 9: 3741.0m-3739.6m

Light beige color, micritic matrix. Brecciated fabric. Abundant stylolites throughout, core is fracturing along stylolites. Minor shell frags, mollusks although everything is very recrystallized (diagenesis). Wackestone clasts intermixed with mudstone (lighter beige vs slightly darker beige). Mottled appearance. Some intervals appear to be microbial.

Box 8: 3742.5m-3741.0m

Light beige color, micritic matrix. Brecciated fabric. Abundant stylolites throughout, core is fracturing along stylolites. Minor shell frags, mollusks although everything is very recrystallized (diagenesis). Wackestone clasts intermixed with mudstone (lighter beige vs slightly darker beige). Mottled appearance.

Box 7: 3743.9m-3742.5m

Light beige color, micritic matrix. Brecciated fabric. Abundant stylolites throughout, core is fracturing along stylolites. Minor shell frags, mollusks although everything is very recrystallized (diagenesis). Wackestone clasts intermixed with mudstone (lighter beige vs slightly darker beige). Mottled appearance. Calcite filled vugg. Some intervals appear to be microbial. Laminae have been compacted and deformed to create a nodular fabric.

Box 6: 3745.3m-3743.9m

Light beige color, micritic matrix. Brecciated fabric. Abundant stylolites throughout, core is fracturing along stylolites. Minor shell frags, mollusks although everything is very recrystallized (diagenesis). Wackestone clasts intermixed with mudstone (lighter beige vs slightly darker beige). Mottled appearance. Silt laminations are more abundant. Some intervals appear to be microbial.

Box 5: 3746.7m-3745.3m

Light beige color, micritic matrix. Brecciated fabric. Abundant stylolites throughout, core is fracturing along stylolites. Minor shell frags, mollusks although everything is very recrystallized (diagenesis). Wackestone clasts intermixed with mudstone (lighter beige vs slightly darker beige). Mottled appearance. Silt laminations are more abundant.

Box 4: 3748.1m-3746.7m

Same rock type continues until 3748.8m, it then abruptly transitions to a darker grey mudstone with minor carbonaceous laminations. Pyrite formation throughout interval. Wavy, parallel laminations. Minor mixing of the darker grey mudstone with the lighter grey Wackestone (perhaps through bioturbation). Minor clasts (fine-medium grained), calcite or quartz, or rip up clasts from the lighter Wackestone. Above, approximately 0.5m of core is missing, and then it continues into the light beige color, micritic matrix. Brecciated fabric. Abundant stylolites throughout, core is fracturing along stylolites. Minor shell frags, mollusks although everything is very recrystallized (diagenesis). Wackestone clasts intermixed with mudstone (lighter beige vs slightly darker beige). Mottled appearance.

Box 3: 3749.56m-3748.1m

Light beige color, micritic matrix. Brecciated fabric. Abundant stylolites throughout, core is fracturing along stylolites. Minor shell frags, mollusks although everything is very recrystallized (diagenesis). Wackestone clasts intermixed with mudstone (lighter beige vs slightly darker beige). Mottled appearance.

Box 2: 3751m-3749.56m

Light beige color, micritic matrix. Brecciated fabric. Abundant stylolites throughout, core is fracturing along stylolites. Minor shell frags, mollusks although everything is very recrystallized (diagenesis). Wackestone clasts intermixed with mudstone (lighter beige vs slightly darker beige). Mottled appearance. Minor clasts (<1cm-3cm) of calcite, or darker grey mudstones (intraclasts)

Box 1: 3752.4m-3751m

Missing core from 3752.4m-3752.1m. Light beige color, micritic matrix. Brecciated fabric. Abundant stylolites throughout, core is fracturing along stylolites. No visible fossils, everything is very recrystallized (diagenesis). Wackestone clasts intermixed with mudstone (lighter beige vs slightly darker beige). Mottled appearance.

Shell Acadia K-62 Core #6:9.6m Recovered

Box 7: 4843.5m-4842.1m

Dark grey grainstone, made up of >60% ooids, and other shell frags. Only two laminations. Minor clasts (fine-very fine grained), primarily quartz and calcite. One large ~15cm long, mud clast, parallel to coring direction. At 4843.8m, large chambered fossil (ammonite?), all replaced with calcite. Micritic matrix.

Box 6: 4844.8m-4843.5m

Dark grey grainstone, made up of >60% ooids, and other shell frags. Only two laminations. Minor clasts (fine-very fine grained), primarily quartz and calcite. Some intervals are light beige/grey in color, however that is believed to be due to exposure and age (happens to abruptly and randomly). Micritic matrix.

Box 5: 4845.1m-4844.8m

Dark grey grainstone, made up of >60% ooids, and other shell frags. Only two laminations. Minor clasts (fine-very fine grained), primarily quartz and calcite. Micritic matrix.

Box 4: 4847.2m-4845.1m

Dark grey grainstone, made up of >60% ooids, and other shell frags. Laminations become more abundant, as well as parallel and wavy. They are not as “compact”, or none of them are almost stylolites. Minor clasts (fine-very fine grained), primarily quartz and calcite. Micritic matrix.

Box 3: 4848.44m-4847.2m

Dark grey grainstone, made up of >60% ooids, and other shell frags. Only two laminations. Minor clasts (fine-very fine grained), primarily quartz and calcite. Micritic matrix.

Box 2: 4849.7m-4848.44m

Dark grey grainstone, made up of >60% ooids, and other shell frags. Small carbonaceous mudstone laminae throughout, randomly oriented. Some laminations are almost stylolites. Minor clasts (fine-very fine grained), primarily quartz and calcite. Micritic matrix.

Box 1: 4850.9m-4849.7m

Core is missing until 4850.3m. Dark grey grainstone, almost appears as a sandstone, however under hand lens it is obvious they are ooids and VF grained shell frags. Small carbonaceous mudstone laminae throughout, randomly oriented. At 4849.5m, a mudstone lamina is almost a stylolite, it is outlined with pyrite, evident from the oxidation taking place. Minor clasts (fine-very fine grained), primarily quartz and calcite. Micritic matrix.

Cohasset L-97 Core #1: 17.7m Recovered

Box 14: 3407.07m-3406.04m

Light brown/beige Wackestone/mudstone with bivalves and other shell frags. Transition zone has some rip-up clasts/mixing. Calcite filled vugs, and minor mixing of mudstone and Wackestone. Clasts visible throughout, white in color and well-rounded (calcite). Mottled appearance is gone.

Box 13: 3407.77m-3407.07m

3407.4m-3407.77m is the same as box 12. It then abruptly transitions into a light brown/beige Wackestone/mudstone with bivalves and other shell frags. Transition zone has some rip-up clasts/mixing. Calcite filled vugs, and minor mixing of mudstone and Wackestone. Clasts visible throughout, white in color and well-rounded (calcite). Mottled appearance is gone.

Box 12: 3409m-3407.77m

Less brecciated (comparatively), however still an apparent fabric with mixed terrigenous mudstone/lime Wackestone. Nodule clasts throughout from mixing and decompaction. Minor amounts of bivalves. Coral frags dispersed throughout. More abundant in pyrite formation within the mudstone (darker grey) areas, randomly forming, no orientation.

Box 11: 3410m-3409m

Less brecciated (comparatively), however still an apparent fabric with mixed terrigenous mudstone/lime Wackestone. Nodule clasts throughout from mixing and decompaction. Minor amounts of bivalves. Coral frags dispersed throughout. More abundant in pyrite formation within the mudstone (darker grey) areas, randomly forming, no orientation.

Box 10: 3411m-3410m

Becomes less brecciated, however still an apparent fabric with mixed terrigenous mudstone/lime Wackestone. Nodule clasts throughout from mixing and decompaction. Minor amounts of bivalves. Coral frags dispersed throughout. Pyrite formation within the mudstone (darker grey) areas, randomly forming, no orientation.

Box 9: 3413m-3411m

Very brecciated with mixed terrigenous mudstone/lime Wackestone. Nodule clasts throughout from mixing and decompaction. Minor amounts of bivalves. Coral frags dispersed throughout. Pyrite formation within the mudstone (darker grey) areas, randomly forming, no orientation.

Box 8: 3414m-3413m

Similar to second half of box 7, very brecciated with mixed terrigenous mudstone/lime Wackestone. Nodule clasts throughout from mixing and decompaction. Minor amounts of bivalves. Coral frags dispersed throughout.

Box 7: 3416m-3414m

Core is missing from 3416-3415.5m, although below missing section spongy coral continues (perhaps just moved around in box). Below, at 3415.5m, wackestone gets more brecciated and it becomes more mixed terrigenous mudstone/lime Wackestone. There is a large calcite vein (parallel to coring direction) ~30cm long and ~5cm wide.

Box 6: 3417m-3416m

Coral throughout first half of box 6, light beige/brown in color. At 3416.5m, there is a large ~40cm long branching coral, with all of the “branches” replaced with calcite. The base of it is missing in the core, however it then transitions into and spongy coral (no structure, all light beige) with minor carbonaceous laminations in no orientation within the transition zone.

Box 5: 3418m-3417m

Large coral piece (~10-15cm, light brown with calcite filled vugs), with carbonaceous material at base.

Box 4: 3419m-3418m

Coral fragments ~3418.8m (dark black, massive appearance). Light grey carbonate rock, with darker grey carbonaceous material throughout. Core has a mottled appearance. Black organic laminae throughout. No apparent grains and very minor amounts of shell frags (bivalves). Wackestone with >10% grains and matrix supported. All recrystallized. Calcite

filled vugs throughout, porosity is not fabric selective (vuggy). Abundant stylolites throughout core, signifying pressure dissolution. Fabric is brecciated.

Box 3: 3421m-3419m

Light grey carbonate rock, with darker grey carbonaceous material throughout. Core has a mottled appearance. Black organic laminae throughout. No apparent grains and very minor amounts of shell frags (bivalves). Wackestone with >10% grains and matrix supported. All recrystallized. Calcite filled vugs throughout, porosity is not fabric selective (vuggy). Abundant stylolites throughout core, signifying pressure dissolution. Fabric is brecciated.

Box 2: 3422m-3421m

Light grey carbonate rock, with darker grey carbonaceous material throughout. Core has a mottled appearance. Black organic laminae throughout. No apparent grains and very minor amounts of shell frags (bivalves). Wackestone with >10% grains and matrix supported. All recrystallized. Calcite filled vugs throughout, porosity is not fabric selective (vuggy). Abundant stylolites throughout core, signifying pressure dissolution. Fabric is brecciated.

Box 1: 3425m-3422m

Light grey carbonate rock, with darker grey carbonaceous material throughout. Core has a mottled appearance. Black organic laminae throughout. No apparent grains and very minor amounts of shell frags (bivalves). Wackestone with >10% grains and matrix supported. All recrystallized. Calcite filled vugs throughout, porosity is not fabric selective (vuggy). Abundant stylolites throughout core, signifying pressure dissolution. Fabric is brecciated.

PanCanadian Panuke PI-1A Core #1: 1.4m Recovered

Only one box of core, core is very broken up.

Box 1: 4032.8m-4029.28m

Light beige-white in color. Matrix is not calcareous. Took samples. Lots of calcite cements throughout, and abundant calcite filled vugs. Abundance of vugs ~5-10%. Small black carbonaceous laminae dispersed throughout, no orientation to them. No evidence of original fossil material, perhaps was all recrystallized (went through diagenesis?). Minor stylolites.

PanCanadian Panuke H-08 Core #1: 2.96m Recovered

Core was very broken up, and sampled heavily. Difficult to describe, only 2.96m has been recovered however the difference from base to top is 14m, since it is so broken up it is not apparent where the missing core is.

Box 3: 3450.7m-3446m

Another brecciated zone begins (again, cannot see nature of contact). Light beige with calcite cement, abundant shell frags (medium sized), primarily bivalves. Some calcite filled vugs, and one calcite vein. May also contain oncoids and ooids and coral fragments. Coral fragment with bivalve within the infilled spine.

Box 2: 3455m-3450.7

Same as box 1 from 3455.7m-3453.9m. Transitions into brecciated interval (darker beige in color) with carbonaceous laminae dispersed throughout the interval, creating boundaries for the grains. Grains are very coarse (1cm-5cm), non-rounded and non-sorted. Clasts may also be oncoids, have a concentric appearance to some, with a micritic envelope. Appear to mainly consist of calcite. Also consists of fine shell frags. Interval appears “clumpy”. Not sure the nature of contact of base or top of brecciated interval due to only pieces left in boxes. Above brecciated interval @ ~3451.8m large coral fragment ~15cm long and within sample area, another large piece of coral ~20cm with carbonaceous material on top of it, hydrocarbon scent.

Box 1: 3460m-3455m

Light beige in color, calcite cemented, very fine grained with abundant broken shell fragments, (fine-medium in size) primarily bivalves and brachiopods. Some pieces of core have oncoids and ooids. Fine grained clasts (well rounded) throughout interval (calcite and quartz). Grainstone. Minor carbonaceous laminae throughout (chaotic).

PanCanadian Panuke M-79 Core #1: 5.2m Recovered

Box 5: 4533.9m-4532.7m

Very similar to box 4, however more intervals of the coarse grained, well rounded and well-sorted clasts (<1cm-3cm in size). Still have carbonaceous laminations throughout in a light grey, ooid and shell fragment rich Packstone.

Box 4: 4534.96m- 4533.9m

Light grey very fine grained Packstone (ooids and shell frags) with calcareous with carbonaceous, non-planar, wavy laminations (~4-5) throughout, appears as coal. Two intervals @ 4534.0m and 4533.7m of ~8cm thick with medium-coarse grained, well rounded and well sorts clasts of calcite, and quartz (storm deposits). No shell frags within these intervals (that can be seen in the core). Clast rich interval @4533.7m has a wavy, erosional contact with the VF grained Packstone with cross-stratified carbonaceous laminations. Mixed terrigenous mudstone/lime wackestone. Nodular bedding is mainly from differential compaction and burrowing.

Box 3: 4536m-4534.96m

First half of box three (4536m-4535.48m) same as box 2. Mixed terrigenous mudstone/lime wackestone. Light grey with fine black specs (ooids, intraclasts) and shell frags interlayered with small carbonaceous laminations. Fine, well rounded clasts throughout (calcite). Second half of box three (4535.48m-4534.96m) is a transition zone from light grey with the darker grey laminations to dark grey/black with abundant well-rounded and well sorted clasts (calcite) and shell frags. It is an abrupt, non-planar change. Clasts are <1cm-3cm. Black wavy laminations, carbonaceous rich (coaly).

Box 2: 4537m-4536m

Dark grey calcareous cemented Packstone with abundant black specs (almost certain they are ooids, could potentially also be intraclasts (took sample)). Still abundance of white clasts (>10%<20%), calcite or quartz. Becoming more layered, with lighter grey (ooids


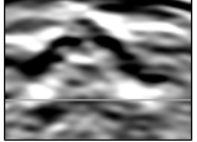

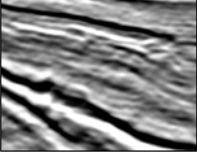
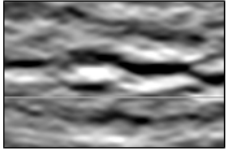
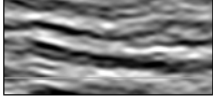
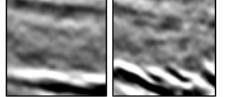

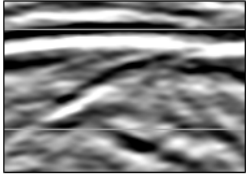
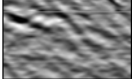
rich, shell frags and intraclasts), 2cm-10cm thick layers, and darker grey with minor shell frags. Layers are non-uniform, perhaps brecciated.

Box 1: 4537.8m-4537m

Light grey with dark grey non-parallel, non-planar, discordant laminations. Calcareous cement, abundant white clasts (calcite) and fine shell fragments (undistinguishable). Near top of box 1, lighter grey material becomes separated by the dark grey laminations.

Appendix E: Seismic facies and traverses

Table E-1: Summary of seismic facies characteristics, geologic interval and examples of the seismic facies from the 3D Sable MegaMerge. See Table 5.1 and Figures 4.13 to 4.18

Seismic Facies Characteristics	Geologic Interpretation	Seismic Facies Examples
Low to high amplitude throughout study area. Parallel to sub-parallel, sometimes chaotic.	Lagoonal, platform interior, High amplitude bursts are low impedance, porous clastics, or dolomitized limestone.	
Structural bump, contractional drape. Noisy, chaotic high amplitudes in low impedance zones.	Reef margin and basinal shale incursions. Transition between the reef margin and proximal foreslope. Typically resistant frame builders creating a raised rim. Diagenesis at the reef margin creates sporadic low impedance porosity which adds to the chaotic signature.	
High amplitude peak-trough pairs. Divergent to concordant, parallel, good continuity.	Carbonate dominated proximal-distal foreslope. Clean microbial limestones on calcareous mudstone pairs (section 5.4.2 Abenaki 4).	
Medium to high amplitudes, generally peak-trough pairs. Displays increasingly more chaotic, discontinuous reflections moving east. Parallel to sub-parallel, some sigmoidal reflections.	Mixed carbonate and siliciclastics. Siliciclastics are interpreted to be the Mic Mac Formation sands which bypassed the carbonate bank and deposited on the proximal foreslope amongst the carbonates of the Abenaki bank (section 5.4.3).	
Low to medium amplitudes, poor continuity. Some high amplitude peak-trough pairs, although generally trough-peak pairs. Mainly sub-parallel, or deformed reflections, some chaotic.	Mixed carbonate and increasing siliciclastics. Proximal to distal foreslope transition. Moving west, more siliciclastics are interpreted from more trough-peak pairs, due to the Sable Delta depositing into the Sable Sub-basin.	
High amplitude trough-peak pairs. Sometimes chaotic, parallel to sub-parallel reflectors.	Prodelta siliciclastics infilling expansion trend (Fig. 4.16, section 5.4.3).	
Downlapping clinofolds, low to medium amplitudes, sub-parallel, relatively continuous (Fig. 5.5).	Proximal to distal foreslope of Abenaki 2 carbonates. Distal toe of Abenaki 2 (section 5.4.2 Abenaki 2).	
High amplitude peak-trough pair. Downlaps onto Mohican. Continuous (Fig. 5.5).	Shelf limestone which grew amongst the platform interior (Figs. 4.13-4.17).	
Angular unconformity. Low to high amplitudes. High amplitudes on the shelf margin, changing to low amplitudes basinward. Mainly chaotic, or deformed reflections.	Angular unconformity interpreted to be due to salt movement. High amplitudes on the shelf due to impedance changes between shelf carbonates and Mohican siliciclastics. Low amplitudes basinward due to little impedance changes between Mohican Formation and Verrill Canyon formations siliciclastics (section 5.4.2).	
Chaotic, low amplitude, poor continuity.	Salt diapirs which moved due to a large influx of siliciclastics from the Sable Delta.	

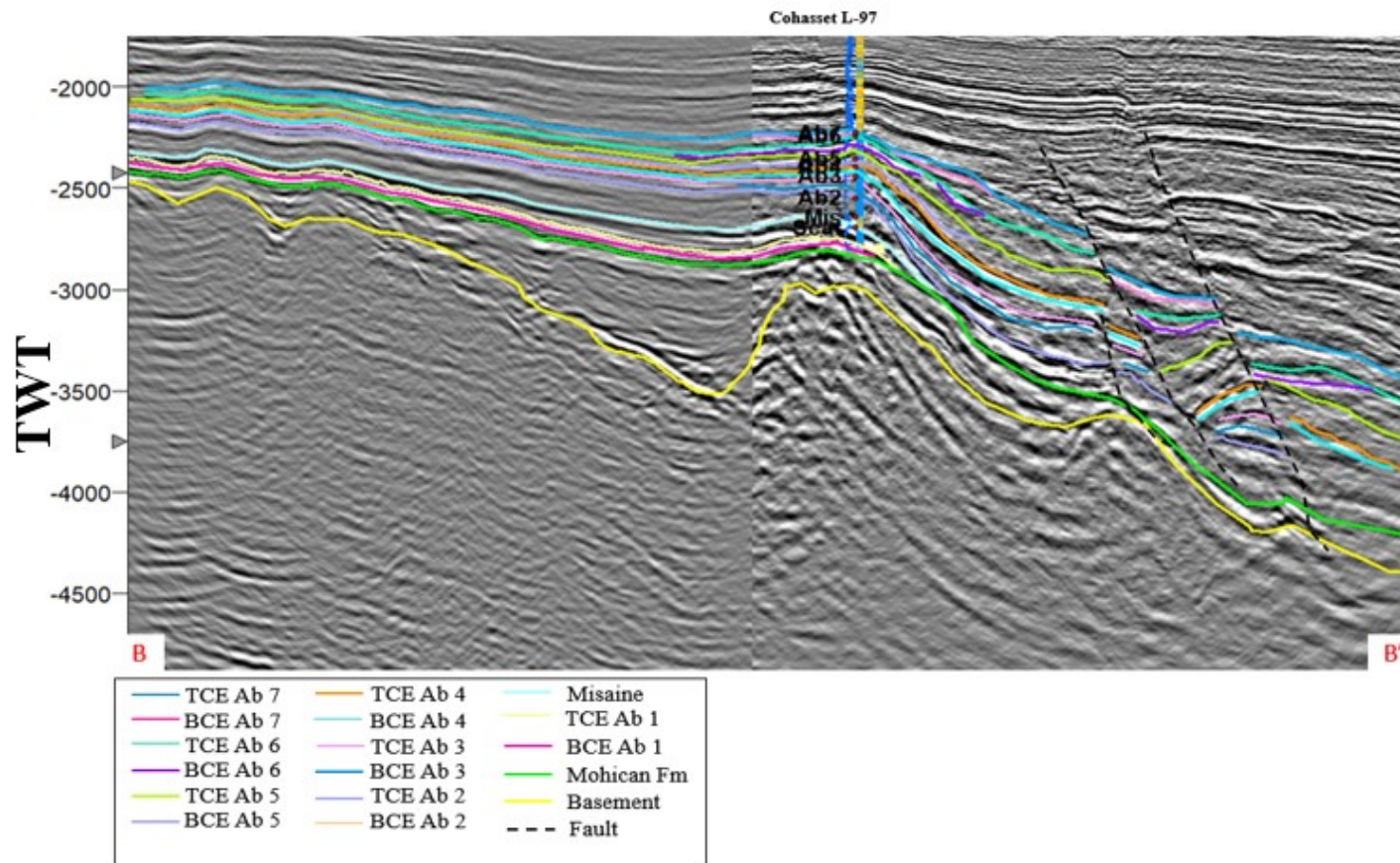


Figure E-1: Seismic traverse showing the transition from continental shelf where the carbonate platform grew, to slope, to distal foreslope/deep basin within the east-central region of the study area. Carbonates were also predominately deposited within this region from the Middle Jurassic to Early Cretaceous, however there is more of a siliciclastic influence in Abenaki 5, 6 and 7 sequences interpreted by the lack of strong amplitude peak-troughs, and the sequences becoming thicker off the bank margin. It can also be observed that within the proximal platform interior, carbonates only grew until Abenaki 4 and it is not until the bank margin that Abenaki 5, 6 and 7 develop.

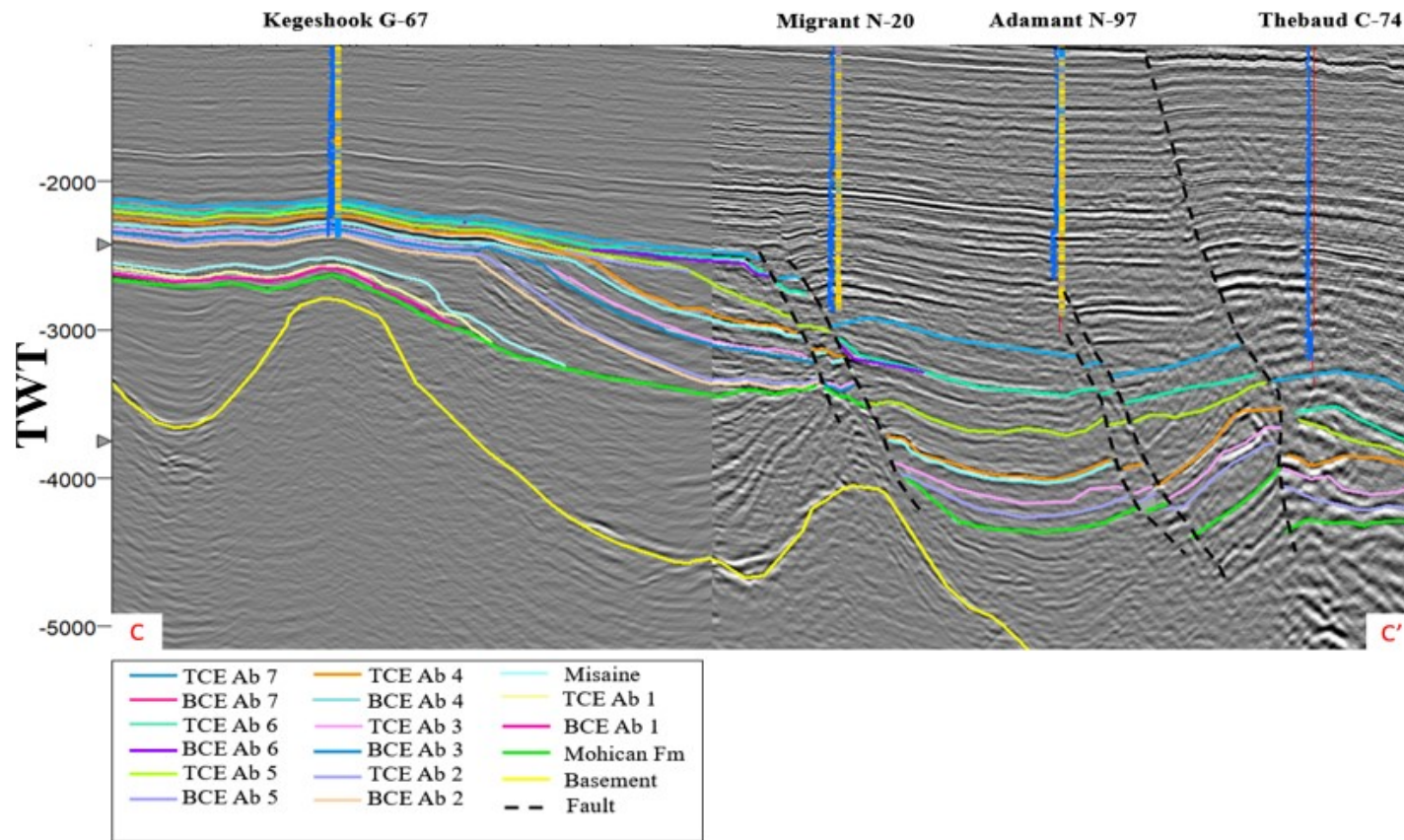


Figure E-2: Seismic traverse showing the transition from continental shelf where the carbonate platform grew, through to the slope, to distal foreslope/deep basin within the central region of the study area. This line demonstrates the extent of the carbonate cycles basinward, and how the carbonate growth of Abenaki 5, 6 and 7 were all affected by the influx of siliciclastics. Migrant N-20 penetrated 1000 m of Jurassic siliciclastics, representing the beginning of the expansion trend caused by the influx of siliciclastics causing sediment loading and salt withdrawal. It can also be observed that within the proximal platform interior, carbonates only grew until Abenaki 4 and it is not until the bank margin that Abenaki 5, 6 and 7 develop.

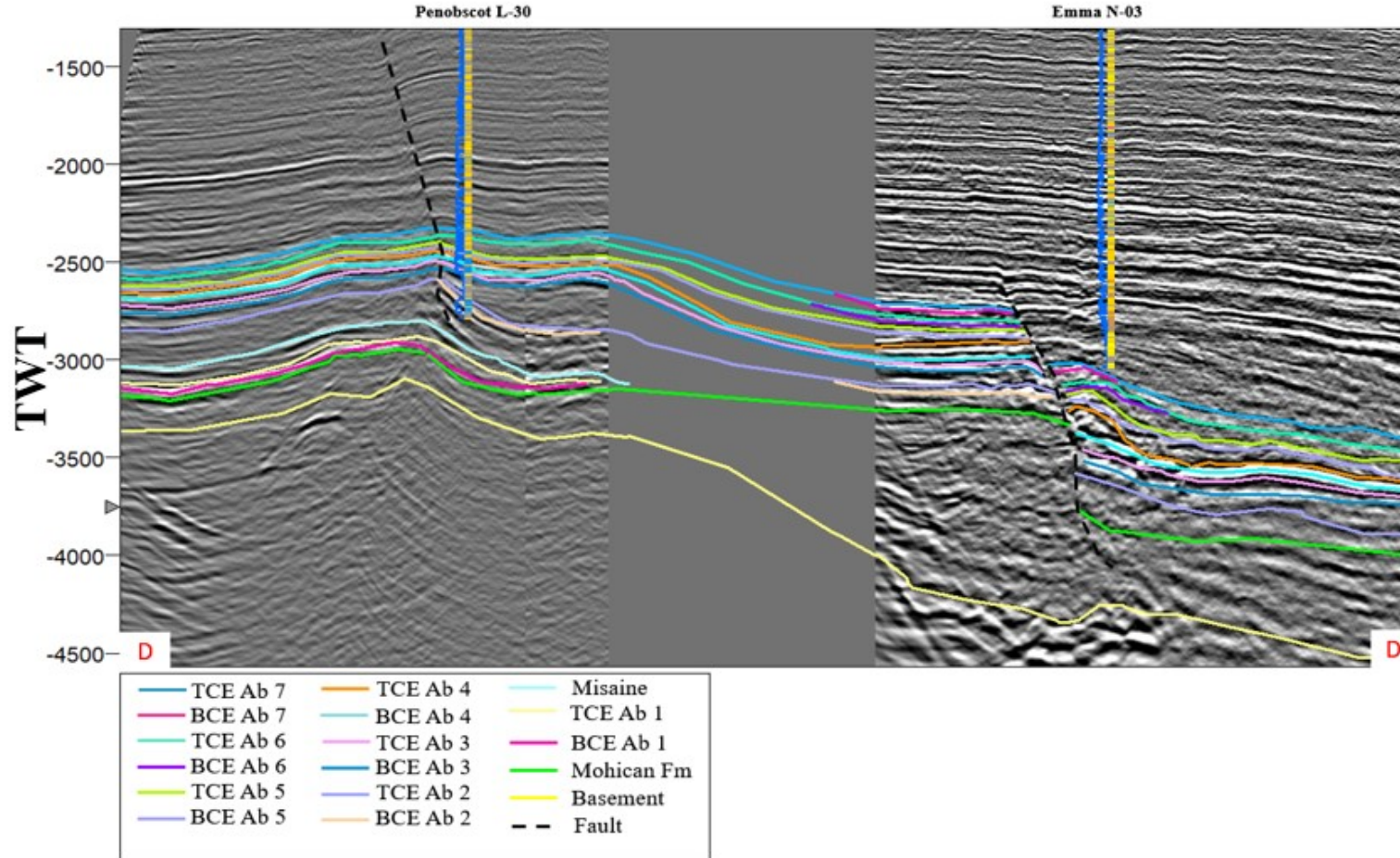


Figure E-3: Seismic traverse showing the transition from continental shelf where the carbonate platform grew, to slope, to distal foreslope/deep basin within the western region of the study area. The grey area between the two wells represent a gap between the seismic surveys. This line shows that in the western region of the study area, near Penobscot L-30, the Abenaki bank only grew until the middle Kimmeridgian (Abenaki 4), and carbonates of Abenaki 5, 6 and 7 were only able to develop on the foreslope of the platform.

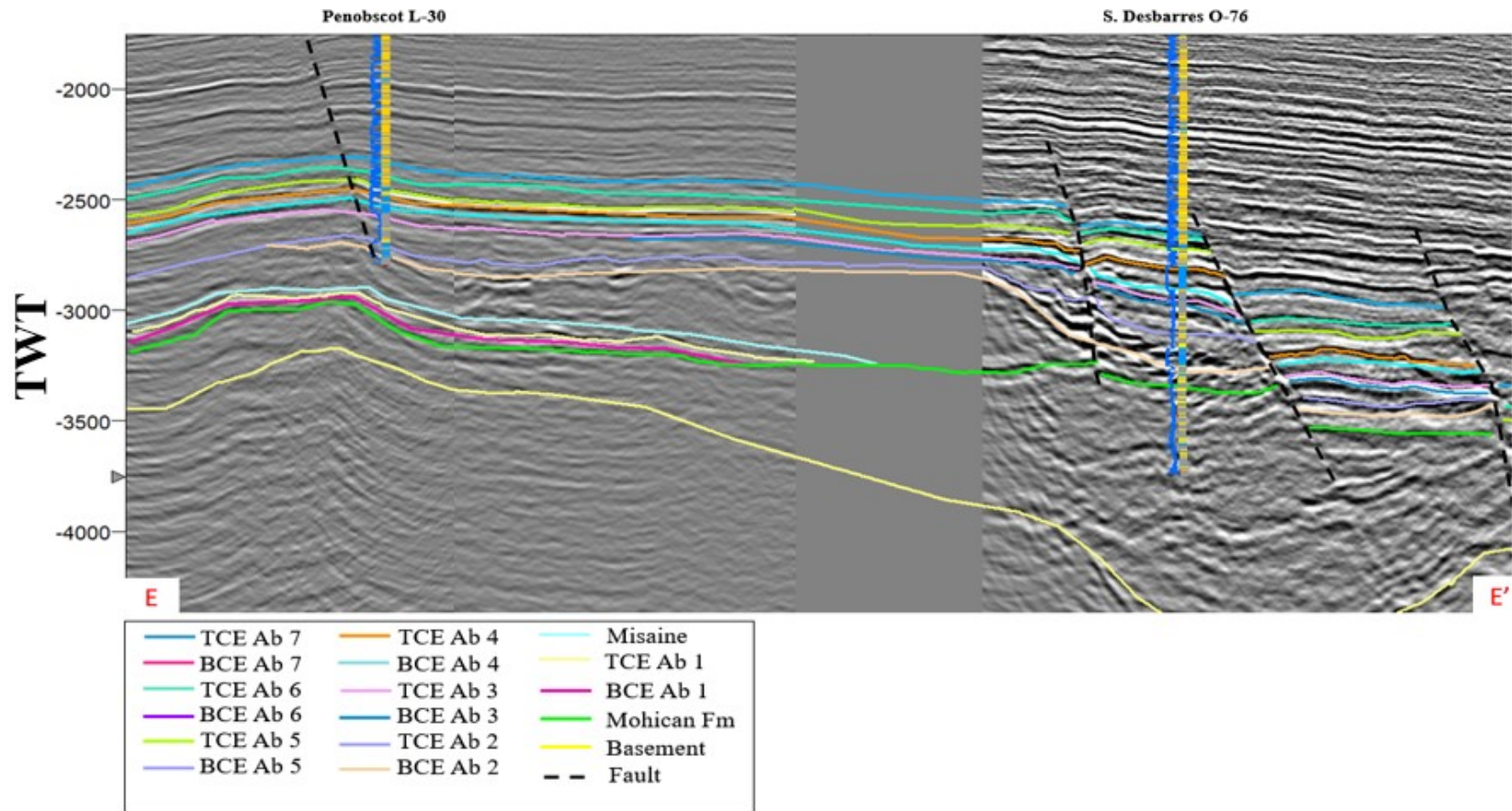


Figure E-4: Seismic traverse showing the transition from continental shelf where the carbonate platform grew, to slope, to distal foreslope/deep basin within the western region of the study area. The grey area between the two wells represent a gap between the seismic surveys. This line shows that in the western region of the study area, near Penobscot L-30, the Abenaki bank only grew until the middle Kimmeridgian (Abenaki 4), and carbonates of Abenaki 5, 6 and 7 were only able to develop on the foreslope of the platform. It also demonstrates that near to the S. Debarres O-76 well, other fourth-order carbonate cycles could develop amongst third-order depositional sequences as carbonates were being shed off the bank during sea-level lowstands.

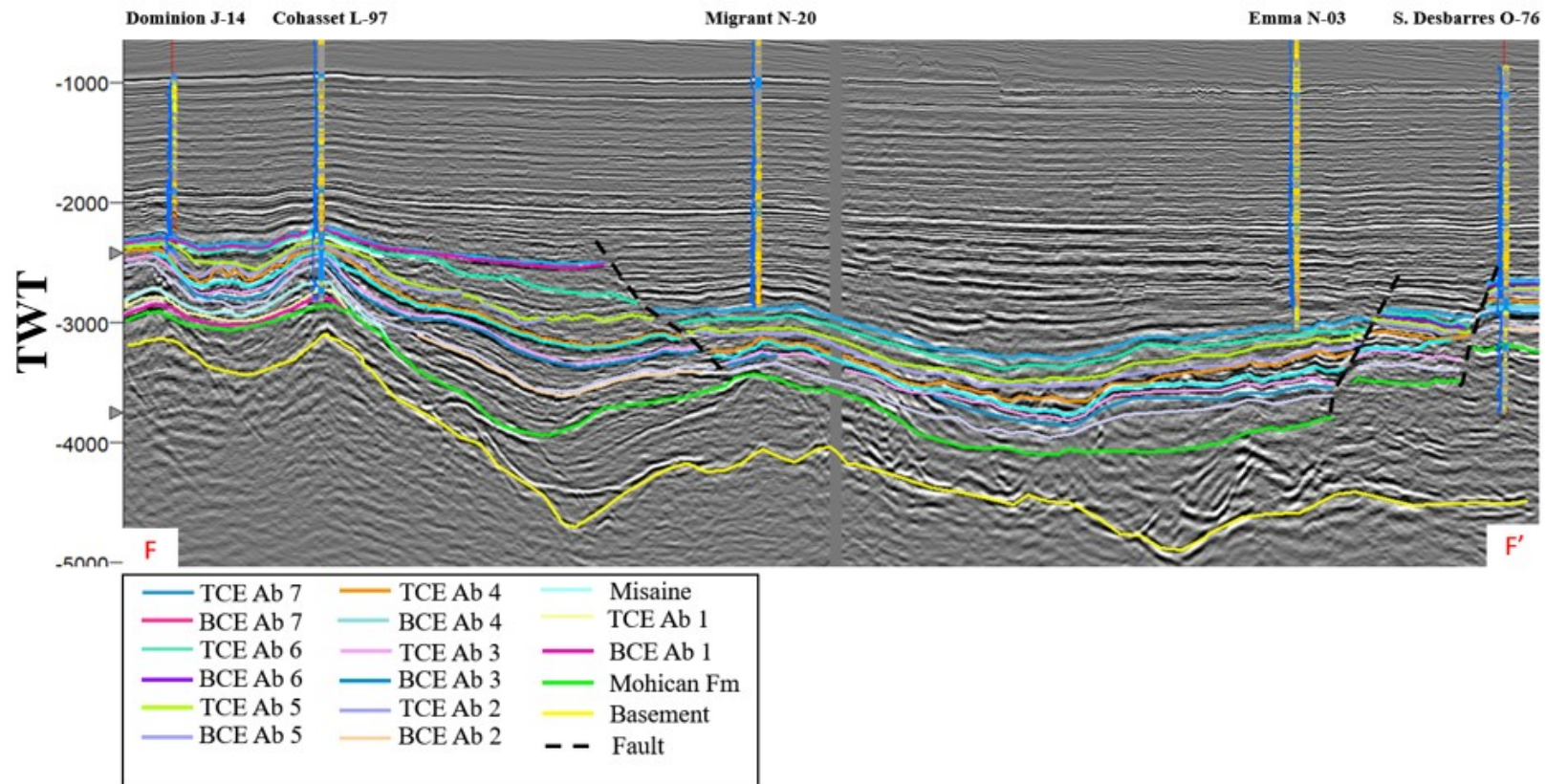


Figure E-5: Seismic traverse showing the west to east transect along strike. It shows all keys wells that were used to identify whether carbonates or siliciclastics prevailed in that specific area. It demonstrates that in the west near Dominion J-14 and Cohasset L-97 (the furthest wells from the Sable Delta in this study) it was predominately a carbonate depositional system and moving eastward to Migrant N-20, siliciclastic influx became evident after the deposition of Abenaki 4. Moving further east to Emma N-03 and S. Desbarres O-76, carbonate deposition is not as prevalent as the east near Dominion J-14 and Cohasset L-97. Under Emma N-03 other fourth-order carbonate cycles were able to develop amongst third-order depositional sequences as carbonates were being shed off the bank during sea-level lowstand.